Neurodevelopmental Deficits and Aberrant Neuron-Neuron Interactions in iPSC-derived Psychiatric Disease Models

Dissertation

zur Erlangung des Grades eines
Doktors der Naturwissenschaften

der Mathematisch-Naturwissenschaftlichen Fakultät
und
der Medizinischen Fakultät
der Eberhard-Karls-Universität Tübingen

vorgelegt
von

Sophia-Marie Hartmann
aus Bad Urach, Deutschland

2025

Tag der mündlichen Prüfung: 13.02.2025

Dekan der Math.-Nat. Fakultät:	Prof. Dr. Thilo Stehle
Dekan der Medizinischen Fakultät:	Prof. Dr. Bernd Pichler
1. Berichterstatter:	Prof. Dr. Hansjürgen Volkmer
2. Berichterstatter:	Prof. Dr. Stefan Liebau
Prüfungskommission:	Prof. Dr. Hansjürgen Volkmer
	Prof. Dr. Stefan Liebau
	Prof. Dr. Jan Benda
	Prof. Dr. Simone Mayer

Erklärung / Declaration:

Ich erkläre, dass ich die zur Promotion eingereichte Arbeit mit dem Titel:

„Neurodevelopmental Deficits and Aberrant Neuron-Neuron Interactions in iPSC-derived Psychiatric Disease Models“

selbständig verfasst, nur die angegebenen Quellen und Hilfsmittel benutzt und wörtlich oder inhaltlich übernommene Stellen als solche gekennzeichnet habe. Ich versichere an Eides statt, dass diese Angaben wahr sind und dass ich nichts verschwiegen habe. Mir ist bekannt, dass die falsche Abgabe einer Versicherung an Eides statt mit Freiheitsstrafe bis zu drei Jahren oder mit Geldstrafe bestraft wird.

I hereby declare that I have produced the work entitled

“Neurodevelopmental Deficits and Aberrant Neuron-Neuron Interactions in iPSC-derived Psychiatric Disease Models”,

submitted for the award of a doctorate, on my own (without external help), have used only the sources and aids indicated and have marked passages included from other works, whether verbatim or in content, as such. I swear upon oath that these statements are true and that I have not concealed anything. I am aware that making a false declaration under oath is punishable by a term of imprisonment of up to three years or by a fine.

Tübingen, den ....

Datum / Date Unterschrift /Signature

TABLE OF CONTENTS

LIST OF FIGURES

LIST OF TABLES

LIST OF ABBREVIATIONS

AC	Adenylyl cyclase
AD2	ASCL1 + DLX2
ANK-3	Ankyrin-3
ASCL1	Achaete-scute homolog 1
AUC	Area under the curve
BDNF	Brain-derived neurotrophic factor
BP	Breakpoints
bp	Base pairs
cDNA	Complementary deoxyribonucleic acid
CHIR99021	highly selective GSK-3 inhibitor
CNTF	Ciliary neurotrophic factor
CNV	Copy number variant
COMT	Catechol-O-Methyltransferase
CRISPR	Clustered regularly interspaced short palindromic repeats
CSF	Cerebrospinal fluid
CTR	Control
DAT	Dopamine transporter
DBH	Dopamine beta-hydroxylase
DDC	Dopa decarboxylase
DEGs	Differentially expressed genes
DISC1	Disrupted in schizophrenia 1
dbcAMP	Dibutyryl cyclic adenosine monophosphate
DIV	Day in vitro
DLX2	Distal-less homeobox 2
DMEM	Dulbecco's Modified Eagle Medium
DMSO	Dimethyl sulfoxide
dNTP	Deoxynucleotide triphosphate
DPBS	Dulbecco's Phosphate-Buffered Saline
DRD	Dopamine receptor
E-I	Excitatory-inhibitory
FBS	Fetal bovine serum
FDR	False discovery rate
FGAs	First-generation antipsychotics
FGF	Fibroblast growth factor
FGFR1	Fibroblast growth factor receptor 1
FOXA2	Forkhead Box A2
FWHM	Full width at half maximum
FZD9	Frzzled-9
GABA	Gamma-aminobutyric acid
GAPDH	Glyceraldehyde 3-phosphate dehydrogenase
GDNF	Glial cell line-derived neurotrophic factor
GFP	Green fluorescent protein
GO	Gene ontology
GPCR	G-protein coupled receptor
GSI	Global synchronization index
GWAS	Genome-wide association study
h	Hours

HC	Healthy control
iDANs	Induced dopaminergic neurons
HCA	High-content analysis
iPSC	Induced pluripotent stem cells
LDN193189	BMP signaling inhibitor
LMX1B	LIM homeobox transcription factor 1-beta
MAP2	Microtubule-associated protein 2
mRNA	Messenger RNA
NAc	Nucleus accumbens
NEAA	non-essential amino acids
NGN2	Neurogenin 2
NMDAR	*N*-methyl-D-aspartate receptor
NPC	Neural progenitor cell
NURR1	Nuclear receptor 4A2
OCT4	Octamer-binding transcription factor 4
PBS	Phosphate-buffered saline
PCR	Polymerase chain reaction
PET	Positron emission tomography
PFA	Paraformaldehyde
PFC	Prefrontal cortex
PLO	Poly-L-ornithine
PMA	Phorbol 12-myristate 13-acetate
PSD	Postsynaptic density
PV	Parvalbumin
RNA	Ribonucleic acid
ROI	Region of interest
RT	Room temperature
rtTA	Reverse tetracycline transactivator protein
RT-PCR	Reverse transcription polymerase chain reaction
RRF	Retrorubal field
SB431542	Activin/BMP/TGF-beta pathway inhibitor
SCZ	Schizophrenia spectrum disorder
SEM	Standard error of the mean
SGAs	Second-generation antipsychotics
smNPC	Small molecule induced neural progenitor cells
SNc	Substantia nigra pars compacta
SNP	Single nucleotide polymorphism
SOX	SRY related HMG box transcription factor
SPECT	Single photon emission computed tomography
SST	Somatostatin
SYN1	Synapsin 1
TetO	Tetracycline operator
TGF	Transforming growth factor
TH	Tyrosine hydroxylase
vGAT	Vesicular GABA transporter
vGLUT	Vesicular glutamate transporter
VMAT	Vesicular monoamine transporter
VTA	Vental tegmental area
XAV939	Tankyrase-(TNKS)-Inhibitor
Y-27632 dihydrochloride	ROCK Inhibitor
˚C	degree celsius

ABSTRACT

Schizophrenia spectrum disorders (SCZ) are severe and complex mental diseases with a multifactorial disease aetiology, which are characterized by the interplay of genetic (e.g. copy number variants) and environmental factors. One major theory in psychiatry proposes aberrant dopamine neurotransmission associated with a hyperdopaminergic state in the striatum and a hypodopaminergic state in the prefrontal cortex contributing to positive and negative/cognitive symptoms, respectively. Detailed mechanistic insight into hypodopaminergic signalling in the mesocortical pathway, particularly the interactions between dopaminergic and glutamatergic neurons, is widely lacking. Another popular hypothesis postulates an imbalance in excitatory and inhibitory signalling in the prefrontal microcircuitry, which is accompanied by aberrant synaptic connectivity and neuronal network deficits. These characteristic features, observed in patients with neuropsychiatric disorders such as SCZ, are thought to result in cognitive symptoms.

To explore the interactions between dopaminergic and glutamatergic neurons in SCZ, a humanized iPSC-based *in vitro* co-culture model derived from patients with idiopathic SCZ was established. In addition, an isogenic co-culture model composed of iPSC-derived glutamatergic and GABAergic cortical neurons (E-I co-culture) carrying 15q13 and 22q11 microdeletions, as genetic risk factors for SCZ, was employed to better understand excitation-inhibition imbalance observed in SCZ and related neuropsychiatric disorders.

Transcriptome analysis of SCZ dopaminergic neurons revealed downregulation of early transcription factors, dopamine metabolism genes, as well as the autoreceptor DRD2 suggesting a hypodopaminergic phenotype and disinhibition of neuronal activity. Cell type-specific analysis revealed increased neuronal activity in both dopaminergic and glutamatergic SCZ neurons in co-culture, which was found to be mainly driven by SCZ dopaminergic neurons and was rescued by a selective DRD2 agonist. In addition, an excess loss of glutamatergic synapses was observed in SCZ co-cultures, whereas dopaminergic synapses remained unaffected. In E-I co-cultures carrying 15q13 and 22q11 microdeletions, a synaptic shift towards increased inhibition was observed, which was accompanied by decreased network activity, but increased synchronicity.

Overall, the established dopaminergic-glutamatergic co-culture model offers the possibility to study mutual interactions between dopaminergic and glutamatergic neurons in more detail and underpins the study of a hypodopaminergic phenotype in SCZ. Furthermore, findings of the microdeletion E-I co-culture system support the hypothesis of an excitation-inhibition imbalance. Although both co-culture systems comprised distinct neuronal compositions, aberrant excitatory synapse formation was identified as an overarching feature.

ZUSAMMENFASSUNG

Das schizophrene Spektrum (SCZ) beinhaltet schwere und komplexe neuropsychiatrische Erkrankungen mit multifaktoriellen Ursachen, die durch ein Zusammenspiel von genetischen Faktoren (z.B. chromosomalen Duplikationen oder Deletionen), sowie verschiedenster Umweltfaktoren gekennzeichnet sind. Eine der wichtigsten Theorien in der Psychiatrie geht von einer gestörten dopaminergen Transmission aus, die mit einem hyperdopaminergen Zustand im Striatum und einem hypodopaminergen Zustand im präfrontalen Kortex einhergeht und damit jeweils zu positiven bzw. negativen/kognitiven Symptomen führt. Detaillierte mechanistische Einblicke zur hypodopaminergen Signalgebung im mesokortikalen Signalweg, insbesondere zu den Wechselwirkungen zwischen dopaminergen und glutamatergen Neuronen, fehlen weitestgehend. Eine weitere Hypothese postuliert ein Ungleichgewicht zwischen exzitatorischen und inhibitorischen Signalen in den Mikroschaltkreisen des präfrontalen Cortex, das zudem von einer aberranten synaptischen Konnektivität und Defiziten in neuronaler Netzwerkaktivität begleitet wird. Diese Merkmale sind charakteristisch für Patienten mit neuropsychiatrischen Störungen wie SCZ und äußern sich in kognitiven Symptomen.

Um die Wechselwirkungen zwischen dopaminergen und glutamatergen Neuronen für SCZ zu untersuchen, wurde ein humanes iPSC-basiertes *in vitro* Ko-Kulturmodell bestehend aus Neuronen, die von Patienten mit idiopathischer SCZ abgeleitet wurden, entwickelt. Darüber hinaus wurde ein isogenes Ko-Kulturmodell aus iPSC-abgeleiteten glutamatergen und GABAergen kortikalen Neuronen (E-I Ko-Kultur) mit 15q13 und 22q11 Mikrodeletionen als genetische Risikofaktoren für SCZ eingesetzt. Mit Hilfe dieses Modells wird versucht, das beobachtete Ungleichgewicht zwischen exzitatorischen und inhibitorischen Signalen in SCZ und ähnlichen neuropsychiatrischen Erkrankungen besser zu verstehen.

Die Transkriptomanalyse dopaminerger SCZ Neuronen ergab eine Herunterregulierung früher dopaminerg-spezifischer Transkriptionsfaktoren, Gene des Dopaminstoffwechsels, sowie des Autorezeptors DRD2, was auf einen hypodopaminergen Phänotyp und eine Disinhibition der neuronalen Aktivität hindeutet. Zelltypspezifische Analysen zeigten eine erhöhte neuronale Aktivität sowohl in dopaminergen als auch in glutamatergen SCZ-Neuronen in den Ko-Kulturen. Diese erhöhte Aktivität war hauptsächlich auf dopaminerge SCZ Neuronen zurückzuführen und konnte durch einen selektiven DRD2 Agonisten ausgeglichen werden. Darüber hinaus wurde in den SCZ Ko-Kulturen ein übermäßiger Verlust glutamaterger Synapsen beobachtet, während dopaminerge Synapsen weitestgehend unbeeinflusst blieben. In den E-I Ko-Kulturen mit Neuronen, die eine 15q13 oder 22q11 Mikrodeletion tragen, zeigte sich eine synaptische Verschiebung hin zu verstärkter Inhibition, die von verringerter Netzwerkaktivität, jedoch erhöhter Synchronizität begleitet wurde.

Insgesamt bietet das neu etablierte, dopaminerge-glutamaterge Ko-Kulturmodell die Möglichkeit, gegenseitige Wechselwirkungen zwischen dopaminergen und glutamatergen Neuronen detaillierter zu untersuchen und bestätigt zusätzlich den hypodopaminergen Phänotyp in SCZ. Darüber hinaus stützen die Ergebnisse aus den E-I Ko-Kultursystemen mit beiden Mikrodeletionen die Hypothese einer Imbalance zwischen exzitatorischen und inhibitorischen Synapsen. Trotz der unterschiedlichen neuronalen Zusammensetzungen der beiden Ko-Kulturmodelle, konnte die aberrante Entwicklung exzitatorischer Synapsen als gemeinsames Merkmal identifiziert werden.

1. INTRODUCTION

1.1 Schizophrenia spectrum disorder

1.1.1 Clinical features

Schizophrenia spectrum disorders (SCZ) are severe and complex mental diseases, which manifest in cognitive, perceptual, and emotional dysfunctions causing a major social burden. The symptoms are relatively heterogenous and comprise three symptom clusters including positive symptoms (hallucinations and delusions), negative symptoms (anhedonia, avolition, emotional blunting) and cognitive impairments (deficits in attention, memory and planning) (1).

SCZ is relatively frequent with a worldwide prevalence of 1 % showing a slightly higher incidence in men than in women (risk ratio men: women 1.4:1) (2, 3). The onset of the disease presents in late adolescence or early adulthood and differs between men and women. While the disease occurs in men between the ages 15-25, in women the onset is in the range of 25-30 years (4, 5). Heart diseases (6) followed by suicide with a 10 % lifetime risk are the most frequent causes of death in SCZ patients (7).

To date, numerous different subtypes of SCZ have been described in the diagnostic tool ‘Diagnostic and Statistical Manual of Mental Disorders’ comprising paranoid, catatonic, disorganized, residual and undifferentiated SCZ. As patients are often diagnosed with more than one subtype, the latest version of the diagnostic tool DSM-5 has removed the classification into subtypes due to the absence of clear boundaries and defined ‘schizophrenia’ as ‘schizophrenia spectrum disorders’ (5, 8). Furthermore, various mental diseases including autism spectrum disorder (ASD), bipolar disorder and major depression share a subset of symptoms that complicate differentiation between them (8). This makes correct diagnosis and therapeutic intervention difficult, especially when the genetic heterogeneity of patients is taken into account.

1.1.2 Current therapeutic strategies

To date, patients with SCZ are treated by antipsychotic medications and clinicians can select from a plethora of approved drugs. However, existing antipsychotics for the treatment of SCZ have notable limitations. Current antipsychotics can be subdivided into two subclasses, typical first-generation (FGAs) and atypical second-generation antipsychotics (SGAs), both of which are selective DRD2 antagonists with an antipsychotic effect. A significant drawback of FGAs is the association with extrapyramidal side effects (e.g., motor side effects, hyperprolactinemia),

which result from the high affinity for DRD2 and the slow dissociation from the receptor leading to a disruption of the physiological dopamine transmission (9). Treatment with SGAs reduces extrapyramidal side effects by modulating mainly the dopaminergic and serotonergic neurotransmitter systems, with low-affinity for DRD2 and high-affinity for the serotonergic receptor 5-HT2A (10). While both FGAs and SGAs primarily alleviating positive symptoms, antipsychotics for treating negative and cognitive symptoms are still limited (11, 12). Although several studies with SGAs have shown amelioration in negative symptoms, the evidence on current treatment options remains unclear (13). A further challenge is the large variability in responsiveness and toleration of the antipsychotic treatment. In around 20-30 % of patients with SCZ, antipsychotic treatment is not effective, which is also due to the heterogeneous disease origin (14). Clozapine, a SGA, is regarded as the gold standard for the therapy of non-responding SCZ patients due to its unique pharmacological profile and studies also reported reduced mortality rates (11, 14, 15). So far, antipsychotic treatment options for SCZ are limited as treatment resistance occurs in up to one third of the patients and treating the negative and cognitive symptoms remains a challenge. Thus, there is an urgent need for new drugs with improved efficacy and better tolerability.

1.2 Dysfunctional neurotransmitter systems in SCZ

1.2.1 The mesocorticolimbic system

Higher cognitive processes, such as decision-making, reward, and working memory are regulated by the modulating neurotransmitter dopamine (16, 17). The ventral midbrain, in which the dopaminergic neurons are located, comprises three main areas: substantia nigra pars compacta (SNc, A9), ventral tegmental area (VTA, A10) and the retrorubal field (RRF, A8) (18). Dopaminergic neurons located in the VTA project rostrally towards limbic and cortical regions, thereby forming two major dopaminergic pathways, the mesocortical and the mesolimbic (19). The mesocortical pathway with dopaminergic projections to the prefrontal cortex (PFC) is essential for higher cognitive processes and emotional responses, whereas the mesolimbic pathway projecting to the nucleus accumbens (NAc) is regarded as reward system and is important for motivation (18, 20, 21). Together, the two pathways form the mesocorticolimbic system (22) and multiple lines of evidence suggests that malfunctions of dopaminergic signalling in these pathways are implicated in the pathogenesis of SCZ (23).

So far, the mesolimbic pathway has been studied in greater depth, as VTA-NAc connections are pivotal in modulating reward and aversion, which also seem to be affected in patients with SCZ (24). Most striatal neurons are medium spiny neurons (MSN), a special type of inhibitory GABAergic projection interneurons, which serve as the primary target for VTA dopaminergic

neurons. These inhibitory projection neurons can be split into two subclasses based on their projection pattern, as well as their differential expression of either dopamine receptor D1 (DRD1) or DRD2 (25, 26). Dopaminergic neurons with projections to the PFC form functional synapses with glutamatergic pyramidal neurons and GABAergic interneurons, particularly parvalbumin (PV)-positive fast-spiking interneurons. Expression of the two dopamine receptor types D1-like receptors (DRD1, DRD5) and D2-like receptors (DRD2, DRD3, DRD4) is found on both pyramidal and GABAergic interneurons (27, 28). In general, dopamine receptors are G protein-coupled receptors (GPCR) and have different modulating properties: D1-like receptors are stimulating as they are coupled to G proteins of the G_s subfamily (G_s and G_{olf}) that activate the adenylyl cyclase (AC) and cAMP production. In contrast, D2-like receptors are coupled to inhibitory G proteins of the subfamily G_i (G_i and G_o) that have an opposing effect on the downstream signalling cascade (29).

1.2.2 The dopamine hypothesis

One of the most accepted theories in psychiatry is the dopamine hypothesis. It was formulated in the 1960s by the discovery of antipsychotic drugs acting as DRD2 antagonists and thereby successfully treating the positive symptoms of SCZ (30). Additionally, findings that drug administration to promote the increase of extracellular dopamine, such as amphetamine, can induce psychotic symptoms similar to those observed in SCZ patients, whereas drugs that deplete dopamine levels can lead to reduced psychosis, formulated the hypothesis of excess dopamine signalling (hyperdopaminergia) (31, 32). Later, the dopamine hypothesis was reconceptualized as new insights from animal studies, as well as post-mortem and imaging data revealed regional distinct aberrations in dopamine signalling (33). Thus, the revised version posits a prefrontal hypodopaminergia resulting in negative symptoms of SCZ, in contrast positive symptoms are assumed to result from striatal hyperdopaminergia based on the response to antipsychotic drug treatment (33, 34, 35). Mainly the positive symptoms can be explained in accordance with the dopamine hypothesis. However, the dopamine hypothesis has its limitations and does not account for all symptom clusters of the disease. Treating negative and cognitive symptoms with antipsychotic drugs results in negligible effects (36). Additionally, neuroanatomical changes including cortical atrophy rather correlate with the severity of negative and cognitive symptoms, but not with psychotic symptoms (37). Thus, the complex psychopathology of SCZ cannot simply be explained by a dysfunction of the dopamine system (38).

Detailed anatomical and biochemical information of dopaminergic aberrations were provided by early post-mortem studies of SCZ patients that reported increased concentrations of dopamine specifically in the NAc and the dorsal striatum (39, 40). More recent studies

demonstrated a significant increase in the rate-limiting enzyme tyrosine hydroxylase (TH) throughout the striatum, which is involved in the synthesis of dopamine indicating elevated dopamine synthesis capacity (41). The strong association between DRD2 and SCZ revealed by genetics supports the idea that the expression of DRD2s is altered in SCZ patients (42). Evidence was provided by several post-mortem studies indicating an elevation in striatal DRD2 binding capacity which was replicated by several *in vivo* imaging studies (43, 44). However, the picture remains complicated as initial findings were inconsistent with more recent results. For example, studies considering subgroups of antipsychotic-naïve patients found no consistent evidence for increased DRD2 expression, while patients who received long-term antipsychotic treatment demonstrated an elevated receptor density which was supported by a positron emission tomography (PET) imaging study comparing DRD2 binding potentials in naïve and treated SCZ patients (45).

Although DRD1 is the major dopamine target in the PFC, the receptor has been less thoroughly studied. Studies focusing on receptor densities yielded heterogenous results. While most drug-naïve patients showed elevated DRD1 density in the PFC (46, 47), chronically medicated patients depicted widespread cortical and striatal reductions (48). Despite the apparent inconsistencies in the reports of DRD1 densities, a link between altered DRD1 binding potential and impaired cognitive function has been hypothesized as manifested in impaired working memory (44). The concept of cortical hypodopaminergia in SCZ was supported by some post-mortem studies demonstrating decreased expression of TH in the PFC (49) and additional PET analysis revealed blunted amphetamine-induced dopamine release capacity in the cortex of SCZ patients that correlated with cognitive deficits (50).

1.2.3 The glutamate hypothesis

A potential involvement of glutamate in the pathology of SCZ was first postulated in 1990 and built on the discovery that dissociative anaesthetics, such as ketamine and phencyclidine (PCP), induced SCZ-like symptoms that mimic not only positive, but also negative and cognitive symptoms in healthy volunteers and additionally worsened the effect in SCZ patients (38, 51, 52). The fact that ketamine and PCP are noncompetitive antagonists of the *N*-methyl-D-aspartate receptor (NMDAR), which can cause psychosis, led to the assumption that SCZ might also be caused by NMDAR hypofunction (53). Meta-analysis of post-mortem studies revealed decreased transcript and protein expression of GluN1, a subunit of the NMDAR, in the PFC, dentate gyrus and left hippocampus of SCZ patients, whereas other subunits (GluN2, GluN3) remained unaltered (54, 55). Supporting evidence for the NMDAR hypofunction hypothesis can be found in numerous pharmacological, neurodevelopmental and genetic animal models. Administration of NMDAR antagonist results in cognitive and behavioural

features comparable to those observed in SCZ patients. Genetic animal models with a knockout in the SCZ risk gene *SRR* encoding the enzyme serine racemase (SR), demonstrated a significant lack of D-serine in the cortex contributing to cognitive symptoms comparable to those observed in SCZ (56). It is assumed that astrocytes are the primary source of L-serine, that is synthesized from glucose. At the postsynaptic densities, the transformation of L-Serine to D-Serine via SR occurs, a process referred to as 'serine shuttle'. The accumulation of D-serine and SR at the postsynaptic sites in cortical neurons ensures proper NMDAR function (38). Finally, antagonism of the NMDAR has also been shown to reduce GABAergic interneuron activity resulting in an increased firing rate of pyramidal neurons due to disinhibition. However, the mechanism leading to reduced GABAergic activity has not been fully elucidated (57).

Although recent evidence points towards aberrant signalling in dopaminergic, glutamatergic, serotonergic and γ-aminobutyric acid (GABA) signalling, the dopamine and glutamate hypothesis are still leading pathophysiological mainstays of SCZ and are not mutually exclusive (58). Both hypotheses were initially formulated based on pharmacological and post-mortem studies and new evidence, particularly from *in vivo* imaging studies, refined the role of both neurotransmitters in the SCZ. While the evidence strongly supports presynaptic dopamine dysfunction and its association with psychotic symptoms, NMDAR hypofunction seem to better account for negative and cognitive symptoms. Thus, combinatory effects of both may account for clinical aspects of SCZ patients. One alternative explanation posits that dopaminergic alterations in the mesolimbic system occur secondary in response to altered cortical neuron function as glutamatergic neuron projections from the cortex regulate midbrain dopaminergic neurons. Altered microcircuits in frontal cortical regions could lead to disinhibition of mesolimbic dopaminergic neurons which in turn might induce psychotic symptoms (59).

1.3 Aetiology and neurodevelopmental hypothesis

Extensive evidence pinpoints towards a multifactorial combination of both genetic and environmental factors, that contribute to the aetiology of SCZ and thus making the study of the disorder more complicated. Meta-analysis based on twin and family studies of SCZ revealed a strong genetic impact with an estimated heritability ranging from 64-81 % (60, 61). Within the last ten years, genome-wide association studies (GWAS) identified over 200 genetic SCZ risk loci and shed light on the polygenic nature of SCZ. Some of the genes identified in these studies were linked to DRD2 and glutamatergic neurotransmission, while others were primarily involved in synapse organization, differentiation and transmission (62). However, none of the identified genes linked to SCZ were found to be sufficient to develop SCZ and therefore, several risk genes are combined to so called polygenic risk-scores (63, 64). Moreover, genetic

analysis have found several copy number variants (CNV) with differentially expressed genes being associated with SCZ and identified chromosomal deletions in the 1q21, 15q13 and 22q11 loci to be addressed more detailed in section 1.4 (65, 66). Other genetic risk factors, that have been found to increase the risk of developing mental illnesses, are chromosomal translocations. One predominant translocation, which was originally discovered in a Scottish family with high rates of mental illnesses, affects the gene *Disrupted-in-Schizophrenia 1* (*DISC1*) (67). The scaffolding protein DISC1 plays fundamental roles in neurodevelopment and its large interaction network makes the protein an attractive target for extensive studies in both humans and animals (68).

Despite the large genetic element, early and late environmental insults have been linked to an increased risk of developing SCZ. Prenatal factors such as complications during pregnancy (infection, malnutrition, psychosocial stress) (69), as well as childhood adversity and trauma (70) have been linked to an increased risk. Later environmental factors that favour the vulnerability to develop the neuropsychiatric disorder include childhood trauma, drug abuse and immigration (70, 71, 72). In 1986, Weinberger first introduced the neurodevelopmental hypothesis proposing an interplay of genetic and environmental factors leading to developmental abnormalities in the brain, while symptoms of SCZ first appear in early adulthood (73). A ‘two-hit’ model was raised assuming that the interplay between perinatal insults of genetic and/or environmental origin as ‘first hit’ results in a primed stage, while a ‘second hit’ during essential brain development phases in young adulthood leads to an excessive loss of synapses and could thus explain dysfunctions in the brain (74). However, due to the complexity of the disease, the ‘two-hit’ hypothesis is considered as a too simplistic model to fully explain the aetiology. Recently, multifactorial conceptualizations have emerged that point to an interplay of multiple hits across major neurodevelopmental milestones as contributing factors to the development of SCZ (75, 76).

1.4 CNVs as genetic risk factor for neuropsychiatric disorders

In general, CNVs refer to changes in the number of copies of particular genome segments that can either be repeated or deleted (duplications and deletions) and can differ from one individual to another. As consequence, different effects were reported ranging from no effects, through morphological and metabolic alterations to significant contribution to both rare and common genetic disorders (77). As outlined above, the aetiology of SCZ is multifactorial and based on complex genetic and environmental interactions. Among various genetic alterations identified in SCZ patients, recent studies suggest that CNVs are the most common genetic alterations that may play an important role in vulnerability to the disorder (78, 79). Although there are some basic criteria such as defined size (50 bp to 3 Mb), the definition of CNVs is quite

ambiguous due to their heterogenous occurrence (80). It has been demonstrated that some CNVs are heritable, whereas de novo CNVs can occur spontaneously (81, 82). In recent years, technological advances improved the resolution for detection of genetic variations, revealing that 70 % of all individuals possessed at least one rare CNV (83). Interestingly, genome-wide scans have demonstrated a twofold increase of rare and de novo CNVs in patients with SCZ and ASD in comparison to healthy individuals (84), and an even higher rate in neurodevelopmental and intellectual disability disorders (85). To study the association between neuropsychiatric disorders and pathogenic CNVs in specific regions, large sample sizes are indispensable. In 2017, a genome-wide study that including more than 20.000 SCZ cases and controls identified several CNV loci that were linked to SCZ, such as for example 15q13 and 22q11 (86). It is worth mentioning that CNVs associated with SCZ lack diagnostic specificity and many can increase the risk for other neuropsychiatric disorders such as ASD, attention-deficit hyperactivity disorder and intellectual disability (87).

1.4.1 The 15q13 microdeletion syndrome

The proximal part of chromosome 15q contains the most genetically unstable region with a size of 2.5 Mb due to the six low-copy repeat elements between breakpoints (BP) 1-6. Recurrent deletions between BP1 or BP2 and BP3 can lead to Prader-Willi syndrome or Angelman syndrome, respectively, whereas 15q13 microdeletions occur more distally, typically at BP4-BP5 (88). This rare microdeletion is strongly linked with numerous neurodevelopmental disorders (intellectual disability, ASD and SCZ) and can increase the risk for developing SCZ by the factor ten (89, 90, 91). Typically, patients are heterozygous for the 15q13 microdeletion, spanning two putative pseudo genes, one microRNA gene and six protein-coding genes, among which, the two protein-coding genes *OTUD7A* and *CHRNA7* were identified as possible SCZ risk genes (92). *OTUD7A* encodes a deubiquitinase that is found to regulate spine formation of cortical neurons. Animal studies including mice deficient in *Otud7a* depicted decreased dendritic spine density as well as reduced excitatory postsynaptic current (93) and similar results were obtained from a study of iPSC-derived excitatory cortical neurons with a loss of function mutation in *OTUD7A* demonstrating reduced dendritic complexity, low level of synaptic proteins like GluA1 and PSD95 and disturbed neuronal network formation (94). Originally, the cholinergic receptor nicotinic alpha 7 subunit (*CHRNA7*) was considered as major genetic driver due to its function as neuronal ligand-gated ion channel and the observation that receptor agonists improved cognition in SCZ patients (95). However, mice deficient in *Chrna7* were not able to fully reiterate neuropsychiatric and behavioural phenotypes observed in humans (96). Additionally, several heterozygous 15q13 microdeletion mouse models (*Df(h15q13)/+*) according to the human CNV were generated revealing

phenotypes similar to those observed of SCZ patients for example, neuronal excitability changes, memory deficits and increased sensitivity to stress (97, 98).

1.4.2 The 22q11 microdeletion syndrome

The 22q11 microdeletion syndrome, also referred to as velocardiofacial syndrome or Di George syndrome, represents the most prevalent microdeletion syndrome, occurring at an incidence rate of 0.0025 % (99). This microdeletion syndrome is characterized by a relatively large hemizygous deletion (up to 3 Mb) in genomic sequences of chromosome 22 including 35-60 known genes (100, 101). Most strikingly, patients that carry a 22q11 microdeletion have a 20-25 % elevated risk of developing SCZ, which is also increased for other neurodevelopmental disorders including intellectual disability (~ 45%), attention deficit- hyperactivity disorder (~ 35%), anxiety disorder (~ 35%) and ASD (10–40%) (102). Typical hallmarks for the 22q11 microdeletion syndrome are learning difficulties, cardiac anomalies, immune deficiencies and endocrine abnormalities (103). Several genes encompassed by the microdeletion have been proposed as potential candidate genes. One of those candidate genes is *COMT* encoding the catabolic enzyme catechol-O-methyltransferase, which is involved in dopamine inactivation and degradation. Mutations in the *COMT* gene are believed to elevate the risk of SCZ and may contribute to its pathogenesis, as a poor clearance function of dopamine in the PFC has been reported (104). Another gene located in the 22q11 microdeletion loci is *DGCR8*. The gene is important for mi-RNA processing and was linked to SCZ based on findings in hemizygous *Dgrc8* deficient mouse models that depicted incomplete dendritic spine structure and reduced numbers of cortical neurons in the prefrontal cortex (105). Deficits in *DGCR8* were observed to lower miRNA processing resulting in reduced development of dendritic spines in the prefrontal cortex and hippocampus and can lead to altered synapse morphology in the thalamocortical pathway, hippocampus and prefrontal cortex (106, 107). Other genes found in the deleted chromosomal region that were linked to SCZ are for example *PRODH*, that encodes the mitochondrial membrane enzyme proline oxidase (POX) important for converting proline into glutamate, and additionally *ZDHHC8* encoding a palmitoyl transferase and *DGCR2* that encodes a adhesion receptor protein (108, 109, 110). Furthermore, mouse models carrying a hemizygous chromosomal deficiency (*Df(16)A*$^{+/-}$) comparable to the human 22q11 deletion were created and thoroughly studied. Behavioural and morphological characterization of deficient mice revealed specific abnormalities in working memory and fear conditioning, as well as less dendritic complexity and spine density and were able to recapitulate most of the hallmarks observed in 22q11 carriers (111).

1.5 Excitation-inhibition imbalance in prefrontal cortical microcircuitry in SCZ

The human cerebral cortex is organized into six different cortical layers (layers I-VI) in which neurons with unique properties are residing (112). During neurogenesis, neurons generated in the ventricular zone migrate to their appropriate cortical layer with deep layer neurons (layer IV-VI), as the first neurons generated followed by upper layer neurons (I-III) (113). *In vivo*, dopaminergic neurons within the mesocortical pathway project to the prefrontal cortex with highest innervation density observed in layer II and layer V-VI forming symmetric synapses with excitatory pyramidal neurons, as well as interneurons (114). In the cortex, excitatory glutamatergic pyramidal and inhibitory GABAergic interneurons are the two main neuronal populations found (ratio excitatory: inhibitory 80:20) (115). Cortical interneurons are divers and differ in morphology, their connectivity to pyramidal neurons, and expression of subtype specific molecular markers. The largest group of cortical interneurons are PV-positive interneurons, followed by a subtype of interneurons that are positive for the neuropeptide somatostatin (SST) (116, 117). In healthy brains, the balance of excitatory and inhibitory information is precisely regulated by various developmental processes that are crucial for proper synapse formation and function of cortical microcircuits (118). Increasing evidence points towards a deficit in the precisely regulated cortical balance between excitation and inhibition (E-I) as one biological consequence in SCZ, referring to disproportions in excitatory and inhibitory synaptic inputs which is supported by post-mortem, genetic and electrophysiological studies. For example, several post-mortem studies have demonstrated reduced levels of the neurotransmitter GABA in the cerebrospinal fluid (CSF) of patients with SCZ in comparison to healthy controls (119). In contrast, heterogenous findings of glutamate concentrations in the CSF of SCZ patients were reported. While first studies demonstrated reduced CSF glutamate levels (120, 121), a recent meta-analysis comprising 230 SCZ patients and 294 healthy controls reported significantly increased glutamate levels (122). Additionally, synaptic protein levels as well as dendritic spine densities have been investigated showing significantly lower protein levels of the major synaptic vesicle protein synaptophysin found in presynaptic terminals, and reduction in postsynaptic markers such as PSD95 in frontal cortical regions in post-mortem brains (123, 124). Altered expression levels of genes involved in glutamate and GABA neurotransmission were identified for the vesicular glutamate transporter-1 (vGLUT1) and glutamic acid decarboxylase 67 (GAD67), the GABA synthesizing enzyme, which were both downregulated in SCZ patients (119, 125). On network level, cortical fast-spiking PV-positive interneurons provide inhibitory input to pyramidal neurons and are the major driver of γ-oscillations (126). Abnormal γ-band frequencies can contribute to impaired

working memory as well as sensory processing, which has already been observed in SCZ patients (127, 128).

Based on these findings, it has been assumed that a local imbalance of excitatory and inhibitory synaptic input might lead to a more global impairment in network activity and synchronicity (129). The understanding of how E-I imbalance contributes to the symptoms of SCZ, could lead to improvements in innovative treatment options and diagnostic targets.

1.6 Disease modelling using human iPSC-based *in vitro* model systems

Until recently, patient studies comprising post-mortem tissue samples and brain imaging, as well as numerous animal models contributed to valuable findings in SCZ but have their limitations. Post-mortem studies only provide a snapshot at the time of death and cannot capture dynamic alterations in the brain. Chronic antipsychotic treatment during the patient's lifetime may heavily influence the outcomes as well (130). One major critical aspect in human disease modelling is the requirement of physiologically relevant *in vivo* or *in vitro* model systems that accurately recapitulate the underlying disease pathophysiology. Hence, animal models are used most frequently as they allow for a more dynamic investigation throughout different developmental stages and can link cellular and molecular mechanisms to behavioural observations. However, most studies make use of rodent models, which are unable to fully reflect the complexity of the human brain and additionally, inherited differences between rodent and human can be found in transcriptomic signatures (131). Consequently, high failure rates in pharmacological research and development are reported due to difficulties in the translation from rodent models to humans (132). One powerful approach for the *in vitro* study of neurodevelopmental and neuropsychiatric disorders is represented by induced pluripotent stem cells (iPSC), that offer hope for regenerative and personalized medicine (133).

1.6.1 Characteristic features of human iPSC

Pluripotent stem cells possess the ability to continuously self-renew and can differentiate into cells from all three germ layers: mesoderm, ectoderm and endoderm (134). These cells are derived from the inner cell mass of the blastocyst, which will later form the complete embryo (135). In 1981, first isolation and cultivation of pluripotent stem cells was achieved by using *in vitro* cultures of mouse blastocysts that were assigned as embryonic stem cells (ESC) (136). As research with human ESC faces ethical and political challenges, new techniques have been established to generate pluripotent stem cells (137). In 2006 and 2007, important breakthroughs in stem cell research were achieved by Takahashi & Yamanaka, who showed successful reprogramming from human somatic cells into iPSC by artificial overexpression of

four transcription factors, the so called ‘Yamanaka factors’: *OCT4*, *SOX2*, *cMYC* and *KLF4* (138, 139). Nowadays, iPSC can be derived from almost every somatic cell type including fibroblasts, blood cells and keratinocytes and additionally, various reprogramming strategies such as integrative and non-integrative, viral and non-viral are described (140, 141, 142). The fact that iPSC conserve the genetic background of a donor and cells can be differentiated into various disease-relevant cell types has made stem cell research indispensable for *in vitro* disease modelling.

1.6.2 *In vitro* disease modelling using human iPSC

For the identification and characterization of common disease-related phenotypes, there are two different strategies using *in vitro* iPSC models. First, iPSC can be derived from genetically heterogenous patients, which is of great importance when studying diseases with a polygenic architecture, such as SCZ. However, the considerable high variability among the individual patients makes the study of SCZ challenging. Usually, these studies benefit from large cohort sizes comprising numerous donors as well as several clonal lines to detect small effects and to increase statistical power (143). To circumvent patient line variations, isogenic iPSC lines can be used to identify phenotypic features of a disease-relevant gene mutation or chromosomal deletions/duplications of interest. Recent advances in the field of gene editing offer new possibilities, for example clustered regularly interspaced short palindromic repeats (CRISPR)-Cas9, which can be employed to introduce or correct mutations while preserving the basic genetic framework (132).

1.6.3 Differentiation of iPSC-derived neurons

Up to now, a plethora of protocols for the differentiation of iPSC into numerous neuronal cells have been established that hold immense potential for the study of the underpinning disease pathophysiology. The right choice of differentiation protocol is relatively important, as reproducibility and patterning consistencies are most critical for the field. Additionally, homogenous neuronal populations are of great importance, especially when comparing differentiated neurons from healthy controls versus patients (144). Two main approaches can be employed for the differentiation of iPSC into neurons. The first approach (‘directed differentiation’) is based on the defined addition of growth factors and cytokines at a specific time manner that aims to mimic signalling processes *in vivo*. Although patterning and specification of neural cells can be pursued more closely, these cultures often result in heterogeneous cell populations containing a mixture of different types of neurons and glial cells. In addition, huge variability among differentiations can be observed which often lack

defined ratios of generated neurons and usually, these cultures require a significant longer differentiation period. In contrast, the second approach requires a manipulation in gene expression as differentiation is forced via overexpression of lineage-specific transcription factors. This differentiation process is much faster than the chemically induced one and yields more homogeneous neural populations. Moreover, this artificial overexpression represents a versatile method as is can be reversible or irreversible and persistent or transient (145).

While recent studies that focus on cortical glutamatergic and cortical GABAergic neurons make use of induced differentiation by overexpression of lineage-specific transcription factors, only few studies reported the generation of dopaminergic neurons by this artificial approach. Cortical glutamatergic and cortical GABAergic neurons are generated by overexpressing the respective lineage-specific transcription factors *Neurogenin 2* (NGN2) (146) and *ASCL1+DLX2* (AD2) (147), while dopaminergic neurons can be induced by the combined overexpression of the transcription factors *ASCL1+LMX1B+NURR1* (ALN) (148). In these differentiation protocols, transient overexpression of respective transcription factors is based on the Tet-On expression system that can be induced by adding doxycycline. The addition of doxycycline leads to a binding of the reverse tetracycline transactivator (rtTA) to the response element (TRE), which initiates gene transcription and thus allows for precise induction (149). Another advantageous aspect of induced differentiations is the possibility of incorporating an antibiotic resistance gene into the plasmid, which makes it possible to select only transduced cells during differentiation and thus yielding more homogenous neuronal populations.

1.6.4 State-of-the-art - Modelling neurodevelopmental disorders using iPSC

Besides many advantages, iPSC models represent an appropriate *in vitro* model system, especially suitable for neurodevelopmental and early onset disorders such as SCZ. In principle, neural cells derived from iPSC can faithfully mimic certain aspects of human embryonic brain development, which was confirmed by RNA expression profiling (150, 151).

Over the past decade, numerous studies have generated iPSC-based neuronal models that has helped to improve the understanding of SCZ-related phenotypes. The focus of these studies varies including neurons derived from patients with idiopathic SCZ as well as isogenic models with specific genetic alterations such as CNVs or mutations in *DISC1* (152). Several approaches comprising functional and morphological assays, transcriptome profiling, and many other experiments were carried out on neural progenitor cells (NPC), mixed neural populations, as well as more homogenous neural subpopulations, mainly on NGN2-derived glutamatergic neurons (153).

Studies focusing on forebrain NPC derived from patients with idiopathic SCZ identified several phenotypic features during early neurodevelopment such as perturbed WNT signalling (154), abnormalities in the FGFR1 pathway (155), as well as neural migration deficits and increased oxidative stress (156). Following a directed differentiation strategy, neural cultures often comprise a mixture of various neuronal cell types such as glutamatergic, GABAergic and dopaminergic neurons (157). One major finding in these neural cultures were deficits in neurite length and outgrowth as an important aspect in neurodevelopment. In addition, reduced neuronal connectivity as shown by decreased expression of synaptic puncta markers, altered WNT signalling and reduced calcium activity has been described in SCZ neurons (157, 158). Alterations in spontaneous neuronal activity and excitability of 2D neural cultures enriched for glutamatergic neurons and 3D organoids has also been reported in a study with patients diagnosed with 22q11 microdeletion syndrome (159), which was accompanied by aberrant gene expression of genes involved in essential processes such as apoptosis, cell cycle and the MAPK pathway (160). An important aspect to consider is that excitatory glutamatergic neurons are the major neuronal subtype generated in these mixed cultures, thus allowing to mainly study glutamatergic phenotypes, but are less suitable to study other SCZ-relevant neural subtypes (152). In recent years, the number of SCZ iPSC studies focusing on NGN2-derived glutamatergic neurons (161, 162, 163) and AD2-derived GABAergic interneurons (164, 165) has increased, demonstrating differences in their transcriptomic profile as well as alterations in synapse formation. Additionally, co-cultures comprising defined ratios of NGN2 and AD2 neurons as well as neurons and glial cells have emerged, that allow to study SCZ characteristic features in a more physiologically relevant culture system (164, 165, 166).

Although aberrant dopamine signalling has also been implicated in the pathophysiology of SCZ and current antipsychotic treatments interfere with the dopamine system, less is known about disease-related alterations of iPSC-derived dopaminergic neurons and their interactions with other neuronal cell types. So far, only few studies made use of dopaminergic neuronal cultures to study SCZ, which resulted in inconsistent and unreproducible results, most likely due to the low differentiation efficiencies reported. These findings ranged from no differences between CTR and SCZ dopaminergic neurons to differentiation deficits and increased dopamine release in SCZ neurons (167, 168, 169). To date, there is no known study that has analysed the transcriptomic profile of iPSC-derived dopaminergic SCZ neuron. Thus, there is a tremendous lack of available data from SCZ studies focusing on iPSC-derived dopaminergic neurons and their interactions with other neuronal cell types. The use of more robust differentiation protocols for the generation of dopaminergic neurons will help to open new avenues and to identify and characterize dopaminergic neuron-specific abnormalities in SCZ.

1.7 Aim of this thesis

As described, SCZ is a complex and heterogenous neuropsychiatric disorder with a multifactorial disease aetiology. Several hypotheses propose early neurodevelopmental alterations, as well as aberrations in neurotransmitter signalling and neuron-neuron interactions, which might result in aberrant neuronal functionality and synapse formation. The aim of this thesis is to study the reciprocal neuron-neuron interactions between dopaminergic and glutamatergic neurons as well as glutamatergic and GABAergic neurons, in order to identify and characterize functional and morphological SCZ and other neuropsychiatric disease-related phenotypes. For this purpose, two iPSC-based *in vitro* co-culture model systems derived from idiopathic and isogenic iPSC lines that differ in their neuronal composition will be employed.

To decipher possible disease-related features, the focus of this study will be on the following aspects:

1) **Identification of a dopaminergic differentiation protocol yielding homogenous dopaminergic neuron populations.** Using iPSC lines with distinct genetic backgrounds, two dopaminergic differentiation strategies will be evaluated and characterized regarding differentiation efficiency and reproducibility. Homogenous neuronal populations are of great importance, especially when comparing neurons from healthy controls versus patients. Therefore, this experiment is an important groundwork for following experiments.

2) **Analysis of the dopaminergic neuron transcriptome to determine the neurodevelopmental state and to identify deregulated genes in SCZ neurons.** Although multiple lines of evidence suggest aberrations in the dopaminergic system in SCZ, so far only few studies focused on iPSC-derived dopaminergic neurons. To shed light on the developmental state and to identify possible differentially expressed genes in SCZ dopaminergic neurons, RNA sequencing will be employed. This is particularly relevant, as potential deregulated genes might result in SCZ-related phenotypes.

3) **Analysis of aberrant neuronal activity in dopaminergic-glutamatergic SCZ co-cultures.** Previous iPSC-based research has been mainly focusing on neuronal cells cultured individually, whereas less is known on the interaction between dopaminergic and glutamatergic neurons. For this purpose, an iPSC-based co-culture system comprising dopaminergic and glutamatergic neurons at defined ratios will be established and used to study functional phenotypes in SCZ. In addition, putative functional consequences of

aberrant gene expression in SCZ patient-derived dopaminergic neurons will be studied. Cell type-specific spontaneous single-cell activity will be measured in dopaminergic and glutamatergic neurons cultured individually, as well as in dopaminergic-glutamatergic co-cultures.

4) **Analysis of aberrant synapse formation in SCZ co-cultures.** To gain further insight into dopaminergic-glutamatergic neuron interactions and to identify possible synaptic phenotypes, synapses were analysed in a cell type-specific manner to decipher the neuronal origin of potential alterations. Aberrant synapse formation and destabilization may contribute to putative functional aberrations.

5) **Analysis of aberrant synaptic connectivity and neuronal functionality in an isogenic microdeletion disease model as genetic risk factor for SCZ.** In the second part of this thesis, isogenic disease models carrying a 15q13 and a 22q11 microdeletion as a high-risk factor for SCZ will be employed. Excitatory-inhibitory imbalances in the developing cortical microcircuitry are thought to contribute to the pathology of neuropsychiatric disorders. To this end, an iPSC-based co-culture system comprising glutamatergic and GABAergic interneurons will be used to decipher synaptic phenotypes and functional abnormalities on single-cell and network level.

2. MATERIAL AND METHODS

2.1 Material

2.1.1 iPSC lines

Table 1. iPSC lines used in this study. All iPSC lines were fully characterized. iPSC lines (CTR1, CTR2, CTR3, SCZ1, SCZ2, SCZ4, SCZ5) have a unique cell line identifier number and are listed in the Human Pluripotent Stem Cell Registry (Charité, Berlin, www.hpscreg.eu).

iPSC line	Gender	Age at donation	Source cell type	Unique cell line identifier/Source
CTR and idiopathic SCZ iPSC lines				
CTR1	female	neonate	cord blood-derived CD34+ progenitors	TMOi001-A
CTR2	female	28	fibroblast of dermis	NMIi001-A
CTR3	male	49	peripheral blood-derived CD34+ hematopoietic stem/progenitor cells	NMIi010-A
SCZ1	male	37	fibroblast of dermis	NMIi002-A
SCZ2	female	54	fibroblast of dermis	NMIi003-A
SCZ4	male	50	fibroblast of dermis	NMIi004-A
SCZ5	female	27	fibroblast of dermis	NMIi006-A
Isogenic CTR and *PINK1* KO iPSC lines				
HC1	female	not stated	fibroblast of dermis	doi: 10.1371/journal.pone.0059252 doi: 10.1016/j.isci.2020.101797
PINK1 KO Δ 8.9	female			
PINK1 KO Δ40.7	female			
Isogenic CTR and 15q13 and 22q11 deletion iPSC lines				
CTR	Stable NGN2 and AD2 iPSC lines of one isogenic control and three microdeletion lines. Detailed information of the iPSC lines (gender, age at donation, source cell type, generation of microdeletions) can be requested from Prof. Dr. Moritz Rossner (Department of Psychiatry and Psychotherapy, LMU University Hospital, LMU Munich).			
15q13				
22q11 clone1				
22q11 clone2				

2.1.2 General material and equipment

Table 2. General material

Consumables	Manufacturer
37 µM Reversible Strainers	STEMCELL Technologies, Canada
40 µM Cell Strainer	Greiner Bio-One, Germany
96 well µClear® half-area plate, black	Greiner Bio-One, Germany
96 well µClear® plate, black	Greiner Bio-One, Germany

AggreWell™800	STEMCELL Technologies, Canada
Cell culture flasks (25, 75, 175 cm2)	Corning Inc., USA
Cryo tubes	Greiner Bio-One, Germany
Eppendorf Tubes (1.5, 2 ml)	Eppendorf AG, Germany
Falcon Tubes (15, 50 ml)	Greiner Bio-One, Germany
Optical 96 well plates, MicroAmp™	Thermo Fisher Scientific, USA
Optical adhesive covers	Thermo Fisher Scientific, USA
Parafilm	Pechiney Plastic Packaging
Petri dishes	Greiner Bio-One, Germany
Pipette reservoir (50 ml)	Cole-Parmer Essentials, USA
Pipettes CELLSTAR® (5 ml, 10 ml, 25 ml, 50 ml)	Greiner Bio-One, Germany
Pipette tips (10 µl, 100 µl, 1000 µl)	TipOne STARLAB GmbH, Germany
Ultra-low attachment plates	Greiner Bio-One, Germany
Well plates (96, 48, 24, 12, 6 well)	Corning Inc., USA

Table 3. Equipment (instruments and devices)

Instruments/Devices	**Manufacturer**
Axiovert 200M microscope	Carl Zeiss Microscopy GmbH, Germany
Centrifuge 5804 R	Eppendorf AG, Germany
Centrifuge 5415C	Eppendorf AG, Germany
CO_2 incubator CB 150	WTC Binder, Germany
Eppendorf Research® plus Mechanical Pipette	Eppendorf AG, Germany
Freezer –20 ºC	Liebherr, Switzerland
Freezer –80 ºC	Sanyo, Japan
Freezer –150 ºC	PHCbi, Japan
Gel electrophoresis chamber HU13	Thermo Fisher Scientific, USA
GelDoc Go Imaging System	Bio-Rad Laboratories, USA
ImageXpress Micro Confocal High-Content Imaging System	Molecular Devices, USA
IncuCyte	Sartorius AG, Germany
Mr. Frosty™ Freezing Container	ThermoFisher Scientific, USA
Multipette® plus Repeater® plus	Eppendorf AG
Nanodrop, Spectrophotometer ND-100	Thermo Fisher Scientific, USA
Nucleocounter NC-200	Chemometech A/S, Denmark
pH meter	Mettler Toledo, Germany
Pipette (0.5-10 µl, 10-100 µl, 100-1000 µl)	Eppendorf AG, Germany
Pipetboy	Integra Biosciences GmbH, Germany
Primovert inverted cell culture microscope	Carl Zeiss Microscopy GmbH, Germany
Spinning Disk Confocal Microscope, Cell Observer SD	Carl Zeiss Microscopy GmbH, Germany
StepOnePlus ™ Real-Time PCR System	Applied Biosystems™, USA
Tecan Plate reader	Tecan Trading AG, Switzerland
Thermocycler Biometra TOne	Analytic Jena AG, Germany
Thermomixer (comfort)	Eppendorf AG, Germany
Ultracentrifuge Sorvall™ MX Plus Mikro	Thermo Fisher Scientific, USA
Vortex Genie 2	Scientific Industries Inc., USA
Water bath WBT 6	Carl Roth GmbH

2.1.3 Chemicals and reagents

Table 4. Chemicals and reagents

Chemicals/Reagents	Manufacturer	Catalogue number
1 kb Plus DNA Ladder	New England Biolabs, USA	N3200
Accutase	Sigma-Aldrich, USA	A6964
Agarose Broad Range	Carl Roth GmbH + Co. KG, Germany	T846
AgeI-HF	New England Biolabs, USA	R3552
Ara-c	Sigma-Aldrich, USA	C6645
B-27™ Supplement (50X), minus Vitamin A	Thermo Fisher Scientific, USA	12587010
Blocking Reagent BMB	Roche, Switzerland	11112589001
Bovine Serum Albumin (BSA) Fraction V	Carl Roth GmbH + Co. KG, Germany	1ETA.4
BstBI	New England Biolabs, USA	R0519
Cal-520™ AM	AAT Bioquest Inc., USA	ABD-21130
Calbryte 590™ AM	AAT Bioquest Inc., USA	ABD-20701
Chemically-Defined Lipid Concentrate	Thermo Fisher Scientific, USA	11905031
CHIR99021	Tocris Bioscience, UK	4423
CloneR™ 2	STEMCELL Technologies, Canada	100-0691
Collagenase IV	STEMCELL Technologies, Canada	07909
CutSmart™ Buffer	New England Biolabs, USA	B6004S
DAPT	Sigma-Aldrich, USA	D5942
Dimethylsulfoxid (DMSO)	Carl Roth GmbH + Co. KG, Germany	A994.1
DNase Stop Solution	Promega GmbH, Germany	Z312C-C
Dorsomorphin dihydrochloride	Bio-techne, USA	3093
dNTPs	New England Biolabs, USA	N0447
Doxycycline	Sigma-Aldrich, USA	D9891
Dulbecco's phosphate buffered saline (DPBS)	Thermo Fisher Scientific, USA	14190094
Fetal Bovine Serum (FBS)	Thermo Fisher Scientific, USA	102700106
Fibronectin	Sigma-Aldrich, USA	F1141
G418	Carl Roth GmbH + Co. KG, Germany	2039
Gel Loading Dye, Purple (6X)	New England Biolabs, USA	B7024S
Glucose solution	Thermo Fisher Scientific, USA	A2494001
GlutaMAX (100X)	Thermo Fisher Scientific, USA	35050038
HEPES (1M)	Thermo Fisher Scientific, USA	15630056
Laminin	Sigma-Aldrich, USA	L2020
L-Ascorbic acid	Sigma-Aldrich, USA	A2078
LDN193189	STEMCELL Technologies, Canada	72147
Lipofectamine™ 2000	Thermo Fisher Scientific, USA	11668019
Matrigel ® hESC-qualified Matrix	Corning Inc., USA	354277
Midori Green Advance	NIPPON Genetics EUROPE GmbH, Germany	MG04

N2 Supplement (100X)	Thermo Fisher Scientific, USA	17502048
N6,2′-O-Dibutyryladenosine 3′,5′-cyclic monophosphate sodium salt (dbcAMP)	Sigma-Aldrich, USA	D0627
Non-essential amino acids (NEAA)	Thermo Fisher Scientific, USA	11140035
Nuclease-free water	New England Biolabs, USA	B1500S
One Shot™ Top 10 chemically competent E. coli	Thermo Fisher Scientific, USA	C404003
Paraformaldehyd (PFA)	Carl Roth GmbH + Co. KG, Germany	0335
PD0325901	Sigma-Aldrich, USA	PZ0162
Penicillin-Streptomycin (100X)	Thermo Fisher Scientific, USA	15140122
Platinum II Taq Hot-Start DNA Polymerase, Platinum II PCR Buffer (5X), Platinum GC Enhancer	Thermo Fisher Scientific, USA	14966001
Poly-L-ornithine hydrobromide	Sigma-Aldrich, USA	P3655
Poly-L-ornithine solution	Sigma-Aldrich, USA	P4957
Pramipexole dihydrochloride	MedChemtronica AB, Sweden	HY-17355
Primer „random“ (dN6-Primer)	Roche, Switzerland	11034731001
Propidium Iodide solution	BioLegend, USA	421301
Purmorphamine (PMA)	Enzo Biochem Inc., USA	ALX-420-045
Puromycin	Thermo Fisher Scientific, USA	11113803
Ready-to-Use Packaging Plasmid Mix (pCPack2 Lentiviral Packaging Plasmid Mix)	Cellecta, Inc., USA	CPCP-K2A
RNAse A	New England Biolabs, USA	T3018L
RQ1 DNase 10X Reaction Buffer	Promega GmbH, Germany	M198A-C
RQ1 RNase-free DNase	Promega GmbH, Germany	M6101
SB431542	STEMCELL Technologies, Canada	72232
SCH 39166 hydrochloride	MedChemtronica AB, Sweden	HY-14689
SKF 38393	MedChemtronica AB, Sweden	HY-12520A
Sodium pyruvate (100 mM)	Thermo Fisher Scientific, USA	11360070
STEMdiff™ Neural Rosette Selection Reagent	STEMCELL Technologies, Canada	05832
SU05402	Sigma-Aldrich, USA	SML0443
Sulpiride	MedChemtronica AB, Sweden	HY-B1019
Triton-X-100	Carl Roth GmbH + Co. KG, Germany	3051
Trypsin/EDTA 0.025 %	Thermo Fisher Scientific, USA	25300054
T4 DNA Ligase, T4 DNA Ligase Reaction Buffer	New England Biolabs, USA	M0202
XAV939	Sigma-Aldrich, USA	X3004
Y-27632	STEMCELL Technologies, Canada	72304

2.1.4 Cytokines

Table 5. Cytokines

Cytokine	Manufacturer	Catalogue number
Recombinant Human BDNF	PeproTech, Inc., USA	450-02
Recombinant human CNTF	PeproTech, Inc., USA	450-13
Recombinant Human GDNF	PeproTech, Inc., USA	450-10
Recombinant Human FGF-8a	PeproTech, Inc., USA	100-25A
Recombinant Human TGF-β3	PeproTech, Inc., USA	100-36E

2.1.5 Cell culture media composition

Table 6. Commercially available media

Medium	Manufacturer	Catalogue number
BrainPhys Neuronal Medium	STEMCELL Technologies, Canada	05790
DMEM, high glucose, GlutaMAX™ supplement	Thermo Fisher Scientific, USA	10566016
DMEM/F12, no glutamine	Thermo Fisher Scientific, USA	21331020
mTeSR™ Plus	STEMCELL Technologies, Canada	100-0276
Neurobasal™ medium	Thermo Fisher Scientific, USA	21103049
Neurobasal™-A medium	Thermo Fisher Scientific, USA	10888022
Opti-MEM™	Thermo Fisher Scientific, USA	31985070
STEMdiff™ Neural Induction Medium	STEMCELL Technologies, Canada	05839
STEMdiff™ Neural Progenitor Medium	STEMCELL Technologies, Canada	05833

Table 7. Astrocyte cultivation medium

Component	Final concentration
DMEM, high glucose, GlutaMAX™ supplement	1 X
FBS	10 %
Penicillin-Streptomycin	1 %
Sodium pyruvate	1 % (1mM)
GlutaMAX	1 %

Table 8. HEK293FT culture and transfection media

Component	Final concentration
Culture medium	
DMEM, high glucose, GlutaMAX™ supplement	1 X
FBS	10 %
NEAA	1 %
Penicillin-Streptomycin	1 %
G418	500 µg/ml
Transfection medium	
Opti-MEM™	1 X

FBS	5 %
Penicillin-Streptomycin	1 %

Table 9. smNPC differentiation and maintenance media (iPSC → smNPC)

Component	Final concentration
Basal medium	
DMEM/F12	50 %
Neurobasal™-A medium	50 %
GlutaMAX	1 %
Penicillin-Streptomycin	1 %
EB medium (days 0-2)	
SB431542	10 µM
Dorsomorphin	1 µM
CHIR99021	3 µM
PMA	0.5 µM
N2B27 medium (days 2-4)	
B27 minus vitamin A	1 %
N2	0.5 %
SB431542	10 µM
Dorsomorphin	1 µM
CHIR99021	3 µM
PMA	0.5 µM
smNPC maintenance medium (days 4-∞)	
B27 minus vitamin A	1 %
N2	0.5 %
CHIR99021	3 µM
PMA	0.5 µM
L-Ascorbic acid	150 µM

Table 10. iDAN differentiation and maturation media (smNPC → iDAN)

Component	Final concentration
Basal medium	
DMEM/F12	50 %
Neurobasal™-A medium	50 %
GlutaMAX	1 %
Penicillin-Streptomycin	1 %
Patterning medium (days 0-7)	
B27 minus vitamin A	1 %
N2	0.5 %
BDNF	20 ng/ml
FGF- 8a	10 ng/ml
PMA	1 µM
L-Ascorbic acid	200 µM
Maturation medium (days 7-14)	
B27 minus vitamin A	1 %
N2	0.5 %
BDNF	10 ng/ml
GDNF	10 ng/ml
TGF- β3	1 ng/ml
dbcAMP	500 µM

DAPT	10 µM

Table 11. Induction medium (ALN neurons)

Component	Final concentration
DMEM/F12	50 %
GlutaMAX	1 %
Penicillin-Streptomycin	1 %
Sodium pyruvate	1 % (1mM)
B27 minus vitamin A	2 %
N2	1 %

Table 12. Neuron medium (ALN neurons)

Component	Final concentration
BrainPhys Neuronal Medium	50 %
GlutaMAX	1 %
Penicillin-Streptomycin	1 %
Sodium pyruvate	1 % (1mM)
B27 minus vitamin A	2 %
N2	1 %
BDNF	20 ng/ml
GDNF	20 ng/ml
L-Ascorbic acid	200 nM
dbcAMP	500 µg/ml
Laminin	1 µg/ml

Table 13. Differentiation medium of stable NGN2-based iPSC to DIV3 iNeurons

Component	Final concentration
N2 medium (days 0-3)	
DMEM/F12	50 %
HEPES	15 mM
Penicillin-Streptomycin	1 %
NEAA	1 %
GlutaMAX	1 %
Glucose	1.5 %
SB431542	10 µM
XAV939	1 µM
LDN193189	100 nM

Table 14. Differentiation medium of stable AD2-based iPSC to DIV8 iNeurons

Component	Final concentration
IPS-SLX medium (days 0-1)	
mTeSR™ Plus	100 %
SB431542	10 µM
XAV939	5 µM
LDN193189	250 nM
IPS-SDP medium (days 1-2)	

mTeSR™ Plus	100 %
SB431542	10 µM
XAV939	5 µM
LDN193189	250 nM
SU05402	10 µM
DAPT	10 µM
PD0325901	8 µM
N2B27 basal medium	
Neurobasal™ medium	100 %
GlutaMAX	1 %
B27 minus vitamin A	2 %
N2	1 %
IPS/N2B27 medium (days 2-5)	
mTeSR™ Plus	66 %
N2B27 basal medium	33 %
SB431542	10 µM
XAV939	5 µM
SU05402	10 µM
DAPT	10 µM
PD0325901	8 µM
N2B27/IPS medium (days 5-8)	
N2B27 basal medium	66 %
mTeSR™ Plus	33 %
SU05402	10 µM
DAPT	10 µM
PD0325901	8 µM

Table 15. Freezing medium of iNeurons

Component	Final concentration
DMEM/F12	50 %
HEPES	15 mM
FBS	40 %
DMSO	10 %

Table 16. Differentiation medium of stable NGN2-AD2 iNeurons co-culture

Component	Final concentration
NB27+ medium (days 0-11)	
Neurobasal™ medium	100 %
FBS	2 %
NEAA	1 %
GlutaMAX	1 %
Glucose	1.5 %
Penicillin-Streptomycin	1 %
B27 minus vitamin A	2 %
BDNF	10 ng/ml
GDNF	10 ng/ml
CNTF	10 ng/ml
Laminin	1 µg/ml
dbcAMP	250 µM
L-Ascorbic acid	100 µM

Ara-c (days 4-7)	2 µM
NB27 medium (days11-21)	
Neurobasal™ medium	100 %
FBS	2 %
NEAA	1 %
GlutaMAX	1 %
Glucose	1.5 %
Penicillin-Streptomycin	1 %
B27 minus vitamin A	2 %
BDNF	10 ng/ml
GDNF	10 ng/ml
CNTF	10 ng/ml
Laminin	1 µg/ml
BrainPhys medium (days21-42)	
BrainPhys Neuronal Medium	100 %
FBS	2 %
NEAA	1 %
GlutaMAX	1 %
Glucose	1.5 %
Penicillin-Streptomycin	1 %
B27 minus vitamin A	2 %
BDNF	10 ng/ml
GDNF	10 ng/ml
CNTF	10 ng/ml
Laminin	1 µg/ml

Table 17. Tyrode buffer composition

Component	Final concentration
NaCl	135 mM
KCl	5 mM
D-Glucose	10 mM
$MgCl_2$ x 6 H_2O	0.2 mM
HEPES buffer	10 mM
$CaCl_2$ x 2 H_20	2.5 mM

2.1.6 Antibodies

Table 18. Primary antibodies

Antibody target	Species	Manufacturer	Catalogue Number	Dilution
ANK-3	mouse IgG2a	NeuroMab, University of California, USA	AB_10697718	1:5
βIII-tubulin	mouse IgG2a monoclonal	STEMCELL Technologies, Canada	60100	1:250
βIII-tubulin	rabbit IgY polyclonal	Synaptic Systems, Germany	302302	1:250
BRN2	rabbit IgG	Cell Signaling Technology, USA	12137	1:500
CTIP2	rat IgG	Abcam, UK	ab18465	1:500

FOXA2	mouse IgG2a monoclonal	Santa Cruz Biotechnology, USA	sc-101060	1:200
Gephyrin	mouse IgG1, clone mAb7a	Synaptic Systems, Germany	147021	1:400
GFAP	rabbit	Agilent Technologies, USA	Z0334	1:500
Hoechst 33258	-	Sigma-Aldrich, USA	861405	1:800
MAP2	chicken IgY	Thermo Fisher Scientific, USA	PA1-10005	1:2500
MAP2	rabbit polyclonal	Synaptic Systems, Germany	188002	1:500
Nestin (JP63)	mouse IgG	Synaptic Systems, Germany	312011	1:1000
PAX6	mouse IgG2a	BioLegend, USA	862001	1:200
PSD95 (PDZ domain)	rabbit IgG1	Synaptic Systems, Germany	124008	1:500
SOX1	rabbit	Abcam, UK	ab22572	1:500
SOX2	rabbit	Cell Signaling Technology, USA	3579S	1:400
Synapsin1 (SYN1)	mouse IgG1 monoclonal	Synaptic Systems, Germany	106011	1:1000
TH	chicken IgY	Abcam, UK	ab76442	1:1000
vGAT	rabbit	Synaptic Systems, Germany	131003	1:500
vGLUT1	mouse IgG	Synaptic Systems, Germany	135511	1:300

Table 19. Secondary antibodies

Antibody target	Species	Manufacturer	Catalogue Number	Dilution
Alexa Fluor 405	goat anti-chicken IgY (H+L) Alexa Fluor 405	Thermo Fisher Scientific, USA	A-31553	1:150
AlexaFluor 488	goat anti-chicken IgY (H+L)	Thermo Fisher Scientific, USA	A-11039	1:400
AlexaFluor 647	goat anti-chicken IgY (H+L)	Thermo Fisher Scientific, USA	A-21449	1:400
AlexaFluor 647	goat anti-rat IgY (H+L)	Thermo Fisher Scientific, USA	A-21247	1:1000
Cy3-AffiniPure	goat anti-mouse IgG (H+L)	Jackson ImmunoResearch, UK	115-165-146	1:500
Cy3-AffiniPure	goat anti-rabbit IgG (H+L)	Jackson ImmunoResearch, UK	111-165-144	1:500
Cy5-AffiniPure	goat anti-mouse IgG (H+L)	Jackson ImmunoResearch, UK	115-175-146	1:500
Cy5-AffiniPure	goat anti-rabbit IgG (H+L)	Jackson ImmunoResearch, UK	111-175-144	1:500

2.1.7 Plasmids

Table 20. Plasmids

Plasmid	Manufacturer	Catalogue Number	Reference
pLV-TetO-hNGN2-eGFP-Puro	Addgene	79823	doi: 10.1016/j.ymeth.2015.11.019.
pLV-TetO-ASCL1-LMX1B-NURR1	Addgene	43918	doi: 10.1371/journal.pone.0028719
pLV-FUdeltaGW-rtTA	Addgene	19780	doi: 10.1016/j.stem.2008.08.003
pEF-Synaptophysin-mRuby	Addgene	188980	doi: 10.1016/j.neuron.2018.04.022

2.1.8 Oligonucleotides

Table 21. Oligonucleotides

Oligo name	Sequence (5' - 3')	Amplicon length (in bp)
P2A-Puro_fw	TCCGGCTTCGAAGCCACGAATTTCTC	688
P2A-Puro_rv	ATCGATTACCGGTTCAGGCACCGG	
ALN-Puro_Seq1	CCCAGAACTTCGTACCCTTTGCAC	-
ALN-Puro_Seq2	TTCTACGAGCGGCTCGGCTTCA	-

2.1.9 Commercially available kits

Table 22. Commercially available kits

Kit Name	Manufacturer	Catalogue Number
Lenti-X p24 Rapid Titer Kit	Takara Bio Inc., Japan	632200
QIAamp DNA Mini Kit	Qiagen, Germany	51304
QIAquick Gel Extraction Kit	Qiagen, Germany	28704
QIAquick PCR Purification Kit	Qiagen, Germany	28104
QIAGEN Plasmid Midi Kit	Qiagen, Germany	12143
RNeasy Mini Kit	Qiagen, Germany	74104
RQ1 RNase-Free DNase	Promega GmbH, Germany	M6101
STEMdiff™ SMADi Neural Induction Kit	STEMCELL Technologies, Canada	08581

2.1.10 Software

Table 23. Software

Software	Company	Version
CorelDRAW (64-bit)	Corel Corporation, Canada	X7
Fiji (based on Image J2)	National Institutes of Health, USA (Image J)	2.9
GraphPad Prism	GraphPad Software, USA	10.2.3
Jupyter Notebook (Python 3)	Project Jupyter	6.4.8
Imaris Bitplane	Oxford Instruments, UK	10.0.0
IncuCyte® S3 Basic Analyzer	Sartorius AG, Germany	-
MetaXpress	Molecular Devices, USA	
Origin® (64-bit)	OriginLab Corporation, USA	2016G
SnapGene Viewer	SnapGene, USA	5.3.1
Zen (blue edition)	Zeiss, Germany	3.0

2.2 Cell culture methods

2.2.1 General iPSC line information

All iPSC lines have previously been fully characterized and described. For additional information on all lines refer to **Table 1**.

2.2.1.1 CTR and idiopathic SCZ iPSC lines

Five iPSC lines used in this study were generated from dermal fibroblasts of one healthy volunteer (CTR2) and four patients diagnosed with schizophrenia-spectrum disorder (SCZ1, SCZ2, SCZ4, SCZ5). These lines were generated by Dr. Ricarda Breitmeyer and Sabrina Vogel in the Molecular Neurobiology group at the NMI in Reutlingen in cooperation with the Department of Psychiatry, University Hospital, Tübingen (authorized by the Ethics Committee of the University Hospital and Faculty of Medicine, Tübingen). Therefore, dermal fibroblasts were reprogrammed via non-integrative episomal reprogramming as previously described (170). Another healthy control iPSC line (CTR1) was commercially acquired from Thermo Fisher Scientific that was originally reprogrammed from umbical cord blood-derived CD34-positive progenitor cells by non-integrative transfection (171). The third healthy control iPSC line (CTR3) was successfully reprogrammed via integration-free episomal reprogramming of peripheral blood derived hematopoietic stem cells and was a kind gift from the Tumorbiology group at the NMI in Reutlingen (172).

2.2.1.2 Isogenic control and *PINK1* KO iPSC lines

The healthy control iPSC line HC1 and the two *PINK1* KO lines were a kind gift from Dr. Julia Fitzgerald at the Hertie Institute for Clinical Brain Research in Tübingen. iPSC from a healthy individual were obtained from dermal skin fibroblasts and reprogrammed using a retroviral reprogramming strategy overexpressing the plasmids OCT4, SOX2, KLF4, c-MYC as previously described (173). Transfection of HC1 iPSC with a TALEN directed to exon 1 resulted in two distinct monoclonal iPSC lines carrying a homozygous deletion of *PINK1* (PINK1 KO-Δ8.9 and PINK1 KO-Δ40.7) (174).

2.2.1.3 Isogenic control and 15q13 and 22q11 microdeletion lines

Stable NGN2 and AD2 iPSC comprising an isogenic control (CTR) and three microdeletion lines (15q13, 22q11 clone1, 22q11 clone2) were a kind gift from Prof. Dr. Moritz Rossner at the Department of Psychiatry and Psychotherapy, LMU University Hospital in Munich.

2.2.2 Matrigel coating

To ensure proper proliferation and to keep pluripotent characteristics, stem cell cultures were maintained on culture vessels coated with Matrigel, a murine basement membrane extract that supports feeder-free expansion of iPSC. For coating, Matrigel was diluted 1:100 in cold DMEM/F12 and added to appropriate culture vessels (e.g. 1 ml Matrigel/ one well on 6-well plate). Incubation at 37 °C for at least 30 minutes was sufficient. Freshly diluted Matrigel could be stored for up to one week at 4 °C. To prevent gelling of Matrigel, work was performed on ice.

2.2.3 PLO/laminin coating

For the cultivation of neuronal progenitor cells (NPC) and differentiation of neurons, 20 % of poly-L-ornithine (PLO) diluted in DPBS was added to appropriate culture vessels (e.g. 1 ml PLO-solution/ one well of 6-well plate). After the incubation of 2 h at RT, plates were washed once with DPBS and once with DMEM/F12. In a second coating step, plates were incubated overnight at 37 °C with 10 µg/ml laminin diluted in DMEM/F12. The following day, coated vessels were locked with parafilm to prevent drying out and further stored at 4 °C for up to one week.

2.2.4 PLO-hydro/laminin/fibronectin coating

For the co-cultivation of stable NGN2-AD2 iNeurons, plates were coated with 0.75 % poly-L-ornithine hydrobromide (PLO-hydro) diluted in DPBS and incubated overnight at 37 °C. The next day, PLO-hydro-solution was removed, and plates were washed three times with DPBS. In a second coating step, 1 % laminin + 2 % fibronectin diluted in DPBS were added to appropriate culture vessels, followed by an overnight incubation at 37 °C. The following day, coated vessels were locked with parafilm to prevent drying out and further stored at 4 °C for up to one week.

2.2.5 iPSC propagation and maintenance

Stem cell cultures were maintained on Matrigel-coated 6-well plates in mTeSR™ Plus medium + 1 % Penicillin-Streptomycin at 37 ˚C in humified 5 % CO_2 atmosphere. Daily medium changes were performed and once cells reached 80-90 % of confluence, cells were enzymatically passaged using Accutase to obtain single-cell suspensions. For this purpose, the cell culture medium was extracted and Accutase was added (1 ml of Accutase/ one well of

6-well plate). After an incubation period of 3-5 minutes at 37 °C, cells start to detach, and the enzymatic reaction was stopped by adding DMEM/F12 at a ratio of 1:2. After the centrifugation for 3 minutes at 300 xg, the supernatant was discarded and cells counted using the Nucleocounter NC-200. For iPSC cultivation, $1.05x10^4$ viable iPSC/cm^2 were added onto one well of a 6-well plate filled with mTeSR™ Plus medium + 1 % Penicillin-Streptomycin supplemented with 10 µM Y-2763 (ROCK inhibitor). iPSC reaching a passage of 40 were discarded and cells with lower passage numbers were thawed.

2.2.6 NPC differentiation

NPC were generated using the STEMdiff™ SMADi Neural Induction kit according to the manufacturer's instructions. For this purpose, iPSC were enzymatically detached and $2x10^6$ cells were seeded per well onto a before with Anti-Adherence Rinsing Solution-treated AggreWell™ 800 24-well plate, which was then centrifuged for 1 minute at 100 xg to allow proper embryoid body (EB) formation. Partial daily medium changes with STEMdiff™ Neural Induction Medium + 1 % Penicillin-Streptomycin were performed for six days to facilitate EBs formation. On day seven, EBs were collected and filtered using a 37 µm reversible strainer to get rid of single cells. EBs that were beforehand harvested in one well on the AggreWell™ 800 24-well plate, were then replated onto one PLO/Lam-coated well of a 6-well plate after filtering. After seven days with daily medium changes in STEMdiff™ Neural Induction Medium + 1 % Penicillin-Streptomycin, neural rosettes were formed, which could be detached by the addition of STEMdiff™ Neural Rosette Selection Reagent for 1.5 h at 37 °C. Dissociated neural rosettes were gently washed with DMEM/F12 and neural rosettes-solution was centrifuged for 3 minutes at 300 xg. Beforehand, 6-well plates were PLO/Lam-coated and selected neural rosettes were seeded in STEMdiff™ Neural Induction Medium + 1 % Penicillin-Streptomycin. Once the resulting NPCs reached 90 % of confluence, cells were enzymatically dissociated with Accutase and seeded onto PLO/laminin-coated 6-well plates in Neural Progenitor Medium supplemented with 1 % Penicillin-Streptomycin at a density of $1.05x10^4$ cells/cm^2.

2.2.7 NPC propagation and maintenance

NPC maintenance was performed in STEMdiff™ Neural Progenitor Medium + 1 % Penicillin-Streptomycin on PLO/Lam-coated 6-well plates at 37 °C and 5 % CO_2 atmosphere with full medium changes every second day. NPC cultures reaching 80-90 % of confluence, were enzymatically dissociated using Accutase. After a 3-5 min Accutase-treatment at 37 °C, cells detached and the enzymatic reaction was stopped by adding DMEM/F12 at a ratio of 1:2. The single cell suspension was then centrifuged for 3 minutes at 300 xg, the supernatant was

discarded and cells counted using the Nucleocounter NC-200. Per well of a 6-well plate, $1.05x10^4$ cells/cm^2 were seeded for routine propagation. NPC with passage numbers until 10 were used for differentiations, while NPC with higher passage numbers were discarded.

2.2.8 Cryopreservation and thawing of iPSC and NPC

For thawing of cryopreserved iPSC and NPC, vials were shortly put into a water bath at 37 °C for a few minutes until only the core remained frozen. Cells were then gently resuspended and transferred to a 15 ml falcon tube containing 3 ml of pre-warmed DMEM/F12. After centrifugation for 3 minutes at 300 xg, the supernatant was discarded and iPSC and NPC were resuspended in mTeSR™ Plus medium + 1 % Penicillin-Streptomycin supplemented with 10 µM Y-27632 to enhance single cell survival and in STEMdiff™ Neural Progenitor Medium + 1 % Penicillin-Streptomycin, respectively. Cells were then seeded into their previously Matrigel- or PLO/laminin-coated growth vessels.

For freezing, single cell suspensions of iPSC and NPC were generated as described. Cells were then centrifuged for 3 minutes at 300 xg and resuspended into 1 ml of their appropriate cell culture medium + 10 % DMSO. Per cryovial, $1x10^6$ cells were added and cryovials were frozen at -80 °C in Mr. Frosty™ freezing containers overnight to ensure a stable cooling. For long-term storage, cryovials were transferred at -150 °C or in liquid nitrogen tanks.

2.2.9 Dopaminergic and glutamatergic neuron differentiation

iPSC-derived neurons can be obtained by different strategies. One strategy is the ‘directed differentiation’ that mimics the *in vivo* development by adding small molecules in a specific concentration and time manner. Lentiviral transduction and overexpression of the key transcription factors represents another approach to rapidly and directly convert iPSC into neurons (175).

2.2.9.1 Differentiation of dopaminergic neurons (iDANs) via growth factors

Generation of induced dopaminergic neurons via ‘directed differentiation’ was based on two differentiation steps. First, iPSC were differentiated into small molecule neuronal progenitor cells (smNPC) and further differentiation into induced dopaminergic neurons (iDANs). This differentiation process is based on the protocol developed by Reinhardt et al. (173). Therefore, iPSC were seeded onto Matrigel-coated 6-well plates with $1.05x10^4$ viable iPSC/cm^2 in mTeSR™ Plus medium + 1 % Penicillin-Streptomycin supplemented with 10 µM Y-27632. After 3-4 days, medium-sized iPSC colonies were detached by addition of 1 mg/ml Collagenase IV for 1 h at 37 °C. Detached colonies were collected in 15 ml falcon tubes. When all colonies

have sunk, the supernatant was removed, and cells were transferred onto ultra-low attachment culture vessels in EB medium for 48 h. In a 2 days rhythm, medium was first changed to N2B27 medium and then to smNPC maintenance medium. EBs were then triturated into smaller fragments with a 1 ml pipette and 10-15 EBs were plated onto one well of a Matrigel-coated 12-well plate. Full medium changes with smNPC Maintenance medium were performed every second day and cells were passaged once a week using Accutase. Per well of a 6-well plate, $1.05x10^4$ cells/cm^2 were seeded for routine passaging. smNPC with passage numbers greater than four, were used for iDAN differentiations.

On DIV0, once smNPC reached 80-90 % confluence, cells were enzymatically detached with Accutase and centrifuged for 3 minutes at 300 xg. After removal of the supernatant, cell pellets were resuspended in DMEM/F12 and $3.9x10^4$ cell/cm^2 cells were seeded onto previously Matrigel-coated 12-well plates in Patterning medium supplemented with 10 µM Y-2763. Full medium changes with Patterning medium were performed every second day until DIV7.

After seven days in Patterning medium, cells were detached as described. In total, $2.5x10^5$ cells/cm^2 were seeded onto one well of a Matrigel-coated 96-well plate in Maturation medium. After 2-3 h, murine astrocytes were added to each well in a neuron-astrocyte ratio of 4:1 ($6.25x10^4$ cells/cm^2 astrocytes/well). For further maturation, cells were cultured in Maturation medium until DIV14, and medium change was performed every other day.

2.2.9.2 Differentiation of dopaminergic neurons (ALN) via overexpression of the transcription factors *ASCL1/LMX1B/NURR1*

The induction of dopaminergic neurons via lentiviral overexpression of *ASCL1-LMX1-/NURR1* (ALN) was achieved according to the already published protocol with slight modifications and started from iPSC (148). On DIV0, iPSC were enzymatically detached using Accutase, centrifuged for 3 minutes at 300 xg and counted as already described. Cells were diluted in mTeSR™ Plus medium + 1 % Penicillin-Streptomycin supplemented with 10 µM Y-2763 to obtain a final cell concentration of $7.89x10^4$ iPSC/cm^2. For transduction of iPSC, the two lentiviral constructs FUdeltaGW-rtTA and TetO-ALN-Puro were added to the single cell suspension to induce the overexpression of *ALN-Puro* under the control of the Tet-On system (**Table 20**). Subsequently, the iPSC-lentiviral suspension was plated onto Matrigel-coated 12-well plates. After overnight incubation on DIV1, medium was replaced by Induction medium containing 1 µg/ml of doxycycline to start transgene overexpression of *ALN-Puro*. On DIV2, selection of transduced cells was initiated by medium replacement with Induction medium supplemented with 1 µg/ml of doxycycline and 1 µg/ml of the antibiotic puromycin, which was repeated until DIV5, as there were no longer dead cells visible. On DIV6 and DIV7, 2 µM Ara-c was initiated and added to the Induction medium with 1 µg/ml of doxycycline, as early

processes began to extend from the cell body to get rid of non-differentiating cells. Until DIV10, full medium changes with Induction medium supplemented with 1 µg/ml of doxycycline were performed daily. For culturing ALN neurons separately in monocultures, immature neurons were detached with Accutase on DIV10, resuspended in Neuron medium + 1 µg/ml of doxycycline, and plated at a density of $1.56x10^5$ cells/cm^2 onto PLO/Lam-coated 96-half-well plates. After neuronal attachment, $3.9x10^4$ cells/cm^2 murine astrocytes were added to neurons at a neuron-astrocyte ratio of 4:1. Half medium changes with Neuron medium were performed every other day to dilute out doxycycline. On DIV24, a full medium change with Neuron medium + 1 µg/ml doxycycline was performed for the final differentiation process. On DIV28, cellular assays were performed.

2.2.9.3 Differentiation of glutamatergic neurons (NGN2-GFP) via overexpression of *Neurogenin2-GFP*

The generation of NGN2-GFP neurons was performed according to a published protocol with slight modifications and started from NPC (146). Therefore, NPCs were seeded at a density of $5.26x10^4$/cm^2 onto Matrigel-coated 12-well plates in Neural Progenitor medium + 1 % Penicillin-Streptomycin at DIV-1. The following day, NPCs were transduced with the two lentiviral constructs FUdeltaGW-rtTA and pLV-TetO-hNGN2-eGFP-Puro, to induce the overexpression *NGN2-GFP* under the control of the Tet-On system (**Table 20**). The following day, medium was replaced by Neural Progenitor medium + 1 % Penicillin-Streptomycin containing 1 µg/ml of doxycycline. After 24 h (DIV2), the selection of transduced cells was initiated by adding Neural Progenitor medium + 1 % Penicillin-Streptomycin + 1 µg/ml of doxycycline + 2 µg/ml of the antibiotic puromycin. Selection was performed until DIV3, when cells were detached for seeding in monocultures. Therefore, immature neurons were detached with Accutase, resuspended in Neuron medium supplemented with 1 µg/ml of doxycycline, and seeded at a density of $1.25x10^5$ cells/cm^2 on PLO/Lam-coated 96-half-well plates. After neuronal attachment, $3.125x10^4$ cells/cm^2 murine astrocytes were added to neurons at a neuron-astrocyte ratio of 4:1. Half medium changes with Neuron medium were performed every other day to dilute out doxycycline. On DIV24, a full medium change with Neuron medium + 1 µg/ml doxycycline was performed for the final differentiation process. On DIV21, cellular assays were performed.

2.2.9.4 ALN-NGN2 co-culture setup

For co-cultivation of dopaminergic and glutamatergic neurons, ALN and NGN2-GFP neurons were generated as described in sections 2.2.9.2 and 2.2.9.3. After initial differentiation steps, pre-differentiated ALN neurons on DIV10 and NGN2-GFP neurons on DIV3 were detached

with Accutase and counted. Immature neurons were seeded into co-cultures at a total seeding density of 1.56x10^5 cells/cm^2 onto one well of a PLO/Lam-coated 96-half-well plate in Neuron medium supplemented with 1 µg/ml of doxycycline. The ALN-NGN2-GFP neurons ratio was 50:50. After neuronal attachment, 3.9x10^4 cells/cm^2 murine astrocytes were added to the co-culture. On DIV24 of ALN neurons, a full medium change with Neuron medium + 1 µg/ml doxycycline was performed for the final differentiation process. On DIV28 of ALN neurons, cellular assays were performed. A schematic overview of the differentiation processes is depicted in **Figure 1**.

The seven iPSC lines were individually differentiated either into ALN-induced or NGN2-induced neurons. For the first part of experiments, the respective ALN neuronal lines were seeded with their matching NGN2 neuronal lines into co-culture. In a second part, the three CTR lines were combined into a CTR population and all four SCZ lines were mixed into a SCZ population. With that approach it was possible to generate a mixed co-culture setup comprising four combinations: CTR ALN + CTR NGN2, SCZ ALN + CTR NGN2, CTR ALN + SCZ NGN2 and SCZ ALN + SCZ NGN2. All other parameters (cell density/well, cultivation period, ect.) remained the same.

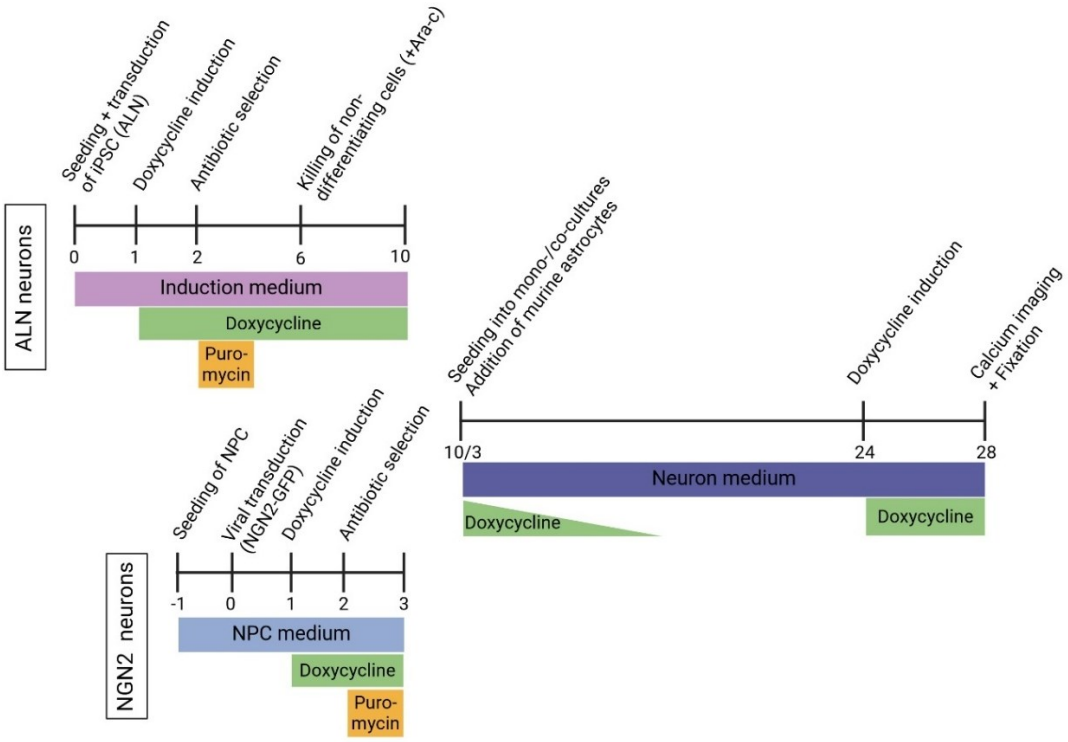

Figure legend on the next page

Figure 1. Schematic overview of ALN and NGN2 differentiation and seeding into monocultures or ALN-NGN2 co-cultures. iPSC are transduced with the lineage-specific transcription factors ALN, whereas NPC are transduced with the lineage-specific transcription factor NGN2 via lentiviral overexpression. Doxycycline administration and puromycin selection induce transgene expression and selection of infected cells. To kill non-differentiating cells, Ara-c was initiated in ALN neuron differentiation for 48 h. ALN and NGN2 neurons were seeded into mono- or co-cultures. Subsequently, murine

astrocytes were added to improve network maturation. Cultures were cultivated in Neuron medium until DIV28. At DIV24, doxycycline was again added to induce the transgene expression and improve neuronal maturation. Created with BioRender.com.

2.2.10 NGN2 and ASCL1/DLX2 (AD2)-based differentiation of stable iPSC to iNeurons

For the generation of cortical glutamatergic NGN2 and GABAergic interneurons, stable transduced iPSC with either NGN2 or AD2 were employed. Differentiation protocols based on the Tet-On system were established by the Department of Psychiatry and Psychotherapy, LMU University Hospital at the LMU in Munich and kindly provided. Induced cortical glutamatergic NGN2 neurons were generated according to previous protocols with slight modifications (176, 177, 178). In a first step, stable NGN2 and AD2-based iPSC were pre-differentiated to DIV3 and DIV8 iNeurons, respectively and frozen. In a second step, frozen iNeurons were thawed and seeded into a NGN2-AD2 co-culture setup

2.2.10.1 NGN2-based differentiation of stable iPSC to DIV3 iNeurons

Stable iPSC-derived NGN2 iNeurons were generated as follows: On DIV0, stable NGN2-iPSC were enzymatically detached using Accutase. After the centrifugation for 3 minutes at 300 xg, cells were resuspended and counted. Required number of 6-well plates were coated with Matrigel beforehand, and $1.05x10^5$ cell/cm^2 were seeded in mTeSR™ Plus medium + 1 % Penicillin-Streptomycin supplemented with 10 µM Y-2763 and 2 µg/ml doxycycline. The next two days (DIV1+ DIV2), full medium changes were performed with N2-medium + 2 µg/ml doxycycline. At DIV3, pre-differentiated NGN2 iNeurons were detached with Accutase, centrifuged for 3 minutes at 300 xg and resuspended in iNeuron freezing medium (**Table 15**). Per cryovial, $1x10^6$ cells were added and cryovials were frozen at -80 °C in Mr. Frosty™ freezing containers overnight to ensure a stable cooling. For long-term storage, cryovials were transferred at -150 °C or in liquid nitrogen tanks.

2.2.10.2 ASCL1/DLX2 (AD2)-based differentiation of stable iPSC to DIV8 interneurons

On DIV0, stable AD2-iPSC were enzymatically detached using Accutase. After the centrifugation for 3 minutes at 300 xg, cells were counted. Required number of 6-well plates were coated with Matrigel beforehand, and $1.05x10^5$ cell/cm^2 were seeded in IPS-SLX medium supplemented with 10 µM Y-2763 and 2 µg/ml doxycycline. The following day (DIV1), medium was replaced by IPS-SDP medium + 2 µg/ml doxycycline. At DIV2, medium was replaced by IPS/N2B27 medium + 2 µg/ml doxycycline. Full medium change to N2B27/IPS medium +

2 µg/ml doxycycline was performed at DIV5, which was repeated until DIV8. Pre-differentiated iNeurons were detached and frozen in iNeuron freezing medium as described in section 2.2.10.1.

2.2.10.3 NGN2-AD2 co-culture setup

For the co-cultivation of stable NGN2 and AD2 at DIV0, cryopreserved iNeurons were always freshly thawed. Thawed iNeurons were then gently transferred to a 15 ml falcon tube containing 3 ml of pre-warmed DMEM/F12 and carefully resuspended. After centrifugation for 3 minutes at 300 xg, the supernatant was discarded and iNeurons were resuspended in NB27+ medium supplemented 10 µM Y-2763 and 2 µg/ml doxycycline. Cell suspensions of AD2 iNeurons were passed through a 40 µm cell strainer and collected in a new 15 ml falcon tube to get rid of cell clusters formed during the pre-differentiation step. After counting, a total number of $1.56x10^5$ cells/cm^2 were seeded onto one well of PLO-hydro/laminin/fibronectin-coated 96-well plates in NB27+ medium supplemented with 2 µg/ml doxycycline with a NGN2-AD2 ratio of 80:20. After 24 h of neuronal attachment, full medium change was performed with NB27+ medium + 2 µg/ml doxycycline and $3.125x10^4$ murine astrocytes/cm^2 were seeded to each well. To kill remaining non-differentiating cells and to inhibit proliferation of astrocytes, a full medium change with NB27+ medium + 2 µg/ml doxycycline + 2 µg/ml Ara-c was performed at DIV4, which was repeated at DIV7. Half medium changes were performed from DIV11 on until DIV14 with NB27 medium + 2 µg/ml doxycycline. At DIV18, doxycycline was diluted out with a half medium change to NB27 medium. Starting from DIV21, BrainPhys medium was initiated with half medium changes every third day. Neurons were cultured until DIV42, when cellular assays were performed, and cells fixed. A schematic overview of the differentiation processes is depicted in **Figure 2**.

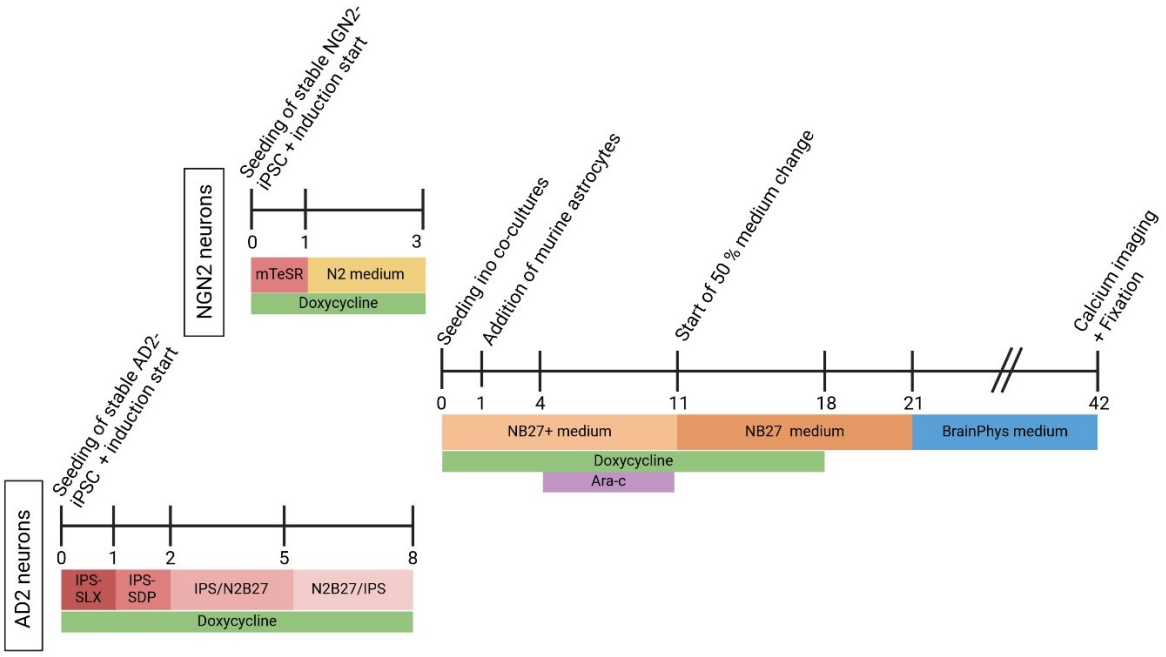

Figure 2. Schematic overview of NGN2 and AD2 iNeuron differentiation and seeding into E-I co-cultures. Differentiation of stable NGN2 and AD2 iPSC is induced by the administration of doxycycline. NGN2 are pre-differentiated for 3 days, whereas AD2 are pre-differentiated for 8 days before seeding into co-culture (DIV0). At DIV1, murine astrocytes are added. Doxycycline administration is performed until DIV18 to induce transgene expression and Ara-c is added for 5 days to kill non-differentiating cells. Co-cultures were cultivated in NB27+ for 11 days, followed by the cultivation in NB27 medium for 10 days and in BrainPhys medium until the end of the culture period (DIV42). Created with BioRender.com.

2.2.11 Preparation of murine astrocytes

P1 pups of the wildtype mice RjOrl:SWISS strain (Janvier-Labs) were used for the isolation of astrocytes (179). In a first step, the head of the newborn pups was separated from the rest of their bodies. Next, the scalp was carefully removed, and the underlying skullcap was cut open from caudal to rostral along the visible midline that separates the two hemispheres, which was then carefully pressed outwards. The brain, that was now easily accessible, was removed with a small spoon and immediately transferred into ice-cold DPBS + 15 mM HEPES buffer + 1 % Penicillin-Streptomycin. The olfactory bulbs and the cerebellum were separated from the cortex using sharp scissors and the meninges were carefully removed with fine forceps under a stereomicroscope. The hemispheres were then isolated and when visible, hippocampi were removed. Cortices were cut into smaller fragments and stored on ice in a falcon tube containing DPBS + 15 mM HEPES buffer + 1 % Penicillin-Streptomycin until further processing. Once all cortices were prepared, DPBS solution was removed from the tube and 5 ml of trypsin/EDTA 0.025 % were added and carefully resuspended. This was followed by an incubation step of 20 minutes in a 37 °C water bath. Finally, trypsin/EDTA solution was replaced by 5 ml of Astrocyte medium (**Table 7**), and cell suspension was resuspended up to 30 times to break up

the large fragments. T75 cell culture flask containing 20 ml of cultivation medium were prepared for further cultivation of isolated cortical cells and cell fragments. Per T75 flask, 4 cortices were added and incubated at 37 °C and 8 % of CO_2. Every other day, full medium changes were performed. After one week, astrocytes were passaged once to get rid of neurons, microglia and oligodendrocytes. After expansion, cells were frozen with passage 1 in cryovials containing $1x10^6$, $2x10^6$ and $5x10^6$ cells/vial in a freezing medium consisting of 90 % FBS + 10 % DMSO.

For cultivation, astrocytes were cultured on uncoated 6-well plates in Astrocyte medium. Full medium changes were performed every other day. For dissociation, astrocytes were washed once with DPBS and then enzymatically detached with trypsin/EDTA 0.025 %. The enzymatic reaction was terminated by adding DMEM/F12, and cells were centrifuged for 3 minutes at 300 xg. For neuronal differentiations, astrocytes in early passages up to P2 were used. Astrocytes were added to the neuronal culture, either freshly thawed P1 astrocytes or cultured P2 astrocytes, which were then detached.

2.2.12 Lentivirus production

To produce third generation lentiviruses, the specialized HEK293FT cell line was used. This cell line stably expresses a neomycin resistance gene, which allows for a cultivation under G418 selection in HEK293FT culture medium (**Table 8**).

2.2.12.1 Transfection of HEK293FT

Prior to transfection, cells were washed once with DPBS and dissociated using trypsin/EDTA 0.025 %. The reaction was stopped using DMEM/F12 and detached cells were centrifuged for 3 minutes at 300 xg. $5x10^5$ viable cells were seeded per T175 flask in HEK293FT cultivation medium without G418 and cultivated at 37 °C and 8 % CO_2. For the generation of a lentiviral construct at least two T175 flasks were used. When HEK293FT reached 80-90 % of confluence, cells were ready to transfect or otherwise transfection was postponed to the next day. For transfection, a plasmid-mix containing 27 µg lentiviral packaging mix + 18 µg plasmid DNA in 4.5 ml Opti-MEM™ and a lipofectamine-mix containing 108 µl Lipofectamine™ 2000 in 4.5 ml Opti-MEM™ were prepared. Both mixes were incubated for 5 minutes at RT in separate reaction tubes. The plasmid-mix was then carefully added to the lipofectamine-mix, without resuspending or inverting, and incubated for further 20 minutes at RT. Meanwhile, the cell culture medium of HEK293FT was discarded and changed to 20 ml of transfection medium. After the incubation step, the plasmid-lipofectamine-mix was added to the HEK293FT in transfection medium (9 ml mix per T175 flask). The flasks were swirled carefully and slowly and incubated at 37 °C and 5 % of CO_2. The following days, the collection of supernatants (48

h and 72 h) was performed under biological safety level 2 conditions. The supernatants were transferred in 50 ml falcon tubes and stored at -80 °C. After collection of the 48 h supernatant, 30 ml of fresh transfection medium was added carefully to HEK293FT cells, while after collection of the 72 h supernatant, cell culture flasks were discarded.

2.2.12.2 Virus preparation

For virus preparation, collected lentiviral suspensions in 50 ml falcon tubes were thawed either overnight at 4 °C or in a water bath at 37 °C for around 1 h. Lentiviral suspension were passed through sterile filters, pipetted into appropriate centrifugation tubes and ultracentrifuged at 19.600 xg for 80 minutes at 4 °C. After carefully removing the supernatant, tubes with the opening downwards were placed on sterilized tissue paper allowing the residual liquid to drain off. Without mixing, 100 µl of PBS + 1 % BSA were carefully pipetted to the viral pellets, and tubes that were sealed with Parafilm were stored over night at 4 °C. After 24 h, generated pellets were resuspended carefully, aliquoted and stored at -80 °C.

2.2.12.3 Determination of lentiviral titers

The Lenti-X p24 Rapid Titer Kit was used to perform lentiviral titer determination following the manufacturer's instructions. Briefly, lentiviral suspensions were diluted to concentrations of 10^{-5} and 10^{-10} and plotted against a p24 standard curve. Resulting lentiviral concentrations were in a range from $5x10^{10}$ to $5x10^{11}$ particles per ml. Cells were transduced with lentiviral concentrations of approximately 10 ng/ml or $2x10^{8}$ particles/ml.

2.3 Cellular assays

Cellular assays were performed with different neuronal cell types and different mono-/co-culture setups at their respective timepoint of differentiation.

Main culture types are listed in the following:

I. **smNPC-derived iDANs monocultures**
   - neurite outgrowth assay was performed at DIV4
   - all other cellular assays were performed at DIV14

II. **ALN-NGN2 mono- and co-cultures** (DIV0 indicates ALN-induction start)
   - cellular assays were performed at DIV28 of ALN neurons
   - at this time point NGN2-GFP neurons were at DIV21

III. **stable iPSC-derived NGN2-AD2 co-cultures** (DIV0 indicates co-culture start)

- neurite outgrowth assay was performed at DIV5
- all other cellular assays were performed at DIV42

2.3.1 Neurite outgrowth assay

2.3.1.1 Neurite outgrowth assay with smNPC

Determination of neurite outgrowth of dopaminergic neurons was performed with the directed differentiation protocol starting from smNPC, as the selection step using the lentiviral overexpression protocol generated lot of dead cells making the imaging and further analysis impossible.

Dopaminergic progenitor cells were enzymatically detached using Accutase. At DIV0, $3.125x10^5$ smNPC were seeded onto Matrigel-coated 96-well µClear plates in Patterning medium + 10 µM Y-2763. Per donor, smNPC were seeded into five wells to ensure sufficient technical replicates. Cells were cultured in Patterning medium for three to four days with full medium changes every other day ensuring that cells did not grow too dense. At DIV4, cells were fixed and stained for βIII-tubulin to visualize the neuronal cytoskeleton and Hoechst for nuclear staining as described in 2.3.6. To analyse the outgrowing neurites, the ImageXpress Micro Confocal High-Content Imaging System with a 20x objective was employed. Per well, nine images were acquired, and images were further processed with the software MetaXpress (Molecular Devices) using the 'Neurite Outgrowth' tool. The tool allowed for identification of Hoechst-positive nuclei and outgrowing neurites for which the length was measured automatically. Within individual replicates, thresholds for the detection of Hoechst-positive nuclei and outgrowing neurites were kept constant for all donors. Additionally, the mean value from each well was computed and normalized relative to the control mean.

2.3.1.2 Neurite outgrowth assay of stable NGN2

On DIV0, stable NGN2-based iPSC were seeded into Matrigel-coated transparent 48-well plates at a density of $1.05x10^4$ cells/cm^2 in mTeSR™ Plus medium + 1 % Penicillin-Streptomycin + 10 µM Y-2763 + 2 µg/ml doxycycline. After 24 h (DIV1, t=0), the medium was changed to N2-medium + 2 µg/ml doxycycline to initiate the NGN2 differentiation. Plates were placed in the IncuCyte® Live Cell Analysis System and every 4 h to 6 h brightfield images were acquired with a 10x objective. Per line, cells were seeded into three to four wells and nine images per well were taken. On DIV2, N2 medium change was repeated. At DIV3 and DIV4, medium was changed fully to NB27 medium + 2 µg/ml doxycycline and cells were imaged

without further medium changes until t=120 h. As medium change at DIV3 resulted in detaching and subsequent attaching of cells, tracking of neurites was only possible from timepoint 72 h on. Images were further processed using the IncuCyte® NeuroTrack analysis module. Neurite length (mm) per number of cell body clusters, as well as neurite branch points (mm) per number of cell body clusters were determined for each time point. The analysis parameters were set with a minimum area of 150 µm for the cell body cluster mask and a minimum cell width of 7 µm. Neurite filters were set to a sensitivity of 0.75 including neurites with a width of 1 µm. Imaging methods and filter settings were constant across all independent experiments and images acquired per well were averaged. Timepoint t=72 h was set to 1 for the following reason: during medium change from N2 medium to NB27 medium cells detached and attached again. A plateau of maximum measurable growth was reached at t=120 h. Therefore, the parameters neurite length and neurite branching were analysed at this timepoint.

2.3.2 pLV-EF1α-Synaptophysin-mRuby transduction

For the generation of ALN and NGN2-GFP neurons that overexpress Synaptophysin-mRuby for cell type-specific labelling of presynaptic boutons, iPSC were transduced at DIV0 with the lentiviral vectors pLV-FUdeltaGW-rtTA, pLV-TetO-ALN-Puro and pLV-EF1α-Synaptophysin-mRuby. NPC were transduced with the lentiviral suspension consisting of pLV-FUdeltaGW-rtTA, pLV-TetO-hNGN2-eGFP-Puro and pLV-EF1α-Synaptophysin-mRuby. Further differentiation steps remained the same and are described in sections 2.2.9.2 and 2.2.9.3.

2.3.3 Treatment with a selective DRD2 agonist and antagonist

In one experiment, neurons in ALN-NGN2 co-cultures were treated with a selective DRD2 agonist and antagonist (Pramipexole dihydrochloride a DRD2 agonist, Sulpiride a DRD2 antagonist). Pramipexole, Sulpiride or DMSO only as a solvent control were added to Neuron medium to obtain a final concentration of 10 µM. Treatment was applied for 24 h at 37 ˚C, 5 % CO_2. The next day, calcium imaging was performed as described in section 2.3.4.

2.3.4 Calcium imaging

iDANs and ALN neurons were stained with the green fluorescent calcium indicator 2 µM Cal-520™ diluted in DMEM/F12, whereas NGN2-GFP neurons in monoculture, as well as ALN-NGN2-GFP neurons in the co-culture were stained with 2 µM of the red fluorescent calcium indicator Calbryte™ 590 AM diluted in DMEM/F12. Both dyes were stained for 30 min at 37 °C. Afterwards, cells were washed once with DMEM/F12, and Neuron medium was added.

Neurons were then incubated for 10-15 minutes at 37 °C to allow for recovery, before imaging started. Spontaneous single-cell calcium activity was measured using the Cell Observer SD spinning disk confocal laser scan microscope with a 20x objective and an incubation chamber allowing to record at 37 °C. Therefore, two comparable microscopic areas per well including multiple cells were chosen and recorded for at least 3 minutes at a frame rate of 50 fps. In each biological replicate (one differentiation), two wells per donor were stained and two videos per well were recorded. Recordings were obtained ranging from 3-5 independent neuronal differentiations per donor. To later distinguish between ALN and NGN2-GFP neurons in the co-culture, snapshots of the Calbryte™ 590 AM and GFP signals were taken immediately before starting the recording.

Calcium recordings were further processed in the image processing software Fiji (based on ImageJ). A minimum of five neurons per neuronal subtype and per recording were analysed. Therefore, active neuronal somata were circled with the freehand selection tool and the mean fluorescent intensity of individual neurons were measured over time using the ROI Manager tool. The Origin 2016G Peak Analyzer software (OriginLab Corporation) allowed for processing of these calcium traces. Therefore, the peak analysis tool was used with constant peak detection threshold and constant peak distance within one replicate and calcium traces were normalized to a baseline of 0. Four peak parameters were filtered out: area under the curve (AUC), full width at half maximum (FWHM), amplitude (ΔF/F0) and peak frequency (n peaks/seconds recorded, Hz). Parameters of multiple cells within one well were averaged and normalized to the CTR group for each replicate.

Calcium imaging of stable NGN2-AD2 E-I co-cultures was performed at DIV42. Cells were stained with 2 µM of the red fluorescent calcium indicator Calbryte™ 590 AM diluted in DMEM/F12 as described above. After the incubation period of 30 minutes and washing with DMEM/F12, Tyrode buffer was added to the wells (**Table 17**). This buffer solution has an increased proportion of potassium chloride, which induces the increase of the resting membrane potential and this in turn promotes the generation of action potentials. The buffer was prepared and kindly provided by the electrophysiology group at the NMI in Reutlingen. Calcium imaging of this co-culture followed the same recording and analysis procedure, as described for the ALN-NGN2 co-culture. Except for snapshot taking, as distinction between cell types was not possible.

2.3.5 Global synchronization index (GSI) analysis

Based on recorded calcium imaging data, the GSI was employed to quantify network communications within the cultures and provides a numerical value that describes the level of

synchronization among the spontaneous calcium bursts that occur during recording. Calcium recordings were processed in the image processing software Fiji as described in section 2.3.4. This processed raw data was then transferred into Jupyter Notebook with a Python code, written and kindly provided by Emilio Pardo Gonzalez (Electrophysiology group, NMI, Reutlingen). Mathematical background of GSI determination is described in detail elsewhere (180). The code generates a correlation matrix showing each ROI in comparison with another ROI and computes the GSI for each recording. GSI values were in the range from -1 to 1, whereby values ranging from -1 to 0 indicate no synchronicity, in contrast values ranging from 0 to 1 indicate (partial) synchronicity.

2.3.6 Immunocytochemistry

After several weeks of differentiation, neurons were fixed with 4 % PFA diluted in DPBS for 15 minutes at RT, followed by a DPBS washing step for three times. Next, cells were permeabilized and blocked for unspecific antibody binding using blocking solution consisting of 0.1 % Triton-X100 in DPBS and 1 x blocking reagent BMB for a minimum of 30 minutes at RT. Following blocking, primary antibodies diluted in blocking solution were added in appropriate concentrations and incubated overnight at 4 °C. The next morning, cells were washed three times with DPBS and the secondary antibody solutions (secondary antibodies diluted in blocking solution) were added for 2 h at RT. During this incubation step, the cells were kept on an orbital shaker and protected constantly from light. To stain for DNA, Hoechst dye was diluted in the blocking solution and added 30 minutes before the 2 h incubation time was over. Cells were then washed again three times with DPBS and stored at 4 °C.

2.3.7 Analysis of differentiation efficiency in dopaminergic neuronal cultures

To compare the two dopaminergic neuronal differentiation protocols, the dopaminergic neuronal yield for each approach was determined. Therefore, iDANs and ALN neurons were fixed and stained by immunocytochemistry for the neuronal cytoskeletal marker βIII-tubulin and tyrosine hydroxylase (TH), a dopaminergic neuron marker. Dopaminergic neurons were imaged using spinning disk confocal microscope Cell Observer SD with a 20x objective. Images from 3-5 independent neuronal differentiations (biological replicate) of two CTR donors (CTR1, CTR2) and two SCZ donors (SCZ1, SCZ4) were acquired, without changing laser intensity, exposure time and gain within one biological replicate. Two wells per cell line were stained and five images per well were taken for each replicate. To analyse the differentiation efficiency, the IMARIS Bitplane 10.0.0 software was used. Therefore, the volume of the βIII-tubulin surface (μm^3) and the volume of the TH surface (μm^3) were determined for each image.

To obtain a ratio, the TH surface volume was divided by the respective βIII-tubulin surface volume. Ratios from individual images within one well were averaged.

2.3.8 NGN2 neuronal layer marker quantification

For the quantification of cortical layer marker, NGN2 neurons in monoculture at DIV21 were fixed and stained for the upper-layer marker BRN2 and the deep-layer marker CTIP, as well as Hoechst for visualization of the nucleus. The neuronal marker MAP2 was stained as well, for the validation of neurite formation. Z-stacks were taken with a 20x magnification using the Cell Observer SD spinning disk confocal laser scan microscope. A minimum of two independent differentiations per donor were performed and two images per well with comparable areas were acquired. Further processing was performed in Zen (blue edition, 3.0) by creating orthogonal projections of the taken z-stacks. Exported orthogonal projections were then loaded into Fiji and channels were split. A threshold was set for the channels comprising the BRN2, CTIP and Hoechst signals and the number of particles per channel measured. As the stained markers CTIP and BRN2 are nuclear marker, hence co-localizing with Hoechst, particles positive for CTIP and Hoechst, particles positive for BRN2 and Hoechst, and particles double positive for CTIP and BRN2 were analysed. Number of CTIP-, BRN2- and double-positive cells were divided by the total number of Hoechst-positive cells to obtain ratios. Data obtained from one well was averaged.

2.3.9 Quantification of synaptic marker

To determine synaptic marker expression, ALN-NGN2 neurons in mono or co-cultures were fixed and stained for pre- and postsynaptic markers at DIV28. Stable NGN2-AD2 neurons in co-culture were fixed and stained at DIV42. Z-stacks were taken with a 63x magnification using the Cell Observer SD spinning disk confocal laser scan microscope. Images were acquired from a minimum of three independent neuronal differentiations per donor. Within each biological replicate, two wells per cell line were stained and five areas with comparable MAP2-fibre density were chosen and then imaged.

Further processing of the taken z-stacks was done with the IMARIS Bitplane 10.0.0 software by creating a 3D mask of the MAP2 signal within the z-stack, representing the total neuronal network. This masking step allowed for only detecting synaptic spots laying within the MAP2 volume and not counting any artefacts. The spot detection tool was used to count and quantify synaptic spots laying within the MAP2 mask. In a first step, thresholds for spot intensity and spot size were determined, which were further kept constant for each synaptic marker within a biological replicate. For the quantification of appositions (pre- and postsynaptic marker), the

MATLAB-based ‘Spots Colocalize’ IMARIS XTension plugin was used. According to the resolution limit of the microscope, a maximum spot distance between pre- and postsynaptic spots of 0.2 µm was set.

In the ALN-NGN2 co-culture, GFP-labelling of the NGN2 neurons allowed for distinction between neuronal cell types. As described above, a MAP2 mask was generated to quantify the total volume and total synapse number of the neuronal network. Within the MAP2 mask, a GFP mask was created representing the volume of NGN2 neurons. Again, synaptic spots within the MAP2, as well as within the GFP mask were counted. Volumes and spot numbers from MAP2 and GFP were subtracted from each other to obtain synapse densities on ALN neurons. Synaptic spots were then normalized to the volume of the respective neuronal cell type. Synapses quantified for z-stacks taken within one well were averaged and normalized to the CTR group.

2.3.10 Analysis of AIS length

AIS length was analysed by immunocytochemical staining. For this purpose, ALN and NGN2-GFP neurons in mono- and co-cultures were fixed and stained (see section 2.3.6) for the neuronal cytoskeletal marker βIII-tubulin and the integral membrane protein ankyrin-3 (ANK-3), a major scaffolding protein at the axon initial segment (AIS). Z-stacks were taken from three independent neuronal differentiations with a 63x magnification using the Cell Observer SD spinning disk confocal laser scan microscope. Two wells per cell line were stained and four to five comparable z-stacks per well were acquired. Orthogonal projection images of these z-stacks were generated, exported from the ZEN 3.0 (blue edition) software, and loaded into Fiji. Next, images were split into their different channels to simplify ANK-3 length measurements. The freehand line tool was used to trace ANK-3-positive segments that were then subsequently measured. Per image, four ANK-3-positive segments were measured. In the co-culture, GFP expression of NGN2 neurons allowed to distinguish between ALN and NGN2 neurons as GFP and ANK-3 were co-expressed. Hence, the ANK3-positive segment could be easily assigned to one of the two cell types. Cells showing ANK-3-positive segments without co-expressing GFP were assigned to ALN neurons. Per image, four ANK-3-positive segments for each cell type were measured. The mean ANK-3 length per well and cell type was calculated and normalized to the CTR group within each biological replicate.

2.4 Molecular biology methods

2.4.1 Cloning of a puromycin-resistance gene into the pLV-TetO-ALN plasmid

To allow for a selection step of transduced cells during differentiation, a P2A-Puromycin sequence was inserted at the 3' end of the *ASCL1-LMX1B-NURR1* plasmid as described previously (148). For this purpose, the pLV-TetO-hNGN2-eGFP-Puro plasmid was used as a template, as it contains the desired P2A-Puromycin sequence. Primers were designed to contain the recognition sequences of the two restriction enzymes AgeI and BstBI used for subsequent cloning and append to the amplified P2A-Puromycin sequence (P2A-Puro_fw + P2A-Puro_rv, **Table 21**). The two restriction enzymes are found in the target region of the pLV-TetO-ALN plasmid, thus allowing the insertion of the P2A-Puromycin sequence by restriction digest and subsequent ligation.

2.4.1.1 RT-PCR and gel electrophoresis

A polymerase chain reaction (PCR) was performed to amplify the desired DNA fragment. See **Table 24** and **Table 25** for reaction recipe and temperature profile. 1 % agarose gels were prepared including Midori Green Advance DNA stain (4 µl/100 µl gel) for the visualization of DNA in the gel. PCR products were combined with 1x gel loading dye, loaded on the agarose gel and ran with parameters set to 120 V for 60 minutes. To confirm that PCR was successful, DNA products were visualized using the blue/green LED illumination of the GelDoc Go imaging system. When amplicons had the correct base pair size, PCR products were extracted following the manufacturer's instructions of the QIAquick PCR Purifcation kit.

Table 24. RT-PCR reaction setup

Reagent	**Amount for one reaction (25 µl)**
Platinum II Taq Polymerase	0.19 µl
Platinum GC Enhancer	4.8 µl
5x Platinum II PCR Buffer	4.8 µl
dNTP mix (10 mM)	0.48 µl
Forward primer (10 µM)	1 µl
Reverse primer (10 µM)	1 µl
Nuclease-free water	fill up to 25 µl
Template cDNA	200 ng

Table 25. Temperature profile used for RT-PCR

Step	Temperature	Duration
Initial denaturation	94 ˚C	2 minutes
Denaturation	94 ˚C	30 sec
Annealing	60 ˚C	30 sec
Extension	68 ˚C	30 sec / kb
Final extension	72 ˚C	5 minutes
Holding stage	4 ˚C	∞

2.4.1.2 Restriction digest, ligation and transformation into chemically competent cells

A restriction digest of the purified P2A-Puromycin PCR product, as well as the ALN plasmid was performed by using the two restriction enzymes AgeI-HF and BstBI. Therefore, 1 µl of CutSmart buffer was mixed with 1 µl of AgeI and 1 µl of BstBI, 1 µg of DNA was added and filled up with ddH2O to a total volume of 10 µl, following an incubation step for 2 h at 37 °C on a heating block. Depending on the enzymes used, inactivation with appropriate temperatures was performed for 20 minutes. The digested DNA fragments were then mixed with 1 x gel loading dye and gel electrophoresis was performed to separate the digested DNA fragments as described in section 2.4.2.1. Visualized DNA fragments with expected base pair lengths were isolated from the gel and purified according to the manufacturer's instructions of the QIAquick Gel Extraction Kit.

In a next step, the digested P2A-Puromycin DNA fragment was ligated into the digested ALN plasmid containing sticky ends after digestion with AgeI and BstBI. For ligation, a molar ratio of 1:3 vector to insert was applied (**Table 26**). For calculation of correct molar ratios, the 'NEBio Caclulator®' online tool was used. The mixture was incubated overnight at 16 °C. The next day, the reaction was heat inactivated at 65 °C for 10 minutes. The ligation mixt was either stored at -20 °C or directly transformed into competent cells.

Table 26. Reaction setup used for ligation

Reagent	Amount for one reaction (20 µl)
T4 DNA Ligase buffer (10 X)	2 µl
Vector DNA	0.020 pmol
Insert DNA	0.060 pmol
Nuclease-free water	fill up to 20 µl
T4 DNA Ligase	1 µl

Transformation into chemically competent cells (One Shot TOP10 chemically competent E. coli) was performed following the manufacturer's instructions. Beforehand, LB agar plates were prepared on which 20-100 µl from each transformation vial were spread. Plates were incubated

at 37 °C overnight. After 16 h, grown colonies were picked and transferred into an Erlenmeyer flask containing 50 ml of LB-medium supplemented with the respective antibiotic marker. The bacterial mixture was then incubated at 37 °C overnight in a shaker.

The harvested overnight bacterial culture was purified using the QIAGEN® Plasmid Midi kit and was performed according to the manufacturer's instructions. Purified plasmid DNA was measured at the Nanodrop, Spectrophotometer ND-100. To check whether P2A-Puromycin sequence was successfully inserted into the ALN plasmid, Sanger sequencing of the plasmid was performed by 4base lab AG (Reutlingen) using the sequencing primers ALN-Puro_Seq1 and ALN-Puro_Seq2 (**Table 21**). Successful cloning is shown in **Supplementary Figure 1**.

2.4.2 Cloning of pEF-Synaptophysin-mRuby into a lentiviral backbone

Cloning of pEF1α-Synaptophysin-mRuby into the lentiviral backbone pLV-04CAMKII-s/WPRE and generation of the pEF1α-Synaptophysin-mRuby lentivirus was performed by Lisa-Sophie Wüstner (Molecular Neurobiology, NMI, Reutlingen). Briefly, in a first step, the 04CAMKII promotor of the lentiviral backbone was replaced by the EF1α promotor by using the restriction enzymes ClaI and SpeI that were targeting the 04CAMKII promotor region. RT-PCR allowed for amplification of the EF1α promotor sequence with primers containing the recognition sites of the two restriction enzymes ClaI and SpeI, which were used for subsequent cloning. Restriction digest and ligation of backbone and amplified sequence resulted in the transition plasmid pLV-EF1α/WPRE. Insertion of the Synaptophysin-mRuby sequence in the plasmid pLV-EF1α/WPRE was done by gateway cloning and resulted in the final plasmid pLV-EF1α-Synaptophysin-mRuby, which is shown in **Supplementary Figure 2**.

2.4.3 Transcriptome analysis

Transcriptome analysis was performed with ALN-induced neurons. Neuronal cultures were differentiated until DIV21, as longer cultivation without murine astrocytes was not possible. Neurons were detached enzymatically with Accutase. After centrifugation for 3 minutes at 300 xg, the cell pellet was washed once in DPBS and again centrifuged. Pellets were then frozen immediately at -80 °C. For whole transcriptome sequencing and following differential expression analysis, which were performed by CeGaT GmbH (Tübingen), cell pellets of three independent differentiations were pooled for each donor. GO enrichment analysis was employed using the online PantherDB classification system (https://pantherdb.org/), where statistical enrichment tests for the GO category cellular components (CC) were performed. Hierarchical cluster analysis in the software MeV was carried out with the kind support of Aaron Stahl (Assay Development, NMI, Reutlingen).

The transcriptome data discussed in this thesis are part of a submitted research article and were uploaded to the NCBI's Gene Expression Omnibus (GEO). The data have the GEO Series accession number GSE275064 and are available through the following link: (https://www.ncbi.nlm.nih.gov/geo/query/acc.cgi?acc=GSE275064).

2.5 Statistics

Statistical analysis was performed using GraphPad Prism 10 (GraphPad Software, Inc). Before any statistical test was calculated, outliers were identified by using the Prism 'ROUT' detection tool. By performing normality and lognormality tests, Gaussian distribution was tested using the D'Agostino-Pearson omnibus normality test. Data were regarded as non-normally distributed, if normality test was negative for Gaussian distribution.

For pairwise comparisons, normally distributed data was analysed with unpaired two-tailed t-tests and non-normally distributed data was analysed using an unpaired two-tailed Mann-Whitney U tests.

Group comparisons were analysed by using unpaired ordinary one-way ANOVA with Tukey's multiple comparison tests for normally distributed data. Unpaired Kruskal-Wallis tests with Dunn's multiple comparison post-hoc tests were applied to non-normally distributed data.

Group comparisons with more than one variable, were computed with an ordinary two-way ANOVA with Tukey's or Šídák's multiple comparison test. Statistics were only calculated if three or more biological replicates (independent differentiations) were present.

For each experiment, respective n-numbers and calculated statistical tests can be found in the figure legends. P-values were assigned as follows: *=p≤0.05, **=p≤0.01, ***=p≤0.001, ****=p≤0.0001, ns=not significant.

3. RESULTS

3.1 Comparison of ‘directed’ and ‘lentiviral induced” dopaminergic differentiation

Most published dopaminergic neuron differentiation protocols are based on the addition of growth factors (‘directed differentiation’), which often yields heterogeneous cell populations and additionally demonstrate high variability among differentiations (181). Another differentiation strategy is the lentiviral overexpression of lineage-specific transcription factors to convert iPSC rapidly and directly into dopaminergic neurons resulting in increased dopaminergic neuronal yields (148).

As an important groundwork for this study, two dopaminergic differentiation protocols based on ‘directed differentiation’ and ‘lentiviral overexpression of transcription factors’ were compared by using two different iPSC batches with a distinct disease background, but with the dopaminergic system as the common denominator. The first set included iPSC lines derived from CTR and idiopathic SCZ patients. The second set comprised one isogenic CTR and two *PINK1* K.O. (PINK1 Δ8.9 and PINK1 Δ40.7) iPSC lines that were a kind gift from Dr. Julia Fitzgerald at the Hertie Institute for Clinical Brain Research in Tübingen. PINK1 is a putative mitochondrial serine/threonine kinase playing an important role in the maintenance of mitochondria (182). Mutations in the gene are assumed to be mainly responsible for autosomal-recessive early-onset Parkinson’s disease (PD) (183). Both disorders, SCZ and PD are associated with alterations in dopaminergic neuron projection/circuitry originating from the VTA, as well as the degeneration of dopaminergic neurons in the substantia nigra, respectively (184, 185).

In order to identify the differentiation protocol that yields high dopaminergic neuron purity and less variability among replicates and donors, the differentiation efficiency was assessed. The differentiation strategy that performed best regarding dopaminergic yield was employed for further experiments in this study.

3.1.1 Dopaminergic neurons (iDANs) generated via ‘directed’ differentiation express cell type-specific marker

To evaluate proper dopaminergic neuron generation via directed differentiation based on the protocol developed by Reinhardt et al. (173), neurons were stained for neuronal and dopaminergic neuron-specific markers.

This protocol was based on a two-step differentiation process starting from iPSC via EB formation to smNPC generation (**Figure 3A**). After one week of differentiation, immunocytochemical staining of smNPC revealed robust expression of the neural progenitor markers SOX1, NESTIN, PAX6, GFAP, as well as the neural stem cell marker SOX2. Expression of the transcription factor forkhead box protein A2 (FOXA2) revealed dopaminergic neuron generation and differentiation (**Figure 3B**).

In a second step, generated smNPC were further differentiated into induced dopaminergic neurons (iDANs) (**Figure 3C**). Therefore, smNPC were seeded together with murine astrocytes to improve viability and maturation of dopaminergic neurons cultivated in monocultures. This improvement of neuronal cultures by the addition of murine astrocytes was shown in a previous study by Dr. Ricarda Breitmeyer (Ricarda Breitmeyer, PhD thesis 2021). After two weeks of differentiation (DIV14), immunocytochemical staining was performed and identified the formation of dendrites that were positive for βIII-tubulin and the microtubule-associated protein 2 (MAP2). Co-expression of tyrosine hydroxylase (TH), involved in the synthesis of dopamine (186), as well as FOXA2 confirmed the generation of dopaminergic neurons (**Figure 3C**).

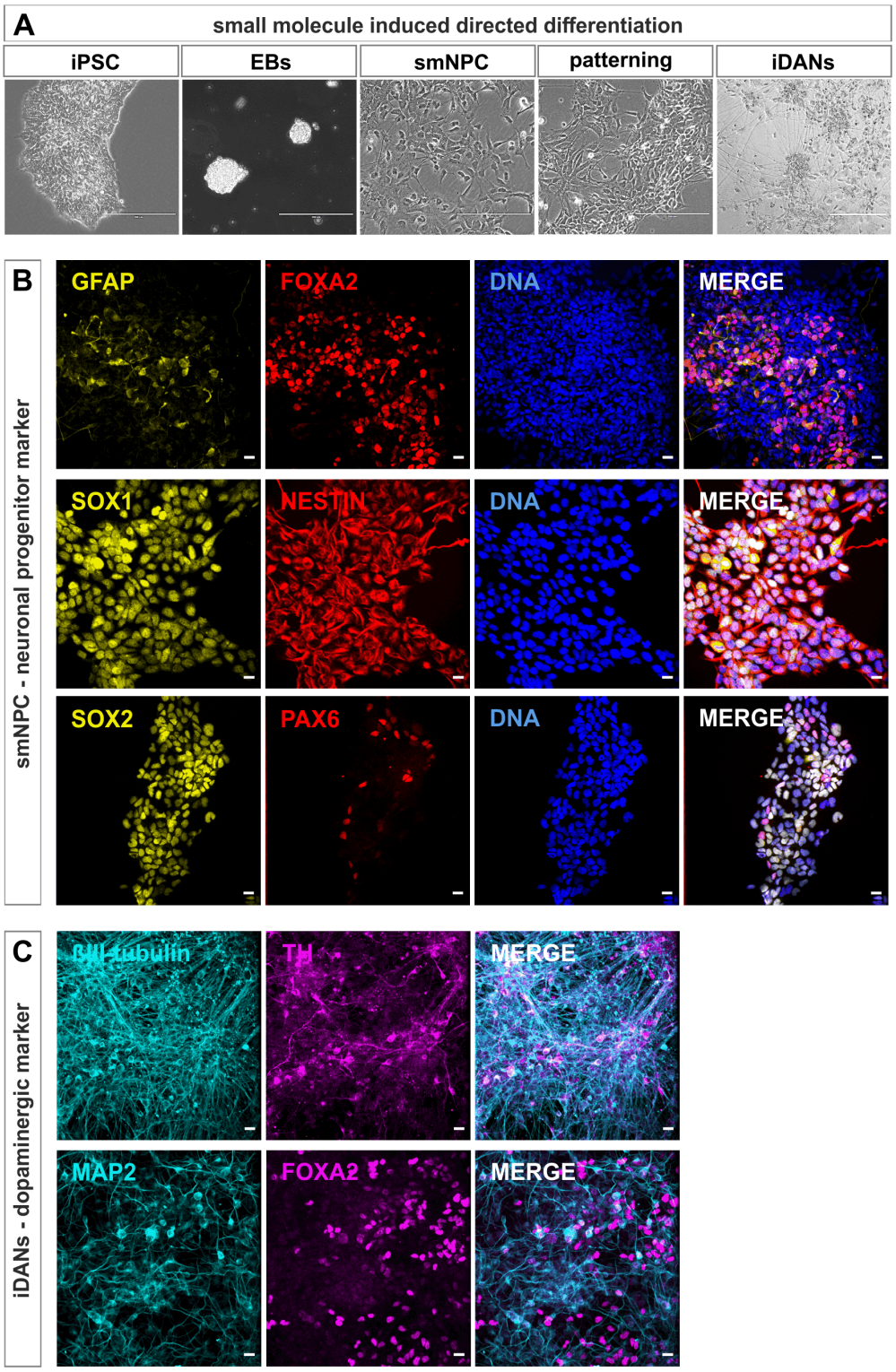

Figure 3. Expression of neural progenitor markers and neuronal markers in 'directed' differentiation of iPSC to dopaminergic neurons. (A) Brigthfield images of intermediate steps required in directed differentiation. Pre-differentiation of iPSC via EB formation to smNPC and further differentiation into iDANs. Scale bars: 200 µm. **(B)** Representative immunocytochemical staining of smNPC positive for neural progenitor markers GFAP, SOX1, NESTIN, PAX6, as well as the neural stem cell marker SOX2 and the early transcription factor FOXA2 involved in dopaminergic differentiation. **(C)** Representative immunocytochemical staining of iDANs expressing the neuronal markers βIII-tubulin and MAP2. Co-expression of markers FOXA2 and TH indicates dopaminergic neuron generation. Scale bars: 20 µm.

3.1.2 Lentiviral overexpression of ALN results in dopaminergic neuronal cells

The generation of ALN-induced dopaminergic neurons followed a described protocol with slight modifications (148). Briefly, iPSC were transduced in suspension with a doxycycline-inducible lentiviral construct overexpressing lineage-promoting transcription factors and differentiated for four weeks (**Figure 4A**). Antibiotic treatment with puromycin allowed for selection of transduced cells in order to maximize purity of cultures. Addition of murine astrocytes improved viability and connectivity of dopaminergic neurons cultivated in monocultures (Ricarda Breitmeyer, PhD thesis 2021).

Immunocytochemical staining of DIV28 ALN-induced neuronal cultures revealed neurons and dendrites positive for the neuronal markers βIII-tubulin and MAP2. Additionally, neurons were stained for the dopaminergic markers TH and FOXA2 co-localizing with Hoechst in the nucleus (**Figure 4B**). This confirmed the generation of dopaminergic neurons via lentiviral induction.

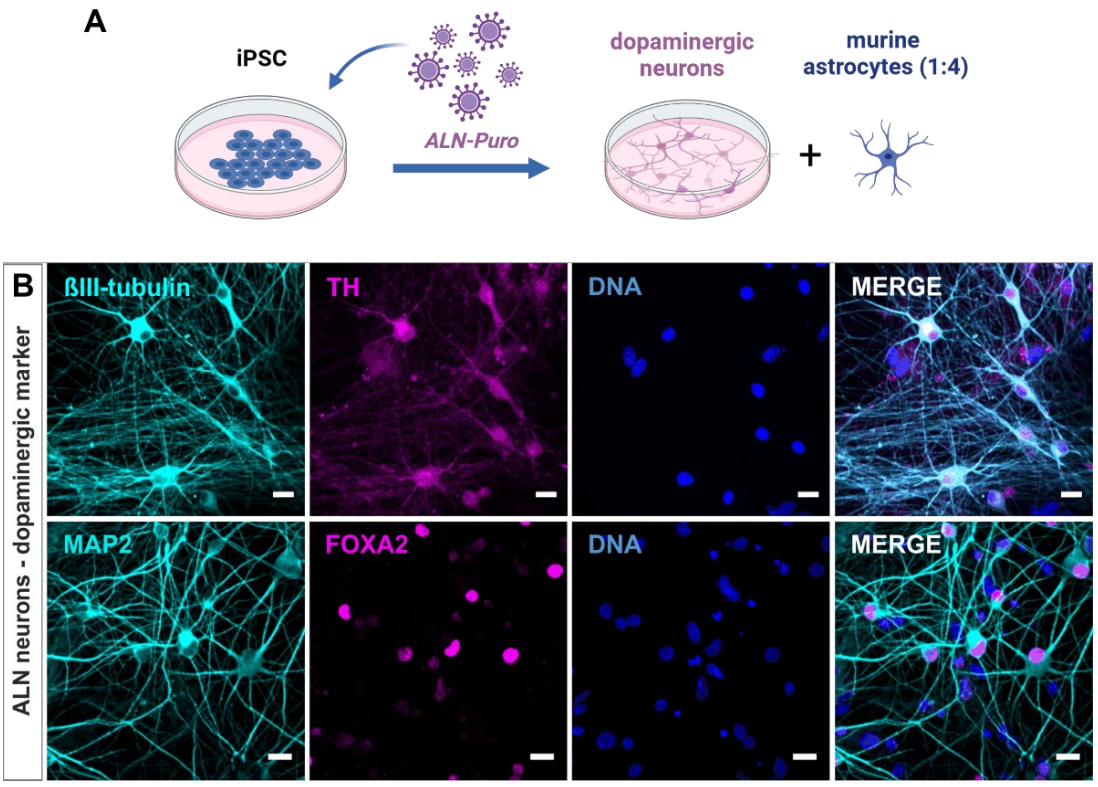

Figure 4. Dopaminergic neuron differentiation via lentiviral overexpression of lineage-specific transcription factors ASCL1-LMX1B-NURR1 results in neurons expressing cell-type specific markers. **(A)** Schematic representation of ALN monoculture setup. iPSC are transduced via lentiviral overexpression of ALN-puromycin for differentiation into dopaminergic neurons (ALN neurons). Primary murine astrocytes are added at a ratio of 1:4. Created with BioRender.com. **(B)** Representative immunocytochemistry (20x) staining of DIV28 ALN neurons positive for neuronal markers βIII-tubulin and MAP2. Co-expression of dopaminergic markers TH and FOXA2, as well as Hoechst for nucleus visualization. Scale bars: 20 µm.

3.1.3 Lentiviral overexpression of *ASCL1-LMX1B-NURR1* leads to increased differentiation efficiency compared to directed differentiation

To assess which differentiation approach leads to a higher yield of dopaminergic neurons, the differentiation efficiency was assessed for both protocols. Thus, the protocols were tested by differentiating both iPSC batches (idiopathic and isogenic iPSC lines) into dopaminergic neurons, respectively. In the first iPSC batch, two CTR lines (CTR1 and CTR2) and two SCZ lines (SCZ1, SCZ2) were picked exemplarily, whereas the second iPSC batch comprised one isogenic CTR and the two iPSC lines carrying a *PINK1* K.O. (PINK1 Δ8.9 and PINK1 Δ40.7). To evaluate the differentiation efficiency, generated neurons were stained for two markers, the neuronal marker βIII-tubulin and the dopaminergic neuron marker TH, which allowed for the analysis and quantification of double-positive neurons.

Generation of dopaminergic neurons via directed differentiation resulted in dopaminergic neuronal yields ranging from 18-35 % for the first batch of iPSC (**Figure 5A**) and revealed variability among independent differentiations. Similar results were obtained for the second batch of iPSC showing a differentiation efficiency in a range of 10-15 % with a more constant yield among differentiations (**Figure 5B**). In contrast, ALN-induced dopaminergic neurons revealed increased differentiation efficiency for both iPSC batches. The two CTR and idiopathic SCZ lines resulted in more homogenous dopaminergic neuron populations reaching a yield of 70-76 % with stable reproducibility among independent differentiations (**Figure 5C**). In addition, the isogenic CTR and the two mutant lines as well yielded higher dopaminergic neuron populations in a range of 50-80 %. Although the second iPSC batch consisted of isogenic lines, the variability among differentiations was relatively high (**Figure 5D**).

Overall, comparison of the two differentiation protocols revealed increased differentiation efficiency by lentiviral transduction of iPSC compared to the directed differentiation protocol. This was validated using iPSC lines with distinct genetic backgrounds and an isogenic model. Noteworthy, differences between CTR and the respective diseased lines were not observed.

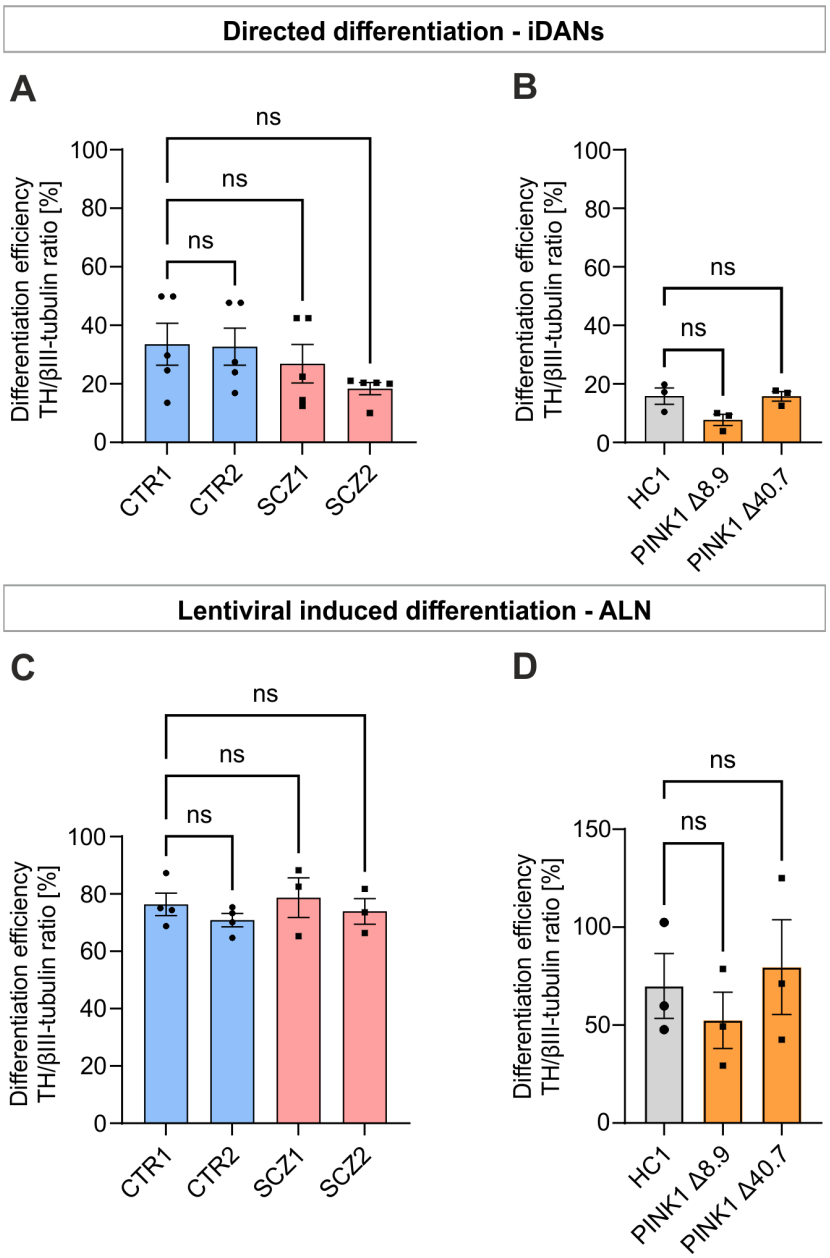

Figure 5. Induced differentiation via lentiviral overexpression of ALN leads to increased dopaminergic neuronal yield compared to directed differentiation. (A-B) Analysis of differentiation efficiency (ratio TH/βIII-tubulin) of directed dopaminergic differentiation protocol for two iPSC batches. **(A)** Analysis of differentiation efficiency for CTR1, CTR2, SCZ1 and SCZ2 (n=5). **(B)** Analysis of differentiation efficiency for HC1, PINK1 Δ8.9 and PINK1 Δ 40.7 (n=3). **(C-D)** Analysis of differentiation efficiency (ratio TH/βIII-tubulin) of lentiviral induced dopaminergic differentiation protocol for two iPSC batches. **(C)** Analysis of differentiation efficiency for CTR1, CTR2, SCZ1 and SCZ2 (CTR n=4, SCZ n=3). **(D)** Analysis of differentiation efficiency for HC1, PINK1 Δ 8.9 and PINK1 Δ 40.7 (n=3). Data points represent averaged values from multiple images taken within two wells per independent differentiation ± SEM. Kruskal Kruskal-Wallis test with Dunn's post-hoc test, ns=not significant.

3.1.4 Distinct calcium properties dependent on the differentiation strategy employed

For further insight into the validity of a disease model, it is imperative to evaluate iPSC-derived neurons on a functional level as well. Depending on the differentiation protocols employed, neurons require a certain time and culture conditions to mature and to demonstrate spontaneous neural activity. Spontaneous synchronous and asynchronous activity is an indicator for the maturation state of the differentiated neuron (144). For this purpose, spontaneous single-cell calcium activity of dopaminergic neurons generated via directed and lentiviral-induced differentiation was analysed. This experiment was performed with the second iPSC batch, since isogenic models usually represent well controllable systems and result in less heterogenous results.

On DIV14 (iDANs) and DIV28 (ALN-induced neurons), spontaneous neuronal activity was determined by calcium imaging. To this end, cells were stained with the green fluorescent calcium indicator Cal^{TM} 520 AM and recorded for 3 minutes. Somatic calcium traces of single neurons were analysed regarding peak frequency as an indicator for the overall activity of the neurons, peak amplitude ΔF/F0 describing the highest fluorescence intensity and as a measure of entered calcium ions. Furthermore, the parameters area under the curve (AUC) and full width at half maximum (FWHM) are surrogates for the calcium flux dynamics occurring during neuronal activity.

Directed differentiation into dopaminergic neurons (iDANs) revealed significantly decreased AUC, FWHM and peak amplitude (ΔF/F0) of PINK1 Δ8.9 and PINK1 Δ40.7 mutant clones compared to the isogenic line HC1, whereas peak frequency was not changed (**Figure 6A-D**). Opposing results were observed in dopaminergic neuronal cultures generated via lentiviral overexpression of ALN. Parameters AUC and FWHM were significantly increased, and the peak amplitude showed a tendency towards elevation in the two mutant *PINK1* cultures. Again, peak frequency was not altered (**Figure 6E-H**).

Taken together, dependent on the differentiation strategy applied, functional characteristics of dopaminergic neurons varies. Since neurons generated via directed differentiation resulted in more heterogenous neuronal populations, this suggests that other neuronal cell types generated could have an impact on neuronal activity. Based on these observations, further experiments in this study were performed using dopaminergic neurons generated via the lentiviral-induced strategy.

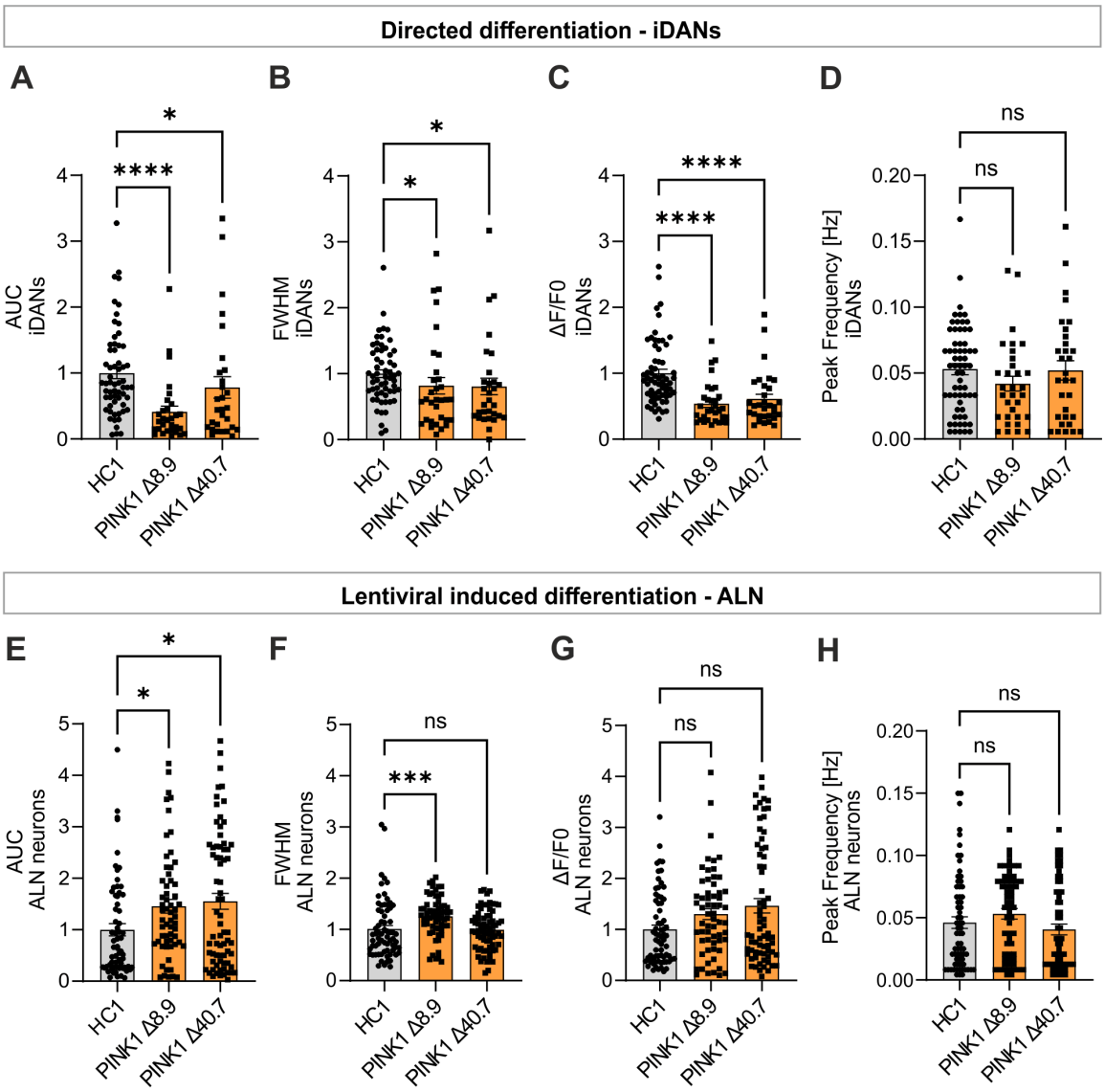

Figure 6. Calcium imaging revealed differentiation-dependent distinct functional properties of generated dopaminergic neurons. (A-D) Analysed calcium imaging parameters of iDANs (directed differentiation). **(A)** AUC of iDANs (HC1 n=60, PINK1 Δ8.9 n=30, PINK1 Δ40.7 n=29). **(B)** FWHM of iDANs (HC1 n=59, PINK1 Δ8.9 n=32, PINK1 Δ40.7 n=30). **(C)** ΔF/F0 of iDANs (HC1 n=63, PINK1 Δ8.9 n=32, PINK1 Δ40.7 n=31). **(D)** Peak frequency of iDANs (HC1 n=62, PINK1 Δ8.9 n=32, PINK1 Δ40.7 n=31). **(E-H)** Analysed calcium imaging parameters of ALN-induced neurons. **(E)** AUC of ALN (HC1 n=64, PINK1 Δ8.9 n=60, PINK1 Δ40.7 n=71). **(F)** FWHM of ALN (HC1 n=68, PINK1 Δ8.9 n=63, PINK1 Δ40.7 n=71). **(G)** ΔF/F0 of ALN (HC1 n=68, PINK1 Δ8.9 n=61, PINK1 Δ40.7 n=69). **(H)** Peak frequency of ALN (HC1 n=68, PINK1 Δ8.9 n=60, PINK1 Δ40.7 n=63). Data points represent values of individual recorded cells ± SEM. Values are normalized to HC1, while values of peak frequency are represented as absolute values. Data were obtained from a minimum of three independent differentiations per donor. Kruskal Kruskal-Wallis test with Dunn's post-hoc test, ns= not significant, *=p≤0.05, ***=p≤0.001, ****=p≤0.0001.

3.2 Transcriptome analysis of ALN neurons confirms a dopaminergic phenotype and identifies differentially expressed genes in SCZ

Before focusing on the transcriptome analysis, the neurite outgrowth and neurite branching ability of dopaminergic progenitor cells (smNPC) were assessed to identify morphological phenotypes during early neurodevelopment in SCZ. After three weeks of differentiation, transcriptome analysis of ALN-transduced neurons comprising the three CTR (CTR1, CTR2, CTR3) and the four idiopathic SCZ (SCZ1, SCZ2, SCZ4, SCZ4) lines was performed to confirm the expression of dopamine-specific markers, as well as to evaluate the neurodevelopmental state and to identify deregulated genes in SCZ neurons compared to healthy controls. To gain further insight into the transcriptomic profile, a hierarchical cluster analysis as well as a gene ontology (GO) enrichment analysis were carried out. Secondly, the developmental state of dopaminergic neurons was evaluated focusing on stem cell and neural progenitor marker genes. In a final step, the expression levels of dopamine metabolism genes and dopamine receptor genes between CTR and SCZ ALN neurons were compared and will be described in the following section.

3.2.1 Neurite outgrowth is unchanged in SCZ smNPC

An important aspect in the study of neurodevelopmental disorders are aberrations that can be observed in early stages of neuronal development. In order to assess early morphological aberrations during development, the neurite outgrowth and neurite branching capacity of smNPC were investigated.

As previous experiments showed that analysis of neurites via lentiviral overexpression was not possible due to the selection step for several days, and Johanna Heider showed that subtle differences in neurite outgrowth are undetectable via forced overexpression of transcription factors (Johanna Heider, PhD thesis 2024), the directed differentiation of iPSC into smNPC was employed for this experiment. These neural progenitor cells represent an earlier phase of development compared to the DIV21 old ALN neurons.

To analyse neurite outgrowth and neurite branching of iPSC-derived dopaminergic neurons, iPSC of two CTR lines (CTR2, CTR3) and four SCZ lines (SCZ1, SCZ2, SCZ4, SCZ5) were differentiated into smNPC via directed differentiation for four days (for more details see section 2.3.1.1). Automated analysis using the ‘Neurite Outgrowth’ tool revealed no differences in neither mean neurite outgrowth per cell nor in mean neurite branching per cell between CTR and SCZ smNPC (**Figure 7A,B**). These results indicate that there are no basic differences in early development at the morphological level.

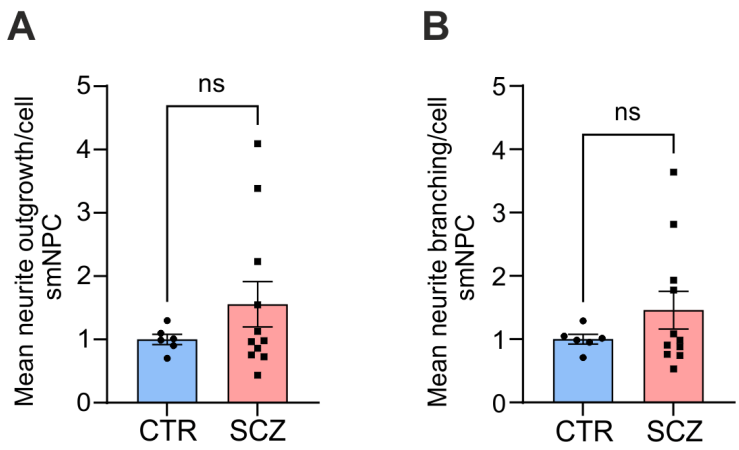

Figure 7. Unaltered neurite outgrowth of dopaminergic progenitor cells. (A-B) Mean neurite outgrowth per cell and mean neurite branching per cell. iPSC were differentiated to smNPC via directed differentiation until DIV4. Per well, nine High-Content images were acquired and processed with the 'Neurite Outgrowth' tool. Within individual replicates, thresholds for nuclei and neurite detection were kept constant for all donors. **(A)** Mean neurite outgrowth per cell. **(B)** Mean neurite branching per cell. Data points represent averaged values of the nine acquired images per well ± SEM. Data were obtained from three independent differentiations per donor. Two-tailed Mann Whitney U test, CTR ALN n=6, SCZ ALN n=11, ns=not significant.

3.2.2 RNA expression profiling reveals thousands of differentially expressed genes in SCZ ALN neurons

In total, 1559 DEGs were identified of which 723 genes were downregulated and 836 genes were upregulated (cut-off padj<0.05, **Figure 8A**). Hierarchical cluster analysis of the top 5 % of down- and upregulated DEGs was carried out with the kind support of Aaron Stahl (Assay Development, NMI, Reutlingen), and revealed two subsets of clusters: one cluster comprising CTR ALN neurons (CTR1, CTR2, CTR3) and the second cluster comprising SCZ ALN neurons (SCZ1, SCZ2, SCZ3, SCZ4) (**Figure 8B**). A list with the top 5 % of DEGs, as well as their function and implication in SCZ can be found in **Supplementary Table 1.**

To obtain more insight into deregulated gene sets in the category cellular components (CC; cut-off q-val <0.05), gene ontology (GO) enrichment analysis was performed using the online classification system PantherDB (https://pantherdb.org/) that allows for identification of deregulated pathways from GO databases. Among the most prominent downregulated pathways in CC, gene sets were annotated with cellular anatomical entity, synapse, cellular component and neuron projection (**Figure 8C**). In contrast, gene sets associated with plasma membrane bounded cell projection, apical part of cell, cilium, cell periphery and extracellular matrix were upregulated (**Figure 8D**). A complete list with all gene sets down- and upregulated can be found in Fehler! Verweisquelle konnte nicht gefunden werden..

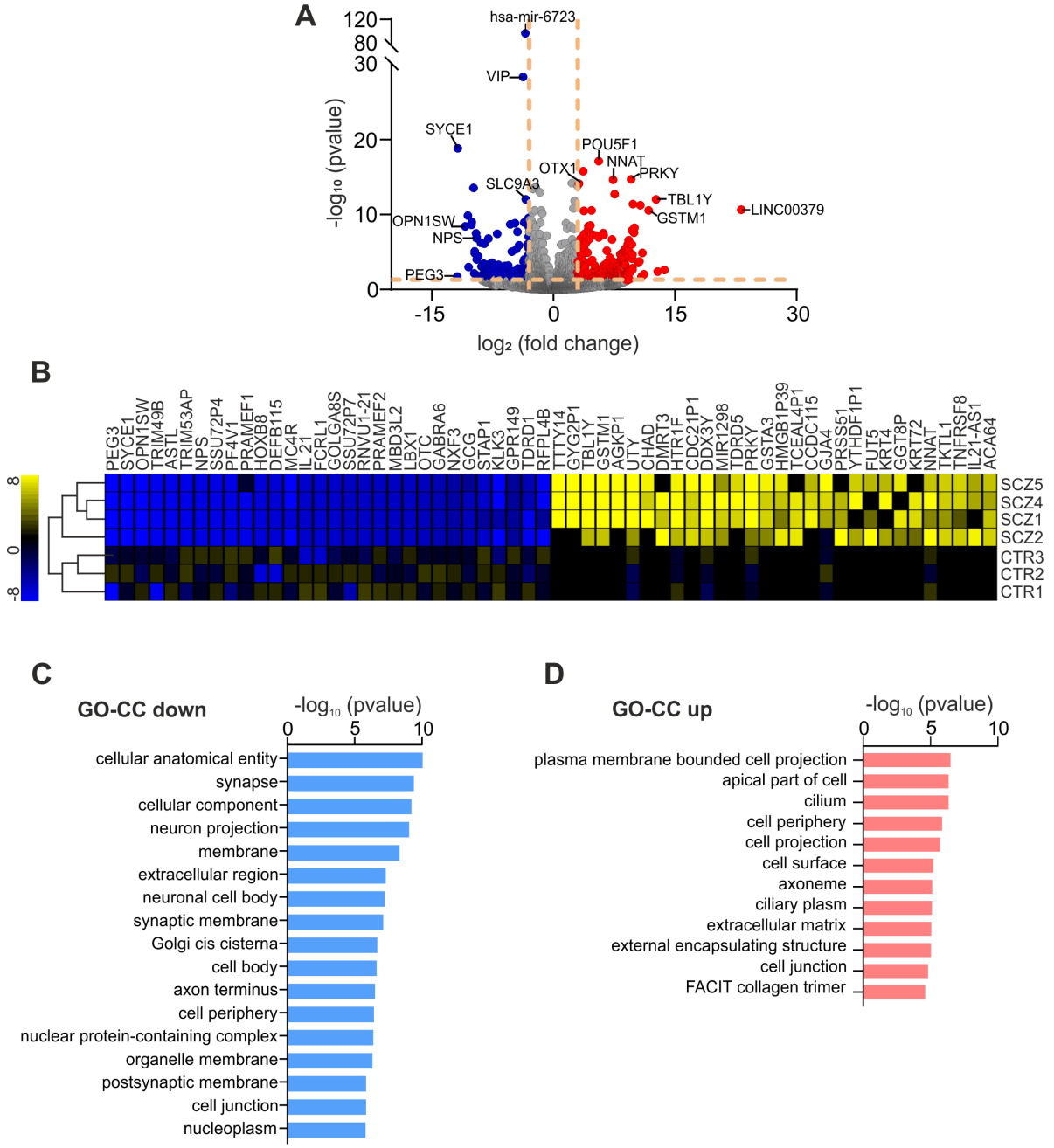

Figure 8. Transcriptome analysis reveals 1559 differentially expressed genes in SCZ ALN neurons. (A) Volcano plot of significantly deregulated genes (cut-off levels for y-axis=1.3 (-log10(pvalue)≤0.05); for x-axis=<3 and >3) depicted by brown lines, blue dots indicate downregulated, red dots indicate upregulated genes) identified by RNA sequencing of ALN neurons differentiated for 21 days (CTR n=3, SCZ n=4). **(B)** Hierarchical cluster analysis of the top 5 % of up- and downregulated DEGs revealed segregation of CTR and SCZ samples. **(C-D)** GO enrichment analysis (PantherDB) identified deregulated gene sets in the category cellular components CC. **(C)** Top 17 downregulated pathways (blue) and **(D)** top 12 upregulated pathways (red) are depicted.

3.2.3 CTR and SCZ ALN neurons differ in their developmental state

To assess the developmental state of ALN neurons and to identify possible developmental differences between CTR and SCZ, the expression levels of stem cell marker and neural progenitor marker genes, as well as early transcription factors were examined in differentiating dopaminergic neurons. It should be noted that the following graphs are normalized read counts and thus, overlapping SEM bars were considered non-different, whereas non-overlapping SEM bars were considered different between CTR and SCZ.

Closer inspection of the normalized read counts revealed upregulation of stem cell marker genes including POU5F1, LIN28A, NANOG and SOX2 (**Figure 9A-D**), as well as neural progenitor marker genes including PAX6 and the progenitor surface marker FGFR1 (**Figure 9E,H)** in SCZ ALN neurons. In contrast, no differences were found for the neural progenitor marker gene NES, whereas FZD9 was downregulated in SCZ ALN neurons (**Figure 9F,G**).

To assess early neurodevelopmental aberrations, a focus was set on early transcription factors that are crucial for dopaminergic neuron differentiation. RNA sequencing of SCZ ALN neurons identified drastic downregulation of gene transcripts for FOXA2, a transcription factor important for midbrain development (187), ASCL1 and LMX1B that are involved in dopaminergic neuronal commitment and proliferation, and NURR1 which is crucial for the expression of dopamine metabolism genes (188) (**Figure 9I-L**).

In summary, RNA sequencing of ALN neurons derived from patients with SCZ revealed increased expression levels of stem cell and neural progenitor marker genes, whereas early transcription factors essential for dopaminergic neuron development and differentiation were downregulated. These findings suggest that SCZ ALN neurons are in a delayed developmental state and aberrant expression of early dopaminergic genes indicates a distinct differentiation state.

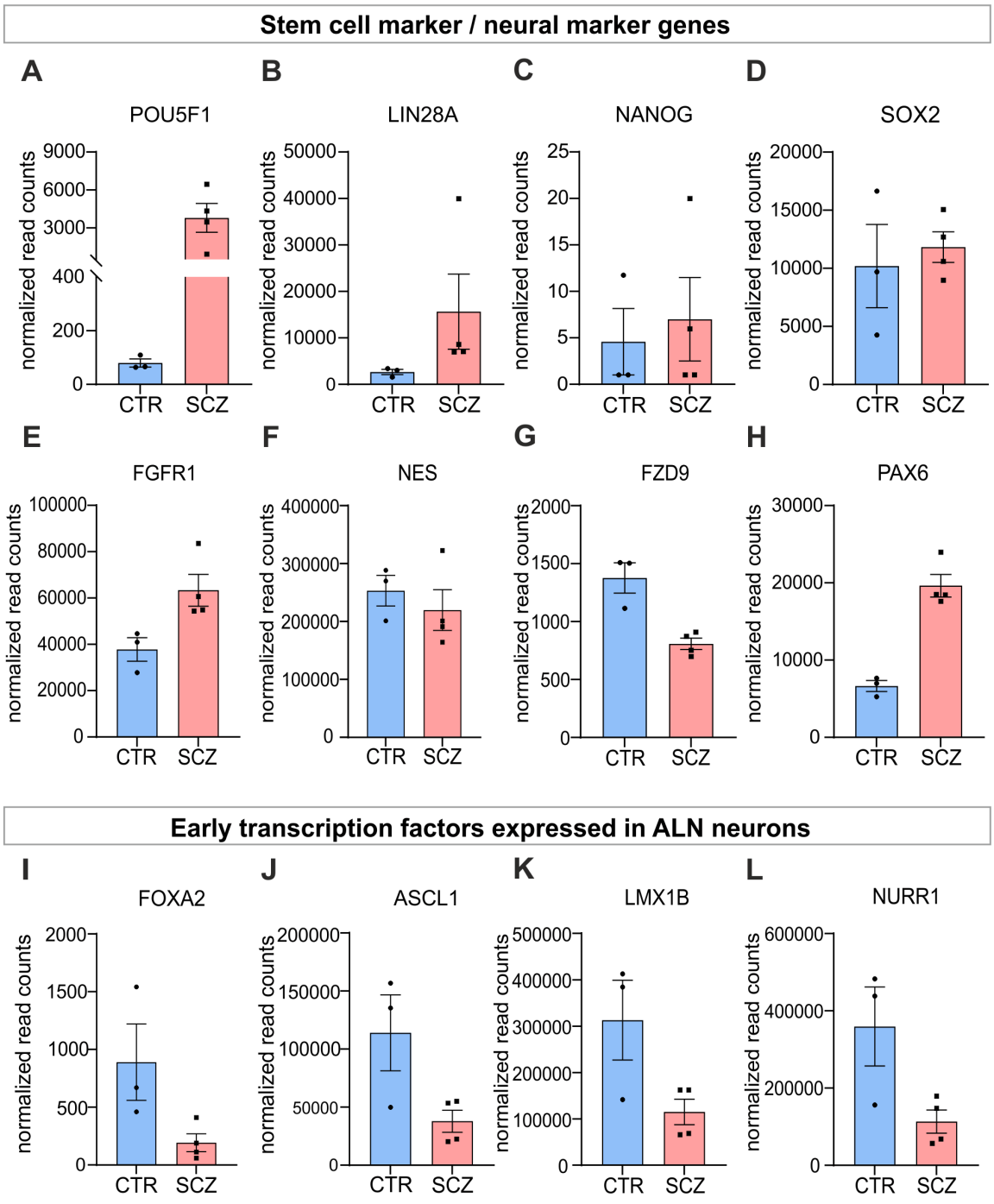

Figure 9. SCZ ALN neurons show distinct developmental and differentiation states. (A-D) Normalized expression of stem cell marker genes **(A)** POU5F1, **(B)** LIN28A, **(C)** NANOG and **(D)** SOX2. **(E-H)** Normalized expression of neural progenitor **(E)** PAX6, **(F)** NES, **(G)** FZD9 and **(H)** FGFR1. **(I-L)** Normalized expression of early transcription factors in dopaminergic neurons **(I)** FOXA2, **(J)** ASCL1, **(K)** LMX1B and **(L)** NURR1. RNA of ALN neurons was extracted after three weeks of differentiation and was derived from three independent differentiations. Normalized read counts depicted as mean ± SEM. (CTR n=3, SCZ n=4).

3.2.4 Downregulation of dopamine metabolism genes in SCZ ALN neurons

As RNA sequencing revealed differences in the developmental state of SCZ ALN neurons and depicted a distinct dopaminergic differentiation state, genes involved in dopamine metabolism might also be affected. For this reason, this chapter focuses on dopamine metabolism genes.

Normalized read counts of genes involved in dopamine synthesis TH, dopamine beta-hydroxylase (DBH), aromatic l-amino acid decarboxylase (DDC) were found to be significantly downregulated in SCZ ALN neurons (**Figure 10A-C**). In contrast, COMT, the gene encoding the catechol-O-methyltransferase, which is important for the inactivation and clearance of dopamine (189) was upregulated (**Figure 10D**). Furthermore, downregulation of genes SLC18A1 and SLC18A2 encoding for the vesicular monoamine transporter 1 and 2 (VMAT1, VMAT2) was observed (**Figure 10E,F**). VMAT1 and VMAT2 are important for the transfer of cytosolic dopamine into synaptic vesicles. In addition, the dopamine transporter (DAT) was drastically downregulated, that is encoded by the SLC6A3 gene (**Figure 10G**).

Overall, transcriptome analysis of SCZ ALN neurons revealed decreased expression of genes involved in dopamine synthesis implying a hypodopaminergic phenotype which was further supported by the upregulation of COMT.

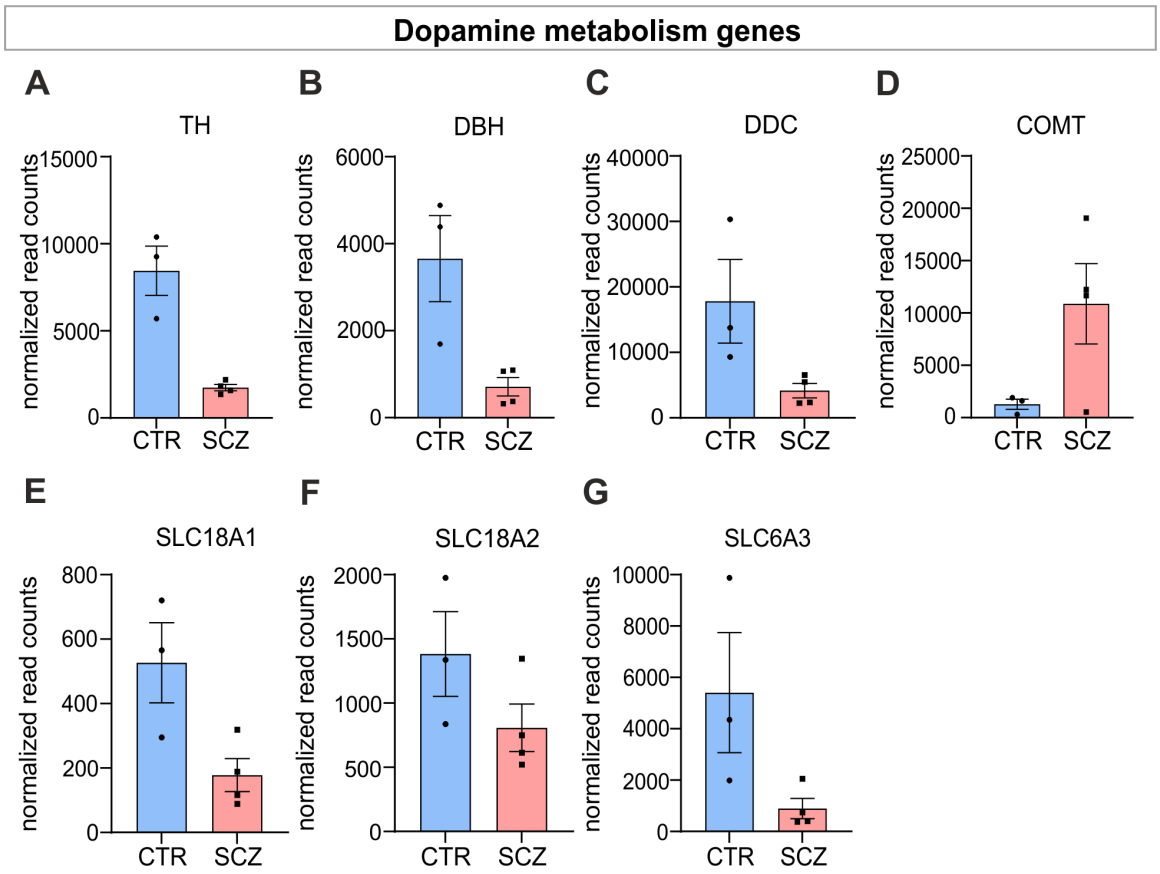

Figure 10. Altered dopamine metabolism in SCZ ALN neurons. **(A-C)** Normalized expression of dopamine synthesis genes **(A)** TH, **(B)** DBH, **(C)** DDC and the dopamine degradation gene **(D)** COMT. **(E-G)** Normalized expression of genes important for the transfer of dopamine into synaptic vesicles **(E)** SLC18A1, **(F)** SLC18A2 and into the cytosol **(G)** SLC6A3. RNA of ALN neurons was extracted after three weeks of differentiation and was derived from three independent differentiations. Normalized read counts depicted as mean ± SEM. (CTR n=3, SCZ, n=4; TH=tyrosine hydroxylase, DBH=dopamine beta-hydroxylase, DDC=L-amino acid decarboxylase, COMT=catechol-O-methyltransferase, SLC18A1/2=solute carrier family 18 member1/2 (encoding for VMAT1/VMAT2), SLC6A3=encoding for DAT).

3.2.5 Altered dopamine receptor DRD2 expression in SCZ ALN neurons

Dopamine metabolism genes were found to be deregulated in SCZ ALN neurons. To assess whether this might interfere with more downstream dopamine signalling pathways, the gene transcripts of all five receptors were examined. Especially, the DRD2 is of great interest as it serves as a dopaminergic autoreceptor regulating feedback-inhibition and controlling the synthesis and release of dopamine (190).

RNA sequencing detected the expression of all five dopamine receptors. However, the expression levels between receptors showed large differences. Highest expression level was found for DRD2 which was strongly decreased in SCZ ALN neurons (**Figure 11B**), while DRD1, DRD3, and DRD5 were hardly detectable (**Figure 11A,C,E**). In addition, DRD4 showed a

moderate expression level with no differences between CTR and SCZ ALN-transduced neurons (**Figure 11D**).

In conclusion, transcriptome analysis of SCZ ALN-transduced neurons demonstrated that among the five identified receptor genes, DRD2 was most abundantly expressed suggesting an inhibitory action. Additionally, DRD2 was found to be downregulated in SCZ ALN neurons which could point towards reduced inhibition in these neurons.

To conclude, differentiation of iPSC into dopaminergic neurons via overexpression of lineage-specific transcription factors resulted in neuronal cells expressing unique marker genes specific for dopaminergic neurons, which was evaluated by RNA sequencing. Moreover, RNA sequencing identified DEGs in SCZ ALN neurons that were mainly associated with synapse and neuron projection, as well as extracellular matrix. Moreover, increased expression of stem cell and neural progenitor marker genes accompanied by reduced expression of core transcription factors crucial for dopaminergic neuron development observed in SCZ ALN neurons suggest a delayed developmental state compared to CTR ALN neurons. Furthermore, this might lead to a hypodopaminergic phenotype, as shown by downregulation of dopamine metabolism genes. The high expression levels of DRD2 support the role of DRD2 as an autoreceptor expressed by dopaminergic neurons. Reduced expression levels of DRD2 in SCZ ALN neurons imply less inhibition in SCZ cultures.

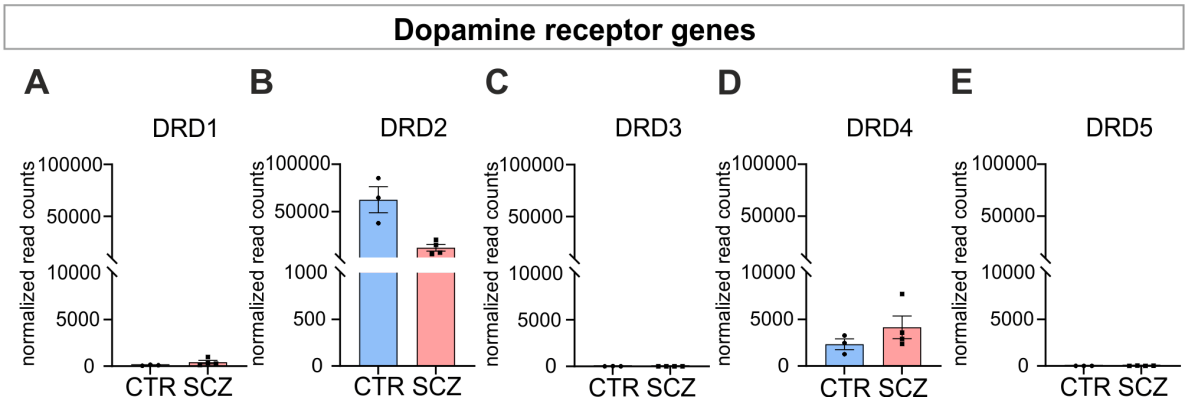

Figure 11. DRD2 expression is decreased in SCZ ALN neurons. (A-E) Normalized expression of D1-like receptors **(A)** DRD1 and **(E)** DRD5 and D2-like receptors **(B)** DRD2, **(C)** DRD3 and **(D)** DRD4. RNA sequencing identified DRD2 as dopamine receptor gene highly expressed, whereas the expression of DRD3 and DRD5 was hardly detectable. RNA of ALN neurons was extracted after three weeks of differentiation and derived from three independent differentiations. Normalized read counts depicted as mean ± SEM (CTR n=3, SCZ, n=4).

3.3 NGN2 neurons mainly express cortical layer II marker

Transcriptome profiling of ALN-derived dopaminergic neurons revealed differences in the developmental state between CTR and SCZ suggesting a developmental delay. To identify whether NGN2-derived glutamatergic neurons as well reveal developmental deficits in SCZ, NGN2 neurons cultured individually were examined. In addition, this experiment served to identify whether differentiated excitatory neurons express telencephalic markers, which was of great importance for following co-culture experiments.

For this purpose, NGN2 neurons differentiated for three weeks and cultivated separately were fixed and stained for the deep-layer marker CTIP (191) and the upper-layer marker BRN2 (192). Hoechst was stained for nucleus visualization and further quantification of layer marker expressions.

Immunocytochemistry revealed that excitatory NGN2 neurons were positive for both layer markers CTIP and BRN2, with a small fraction of neurons that were double positive for both markers (**Figure 12A,B**). For the identification of exact layer marker ratios, numbers of cells positive for CTIP, BRN2 or double-positive were determined and divided by the total number of Hoechst-positive cells. CTR NGN2 neuronal cultures comprised 10 % of CTIP-positive cells, 60 % of BRN2-positive cells and 7 % of cells positive for both markers. Interestingly, in SCZ NGN2 cultures, the ratio of CTIP-positive cells was significantly increased compared to CTR neurons with a total ratio of 27 %. BRN2-positive and double-positive neuronal ratios were unchanged compared to CTR (BRN2+ 62 %, double-positive 16 %, **Figure 12C**).

In summary, the results indicate that NGN2-transduced neurons are telencephalic forming three excitatory cell subpopulations (deep-layer neurons, upper-layer neurons, double-positive neurons). The upper-layer neuronal subpopulation was largest which is important to keep in mind when discussing SCZ-related phenotypes. Furthermore, differences between CTR and SCZ with a higher fraction of deep-layer NGN2 neurons in SCZ suggest altered developmental dynamics.

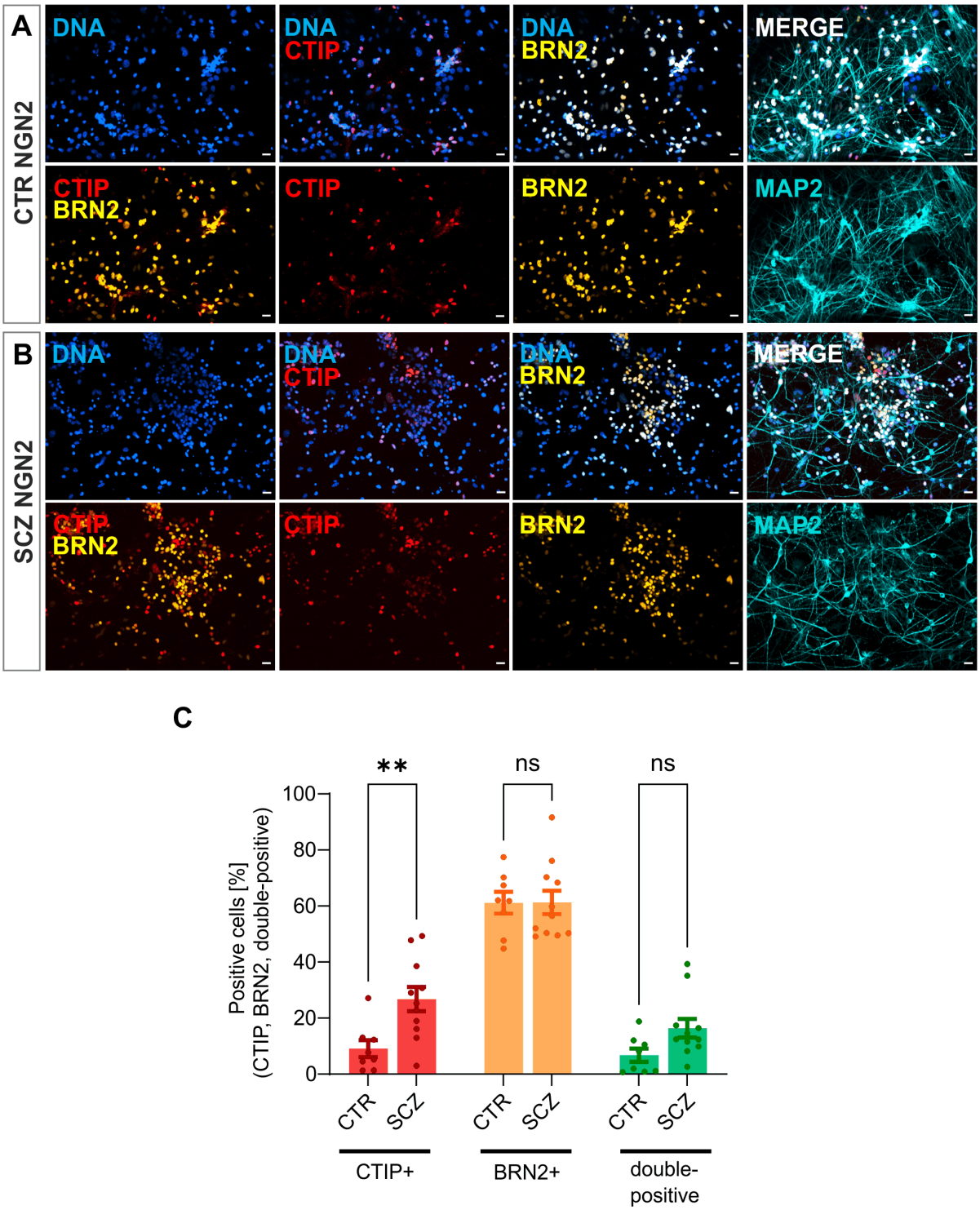

Figure 12. NGN2-induced neurons are positive for deep and upper cortical layer markers. (A) Expression of CTIP and BRN2 in CTR NGN2 neurons at DIV21. **(B)** Expression of CTIP and BRN2 in SCZ NGN2 neurons at DIV21. Scale bars 20 µm. **(C)** Quantification of CTIP, BRN2 and double-positive cells in NGN2 cultures of CTR and SCZ neurons. Data points represent averaged values from two images taken within one well ± SEM. Data were obtained from minimum two independent differentiations per donor. Two-way ANOVA with Šídák's multiple comparison test, CTR n=8, SCZ n=11, **=p≤0.01, ns=not significant.

3.4 Establishment and characterization of an iPSC-derived dopaminergic-glutamatergic co-culture model

In this part, an iPSC-derived co-culture model system comprising dopaminergic and glutamatergic neurons was established to study dopaminergic-glutamatergic neuron interactions in SCZ in more detail. *In vivo*, interactions of those two neuronal cell types can be found within the mesocortical pathway that originates from the VTA in the midbrain and projects into the PFC. In SCZ, several studies propose that the mesocortical pathway is characterized by a hypodopaminergic state. Compared to conventional monocultures, co-cultures comprising more than one cell type in defined ratios can closely recapitulate the *in vivo* situation as they represent more physiologically relevant and complex systems. Additionally, these cultures can be used to study reciprocal interactions of respective cell types affected in the disease.

The established co-culture system consists of dopaminergic and glutamatergic neurons. ALN-derived dopaminergic and NGN2-derived glutamatergic neurons were generated via lentiviral overexpression of the respective lineage-promoting transcription factors, followed by seeding into co-culture. This approach is outlined in section 2.2.9 and is depicted schematically in **Figure 13**.

Additionally, murine astrocytes were co-seeded to increase viability and maturation of neurons which was demonstrated in previous work (Ricarda Breitmeyer, PhD thesis 2021). As described in the first part of this study (section 3.1), the choice of differentiation protocols used represents an important basis as distinct differentiation approaches vary in their reproducibility and neuronal yield.

In a first step, the established ALN-NGN2 neuronal co-culture was characterized to see whether cell type-specific neuronal markers were expressed, and furthermore functional and morphological phenotypes were examined.

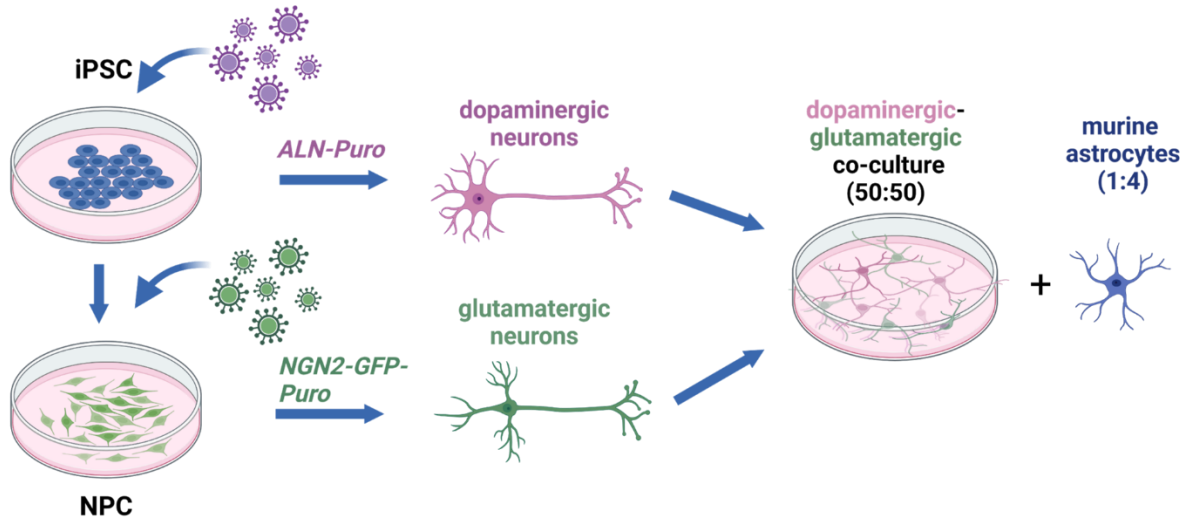

Figure 13. Schematic representation of ALN-NGN2 co-culture setup. Human iPSC are either directly transduced with ALN-puromycin for differentiation into dopaminergic neurons (ALN neurons) or differentiated into NPC by dual SMAD-inhibition. Lentiviral transduction of NPC via NGN2-GFP-puromycin leads to the differentiation into GFP-positive glutamatergic neurons (NGN2 neurons). ALN and NGN2 neurons are seeded into co-cultures at a ratio of 50:50. Primary murine astrocytes are added at a total ratio of 1:4.

3.4.1 Characterization of ALN and NGN2 neurons in co-culture

To check whether ALN- and NGN2-induced differentiations into dopaminergic and glutamatergic neurons were successful in co-culture, immunocytochemical staining of ALN-NGN2 co-cultures was performed at DIV28 (**Figure 14**). In a first step, the expression of neuronal cell type-specific markers in the established ALN-NGN2 co-cultures was exemplary assessed. Therefore, co-cultures were stained with the dopaminergic marker TH, while NGN2 neurons reliably expressed GFP allowing for cell type specific distinction. Neurons positive for TH were identified in co-cultures, as well as neurons expressing GFP, hence indicating the presence of both neuronal cell types after a cultivation period of four weeks (**Figure 14A**). Staining for the neuronal marker MAP2 revealed proper neurite formation with robust expression of the vesicular glutamate transporter 1 (vGLUT1), an excitatory presynaptic marker and synapsin 1 (SYN1), a general presynaptic marker (**Figure 14B,C**).

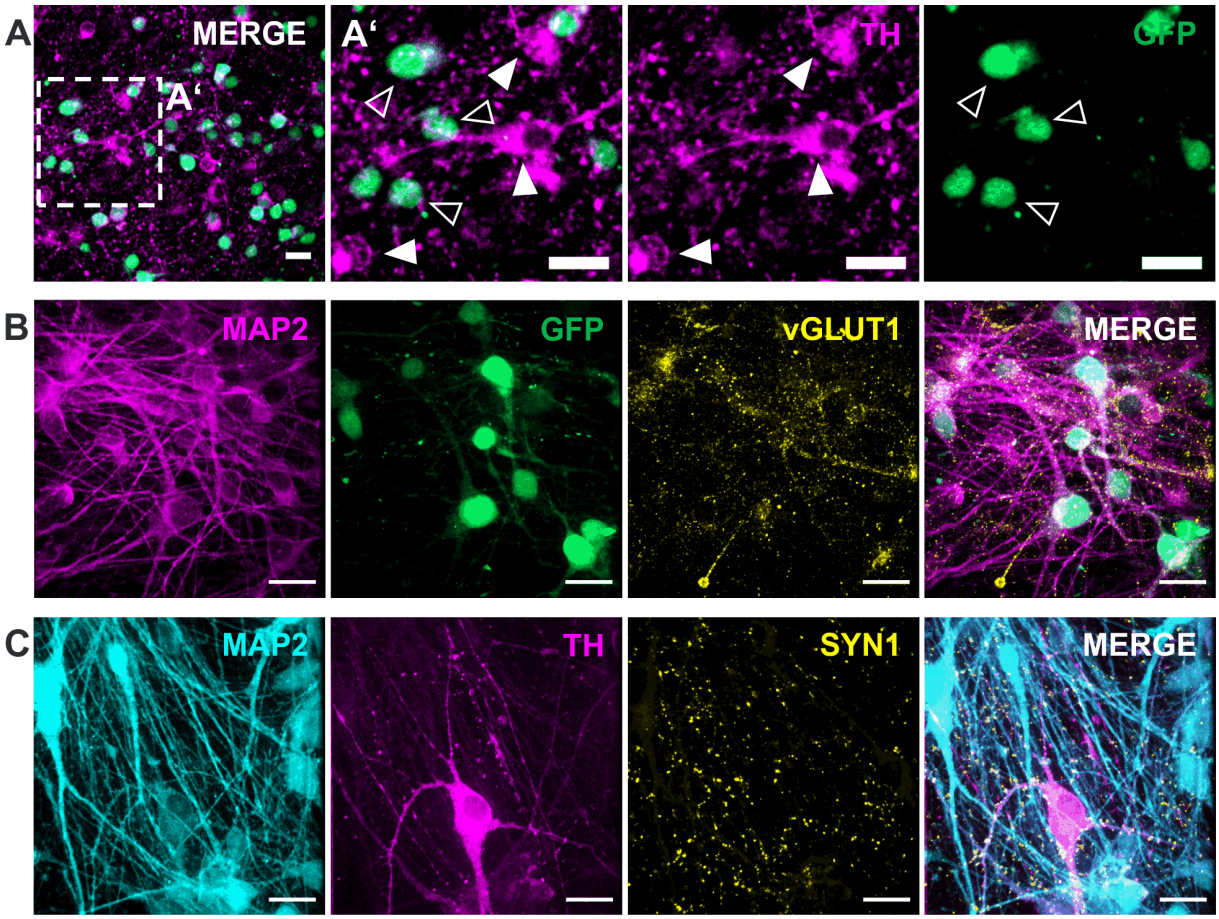

Figure 14. ALN-NGN2 induced neurons in co-culture allow for cell type specific distinction. (A) Immunocytochemical staining of co-cultures showing TH and GFP expression of co-cultured neurons at DIV28. The enlarged section is indicated by the dashed rectangle and depicted in **(A')**. Arrow heads indicate NGN2 neurons, open arrow heads indicate ALN neurons. **(B)** Expression of the neuronal marker MAP2 and glutamatergic presynaptic marker vGLUT1. GFP-labelling indicate generated NGN2 neurons. **(C)** Co-cultures positive for MAP2 and robust expression of the presynaptic marker SYN1. ALN-induced neurons were positive for the dopaminergic marker TH. Scale bars 20 µm.

3.5 Functional characterization of dopaminergic and glutamatergic neurons

To assess functional phenotypes observed in SCZ, neural activity was measured based on spontaneous single-cell activity. To this end, calcium imaging of ALN and NGN2 neurons cultured individually and furthermore of ALN and NGN2 neurons co-cultured was performed.

3.5.1 Unaltered neuronal activity in SCZ dopaminergic and SCZ glutamatergic neurons cultivated separately

As described in section 3.2.5, RNA sequencing suggested a hypodopaminergic phenotype, which was accompanied by decreased expression of the autoreceptor DRD2 involved in inhibitory signalling. To assess whether this might contribute to altered neuronal activity of SCZ ALN neurons, calcium imaging was performed in ALN neurons cultured separately at DIV28.

For this purpose, CTR and SCZ ALN neurons were stained with the green fluorescent calcium indicator Cal^{TM} 520 AM and recorded for 3 minutes (**Figure 15A**). Somatic calcium traces of single ALN neurons were analysed regarding the four parameters AUC, FWHM, ΔF/F0 and peak frequency as described in section 3.1.4.

Comparisons between CTR and SCZ ALN did not reveal differences in AUC and peak amplitude ΔF/F0, whereas FWHM was significantly reduced in SCZ neurons (**Figure 15B-D**). In addition, peak frequency of ALN SCZ neurons was unaltered compared to CTR ALN neurons (**Figure 15E**). Quantitative analysis of individual CTR and SCZ lines can be found in **Supplementary Figure 3A-D**.

In a further experiment, calcium dynamics in NGN2 neuronal cultures were assessed. For this purpose, NGN2 neurons were stained with the red fluorescent calcium dye Calbryte^{TM} 590 AM (**Figure 16A**) and again spontaneous single cell calcium activity was measured over a period of 3 minutes in unstimulated neuronal cultures at DIV21. Analysis of the four parameters AUC, FWHM, ΔF/F0 and peak frequency did not show any differences between CTR and SCZ NGN2 neurons (**Figure 16B-E**). Quantitative analysis of individual CTR and SCZ lines can be found in **Supplementary Figure 3E-H**.

To conclude the results observed in ALN and NGN2 monocultures obtained by calcium imaging of spontaneous single-cell activity, revealed unaltered calcium activity patterns in SCZ neuronal cultures.

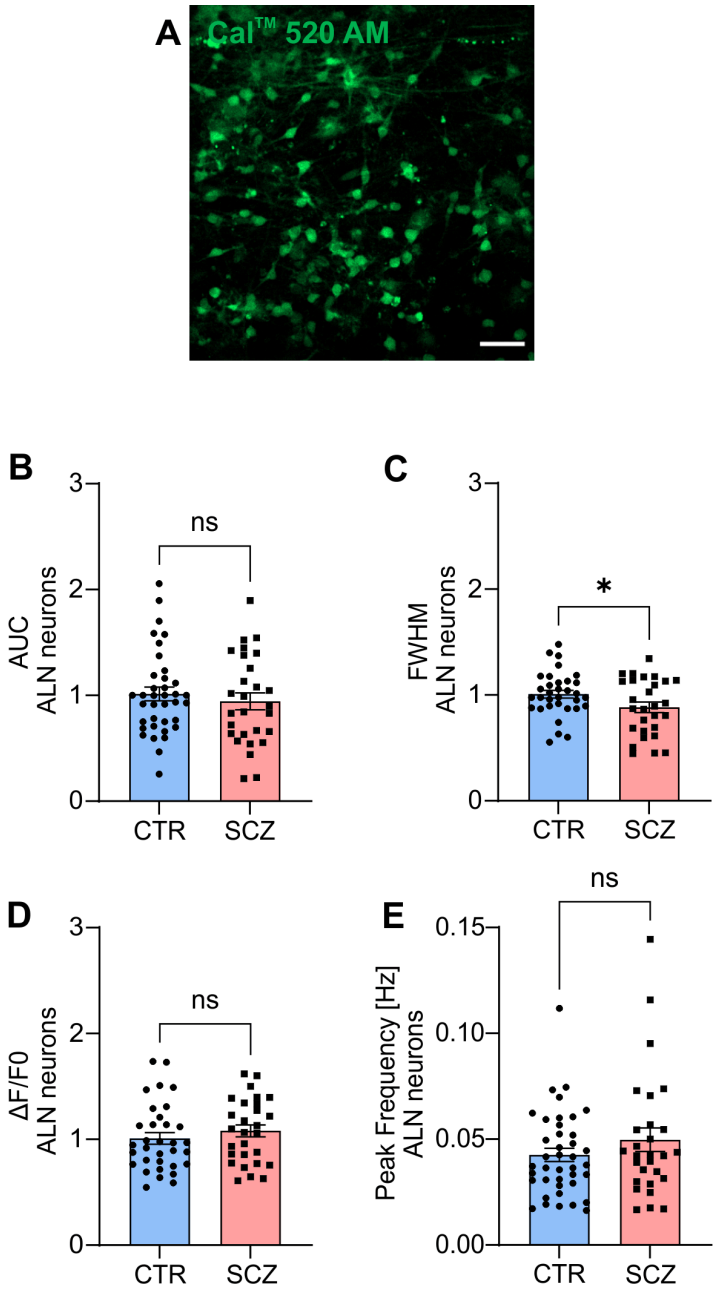

Figure 15. Unaltered calcium activity of SCZ ALN neurons cultured individually. (A) ALN neurons are stained with the green fluorescent calcium indicator Cal™ 520 AM and were recorded over a period of 3 minutes. Scale bars: 50 µm. **(B-E)** Mean peak parameters are indicated: area under the curve (AUC), full width at half maximum (FWHM), amplitude (ΔF/F0) and peak frequency (Hz). **(B)** AUC. Two-tailed Mann Whitney U test (ns=not significant; CTR n=37, SCZ n=28). **(C)** FWHM. Two-tailed unpaired t test (*=p≤0.05; CTR n=33, SCZ n=28). **(D)** ΔF/F0. Two-tailed Mann Whtiney U test (ns=not significant; CTR n=33, SCZ n=28). **(E)** Peak frequency. Two-tailed Mann Whitney U test (ns=not significant; CTR n=40, SCZ n=28). Data points represent averaged values from multiple neurons recorded within an individual well ± SEM. Values are normalized to CTR, while values for peak frequency are represented as absolute values. Data were obtained from a minimum of three independent differentiations per donor.

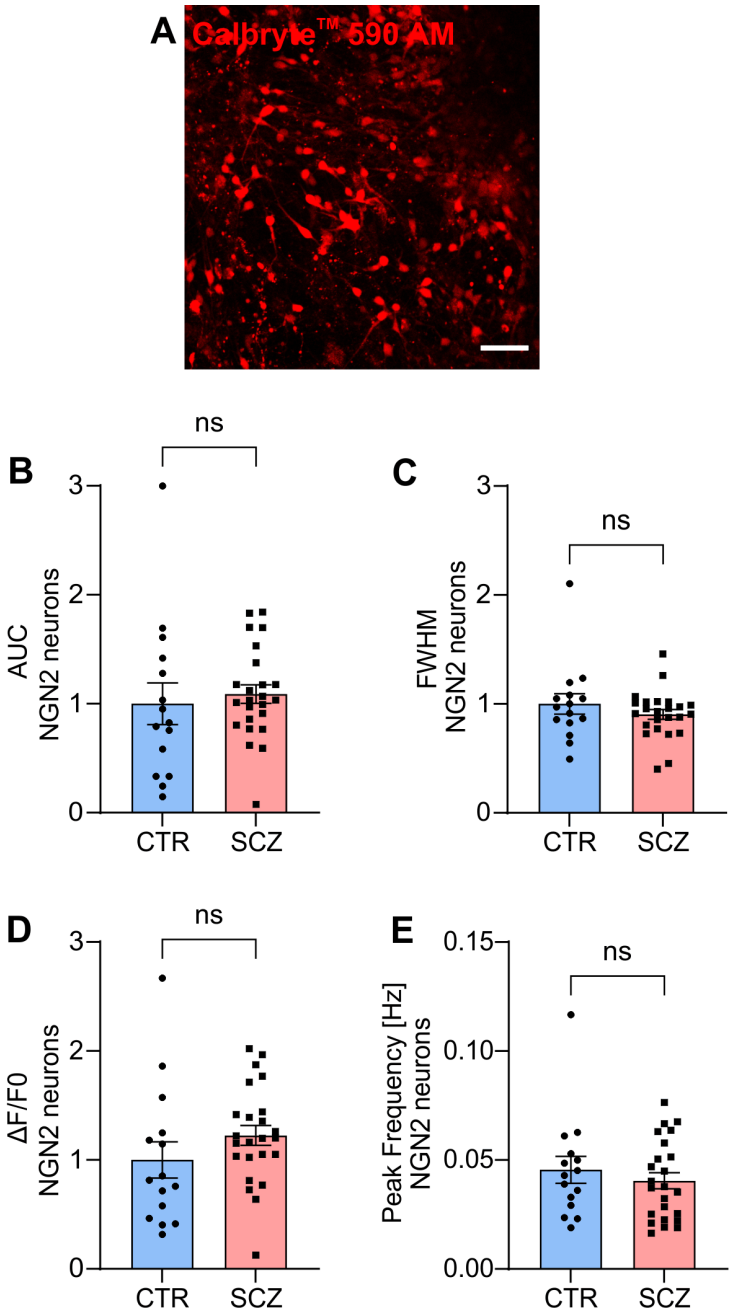

Figure 16. Unaltered calcium activity of SCZ NGN2 neurons cultures individually. (A) NGN2 neurons in monoculture are stained with the red fluorescent calcium indicator Calbryte™ 590 AM and were recorded over a period of 3 minutes. Scale bars: 50 µm. **(B-E)** Mean peak parameters are indicated: area under the curve (AUC), full width at half maximum (FWHM), amplitude (ΔF/F0) and peak frequency (Hz). **(B)** AUC (CTR n=15, SCZ n=24). **(C)** FWHM (CTR n=15, SCZ n=24). **(D)** ΔF/F0 (n=15, SCZ n=24). **(E)** Peak frequency (Hz; CTR n=15, SCZ n=24). Data points represent averaged values from multiple neurons recorded within an individual well ± SEM. Values are normalized to CTR, while values for peak frequency are represented as absolute values. Data were obtained from a minimum of three independent differentiations per donor. Two-tailed Mann Whitney U test, ns=not significant.

3.5.2 Increased spontaneous single-cell activity of SCZ neurons in co-culture

To further examine the dopaminergic-glutamatergic neuron-neuron interactions and to assess altered calcium activity, neurons in co-culture at DIV28 were stained with the red fluorescent calcium dye Calbryte™ 590 AM and subsequent calcium imaging was performed. GFP-labelling of NGN2 neurons allowed for distinction between the two cell types and enabled cell type specific analysis. Neurons double positive for Calbryte™ 590 AM and GFP were considered as NGN2 neurons, while neurons positive for Calbryte™ 590 AM and negative for GFP were assigned as ALN neurons (**Figure 17A**).

The analysis focused on unsynchronized neuronal activity, as CTR and SCZ co-cultures exhibited no synchronous network activity. Exemplary calcium traces of CTR and SCZ ALN and NGN2 neurons in co-culture can be found in **Figure 17B**. Contrary to the observations made in separated ALN and NGN2 neuronal cultures, both ALN and NGN2 neurons in co-culture exhibited significantly increased peak frequencies in SCZ cultures (**Figure 17B,F,J**). As observed in individual cultures, SCZ ALN neurons in co-culture exhibited decreased FWHM, whereas the other parameters AUC and ΔF/F0 were unchanged compared to CTR (**Figure 17C-E**). The parameters AUC, FWHM and ΔF/F0 were unaltered in SCZ NGN2 neurons (**Figure 17G-I**). Quantitative analysis of individual CTR and SCZ lines of ALN and NGN2 neurons can be found in **Supplementary Figure 4**.

Overall, alterations of basal spontaneous activity were observed for both neuronal cell types in SCZ co-culture. Notably, the peak frequency, as the common parameter altered in ALN and NGN2 neurons in SCZ co-cultures depicted a significant increase reflecting a general calcium overactivity in SCZ co-cultures and moreover implies overall increased activity in SCZ co-culture systems. The observed increased neuronal activity in SCZ ALN neurons supports the hypothesis of a hypodopaminergic phenotype as suggested by the transcriptome data, which is marked by reduced expression of dopamine metabolism genes and the autoreceptor DRD2. However, as increased peak frequency was only observed in SCZ co-cultures but not in individual cultures indicating that the interaction between the two neuronal cell types might be required for the hyperactive state.

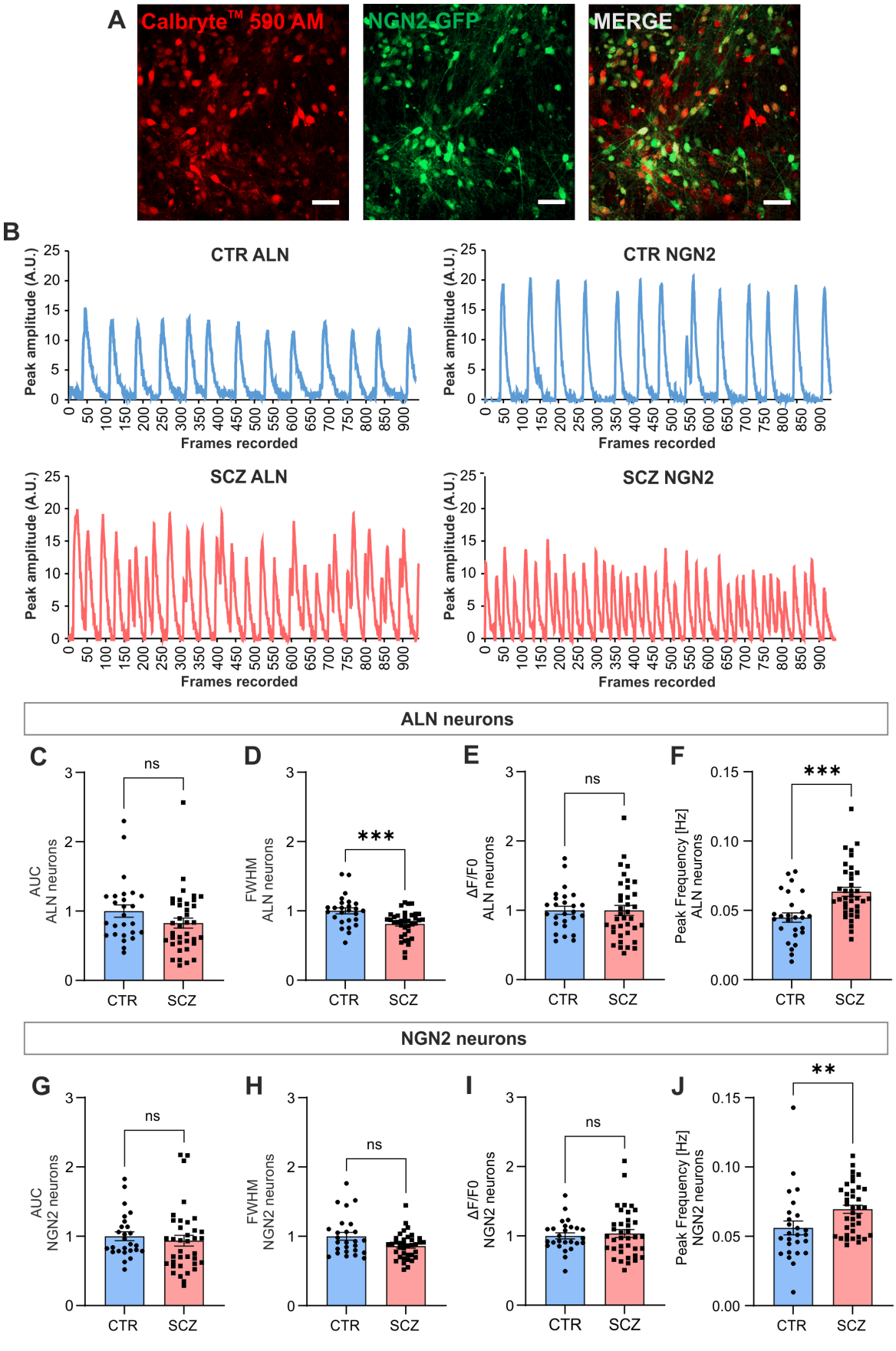

Figure legend on the next page

Figure 17. SCZ neurons in co-culture exhibit increased calcium activity. (A) Neurons in ALN-NGN2 co-cultures stained with the red fluorescent calcium indicator Calbryte 590 AM. NGN2 neurons express GFP, allowing the discrimination of ALN from NGN2 neurons in co-cultures (arrow head indicate NGN2 neuron; open arrow head indicate ALN neuron). Scale bars: 50 µm. **(B)** Representative calcium traces recorded for 3 min from spontaneously active CTR ALN and SCZ ALN neurons, as well as from CTR NGN2 and SCZ NGN2 neurons. **(C-J)** Mean peak parameters are indicated: area under the curve (AUC), full width at half maximum (FWHM), amplitude (ΔF/F0) and peak frequency (Hz) of ALN neurons and NGN2 neurons. **(C)** AUC of ALN neurons (CTR n=26, SCZ n=37). **(D)** FWHM of ALN neurons (CTR n=26, SCZ n=37). **(E)** ΔF/F0 of ALN neurons (CTR n=26, SCZ n=37). **(F)** Peak frequency of ALN neurons (CTR n=26, SCZ n=37). **(G)** AUC of NGN2 neurons (CTR n=26, SCZ n=37). **(H)** FWHM of NGN2 neurons (CTR n=26, SCZ n=37). **(I)** ΔF/F0 of NGN2 neurons (CTR n=26, SCZ n=37). **(J)** Peak frequency of NGN2 neurons (CTR n=26, SCZ n=37). Data points represent averaged values from multiple neurons recorded within an individual well ± SEM. Values are normalized to CTR, while values for peak frequency are represented as absolute values. Data were obtained from a minimum of three independent differentiations per donor. Two tailed Mann Whitney-U tests, **=p≤0.01, ***=p≤0.001, ns=not significant.

3.5.3 SCZ ALN neurons as possible driver for elevated neuronal activity in co-cultures

To further elucidate the neuronal cell type responsible for increased activity in the SCZ co-culture and to strengthen the hypothesis of a hypodopaminergic phenotype with less inhibition, mixed co-cultures were generated. This work was part of a Master's thesis and initial experiments were performed by Patricia Pizarro Garcia, a master student under my supervision (Patricia Pizarro Garcia, Master's thesis, 2023).

Seeding into mixed co-cultures, as well as calcium imaging recordings were performed by Patricia Pizarro Garcia. Analysis of calcium imaging data was performed by both of us.

For this purpose, the three CTR and four SCZ iPSC lines were individually pre-differentiated into either ALN-induced or NGN2-induced neurons following the described strategy. The three CTR lines were mixed into a CTR populations and the four SCZ lines were mixed into a SCZ population at equal ratios for each line. This allowed for seeding the CTR and SCZ neuronal populations into mixed co-cultures with following four permutations as shown in **Figure 18A**. All other parameters such as cell density per well and differentiation time remained the same.

At DIV28, the neurons in the mixed co-cultures were stained with the red fluorescent calcium dye Calbryte™ 590 AM and subsequent spontaneous single cell calcium activity was measured. Again, GFP-labelling of NGN2 neurons allowed for cell type specific analysis.

In accordance with the findings shown in the previous co-culture experiment (**Figure 17F,J**), both ALN and NGN2 neurons demonstrated increased peak frequency in the SCZ combination (SCZ ALN+SCZ NGN2) compared to CTR co-cultures (CTR ALN+CTR NGN2) (**Figure 18E,I**), while other parameters such as AUC, FWHM and ΔF/F0 remained unaltered (**Figure 18B-D,F-H**). Additionally, the co-culture combinations SCZ ALN+CTR NGN2 showed equally increased peak frequency of ALN neurons in comparison to the CTR culture, which was not observed for co-cultures comprising CTR ALN+SCZ NGN2 neuronal combinations (**Figure 18E**).

When focusing on NGN2 neurons, a moderate increase in peak frequency was identified in the combination of SCZ ALN+CTR NGN2 and CTR ALN+SCZ NGN2 neurons which did not reach the level of significance (**Figure 18I**).

Overall, the mixed co-culture model supports the findings of the previous calcium imaging experiment in SCZ ALN-NGN2 co-cultures showing increased neural activity in SCZ neurons. In addition, these results suggest that the presence of SCZ ALN neurons in the co-culture irrespective of the NGN2 phenotype can lead to elevated activity and thus underlines the hypothesis of a hypodopaminergic phenotype with less inhibition in SCZ ALN neurons.

Despite this, the results suggest that SCZ ALN neurons are not sufficient to induce elevated activity in NGN2 neurons, which is rather induced by the combination of both SCZ neuronal cell types indicating that SCZ NGN2 specific properties are needed.

To sum it up, the observations made in mixed co-cultures identify SCZ ALN neurons as possible driver for increased activity in co-cultures.

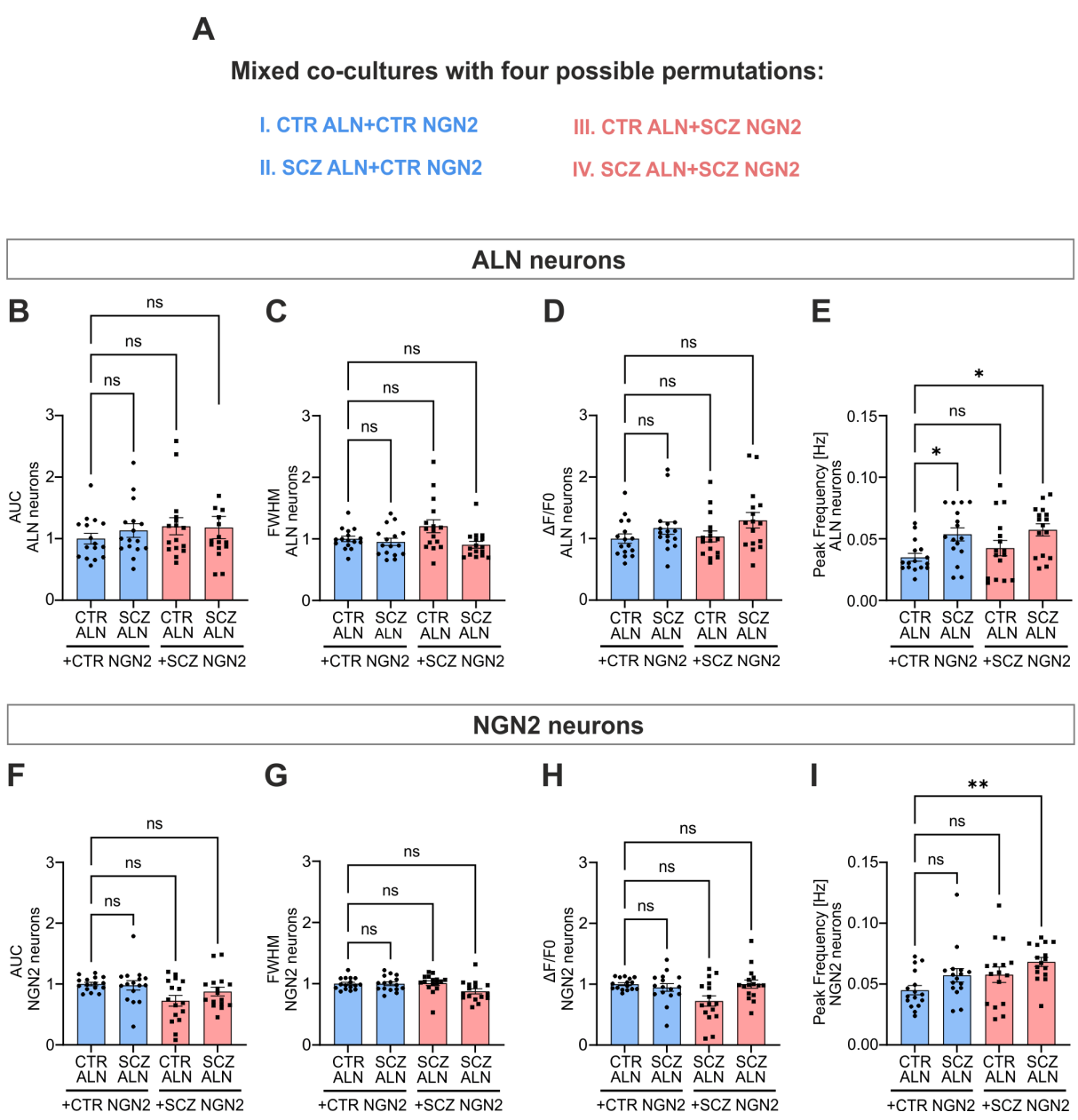

Figure 18. Mixed co-cultures of ALN-NGN2 neurons reveal SCZ ALN neurons as possible driver for increased activity. (A) Overview of experimental design. Four possible co-culture combinations were generated: CTR ALN+CTR NGN2, SCZ ALN+CTR NGN2, CTR ALN+SCZ NGN2, SCZ ALN+SCZ NGN2. **(B-I)** Mean peak parameters are indicated: area under the curve (AUC), full width at half maximum (FWHM), amplitude (ΔF/F0) and peak frequency (Hz) of ALN neurons and NGN2 neurons. Values are normalized to CTR, while values for peak frequency are represented as absolute values. **(B)** AUC of ALN neurons. **(C)** FWHM of ALN neurons. **(D)** ΔF/F0 of ALN neurons. **(E)** Peak frequency of ALN neurons. **(F)** AUC of NGN2 neurons. **(G)** FWHM of NGN2 neurons. **(H)** ΔF/F0 of NGN2 neurons. **(I)** Peak frequency of NGN2 neurons. Data points represent averaged values of multiple neurons recorded within an individual well ± SEM. Data were obtained from five independent differentiations per combination. Kruskal-Wallis test with Dunn's post-hoc test, for each combination n=16, *=p≤0.05, **=p≤0.01, ns=not significant.

3.5.4 Increased activity in SCZ co-cultures can be rescued by a selective DRD2 agonist

As RNA sequencing of SCZ ALN neurons revealed reduced expression levels of DRD2 and SCZ co-cultures exhibited increased activity suggesting overall less inhibition, calcium peak frequencies in the presence of a selective DRD2 agonist or a selective DRD2 inhibitor were assessed.

To this end, pre-differentiated ALN and NGN2 neurons were seeded into CTR or SCZ populations at equal cell ratios for each line. Co-cultures were treated for 24 h with either DMSO as a solvent control, 10 µM Pramipexole dihydrochloride, a selective DRD2 agonist or 10 µM Sulpiride, a selective DRD2 antagonist, and subsequent calcium imaging was performed.

When comparing peak frequencies of CTR and SCZ co-cultures in both ALN and NGN2 neurons treated with DMSO, again elevated peak frequency was detected supporting the previous observations in the SCZ situation. However, application of Pramipexole completely rescued elevated peak frequencies of SCZ ALN and SCZ NGN2 lines to baseline activity as compared to DMSO treated control populations, whereas no effect was observed with CTR ALN and CTR NGN2 neurons (**Figure 19A,B**). In contrast, treatment with Sulpiride, the selective DRD2 antagonist did not affect calcium activity neither in CTR nor in SCZ populations of ALN and NGN2 neurons (**Figure 19A,B**). Other calcium parameters (AUC, FWHM, ΔF/F0) remained unaffected and can be found in **Supplementary Figure 5**.

To sum up, calcium imaging confirmed the increase of neuronal activity in both ALN and NGN2 SCZ neurons compared to CTR. The observed rescuing effect suggests that calcium activity is regulated by DRD2-dependent mechanisms in both ALN and NGN2 neurons. Since this phenotype was not observed in CTR neurons, this implies that the hypodopaminergic phenotype is responsible for increased activity in SCZ neurons and activation of DRD2 could then lead to increased inhibition, thus leading to a rescue. Moreover, the findings assume the expression of DRD2 in both neuronal cell types.

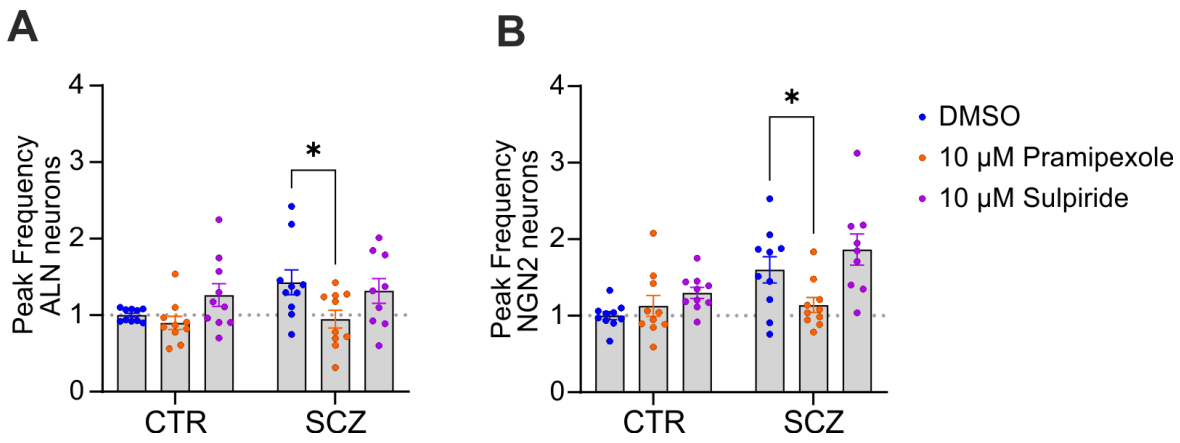

Figure 19. Treatment with a selective DRD2 agonist can rescue increased peak frequency in SCZ co-cultures. (A-B) Analysis of spontaneous calcium activity after 24 h treatment with DMSO (solvent control), 10 µM Pramipexole (DRD2 agonist) and 10 µM Sulpiride (DRD2 anatgonist). Recordings were performed for 4 minutes. **(A)** Peak frequency of ALN neurons. **(B)** Peak freqeuncy of NGN2 neurons. Values are normalized to CTR DMSO. Data points represent averaged values of multiple neurons recorded within an individual well ± SEM. Data were obtained from five independent differentiations. Two-way ANOVA with Tukey's multiple comparison test, DMSO n=10, CTR Pramipexole n=10, CTR Sulpiride n=10, SCZ DMSO n=10, SCZ Pramipexole n=10, SCZ Sulpiride n=9, *=p≤ 0.05.

3.6 Decreased AIS length in SCZ patient-derived neurons

In a next part, the axon initial segment (AIS) was examined to assess whether homeostatic AIS length regulation can be observed in response to increased neuronal activity in SCZ co-cultures. Hence, the analysis of AIS length displays an indirect measure for altered neuronal activity. Ankyrin-3 (ANK-3) is considered as AIS marker as it is the major scaffolding protein important for ion channel and cell adhesion molecule clustering at the AIS to regulate action potential initiation and to ensure proper neuronal excitability (193, 194). Therefore, ANK-3 was used to determine axon length in ALN and NGN2 neurons in co-culture in the following experiment.

3.6.1 Decreased AIS length in SCZ ALN-NGN2 co-cultures

To assess whether the AIS length is regulated in a homoeostatic manner in response to increased neuronal activity in the SCZ co-culture model, the ANK-3 length of ALN and NGN2 neurons in co-culture was analysed. For this purpose, co-cultured neurons at DIV28 were fixed and stained for three markers, the neuronal marker βIII-tubulin, the dopaminergic marker TH and the AIS marker protein ANK-3. Only segments double-positive for βIII-tubulin and ANK-3 were taken into consideration and GFP labelling of NGN2 neurons allowed for distinction between neurons in co-culture.

Neurites positive for βIII-tubulin, TH and ANK-3 were considered as ALN neurons, whereas neurites positive for βIII-tubulin, GFP and ANK-3 were assigned to NGN2 neurons. ANK-3-positive segments are indicated by arrow heads in **Figure 20A.** Cell type specific analysis of ANK-3 length revealed significantly reduced AIS length in both ALN and NGN2 SCZ neurons which may result in a homeostatic response to increased activity (**Figure 20B-C**).

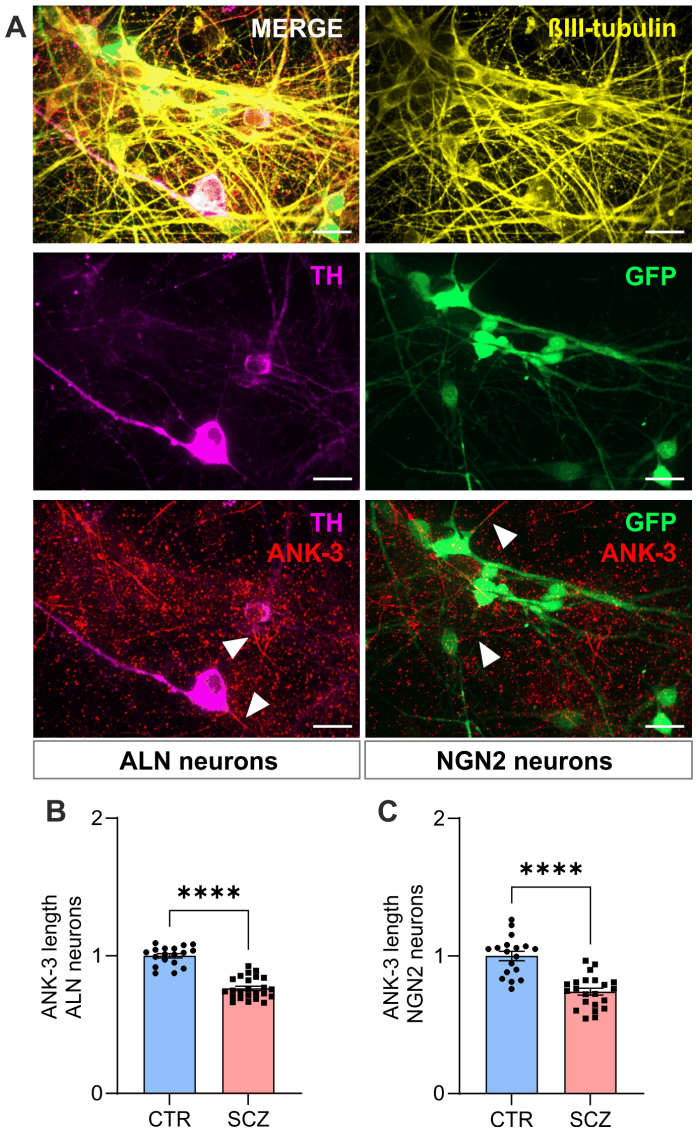

Figure 20. Decreased AIS length in SCZ co-cultures. (A) Immunocytochemistry staining of ALN-NGN2 co-cultures at DIV28 revealed expression of the neuronal marker βIII-tubulin, the dopaminergic marker TH and the AIS marker protein ankyrin-3 (ANK-3). Segments positive for βIII-tubulin, TH and ANK-3 indicate ALN neurons. Segments positive for βIII-tubulin, GFP and ANK-3 indicate NGN2 neurons (ANK-3 positive segments indicated by arrow heads). Scale bars=20 µm. **(B)** Analysis of ANK-3 length in ALN neurons. **(C)** Analysis of ANK-3 length in NGN2 neurons. Data points represent averaged values from individual wells ± SEM. Values are normalized to CTR. Data were obtained from three independent differentiations per donor. Two-tailed unpaired t-test, CTR n=18, SCZ n=24, ****=p≤0.0001.

3.6.2 Reduced AIS length in SCZ ALN and SCZ NGN2 monocultures

To see whether the reduction of the AIS length was a homeostatic mechanism occurring in response to elevated neuronal activity in SCZ co-cultures, AIS length in ALN and NGN2 neurons in monocultures was examined.

In order to do so, ALN neurons cultured individually were fixed and stained at DIV28, while NGN2 neurons in separated cultures were fixed and stained at DIV21. For the analysis of AIS length in ALN neurons, neurites co-expressing βIII-tubulin and ANK-3 were measured as indicated by the arrow head **Figure 21A.** Analysis of the AIS length in ALN neurons revealed a significant decrease in SCZ cultures which was comparable to the effect observed in the co-culture system (**Figure 21B**).

To assess whether reduced AIS length is an intrinsic effect restricted to ALN neurons cultured separately, NGN2 neurons in monoculture were analysed. βIII-tubulin-positive neurites co-expressing GFP and ANK-3 were measured regarding length (**Figure 21C**). In accordance with the findings in ALN monocultures, SCZ NGN2 monocultures demonstrated a drastic decrease in the AIS length (**Figure 21D**).

In summary, analysis of ANK-3 as a marker for AIS revealed significantly shortened segments in SCZ which was not restricted to co-cultures, but as well observed in both ALN and NGN2 neurons cultured separately. These findings revise the hypothesis of a homeostatic AIS regulation in response to increased activity, as altered calcium activity was not observed in ALN and NGN2 monocultures. Thus, the results imply that reduced AIS length is rather an intrinsic mechanism found in SCZ neurons.

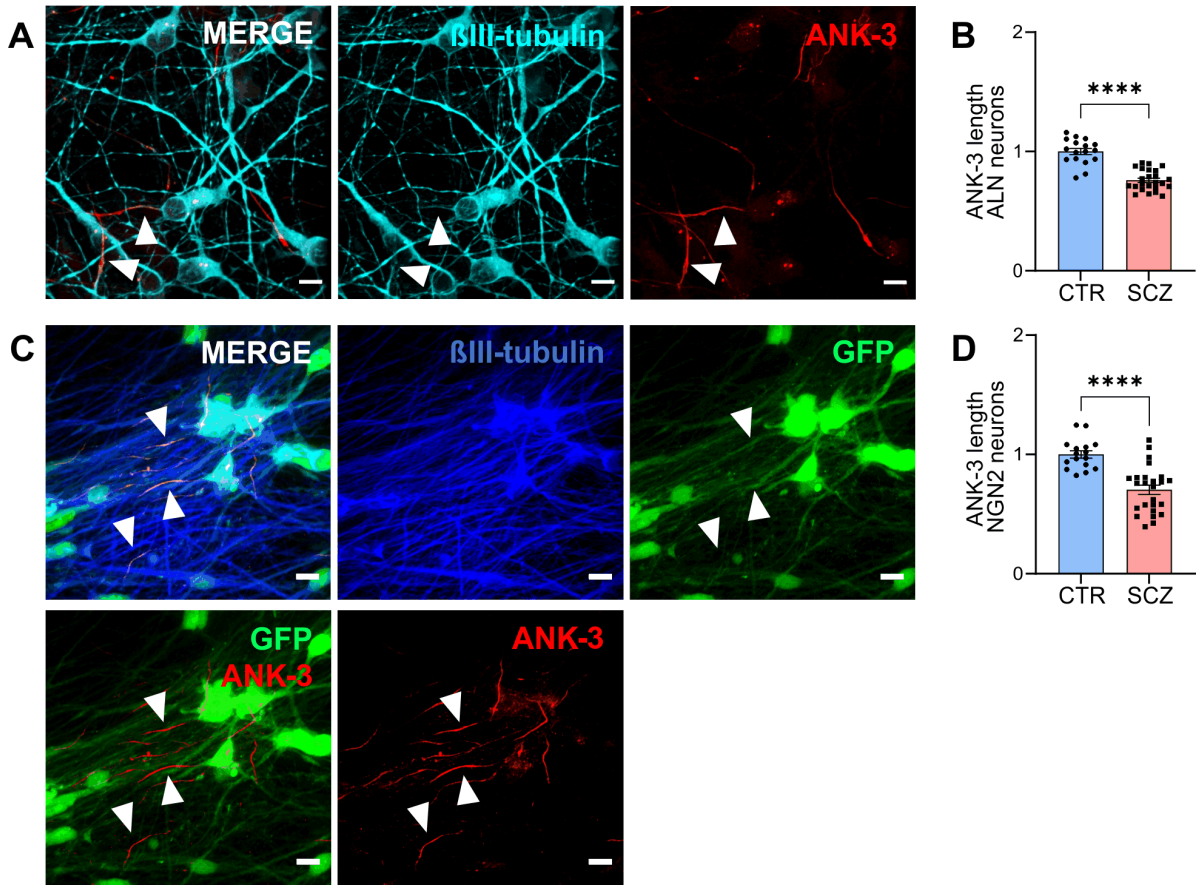

Figure 21. Decreased AIS length in ALN and NGN2 SCZ monocultures. (A) Immunocytochemistry staining of ALN monocultures at DIV28 revealed expression of the neuronal marker βIII-tubulin and the AIS marker protein ankyrin-3 (ANK-3). Segments double-positive for βIII-tubulin and ANK-3 were analysed (indicated by arrow heads). Scale bars=20 µm. **(B)** Analysis of ANK-3 length in ALN neurons. Two-tailed Mann Whitney U test, CTR n=17, SCZ n=24, ****=p≤0.0001. **(C)** Immunocytochemistry staining of NGN2 monocultures at DIV21 revealed expression of the neuronal marker βIII-tubulin, GFP and the AIS marker protein ankyrin-3 (ANK-3). Segments positive for βIII-tubulin, GFP and ANK-3 were analysed (indicated by arrow heads). Scale bars=20 µm. **(D)** Analysis of ANK-3 length in NGN2 neurons. Two-tailed unpaired t-test, CTR n=16, SCZ n=25, ****=p≤ 0.0001. Data points represent averaged values from individual wells ± SEM. Values are normalized to CTR. Data were obtained from three independent differentiations per donor.

3.7 Synaptic phenotypes in SCZ patient-derived neurons

3.7.1 Synapse density in SCZ ALN neuron monocultures is unaltered

RNA sequencing and subsequent GO enrichment analysis of SCZ ALN neurons identified gene sets enriched for ‘synapse’ and ‘neuron projection’ to be downregulated. Therefore, in a first set of experiments, synapse formation in ALN monocultures was assessed to identify possible synaptic aberrations in dopaminergic neurons.

For this purpose, synapse formation was examined by quantifying pre- and postsynaptic markers localizing on MAP2-positive neurites. Co-localization of pre- and postsynaptic spots in close apposition to each other (≤ 0.2 µm) was considered as morphological synapse, since this defined distance matches the microscope’s resolution limit. Another aspect that was considered in the analysis of synaptic markers was the percentage of co-localizing presynaptic spots indicating presynaptic terminals that already made contact to postsynaptic compartments out of the total number of identified presynaptic spots, thus representing a ratio between extra-synaptic and synaptic spots.

At DIV28, ALN neurons cultured separately were stained for the general presynaptic marker synapsin 1 (SYN1) and the postsynaptic density protein 95 marker (PSD95) that were quantified on MAP2-positive dendrites (**Figure 22A**). Presynaptic SYN1-positive densities, as well as postsynaptic PSD95-positive density clusters were unaltered in SCZ ALN neurons compared to CTR (**Figure 22C-D**). Analysis of SYN1 and PSD95 spots in apposition did not reveal alterations between CTR and SCZ cultures (**Figure 22E)** suggesting that morphological synapse formation is unaffected. In addition, the percentage of co-localizing SYN1 spots was unaltered (**Figure 22F**).

In a control experiment, the expression of the excitatory presynaptic marker vGLUT1 in apposition with PSD95 was identified in ALN neurons cultured separately (**Figure 22B**).

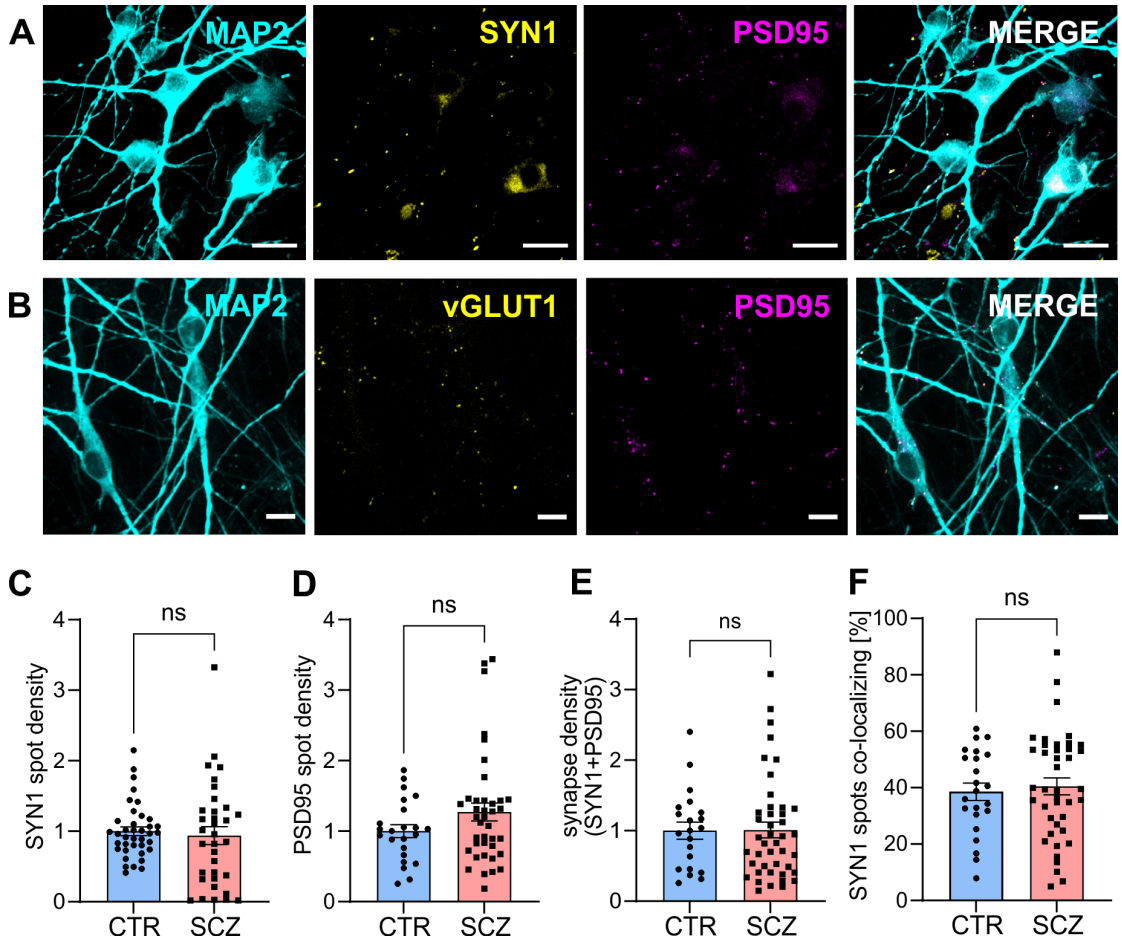

Figure 22. Unaltered synapse density in ALN monocultures. (A) Exemplary immunocytochemistry staining (63x) of the presynaptic marker SYN1, the postsynaptic marker PSD95 on MAP2-positive dendrites in ALN monocultures at DIV28. Scale bars: 10 µm. **(B)** Exemplary immunocytochemistry staining (63x) of the presynaptic marker vGLUT1 and the postsynaptic marker PSD95 on MAP2-positive dendrites in ALN monocultures. Scale bars: 10 µm. **(C-F)** Quantification of pre- and postsynaptic markers on MAP2-positive dendrites. **(C)** SYN1 density quantification. CTR n=38, SCZ n=34. **(D)** PSD95 density quantification. CTR n=23, SCZ n=29. **(E)** Synapse quantification (SYN1+PSD95). CTR n=21, SCZ n=43. **(F)** Percentage of co-localizing SYN1 spots. CTR n=23, SCZ n=41 Data points represent averaged values from individual wells ± SEM. Values are normalized to CTR, while values for SYN1 co-localizing spots are represented as ratio. Data were obtained from minimum of three independent differentiations per donor. Two-tailed Mann Whitney U test, ns=not significant.

3.7.2 Decreased synapse density in SCZ ALN-NGN2 co-cultures

To gain further insight into the interaction between dopaminergic and glutamatergic neurons and to reveal possible aberrations in synapse formation that might contribute to the elevated neuronal activity in SCZ co-cultures, synaptic markers were quantified in the ALN-NGN2 co-culture model. To achieve this, co-cultures were fixed and stained for the general presynaptic marker SYN1, the excitatory presynaptic marker vGLUT1, and the postsynaptic marker PSD95 on MAP2-positive neurons. This approach enabled the quantification of pre-, post- and synaptic densities, as well as the analysis of the percentage of co-localizing presynaptic sites.

Again, co-localization of pre- and postsynaptic spots in close apposition to each other (≤ 0.2 µm) was considered as morphological synapse. GFP-labelling of NGN2 neurons allowed for cell type specific analysis (**Figure 23A, Figure 24A**).

Analysis of general synapse formation and excitatory synapse formation was possible for following combinations:

I. General synapse formation on ALN neurons (SYN1+PSD95 on GFP- cells)
II. General synapse formation on NGN2 neurons (SYN1+PSD95 on GFP+ cells)
III. Excitatory synapse formation on ALN neurons (vGLUT1+PSD95 on GFP- cells)
IV. Excitatory synapse formation on NGN2 neurons (vGLUT1+PSD95 on GFP+ cells)

Quantification of the general presynaptic terminal marker SYN1 revealed significant reduction on both ALN and NGN2 neurons in SCZ co-cultures, as well as a significant loss of morphological synapse densities (SYN1+PSD95) (**Figure 23B,D,F,H**). PSD95-positive clusters were significantly reduced on SCZ ALN neurons (**Figure 23C**), whereas NGN2 neurons did not reveal alterations between SCZ and CTR neurons (**Figure 23G**). Additionally, analysis of co-localizing presynaptic spots, did not show any differences between CTR and SCZ cultures on both ALN and NGN2 neurons suggesting that extra-synaptic and synaptic SYN1-positive terminals were equally reduced in SCZ cultures (**Figure 23E,I**). Quantitative analysis for individual CTR and SCZ lines can be found in **Supplementary Figure 6A,B,E,F.**

Noteworthy, SYN1 is a more general presynaptic marker that is not specific for dopaminergic or glutamatergic terminals. To further elucidate the contribution of both neuronal cell types to excess synaptic loss in SCZ co-cultures, staining for the excitatory presynaptic marker vGLUT1 was applied to mark excitatory synapses. Again, the analysis focused on excitatory presynaptic marker densities (vGLUT1), postsynaptic densities (PSD95) and vGLUT1+PSD95 excitatory synapse densities quantified on MAP2-positive neurons (**Figure 24A**). Presynaptic vGLUT1-positive terminals and excitatory synapse density (vGLUT1+PSD95) showed a tendency towards a decrease but did not reach levels of significance (**Figure 24B,D**). In contrast, excitatory presynaptic and synaptic densities on SCZ NGN2 neurons were reduced compared to CTR neurons (**Figure 24F,H**). Postsynaptic density clusters were unaffected on both ALN and NGN2 SCZ neurons, as well as the percentage of co-localizing vGLUT1 spots (**Figure 24C,E,G,I**). Quantitative analysis of individual CTR and SCZ lines can be found in **Supplementary Figure 6C,D,G,H**.

In summary, synapse analysis in ALN-NGN2 co-cultures revealed an excess loss of synapses on both neurons in SCZ cultures, primarily driven by the loss of presynaptic sites. Synapse-specific quantification in the co-culture demonstrated a reduction of excitatory synapses on SCZ NGN2 neurons, but not on SCZ ALN neurons.

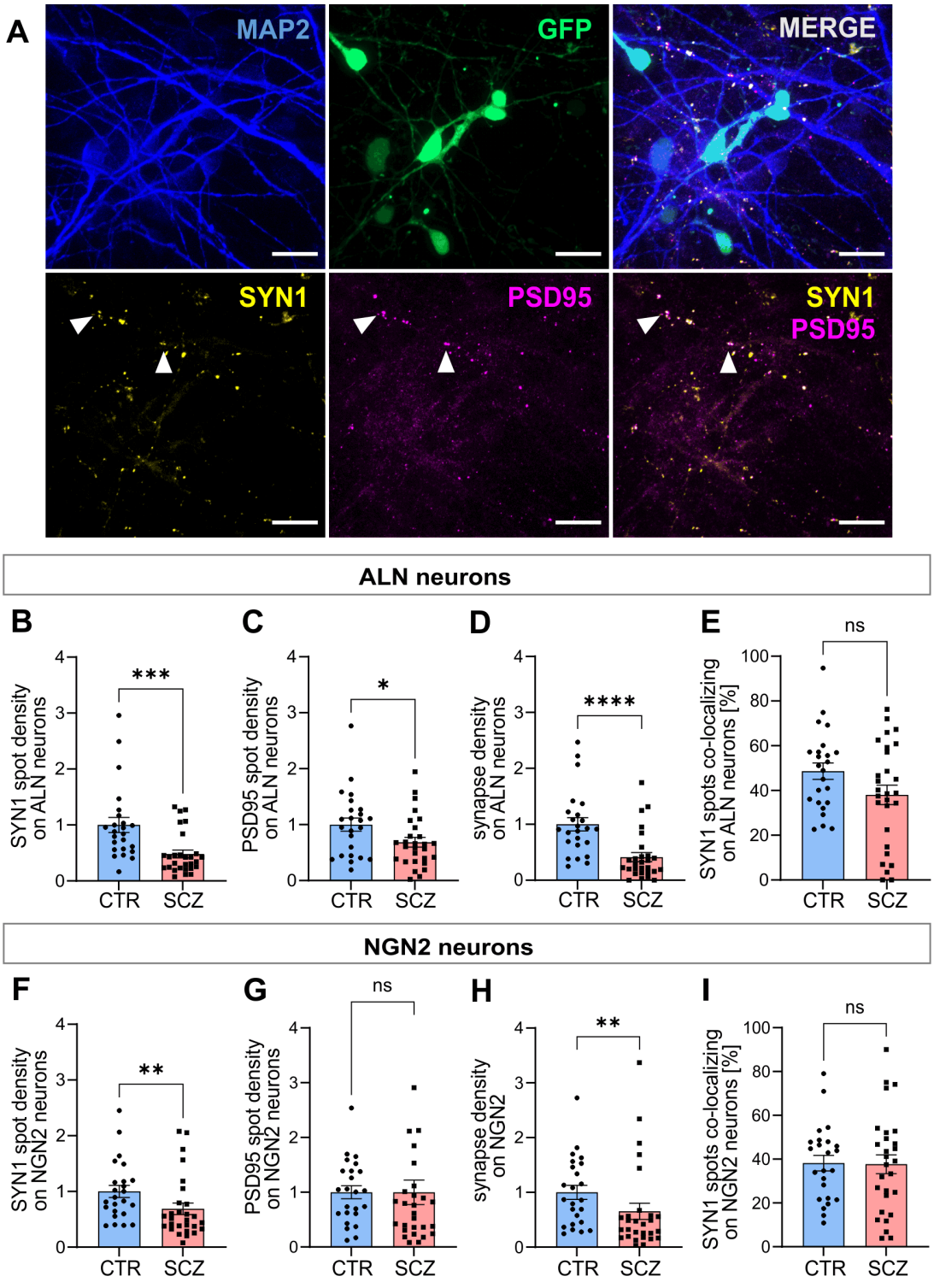

Figure legend continues on the next page

Figure 23. Decreased synapse density in SCZ ALN-NGN2 co-cultures. (A) Immunocytochemistry revealed expression of the general presynaptic marker SYN1, the postsynaptic marker PSD95 on MAP2-positive dendrites in ALN-NGN2 co-cultures at DIV28. Synaptic markers quantified on MAP2-positive/GFP-negative neurons were considered as ALN neurons, whereas synaptic markers counted on MAP2-positive/GFP-positive neurons were considered as NGN2 neurons. Co-localization of SYN1 and PSD95 is considered as morphological synapse (indicated by arrow heads). Scale bars 20 µm. **(B-E)** Quantification of synaptic markers localizing on MAP2-positive/GFP-negative ALN neurons. **(B)** Quantification of SYN1. **(C)** Quantification of PSD95. **(D)** Quantification of synaptic densities (SYN1+PSD95). **(E)** Percentage of SYN1 spots co-localizing. **(F-I)** Quantification of synaptic markers

localizing on MAP2-positive/GFP-positive NGN2 neurons. **(F)** Quantification of SYN1. **(G)** Quantification of PSD95. **(H)** Quantification of synaptic densities (SYN1+PSD95). **(I)** Percentage of SYN1 spots co-localizing. Data points represent averaged values from individual wells ± SEM. Values are normalized to CTR, while values for SYN1 co-localizing spots are represented as ratio. Data were obtained from minimum of three independent differentiations per donor. Two-tailed Mann Whitney U test, CTR n=24, SCZ n=28, *=p≤0.05, **=p≤0.01, ***=p≤0.001, ns=not significant

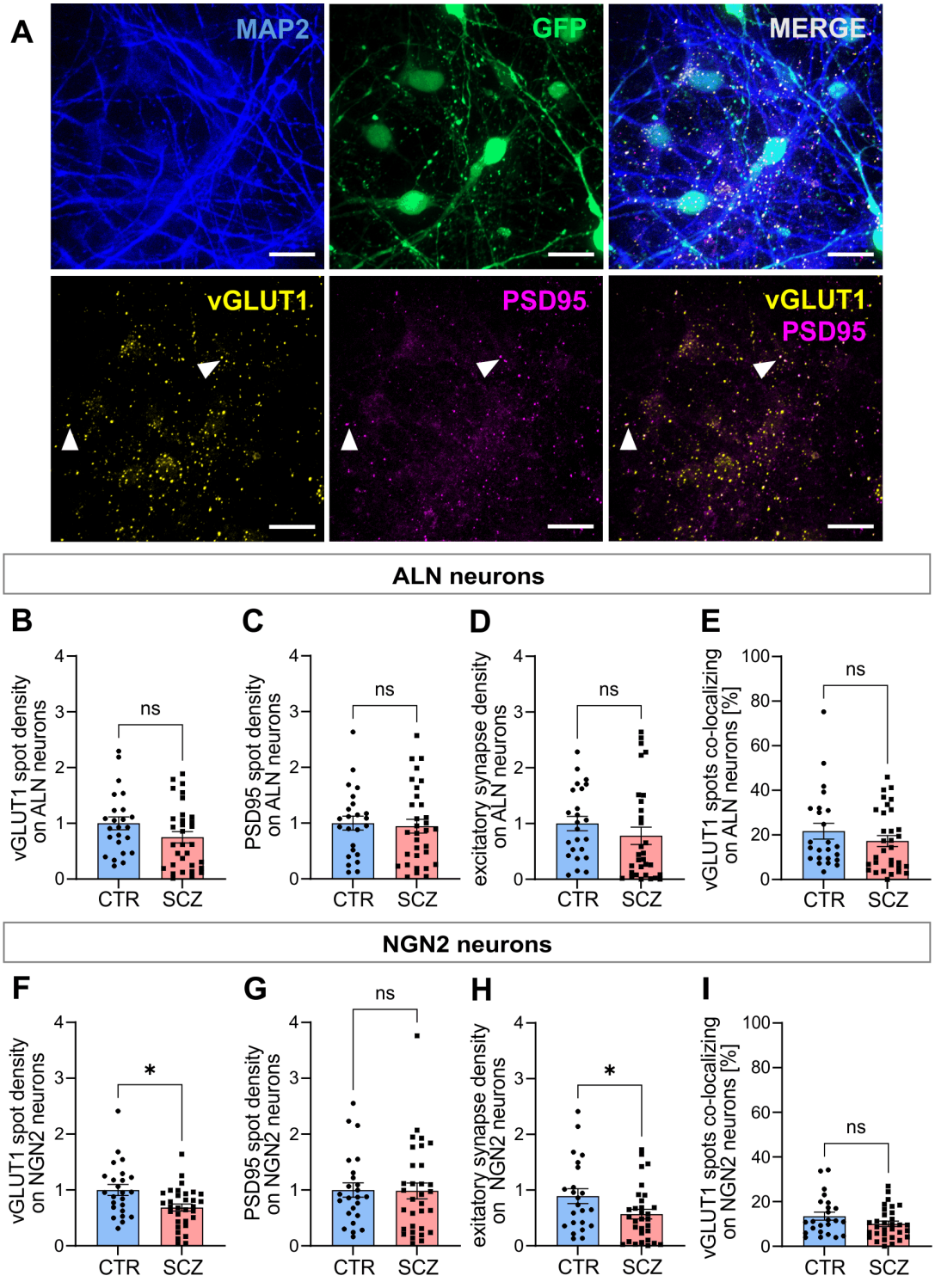

Figure legend on the next page

Figure 24. Decreased excitatory synapse density in SCZ co-cultures. (A) Immunocytochemistry revealed expression of the excitatory presynaptic marker vGLUT1, the postsynaptic marker PSD95 on MAP2-positive dendrites in ALN-NGN2 co-cultures at DIV28. Synaptic markers quantified on MAP2-positive/GFP-negative neurons were considered as ALN neurons, whereas synaptic markers counted on MAP2-positive/GFP-positive neurons were considered as NGN2 neurons. Co-localization of vGLUT1 and PSD95 is considered as morphological synapse (indicated by arrow heads). Scale bars 20 µm. **(B-E)** Quantification of synaptic markers localizing on MAP2-positive/GFP-negative ALN neurons. **(B)** Quantification of vGLUT1. **(C)** Quantification of PSD95. **(D)** Quantification of excitatory synaptic densities (vGLUT1+PSD95). **(E)** Percentage of vGLUT1 spots co-localizing. **(F-I)** Quantification of synaptic markers localizing on MAP2-positive/GFP-positive NGN2 neurons. **(F)** Quantification of vGLUT1. **(G)** Quantification of PSD95. **(H)** Quantification of synaptic densities (vGLUT1+PSD95). **(I)** Percentage of vGLUT1 spots co-localizing. Data points represent averaged values from individual wells ± SEM. Values are normalized to CTR, while values for SYN1 co-localizing spots are represented as ratio. Data were obtained from minimum of three independent differentiations per donor. Two-tailed Mann Whitney U test, CTR n=24, SCZ n=28, *=p≤0.05, ns=not significant.

3.7.3 Development of a lentiviral vector for cell type-specific presynaptic-bouton labelling

As shown in **Figure 22B**, ALN neurons cultured separately were positive for the excitatory presynaptic marker vGLUT1. Thus, the analysis of excitatory presynaptic and synaptic densities in the co-cultures did not allow for a clear discrimination between terminals of dopaminergic and glutamatergic neurons. Furthermore, immunocytochemical staining for typical dopaminergic markers such as DAT or VMAT2 was not successful. Hence, another approach was applied to cell type specifically label dopaminergic and glutamatergic presynaptic terminals in a more reliable manner. A lentiviral vector expressing a synaptophysin (SYP)-mRuby fusion protein to efficiently label presynaptic terminals was generated by Lisa-Sophie Wüstner (Molecular Neurobiology, NMI, Reutlingen) and kindly provided. The map of the generated lentiviral vector pLV-EF1α-Synaptophysin-mRuby can be found in **Supplementary Figure 2**.

The lentiviral vector overexpressing SYP-mRuby was first applied to ALN and NGN2 neurons cultured separately. At DIV28 and DIV21, respectively, neurons were positive for MAP2 and the postsynaptic marker PSD95, which also revealed SYP-mRuby expression in both ALN and NGN2 neuronal cultures (**Figure 25A,F**). In addition, SYP-mRuby was also found in close apposition with PSD95 suggesting the formation of morphological synapses. Quantification of synaptic marker densities in ALN neuronal monocultures, revealed unaltered SYP-mRuby positive terminal density, as well as unaltered PSD95 cluster and synapse (SYP-mRuby+PSD95) densities in SCZ cultures (**Figure 25B-D**). In addition, the percentage of co-localizing SYP-mRuby spots was unchanged between CTR and SCZ (**Figure 25E**).

When analysing SYP-mRuby positive terminals on NGN2 neurons cultured separately a significant reduction was observed in SCZ neurons, which was accompanied by a reduced synapse density (**Figure 25G,I**). In contrast, postsynaptic PSD95 clusters, as well as percentage of co-localizing SYP-mRuby spots was unaltered (**Figure 25H,J**).

Overall, synapse quantification of ALN monocultures revealed no differences between CTR and SCZ, which was replicated by two different approaches: transduction of cells with pLV-EF1α-SYP-mRuby and immunocytochemical quantification of SYN1. In addition, previous studies including the same set of donors observed significant reduction of presynaptic and synaptic densities in SCZ NGN2 monocultures (166), which was also found in transduced SCZ NGN2 neurons. To conclude, the results confirm previous findings and hence demonstrate the validity of the used lentiviral construct for synaptic bouton labelling.

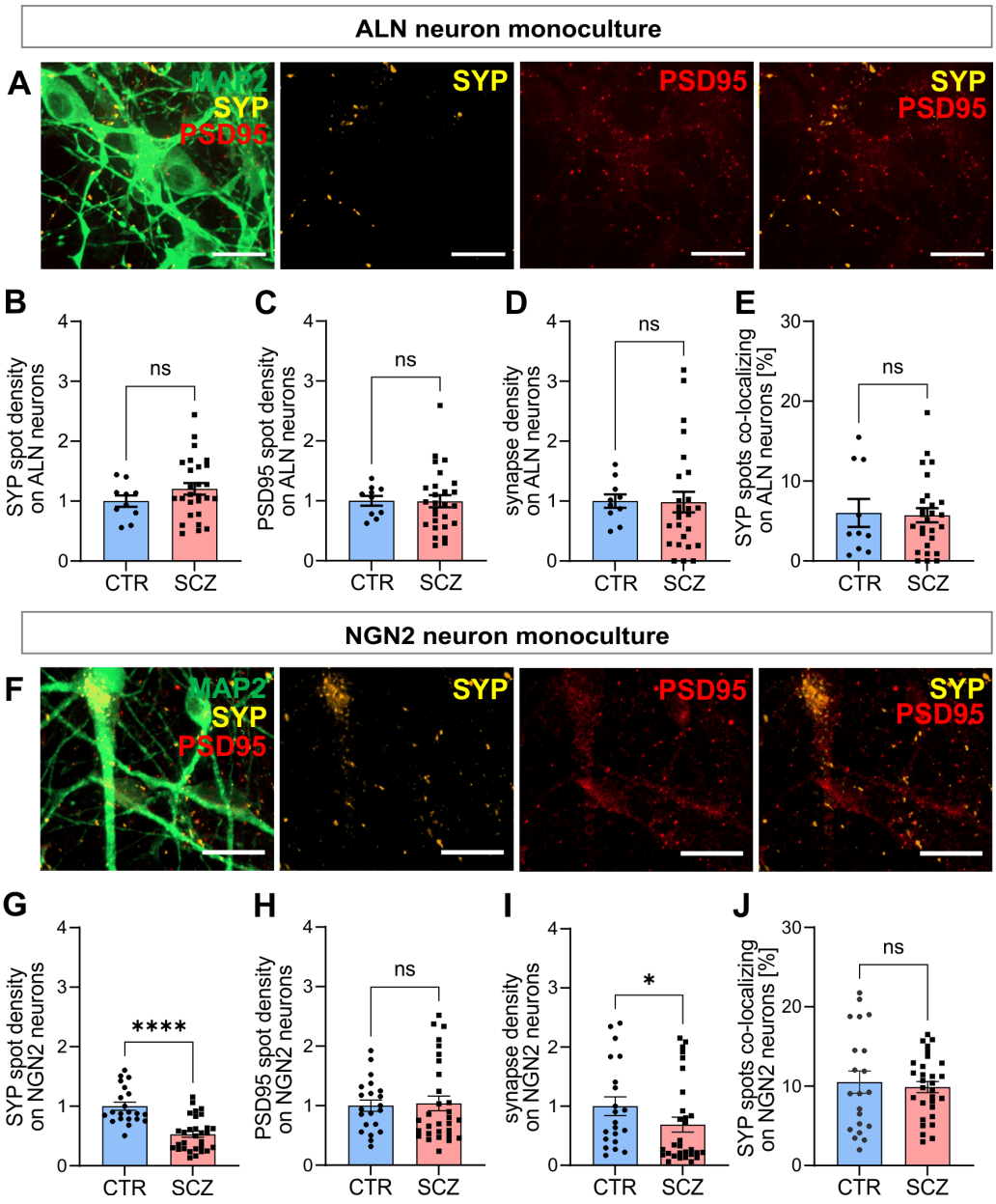

Figure 25. Characterisation of the lentiviral construct pLV-EF1α-Synaptophysin-mRuby for presynaptic bouton labelling in ALN and NGN2 monocultures. (A) Synaptophysin-mRuby transduced ALN neurons in monocultures express SYP-mRuby, the postsynaptic marker PSD95 on MAP2-positive neurons at DIV28. Scale bars 20 µm. **(B-E)** Quantification of synaptic markers on MAP2-positive neurons. **(B)** SYP density quantification. Unpaired t-test, CTR n=10, SCZ n=27. **(C)** PSD95 density quantification. Two-tailed Mann Whitney U test, CTR n=10, SCZ n=27. **(D)** Synapse quantification (SYP+PSD95). Two-tailed Mann Whitney U test, CTR n=10, SCZ n=26. **(E)** Percentage of co-localizing SYP spots. Two-tailed Mann Whitney U test, CTR n=10, SCZ n=27. Data were obtained from four independent differentiations per donor. ns= not significant. **(F)** Synaptophysin-mRuby transduced NGN2 neurons in monocultures express SYP-mRuby, the postsynaptic marker PSD95 on MAP2-positive neurons at DIV21. Scale bars 20 µm. **(G-J)** Quantification of synaptic markers on MAP2-positive neurons. Two-tailed Mann Whitney U test, CTR n=21, SCZ n=30. **(G)** SYP density quantification. **(H)** PSD95 density quantification. **(I)** Synapse quantification (SYP+PSD95). **(J)** Percentage of co-localizing SYP spots. Unpaired t-test two-tailed, CTR n=21, SCZ n=30. Data points represent averaged values from individual wells ± SEM. Values are normalized to CTR, while values for SYN1 co-localizing spots are represented as ratio. Data were obtained from four to five independent differentiations per donor. *=p≤ 0.05, ****=p≤ 0.0001, ns=not significant.

3.7.4 Lentiviral overexpression of Synaptophysin-mRuby allows for cell type-specific presynaptic bouton labelling in ALN-NGN2 co-cultures

To discriminate between ALN- and NGN2-specific presynaptic terminals, the lentiviral vector pLV-EF1α-SYP-mRuby was applied to ALN-NGN2 co-cultures. For this purpose, either ALN or NGN2 neurons were transduced individually with the lentiviral vector prior to seeding into co-culture. ALN neurons transduced with the lentiviral vector were then co-cultured with non-transduced NGN2 neurons. This strategy allowed to selectively label presynaptic terminals of ALN neurons found on ALN neurons (GFP- cells) and on NGN2 neurons (GFP+ cells). NGN2 neurons transduced with the lentiviral vector were co-cultured with non-transduced ALN neurons. Hence, this allowed to selectively label presynaptic terminals of NGN2 neurons found on ALN neurons (GFP- cells) and on NGN2 neurons (GFP+ cells).

In this experiment, the lines CTR1, SCZ1, SCZ2, SCZ4 and SCZ5 were used.

SYP-mRuby positive presynaptic terminal quantification are described following:

I. Dopaminergic presynaptic boutons on ALN neurons (SYP+ on GFP- cells)
II. Dopaminergic presynaptic boutons on NGN2 neurons (SYP+ on GFP+ cells)
III. Glutamatergic presynaptic boutons on ALN neurons (SYP+ on GFP- cells)
IV. Glutamatergic presynaptic boutons on NGN2 neurons (SYP+ on GFP+ cells)

At DIV28, co-cultures were fixed and stained for MAP2 and PSD95. Discrimination between neuronal cell types was ensured by GFP expression of NGN2 neurons.

Successful transduction of ALN neurons in co-culture demonstrated SYP-mRuby-positive terminals on MAP2-positive neurons (**Figure 26A**). Quantification of presynaptic SYP-mRuby-positive terminals derived from ALN neurons did not show any differences in presynapse formation neither on ALN neurons nor on NGN2 neurons between CTR and SCZ co-cultures (**Figure 26B,D**). In addition, PSD95 cluster densities on ALN and NGN2 neurons were unaltered in SCZ cultures (**Figure 26C,E**). Quantitative analysis for individual CTR and SCZ lines can be found in **Supplementary Figure 7A,B**.

Next, transduced NGN2 neurons co-cultured with non-transduced ALN neurons revealed expression SYP-mRuby (**Figure 27A**). SYP-mRuby-positive terminals on both ALN and NGN2 neurons were significantly reduced in SCZ cultures (**Figure 27B,D**). Again, postsynaptic cluster density on SCZ ALN neurons was not affected (**Figure 27C**), whereas a significant increase in postsynaptic density was observed on SCZ NGN2 neurons (**Figure 27E**). Quantitative analysis for individual CTR and SCZ lines can be found in **Supplementary Figure 7C,D**.

In conclusion, the results indicate that mainly presynaptic terminals of SCZ NGN2 neurons are affected, whereas a loss of terminals from ALN neurons was not identified. However, the findings of elevated activity cannot be explained by increased excitatory synaptic input.

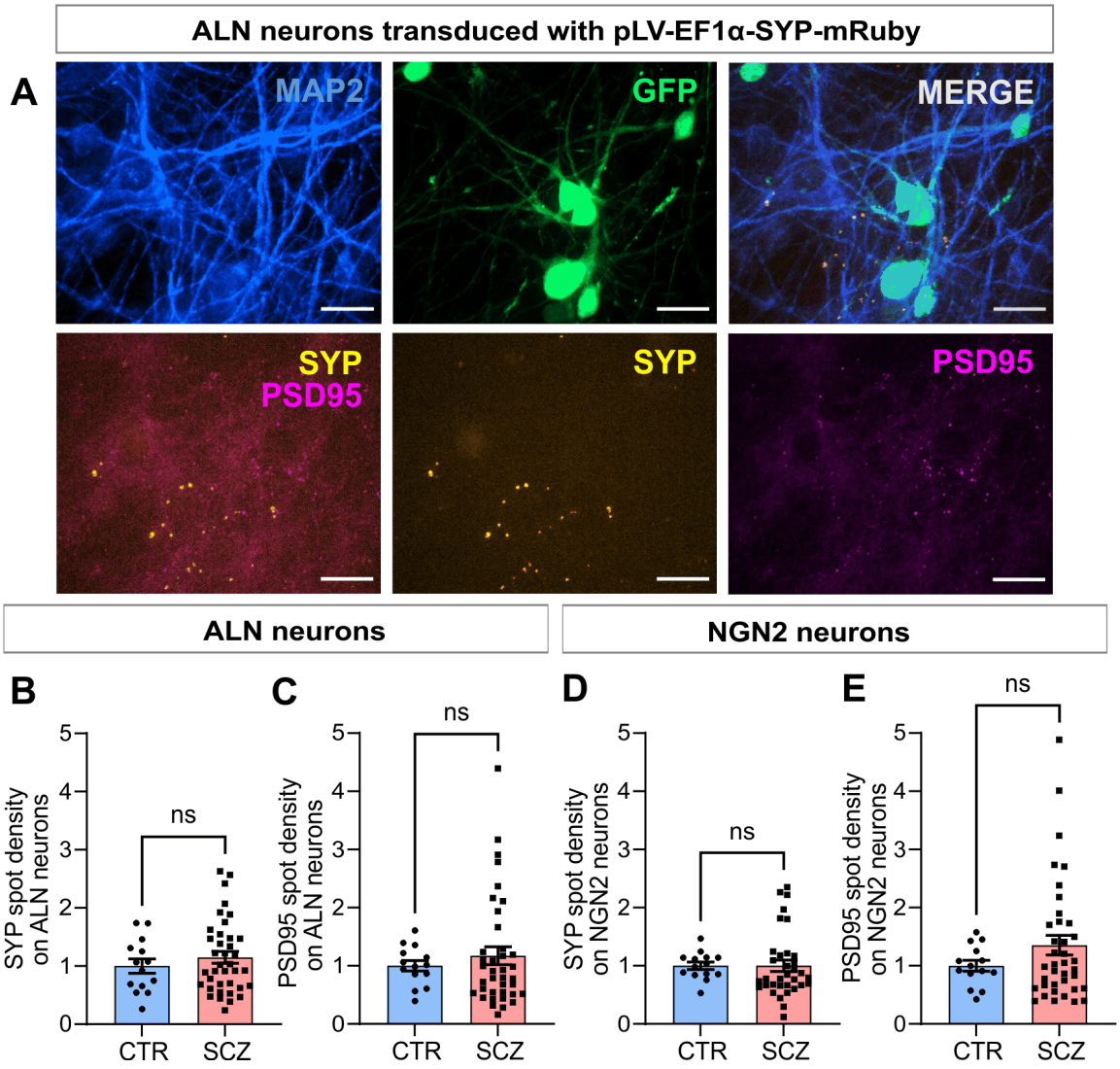

Figure 26. Dopaminergic presynaptic terminal density is unaffected in SCZ ALN-NGN2 co-cultures. (A) Expression of SYP-mRuby indicate successful transduction of ALN neurons prior to seeding into co-culture with NGN2 neurons. Immunocytochemistry reveals expression of the postsynaptic marker PSD95 on MAP2-positive neurons at DIV28. Quantification of SYP-mRuby-positive terminals on MAP2-positive/GFP-negative neurons (ALN) and MAP2-positive/GFP-positive neurons (NGN2). Scale bars 20 µm. **(B+C)** Quantification of presynaptic and postsynaptic markers on ALN neurons. **(B)** Quantification of SYP. **(C)** Quantification of PSD95. **(D+E)** Quantification of presynaptic and postsynaptic markers on NGN2 neurons. **(D)** Quantification of SYP. **(E)** Quantification of PSD95. Data points represent averaged values from individual wells ± SEM. Values are normalized to CTR. Data were obtained from minimum of three independent differentiations per donor. Two-tailed Mann Whitney U test, CTR n=14, SCZ n=38, ns= not significant.

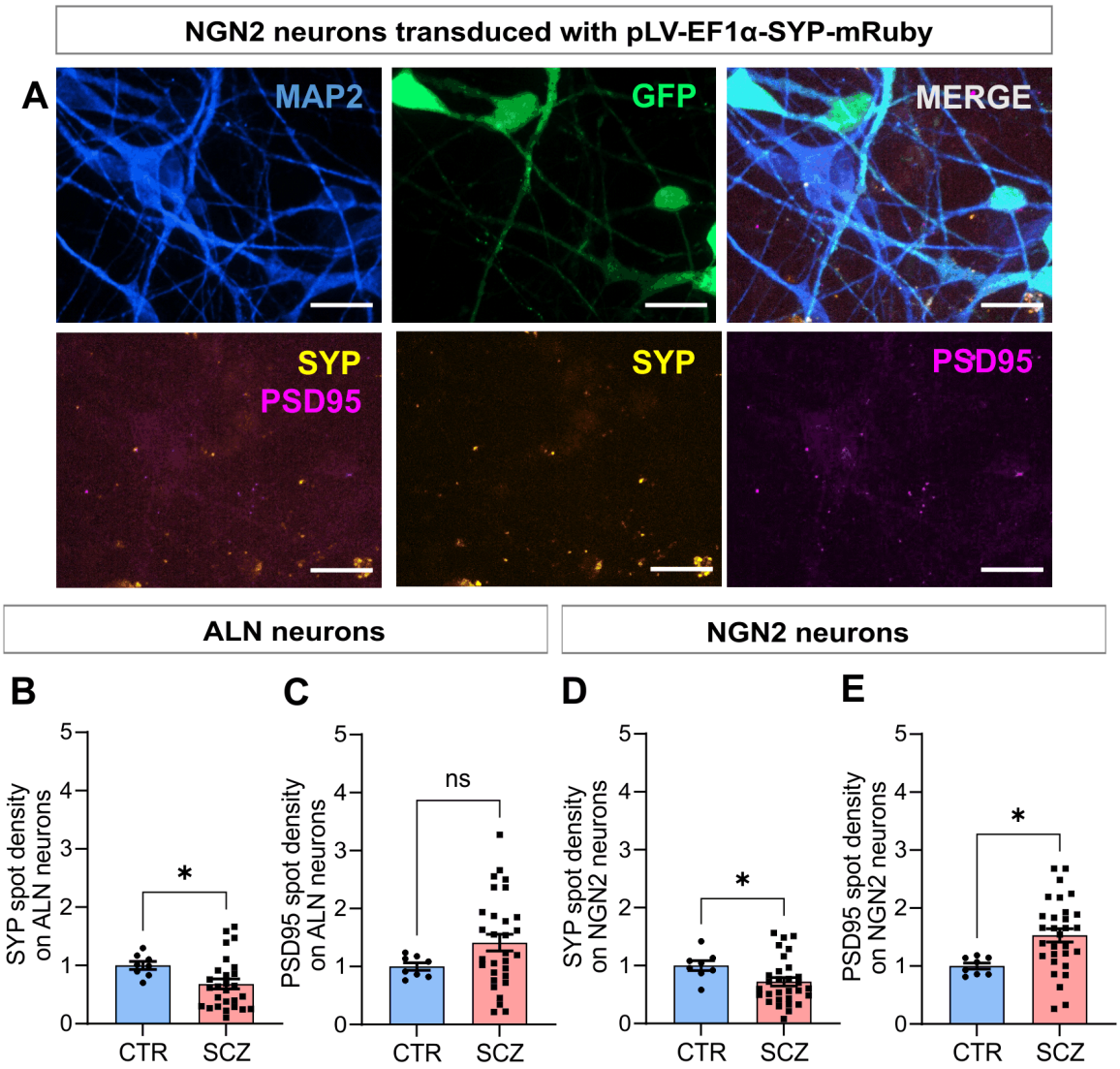

Figure 27. Glutamatergic presynaptic terminal density is decreased in SCZ ALN-NGN2 co-cultures. (A) Expression of SYP-mRuby indicate successful transduction of NGN2 neurons prior to seeding into co-culture with ALN neurons. Immunocytochemistry reveals expression of the postsynaptic marker PSD95 on MAP2-positive neurons at DIV28. Quantification of SYP-mRuby-positive terminals on MAP2-positive/GFP-negative neurons (ALN) and MAP2-positive/GFP-positive neurons (NGN2). Scale bars 20 µm. **(B+C)** Quantification of presynaptic and postsynaptic markers on ALN neurons. **(B)** Quantification of SYP. **(C)** Quantification of PSD95. **(D+E)** Quantification of presynaptic and postsynaptic markers on NGN2 neurons. **(D)** Quantification of SYP. **(E)** Quantification of PSD95. Data points represent averaged values from individual wells ± SEM. Values are normalized to CTR. Data were obtained from minimum of three independent differentiations per donor. Two-tailed Mann Whitney U test, CTR n=8, SCZ n=30, *=p≤0.05, ns= not significant.

3.8 E-I co-culture models with 15q13 and 22q11 microdeletions as genetic risk factors for SCZ show synaptic and functional phenotypes

In the second part of this thesis, isogenic disease models carrying a 15q13 and a 22q11 microdeletion as high-risk factors for SCZ were employed. The focus was set on the interactions between excitatory glutamatergic and inhibitory GABAergic interneurons, as E-I imbalances in the developing cortical microcircuitry are thought to be involved in the pathology of neuropsychiatric disorders.

For this purpose, iPSC-derived glutamatergic and GABAergic neurons were seeded at defined ratios into an E-I co-culture model, which was employed to study possible aberrations in the cortical microcircuitry, as indicated by aberrations in synapse formation and altered neuronal activity. One of the advantages when using isogenic designs is that the genetic makeup remains the same, except for the genetically modified region and thus allowing the study of mutation-relevant phenotypes (143).

The isogenic iPSC lines under study comprising one isogenic CTR and three deletion lines (one clone with a deletion in chromosome 15q13 and two clones with deletions in chromosome 22q11) were a kind gift from Prof. Dr. Moritz Rossner at the Department of Psychiatry and Psychotherapy in Munich. The iPSC lines obtained were stably transduced with the lineage-specific transcription factors *NGN2* or *ASCL1-DLX2* (AD), respectively, and the reverse tetracycline transactivator protein (rtTA) under the operator sequence (TetO) to easily start differentiations by adding doxycycline. For more details on the NGN2-AD2 co-culture setup and refer to section 2.2.10.

3.8.1 Aberrant neurite branching in NGN2 neurons carrying microdeletions

In a first experiment, the neurite outgrowth and neurite branching of pre-differentiated NGN2 neurons carrying microdeletions in comparison to the isogenic CTR were assessed, in order to identify early disease-relevant phenotypes. Individual replicates of this experiment were performed by Sabrina Vogel (Molecular Neurobiology, NMI, Reutlingen).

Neurite outgrowth assays were performed by using the IncuCyte Neurotrack module that allows for detection of live cell dynamics and recognizes outgrowing neurites and cell body clusters in an automated manner (**Figure 28A,** neurites in purple and cell body cluster in orange). Starting from 72 h after neural induction, the isogenic CTR line and the three mutant clones showed a constant increase in neurite length and neurite branch points as depicted in **Figure 28B, Figure 28C**. After 120 h, a plateau in neurite outgrowth was reached showing a trend towards an increase in all three deletion clones (**Figure 28D**). At this timepoint (120 h),

neurite branch points were significantly increased in two mutant clones (15q13 and 22q11 clone2), whereas 22q11 clone1 demonstrated a slight increase which did not reach the level of significance (**Figure 28E**).

To conclude, compared to the isogenic CTR line, the three deletion clones revealed a tendency towards increase in neurite length and demonstrated a significant increase in neurite branch points. The results suggest that already during early neurodevelopmental alterations occur and aberrant neurite outgrowth micht be an early indicator in excitatory glutamatergic neurons.

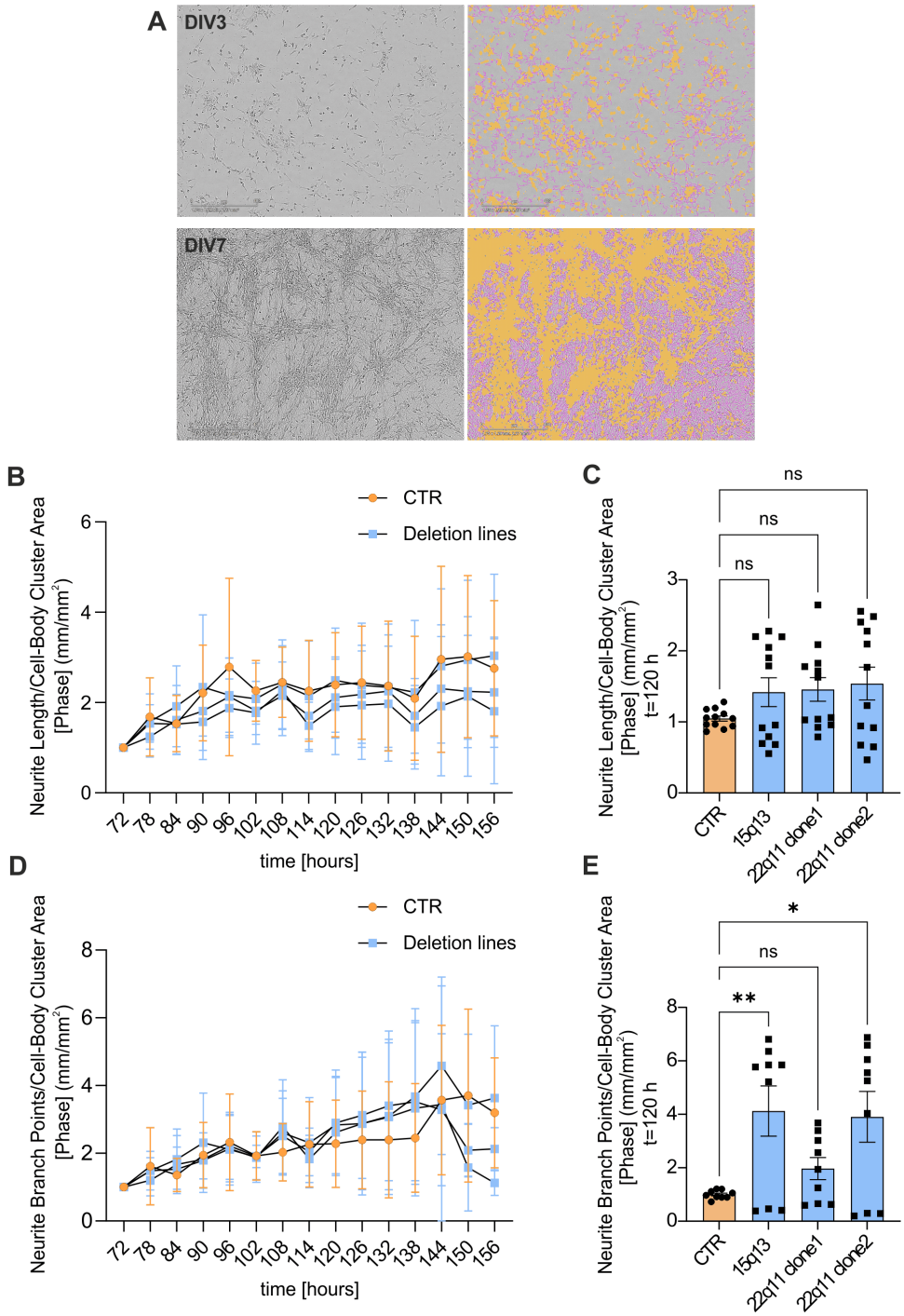

Figure 28. Neurite branching is altered in NGN2 neurons with microdeletions. (A) Exemplary phase contrast image showing the start of outgrowing neurites in NGN2 iNeurons at DIV3 (upper, left) and increased neurite outgrowth at DIV7 (lower, left). The IncuCyte Neurotrack analysis module was used for the detection of neurites (purple) and cell body clusters (orange) (upper and lower, right). Scale bars: 400 µm. **(B-C)** Neurite length per cell body cluster area and neurite branch points per cell body cluster area were measured from timepoint t=72 h to t=156 h. Values are normalized to t=72 h. **(D-E)** Analysis of neurite outgrowth and neurite branch points at t=120 h after plateau is reached. Data points represent averaged values from individual wells ± SEM. Values are normalized to CTR. Data were obtained from four independent differentiations per line. Ordinary one-way ANOVA with Dunnett's post-hoc test, CTR n=12, 15q13 n=12, 22q11 clone1 n=12, 22q11 clone2 n=12, *=p≤0.05, **=p≤0.01, ns=not significant.

3.8.2 Excitatory synapses are reduced in microdeletion E-I co-cultures

E-I synaptic ratios are crucial for the maintenance of cortical balance and essential for proper network formation. To study synaptic phenotypes in E-I co-cultures with neurons carrying a 15q13 and 22q11 microdeletion, stable NGN2 and AD2 iPSC were pre-differentiated separately and seeded into co-culture with a cultivation period of 42 days.

At DIV42, immunocytochemistry staining revealed robust expression of the excitatory presynaptic marker vGLUT1 and the postsynaptic marker PSD95 on MAP2-positive neurons, as well as the formation of morphological excitatory synapses (vGLUT1+PSD95) (**Figure 29A,** co-localization indicated by arrow heads). Quantification of vGLUT1-positive terminals revealed a significant decrease in all three mutant co-cultures (15q13, 22q11 clone1 and 22q11 clone2) compared to the isogenic CTR line (**Figure 29B**), which was accompanied by a reduced excitatory synapse density (**Figure 29D**). However, postsynaptic densities, as well as percentage of co-localizing vGLUT1 spots did not show any alterations compared to CTR (**Figure 29C, Figure 29E**).

Staining for inhibitory synaptic markers revealed the expression of the inhibitory presynaptic marker vesicular GABA transporter (vGAT) and the inhibitory postsynaptic marker Gephyrin on MAP2-positive neurons (**Figure 30A**). Contrary to excitatory synapse results, quantification of inhibitory synaptic markers in CTR and mutant clones did not reveal overt differences in E-I co-cultures. Quantification of vGAT did not reveal any differences between CTR and mutant clones (**Figure 30B**). Postsynaptic Gephyrin-positive compartments were significantly increased in all three mutant clones in comparison to the isogenic CTR (**Figure 30C**), which resulted in a trend towards increased inhibitory synaptic density (vGAT+Gephyrin), especially in 22q11 clone1 (p-value=0.09; **Figure 30D**). The percentage of co-localizing vGAT spots was unaltered (**Figure 30E**).

To summarize, synapse quantification revealed an excess loss of excitatory synapses in mutant E-I co-cultures, which was primarily driven by excitatory presynaptic terminals. In addition, a slight increase in inhibitory synapses, driven by increased inhibitory postsynaptic densities was identified. All in all, these results indicate an imbalance in excitatory and inhibitory synaptic signalling, which could result in elevated inhibition in the co-cultures.

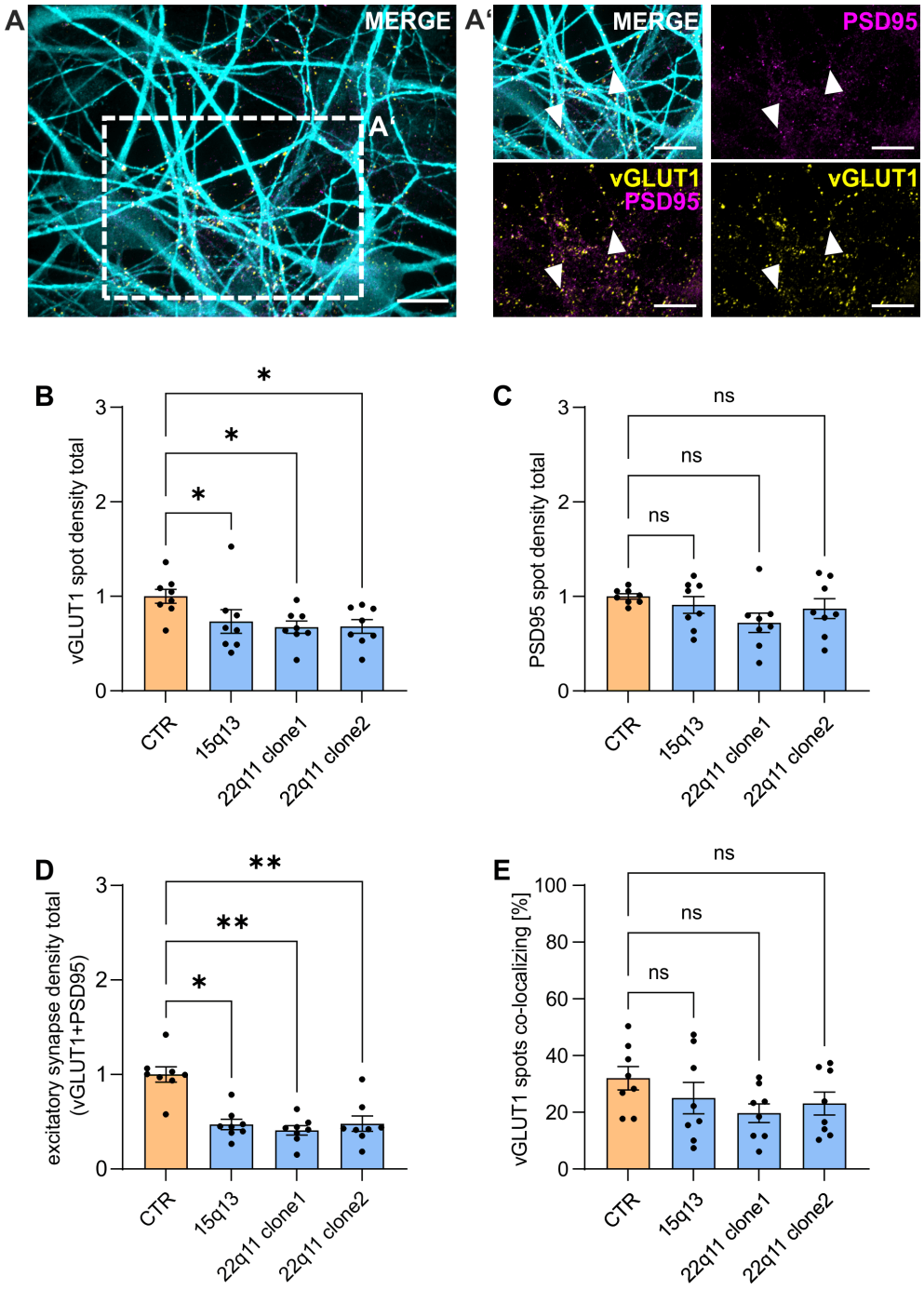

Figure 29. Excitatory synapse density is decreased in microdeletion E-I co-cultures. (A-A') Immunocytochemistry revealed the expression of the excitatory presynaptic marker vGLUT1 and the postsynaptic marker PSD95 on MAP2-positive neurons in E-I co-cultures at DIV42. The enlarged section is indicated by the dashed rectangle depicted in **(A')**. Co-localization of vGLUT1 and PSD95 are indicated by arrows heads. Scale bars 20 µm. **(B-E)** Quantification of synaptic markers localizing on MAP2-positive neuronal cells. **(B)** Quantification of presynaptic density vGLUT1. **(C)** Quantification of postsynaptic density PSD95. **(D)** Quantification of excitatory synaptic density (vGLUT1+PSD95). **(E)** Percentage of vGLUT1 spots co-localizing. Data points represent averaged values from individual wells ± SEM. Values are normalized to CTR, while values for vGLUT1 co-localizing spots are represented as absolute values. Data were obtained from four independent differentiations per line. For **(B+D)** Kruskal-Wallis test with Dunn's post-hoc test. For **(C+E)** Ordinary one-way ANOVA with Dunnett's post-hoc test, CTR n=8, 15q13 n=8, 22q11 clone1 n=8, 22q11 clone2 n=8, *=p≤0.05, **=p≤0.01, ns=not significant.

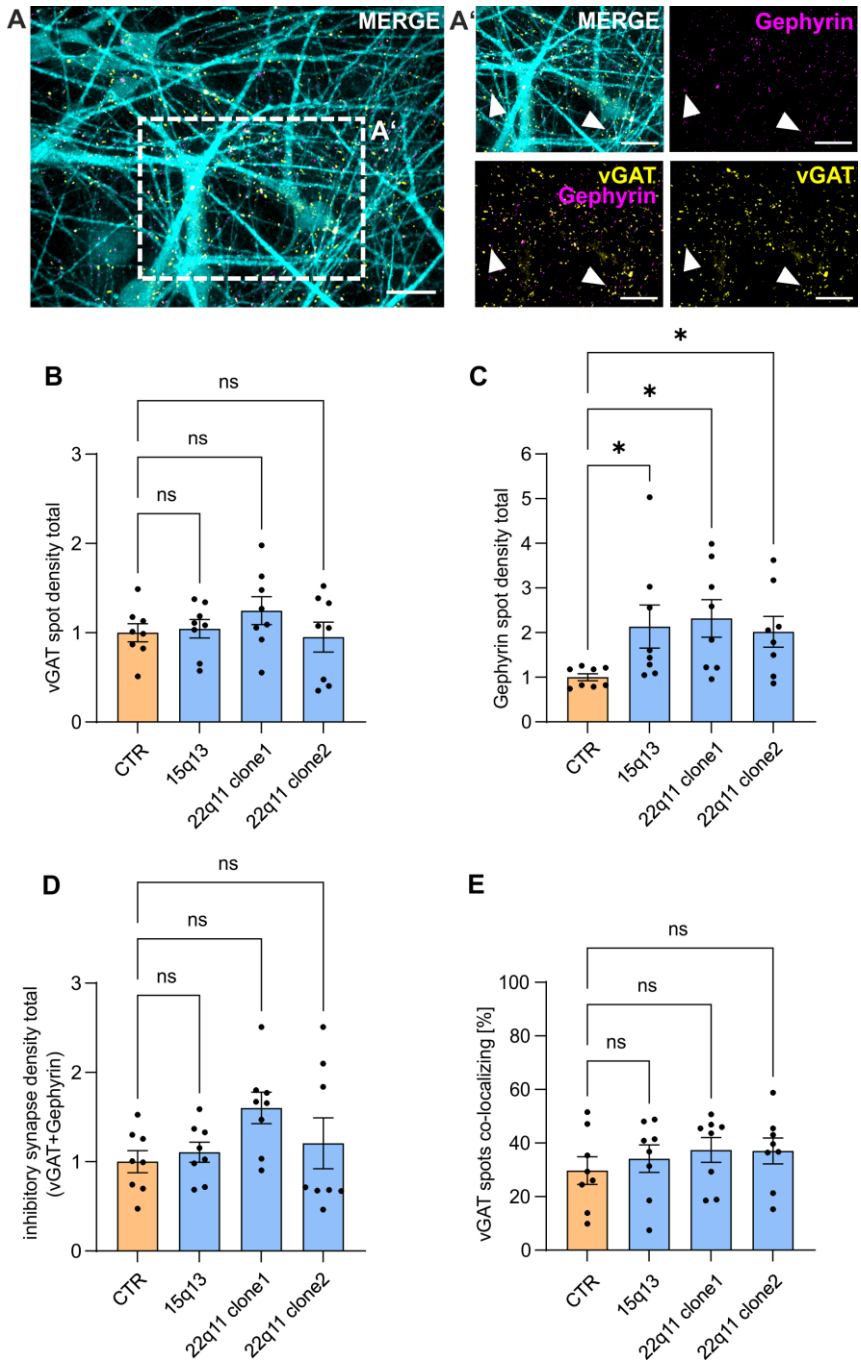

Figure 30. Inhibitory synapses not affected but show increased postsynaptic density in E-I co-cultures with microdeletions. (A-A') Immunocytochemistry revealed the expression of the inhibitory presynaptic marker vGAT and the postsynaptic marker Gephyrin on MAP2-positive neurons in E-I co-cultures at DIV42. The enlarged section is indicated by the dashed rectangle depicted in **(A')**. Co-localization of presynaptic vGAT and postsynaptic Gephyrin are indicated by arrows heads. Scale bars 20 µm. **(B-E)** Quantification of synaptic markers localizing on MAP2-positive neuronal cells. **(B)** Quantification of presynaptic density vGAT. **(C)** Quantification of postsynaptic density Gephyrin. **(D)** Quantification of inhibitory synaptic density (vGAT+Gephyrin). **(E)** Percentage of vGLUT1 spots co-localizing. Data points represent averaged values from individual wells ± SEM. Values are normalized to CTR, while values for vGAT co-localizing spots are represented as absolute values. Data were obtained from four independent differentiations per line. For **(B)** Ordinary one-way ANOVA with Dunnett's post-hoc test. For **(C-E)** Kruskal-Wallis test with Dunn's post-hoc test, CTR n=8, 15q13 n=8, 22q11 clone1 n=8, 22q11 clone2 n=8, *=p≤0.05, ns=not significant.

The comparison of excitatory and inhibitory synaptic ratios between CTR and mutant clones showed a drastic loss of excitatory synapses. Remarkably, the proportion of inhibitory synapses was significantly increased for the mutant 22q11 clone1 compared to the isogenic CTR (**Figure 31**). The identification of altered excitatory-inhibitory synapse ratios imply a synaptic disbalance in the E-I co-cultures carrying microdeletions.

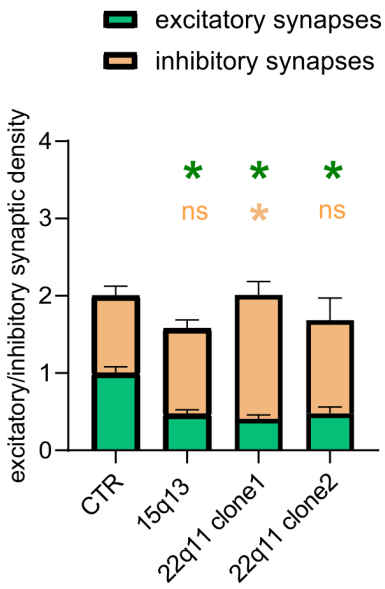

Figure 31. Altered excitatory and inhibitory synapse ratio in mutant E-I co-cultures. Quantification of excitatory (vGLUT1+PSD95) and inhibitory (vGAT+Gephyrin) synapse densities on MAP2-positive neurons in the isogenic CTR and mutant E-I co-cultures. Excitatory and inhibitory synapses were normalized to CTR, respectively. Data were obtained from four independent differentiations per line. Two-way ANOVA with Dunnett's post-hoc test, CTR n=8, 15q13 n=8, 22q11 clone1 n=8, 22q11 clone2 n=8, *=p≤0.05, ns=not significant.

3.8.3 Aberrant neuronal network activity in microdeletion E-I co-cultures

To assess whether the observed synaptic phenotype resulted in functional consequences, spontaneous single-cell calcium activity was measured and analysed. At DIV42, recordings of somatic calcium signals in unstimulated neurons in E-I co-culture over a period of 3 minutes were acquired.

Whenever calcium imaging was performed, the cultivation medium was used as recording buffer. However, calcium recordings of E-I co-cultures performed with neuronal cultivation medium resulted in no measurable activity. Therefore, the recording buffer was changed to Tyrode buffer to facilitate the generation of action potentials, as it contains an increased proportion of potassium chloride, which results in an increased resting membrane potential. Tyrode buffer solution was prepared and kindly provided by the electrophysiology group at the NMI.

Calcium recordings in Tyrode buffer revealed synchronous neuronal activity suggesting that most neurons were involved in network burst activity allowing to analyse single-cell calcium properties of neurons involved in bursting.

Exemplary calcium traces of neurons in E-I co-cultures are depicted in **Figure 32A**. Analysis of the AUC revealed a significant increase in all three mutant E-I co-cultures, with 15q13 showing the greatest increase compared to the isogenic CTR (**Figure 32B**). In addition, significantly increased ΔF/F0 and FWHM were observed for 15q13 E-I co-cultures, while those parameters were found to be slightly increased in 22q11 microdeletion cultures but did not reach the level of significance (**Figure 32C,D**). Remarkably, the peak frequency in 15q13 and 22q11 mutant E-I co-cultures showed a significant decrease in comparison to the CTR culture (**Figure 32E**).

To sum up, E-I co-cultures of stable NGN2 and AD2-derived neurons showed synchronous network activity when recorded in Tyrode buffer suggesting that increasing the membrane potential is necessary to induce measurable neural activity in these co-cultures. Single-cell analysis in mutant E-I co-cultures revealed reduced neuronal activity as observed in the decrease of peak frequency, which might be influenced by altered synaptic connectivity as described above. However, the three mutant clones showed similar activity patterns irrespective of chromosomal deletion, while the 15q13 microdeletion demonstrated the strongest phenotype.

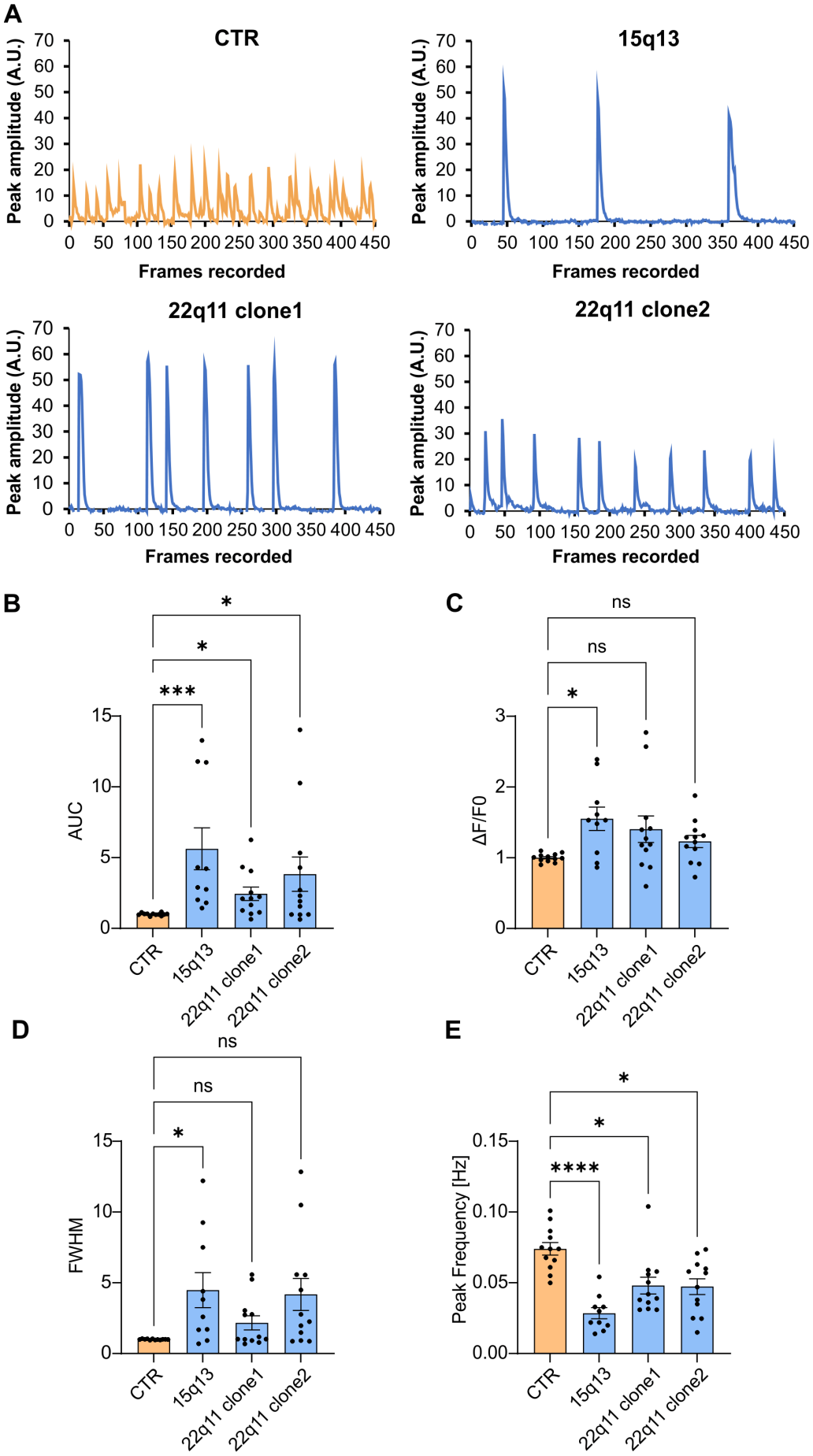

Figure legend on the next page

Figure 32. Altered network activity in microdeletion E-I co-cultures. (A) Exemplary somatic calcium traces of the isogenic CTR, the 15q13 clone, the 22q11 clone1 and the 22q11 clone2. Spontaneous single-cell calcium activity was recorded over a period of 3 minutes. **(B-E)** Mean peak parameters are indicated: area under the curve (AUC), amplitude (ΔF/F0), full width at half maximum (FWHM), and peak frequency (Hz) in E-I co-cultures at DIV42. **(B)** AUC. **(C)** FWHM. **(D)** ΔF/F0. **(E)** Peak frequency. Data points represent averaged values of multiple neurons recorded within an individual well ± SEM. Values are normalized to CTR, while values for peak frequency are represented as absolute values. Data were obtained from minimum 5 independent differentiations per line. Kruskal-Wallis test with Dunn's post-hoc test, CTR n=12, 15q13 n=10, 22q11 clone1 n=12, 22q11 clone2 n=12, *=p≤0.05, ***=p≤0.001, ****=p≤0.0001, ns=not significant.

3.8.4 Increased synchronization in E-I co-cultures carrying microdeletions

One common feature observed in E-I imbalances is disturbed network formation and altered synchronicity. Calcium imaging recordings revealed synchronous network burst activity in isogenic CTR and mutant E-I co-cultures, but additionally identified functional aberrations. To evaluate whether network communications within microdeletion E-I co-cultures are altered, the global synchronization index (GSI) based on the recorded calcium imaging data was assessed. The GSI determines the synchronization among spontaneous calcium bursts that occur during recordings and in addition calculates a numerical value ranging from 0 to 1 as a measure for the extend of synchronicity (0=asynchronous activity, 1=synchronous activity). The GSI was calculated with a Python code written and kindly provided by Emilio Pardo Gonzalez (Electrophysiology, NMI, Reutlingen). In addition to the numeric value, a correlation matrix is generated showing the comparison of each ROI to another (**Figure 33A**).

Applying the calcium raw data to the Python code, generated correlation matrices showing that ROIs (recorded neurons) in mutant E-I co-cultures were more correlated to each other than ROIs recorded in CTR E-I co-cultures, as already indicated by the colour code (**Figure 33A,** blue indicates no correlation (0), red indicates correlation (1)). Moreover, numerical values calculated by the code identified synchronicity in both CTR and mutant E-I co-cultures as values were clearly above 0. However, statistical analysis revealed increased synchronicity in neuronal networks of microdeletion E-I co-cultures compared to the isogenic CTR culture (mean GSI values15q13=0.908, 22q11 clone1=0.886, 22q11 clone2=0.894 and CTR=0.667, **Figure 33B**).

To sum up, results obtained from microdeletion E-I co-cultures identified alterations in early developmental states, as indicated by disturbed neurite branching. Additionally, the ratio of excitatory and inhibitory synapses was significantly altered with mainly excitatory presynapses being affected. Finally, functional analysis revealed altered calcium activity and disturbed

network synchronicity. Overall, the results pinpoint towards imbalances in E-I co-cultures with 15q13 and 22q11 microdeletions.

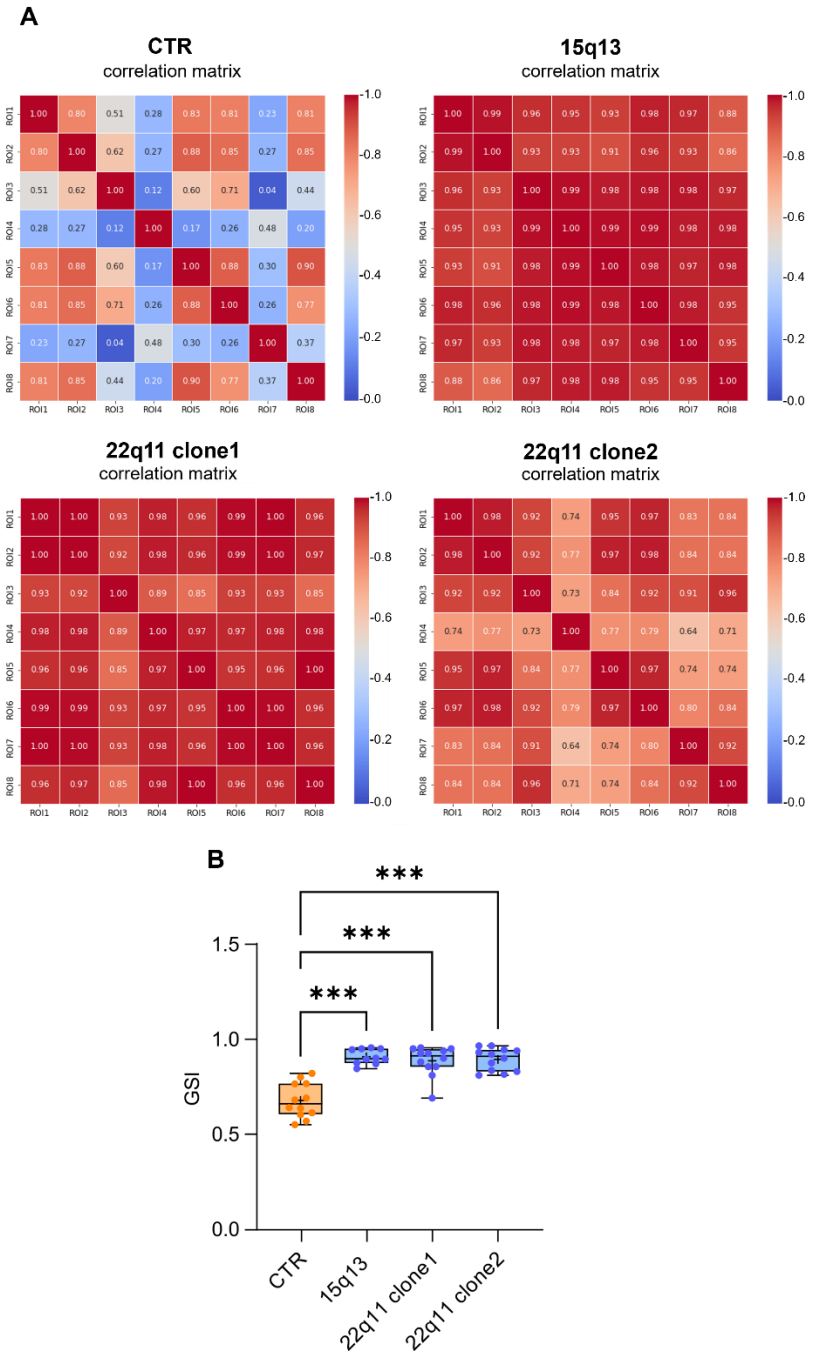

Figure 33. Increased synchronicity in 15q13 and 22q11 microdeletion E-I co-cultures. (A) Exemplary correlation matrix plots of the isogenic CTR, the 15q13 clone, the 22q11 clone1 and the 22q11 clone2. Correlation matrices showing each ROI in comparison to other ROIs calculated within one recording. Obtained values ranging from 0 to 1, with 1 showing correlation. **(B)** Global synchronization index (GSI) as a measure for synchronicity within a recorded well. Calculated GSI values obtained by the Python code ranging from -1 to 0 indicate no synchronicity, whereas values ranging from 0 to 1 indicate synchronicity. Data points represent averaged GSI values obtained from recordings within an individual well ± SEM. Data were obtained from minimum 5 independent differentiations per line. Kruskal-Wallis test with Dunn's post-hoc test, SBA n=12, 15q13 n=10, 22q11 clone1 n=12, 22q11 clone2 n=12, ***=p≤0.001.

4. DISCUSSION

In this study, the major aim was to identify and characterize functional and morphological SCZ-related phenotypes and to study reciprocal neuron-neuron interactions. For this purpose, a co-culture model comprising dopaminergic and glutamatergic neurons derived from SCZ patients was established and further investigated. In the second part of the thesis, an iPSC-derived co-culture model comprising glutamatergic and GABAergic interneurons carrying 15q13 and 22q11 microdeletions as genetic SCZ risk factors were examined.

The following aspects were addressed in this study:

1) **Identification of a dopaminergic differentiation protocol yielding homogenous dopaminergic neuron populations.** In a first step, two differentiation protocols based on different strategies were characterized and compared. The lentiviral induced dopaminergic differentiation protocol resulted in more homogenous dopaminergic neuron populations and was used for following experiments.

2) **Analysis of the dopaminergic neuron transcriptome to determine the neurodevelopmental state and to identify deregulated genes in SCZ neurons.** Transcriptome analysis of ALN-transduced dopaminergic neurons revealed a distinct developmental state in SCZ neurons compared to CTR. In addition, dopamine metabolism genes as well as the inhibitory autoreceptor DRD2 were downregulated suggesting a hypodopaminergic phenotype in SCZ ALN neurons.

3) **Analysis of aberrant neuronal activity in dopaminergic-glutamatergic SCZ co-cultures.** Calcium imaging of SCZ patient-derived co-cultures on single-cell level revealed increased spontaneous activity of both dopaminergic and glutamatergic neurons, which was solely observed in co-cultures. Mixed co-culture models revealed SCZ dopaminergic neurons as a possible driver for elevated activity, suggesting an intrinsic hyperactive state. Stimulation of DRD2 with a selective agonist rescued increased calcium activity in SCZ co-cultures.

4) **Analysis of aberrant synapse formation in SCZ co-cultures.** Synapse quantification in dopaminergic-glutamatergic SCZ co-cultures revealed a significant loss of synapses, which was primarily affecting excitatory synapses. The loss of synapses can be attributed to the drastic loss of presynaptic terminals, as postsynaptic densities remained unchanged.

5) **Analysis of aberrant synaptic connectivity and neuronal functionality in an isogenic microdeletion disease model as genetic risk factor for SCZ.** Analysis of synaptic and functional phenotypes in E-I co-cultures that carried either a 15q13 or a 22q11 microdeletion as genetic risk factors for SCZ, revealed a decrease in excitatory synapses, as well as an increase in inhibitory postsynaptic density in the mutant clones. Moreover, mutant E-I co-cultures exhibited decreased calcium activity compared to the isogenic control line, as well as increased synchronization. These phenotypes might contribute to E-I imbalances in the co-cultures.

4.1 Modelling neurodevelopmental disorders using iPSC

The challenge of linking the polygenic architecture of neurodevelopmental diseases and early onset disorders to cellular and molecular alterations in the brain can be addressed using iPSC-derived neural model systems. What makes them most suitable is that iPSC-derived neuronal models enable the identification of early aberrations in SCZ, as their transcriptomic profile closely resembles those of fetal neurons (195). Additionally, iPSC-derived neurons allow access to critical time periods at various neurodevelopmental states (150, 151), and most importantly preserve the patient's specific genetic background (196). One notable disadvantage is that iPSC-derived neural cultures cannot reflect the perinatal and adult brain, as those neurons lack the complexity of neurons *in vivo* and current cell culture techniques limit the cultivation period *in* vitro (151). Another concern of using iPSC-derived neurons is the low reproducibility found within multiple iPSC lines, as well as among different clones of the same iPSC line. Especially in the field of iPSC-derived dopaminergic neurons, several inconsistencies were found regarding reliability, reproducibility and efficiency. Most dopaminergic differentiation protocols rely on the directed differentiation process from iPSC into dopaminergic neurons with differentiation efficiencies ranging from 5-75 % (144). To date, research on dopaminergic neurons derived from SCZ patients is extremely underrepresented in the iPSC field, although implication of aberrant dopamine signalling in the pathogenesis of SCZ is widely accepted. It is likely, that the inconsistent differentiation results among the studies, as well as the lack of robust phenotype specification protocols could be responsible for the underrepresentation (152).

4.1.1 The choice of the dopaminergic neuron differentiation protocol

As an important basis for this study, two dopaminergic neuron differentiation protocols based on 'directed differentiation' (173) and 'lentiviral overexpression of lineage-specific transcription factors' (148) were compared. The differentiation efficiencies obtained with both strategies

were in line with the results reported in the original studies. Reinhardt et al., reported a variable yield ranging from 35-70 % of dopaminergic neurons obtained via directed differentiation (iDANs) (173), whereas Powell et al., employed the lentiviral overexpression strategy of lineage-specific transcription factors (ALN) and demonstrated a differentiation efficiency ranging from 70-80 %. Possible explanations for the variable dopaminergic differentiation efficiency by the directed approach could be the initial undetermined cell fate, as generated smNPC have the capability to differentiate into both central nervous system and neural crest lineage neurons, which is dependent on the small molecules added. Proper differentiation requires precise combinations and addition of chemicals, while inefficient activation or inhibition of signalling could result in heterogenous neuronal populations (181). A first study, employing the directed differentiation strategy, reported the successful differentiation into midbrain dopaminergic neurons, but was lacking the quantification of dopaminergic neurons generated (197). A follow up study based on a two-step differentiation protocol with first patterning into midbrain floor-plate cells and further patterning into midbrain dopaminergic neurons demonstrated a dopaminergic neuronal yield ranging from 70-80 %. With this approach, the conventional EB formation, as described for the directed differentiation protocol employed in the study presented, is bypassed and produced three times more TH-positive neurons (181, 198).

To date, there are only few established dopaminergic differentiation protocols that make use of lineage-specific transcription factor overexpression. In 2011, a first study demonstrated that the combination of the three lineage-specific transcription *Ascl1*, *Lmx1a/Lmx1b* and *Nurr1* important for midbrain development can rapidly and efficiently induce dopaminergic neurons from mouse and human fibroblasts (199). The transcription factor *ASCL1* is proposed to play essential roles in neuronal commitment and differentiation, whereas *LMX1A*/*LMX1B* and *NURR1* are critical factors during dopaminergic system development and survival (199, 200). Interestingly, trans-differentiation of primary rat cortical neurons by induction of the dopaminergic-specific transcription factors *Nurr1*, *Lmx1a* and *Pitx3* that was not sufficient to induce TH expression in absence of *Ascl1*. TH-positive neurons were only obtained by co-expression of Nurr1 and Ascl1 suggesting that these factors are crucial for proper dopaminergic neuron differentiation (201). First reports using overexpression of the transcription factors *ASCL1*, *LMX1A* and *NURR1* demonstrated a dopaminergic differentiation efficiency with low yields ranging from 5-33 %. Optimization of this one-step protocol with additional expression of the doxycycline inducible reverse tetracycline transactivator for controlled transcription and the incorporation of antibiotic selection cassettes resulted in more homogeneous dopaminergic populations (65-90 %) (148, 202) which is in accordance with the findings in the study presented.

Interestingly, analysis of spontaneous calcium activity revealed distinct firing properties of dopaminergic neurons generated via both differentiation protocols. As directed differentiation resulted in less homogenous dopaminergic neuronal populations, it can be speculated that other neurons generated may have an impact on neuronal properties in these cultures. Therefore, it is crucial to record the number of target neurons and to identify the types of cells produced.

To conclude, directed differentiation protocols resulted in more heterogenous neuron populations, while in contrast, overexpressing lineage-specific transcription factors accelerates the conversion into neuronal cells, resulting in a more consistent differentiation process and more homogenous neuronal populations. Thus, employing induced differentiation protocols will significantly improve the iPSC research and will help to improve the understanding of SCZ-related phenotypes in dopaminergic neurons.

4.2 Early neurodevelopmental aberrations in SCZ neurons

4.2.1 Neurodevelopmental deficits in SCZ ALN neurons

So far, there are three research groups that have employed iPSC-derived dopaminergic neurons from SCZ patients and compared them to CTR lines. Importantly, all three studies made use of directed differentiation protocols and none of them included RNA sequencing (167, 168, 169). In this study, neuronal cultures of ALN-transduced iPSC derived from patients with idiopathic SCZ were employed for the first time to study aberrant dopamine signalling and to reveal SCZ-relevant phenotypes.

Transcriptome analysis of SCZ ALN neurons revealed thousands of DEGs. A closer look revealed increased expression of stem cell marker genes, as well as neural progenitor markers. In accordance with these findings, an iPSC study focusing on SCZ-derived dopaminergic neurons reported abnormal expression of neuronal precursor markers PAX6 and Nestin, which was revealed by immunocytochemistry. While PAX6 was significantly higher expressed, Nestin was significantly reduced in SCZ-derived dopaminergic neurons (169). Although the differentiation into dopaminergic neurons was based on forced expression of the three transcription factors *ASCL1, LMX1B* and *NURR1* in the study presented, gene expression profiling revealed reduced expression levels of these genes in SCZ ALN neurons. This could be explained by the fact, that the endogenous expression levels of these early transcription factors were drastically reduced in SCZ neurons, which might lead to an impaired ability to differentiate properly into dopaminergic neurons. However, it remains to be addressed to what extent ectopic expression of these transcription factors is affecting the endogenous

gene transcript levels, but one could speculate that forced expression is not sufficient to compensate the decreased endogenous expression levels. In the course of dopaminergic neurogenesis, early expression of FOXA2 activates LMX1A/LMX1B, which are involved in early specification into midbrain dopaminergic progenitor cells and play essential roles in regulating cell proliferation (188). Additionally, both transcription factors were found to be essential for regulating synaptic inputs on dopaminergic neurons and dendritic formation (203). After entering the post-mitotic phase, dopaminergic progenitor cells differentiate into mature neurons and express NURR1, which is crucial for dopaminergic neuron development, maturation and function. Moreover, NURR1 is required for the expression of several genes implicated in dopamine synthesis (200). Mice lacking *Nurr1* were not able to generate dopaminergic neurons and died immediately after birth (204). In addition, decreased *NURR1* mRNA levels in the prefrontal cortex were found in SCZ patients' post-mortem brains (205).

4.2.2 Neurodevelopmental deficits in SCZ NGN2 neurons

In a next step, NGN2-derived glutamatergic neurons were stained for deep- and upper-layer markers in order to identify putative neurodevelopmental alterations in SCZ neurons. *In vivo*, newly formed excitatory pyramidal neurons originate from the ventricular zone and migrate though radial migration to their appropriate cortical layers. Cortical deep-layers are formed by neurons that exit the ventricular zone in early neurodevelopmental phases, while neurons formed at later timepoints settle in superficial cortical layers (206). Especially, cortical neurons located in the superficial layers are thought to be involved in enhanced cognitive processes in humans and thus, represent primary targets of neurodevelopmental disorders such as SCZ (207).

Subtype-specification of NGN2 neurons revealed that predominantly upper-layer neurons (BRN2-positive) were generated, whereas deep-layer neurons (CTIP-positive) made up only a small proportion. This indicates that generated NGN2 induced telencephalic glutamatergic neurons in the study are representative for later developmental states. However, CTIP-positive neurons were found to be increased in SCZ cultures compared to CTR suggesting distinct developmental states. This is particularly important to note when synapses are quantified.

Overall, transcriptome analysis in ALN-derived neurons as well as quantification of layer-specific markers in NGN2-derived neurons revealed deficits in the developmental of SCZ neurons suggesting a delayed developmental state. In line with this, previous studies identified early aberrations in SCZ progenitor cells, including deficits in neuronal migration, increased oxidative stress and altered signalling pathways, and one could speculate that these alterations might contribute to aberrations in the development of SCZ neurons (154, 155, 156).

Neurodevelopmental deficits might lead to functional and morphological consequences in differentiated mature neurons in SCZ.

4.3 Altered dopamine metabolism in SCZ ALN neurons

One major finding of the transcriptome analysis was the downregulation of genes involved in dopamine synthesis and transport implying a hypodopaminergic phenotype in SCZ ALN neurons. According to these findings, several patient studies have provided robust evidence of aberrant dopamine signalling in SCZ patients that varies depending on the dopaminergic pathway investigated. Most imaging studies using [^{18}F]-DOPA to examine the dopamine synthesis capacity have found increased striatal uptake in SCZ patients, whereas less metabolic activity was identified in cortical regions (208). So far, VMAT1/VMAT2 activity, as well as expression levels has not been widely examined in SCZ patients. However, one imaging study found normal VMAT2 levels in the striatum of SCZ post-mortem samples (209). In addition, studies on DAT expression are inconsistent, and most reports focus on striatal regions. A recent meta-analysis of post-mortem studies claimed that DAT expression is not altered in SCZ (210), while a PET imaging study reported increased DAT levels restricted to BA 10 without alterations in other cortical regions (211).

Likewise, transcriptome analysis revealed the expression of all five dopamine receptors, with DRD2 being the most abundant DRD expressed in ALN neurons. DRD2 may serve as an autoreceptor of dopaminergic neurons important for controlling feedback inhibition. Upon stimulation of autoreceptors, the excitability of dopamine neurons, as well as the release of dopamine decreases through the control of downstream signalling (190). The expression of DRD2 was found to be drastically decreased in SCZ ALN neurons suggesting less inhibitory signalling. Remarkably, *Drd2*-deficient mice demonstrated reduced expression of Nurr1 and a reduction of mesencephalic TH-positive cells during the embryonic state suggesting an alteration in the dopaminergic neuron development due to the absence of DRD2, which was rescued by the activation of DRD2 (212). The hypothesis of a mutual interaction of both genes was supported by a study reporting modification in the expression levels of DRD2 by gain or loss of Nurr1 (213). In line with this, transcriptome data also revealed decreased expression of both NURR1 and DRD2 in SCZ ALN neurons suggesting that aberrant NURR1 expression might lead to aberrant DRD2 expression levels.

Overall, it can be hypothesized that changes in the expression of early transcription factors during dopaminergic neuron development (as discussed in section 4.2.1) most likely contribute to altered dopamine metabolism in more mature neurons in SCZ. Consistent with this hypothesis, the transcriptome data implies that SCZ ALN neurons exhibit a delayed

developmental state, which could result in a reduced dopamine metabolism and reduced expression of the autoreceptor DRD2.

4.4 Altered neuronal activity in SCZ ALN-NGN2 co-cultures

The decreased expression of the inhibitory autoreceptor DRD2 in SCZ ALN neurons as revealed by transcriptome analysis suggests less inhibition in SCZ neuronal cultures. Therefore, as a next step, calcium imaging was performed to study functional phenotypes in ALN and NGN2 cultures with neurons cultivated separately, as well as in the established ALN-NGN2 co-culture model.

Analysis of calcium imaging performed in both ALN and NGN2 monocultures did not reveal any alterations of neuronal activity between CTR and SCZ. Prior research on iPSC-derived glutamatergic neurons has provided contrasting findings in relation to all parameters. In a first study it was shown that amplitude and numbers of spontaneous calcium transients were unaltered, which is consistent with our observations (157), whereas a second study identified reduced peak frequency and increases in AUC and FWHM in SCZ samples (158). It is important to mention, that differentiation protocols employed by the two studies were based on growth-factors resulting in more heterogenous neuronal populations. A further study, using NGN2-derived glutamatergic neurons of isogenic 16p11.2 duplication and SCZ patient-derived iPSC, observed reduced peak frequency in monocultures, but focused on synchronous neuronal network activity (214).

Interestingly, upon co-cultivation of ALN and NGN2 neurons both exhibited elevated activity in SCZ cultures, suggesting that the interaction between the two neuronal cell types might contribute to this phenotype. The cause behind the increased peak frequency in both SCZ neurons in co-culture remains elusive and need to be further addressed. However, one possible explanation could be the intrinsic hyperactive state of SCZ ALN neurons due to a decreased expression of the autoreceptor DRD2, which was accompanied by reduced dopamine metabolism suggesting a decrease in dopamine release. Therefore, it can be speculated that upon co-cultivation NGN2 neurons try to compensate the reduced dopamine signalling by an increased release of glutamate, which in turn could lead to an activation of ALN neurons. Another possibility could be that NGN2 neurons express other DRDs that may account for increased calcium activity. Moreover, unaltered calcium activity observed in SCZ ALN monocultures suggests an autoregulative mechanism that allows to compensate the hyperactive state.

In addition, the observed intrinsic hyperactive state of SCZ ALN neurons in the mixed co-culture model supports the theory of a hypodopaminergic phenotype and confirms the

hypothesis of reduced inhibition. Additionally, reduced FWHM was as well observed in SCZ ALN monocultures compared to CTR, indicating altered calcium flux dynamics of dopaminergic neurons. A recent co-culture study comprising NGN2 and AD2 neurons derived from the same iPSC lines reported reduced peak amplitude of SCZ NGN2 neurons that showed unsynchronized activity, while the peak frequency was unaltered. Strikingly, when focusing on neurons involved in synchronized burst activity, unaltered peak amplitude but increased peak frequency was demonstrated in both SCZ NGN2 and AD2 neurons (164), suggesting a hyperactive state in this SCZ co-culture model as well, which was restricted to synchronous activity. However, the neurons in the present ALN-NGN2 co-culture exhibited spontaneous single-cell activity but were lacking coordinated network burst firing, which could be explained by the absence of inhibitory interneurons in these cultures. *In vivo*, synchronized bursting activity in the cortex results from the precise interplay of excitation and inhibition predominantly driven by fast-spiking PV-positive interneurons (215).

Moreover, the fact that DRD2 serves as an autoreceptor and upon stimulation decreases the excitability of the neuron, was confirmed by the application of the selective DRD2 agonist Pramipexole that rescued the hyperactive state in SCZ co-cultures, most likely by increasing the inhibition (190). Interestingly, this effect was selective for SCZ neurons but not for CTR neurons, indicating an aberrant DRD2 functionality. The interplay between DRD2 autoreceptors and hyperactivity was demonstrated in autoreceptor-null mice lacking Drd2 on dopaminergic neurons, while other neuronal cell types had normal levels of the receptor expressed at postsynaptic site. These animals demonstrated a hyperactive state due to the lack of dopamine release inhibition (216), which is in accordance with the findings of a hyperactive state in the present SCZ co-culture.

Furthermore, the elevated activity of SCZ NGN2 neurons was also rescued by the selective DRD2 agonist suggesting that DRD2 signalling as well contributes to the activity pattern of NGN2 neurons. *In vivo*, DRD1 and DRD2 are highly expressed in cortical layers II, V, VI on both glutamatergic pyramidal neurons and inhibitory interneurons in the human PFC (114). The expression of activating DRD1 and inhibitory DRD2 in NGN2-transduced iPSC and NPC was demonstrated in several studies (159, 217, 218, 219). However, the cause of elevated calcium activity of SCZ NGN2 neurons remains elusive and needs to be further elucidated.

Overall, the identified hyperactive phenotype in the SCZ co-culture model indicates a mutual interaction of dopaminergic and glutamatergic neurons and could be associated with altered excitatory synaptic input, altered neurotransmitter signalling, signal integration at the postsynaptic site or altered receptor expression. However, one need to bear in mind, that transcriptome analysis was performed with ALN neurons cultured separately, showing distinct phenotypes when co-cultured with NGN2 neurons. Detailed electrophysiological

measurements such as patch-clamp recordings could be performed to address these questions. Typically, antipsychotics are DRD2 antagonists that alleviate positive symptoms by blocking the receptor, while treatment options for negative and cognitive symptoms are relatively rare. This experiment demonstrates that a hypodopaminergic phenotype could be rescued by activating DRD2 and thus leading to reduced neuronal activity. However, *in vivo* the situation is complex as drug administration in a spatially restricted manner is challenging.

4.5 Synaptic aberrations in SCZ-patient derived NGN2 neurons

The brain of SCZ patients is characterized by whole brain volume reductions, especially in grey matter areas such as the prefrontal cortex (220), which is suggested to be due to excess synapse loss (59). Thus, synaptic aberrations were investigated in detail in this thesis using SCZ patient-derived dopaminergic and glutamatergic neurons. The hypodopaminergic phenotype observed in SCZ ALN neurons as revealed by transcriptome analysis suggests a reduction in dopaminergic presynaptic terminals, as DAT levels were reduced. However, synaptic alterations between CTR and SCZ in ALN monocultures were not identified neither by quantification of SYN1 nor by transduction with the fusion protein SYP-mRuby. These results contrasted with a previous study that reported a reduced expression of DAT in SCZ-derived dopaminergic neurons (169). Moreover, a recent study found that only 50 % of the dopaminergic terminals were positive for VMAT2 indicating that not all varicosities are able to release dopamine. This could be explained by the capability of dopaminergic neurons to co-release other neurotransmitters such as glutamate or GABA most likely from distinct terminals (221). Presumably, both approaches staining with SYN1 and overexpression of SYP-mRuby did not exclude varicosities that are not specific for dopamine release, which could explain the contrary results obtained by RNA sequencing and synapse quantification in SCZ ALN monocultures.

Significant reductions of the general presynaptic marker SYN1, as well as synapses (SYN1+PSD95) were observed on both ALN and NGN2 neurons indicating an overall loss of synapses in SCZ co-cultures. In line with these findings, post-mortem studies of SCZ patients reported reduced protein and mRNA levels of synaptic markers in the PFC, such as the synaptic vesicle protein SYP (123), which was confirmed by a recent PET imaging study that identified reduced expression of the synaptic vesicle protein SVA2 in SCZ patient cortices (222). Noteworthy, most SCZ patient studies demonstrated synaptic phenotypes in cortical regions mainly focusing on the local microcircuitry, with few studies including as well subcortical regions such as the hippocampus (124). It is therefore important to note, that the established co-culture system in this study comprises neuronal types that *in vivo* are localized in distinct brain regions.

The fact that dopaminergic neurons can co-transmit glutamate which make up to 30 % of VTA neurons and additionally, these neurons send projections to the prefrontal cortex, is adding a further dimension of complexity (223) and makes quantification of vGLUT1-positive terminals less specific. Transduction of ALN or NGN2 neurons with the lentiviral vector SYP-mRuby before seeding into co-culture and subsequent quantification of SYP-positive presynaptic boutons, revealed consistent findings of reduced presynaptic vGLUT1 density on SCZ NGN2 neurons and reduced SYP-positive density on SCZ ALN neurons. So far, the role of glutamatergic-dopaminergic synaptic innervation in SCZ has not been reported and remains elusive. However, these results indicate that mainly excitatory presynaptic connections onto glutamatergic neurons within cortical microcircuits are disturbed, as well as excitatory inputs onto dopaminergic neurons. In contrast to these findings, a recent study employing co-cultures comprising glutamatergic NGN2-derived and GABAergic AD2-derived neurons representative for the cortical microcircuitry, resulted in unaltered excitatory synaptic input onto SCZ NGN2 neurons, whereas excitatory input onto AD2 neurons was increased (164). These contradictory results indicate that depending on the neuronal composition in the co-culture, the synaptic phenotype may vary, but as well demonstrates aberrant excitatory synapse formation as an overarching phenotype.

In contrast to post-mortem studies, the PSD95 density of SCZ NGN2 neurons was found to be either unaltered or increased, which differed considerably from a recent meta-analysis revealing a significant decrease in density in dendritic spines and reduced PSD95 expression levels predominantly in the PFC (124). Especially in post-mortem studies, the evaluation of dendritic spines represents a proxy of synapse formation as most excitatory synapses in the cortex are formed on spines. However, postsynaptic density in SCZ is relatively frequently studied but findings are often conflicting due to limited number of subjects and the lack of brain region specifications. Interestingly, two research groups found significantly reduced spine density in layer III pyramidal neurons, which was not observed in deep cortical layers, suggesting that aberrant synapse formation is restricted to certain neuronal circuits (224). As immunocytochemistry of NGN2 neurons revealed two subpopulations that were either positive for the deep-layer marker CTIP or the upper-layer marker BRN2 and in addition depicted a small fraction of double-positive neurons, quantification of PSD95 positive clusters should be further investigated in a more NGN2 subpopulation-specific manner.

In summary, the analysis of synaptic phenotypes in ALN-NGN2 co-cultures revealed that mainly excitatory presynaptic terminals are affected, while dopaminergic varicosities were largely unchanged, but should be studied further including more specific dopaminergic synapse markers such as DAT, VMAT1, VMAT2. However, synapse formation is a relatively dynamic process (225) and additional studies should take into consideration to monitor these

synaptic dynamics in earlier, as well as in more mature cultures to reveal possible aberrations occurring at different developmental phases. In addition, it is of great importance to quantify synapses in a more cortical subtype-specific manner, especially against the background of a developmental deficit in SCZ NGN2 neurons. To conclude, it can be assumed that reduced excitatory synaptic signalling is not responsible for increased activity observed in SCZ co-cultures and might be a more general morphological phenotype.

4.6 Excitatory-inhibitory co-culture as a model of the developing cortical microcircuitry

In the second part of this thesis, an iPSC-based co-culture comprising glutamatergic and GABAergic interneurons that carried a 15q13 or a 22q11 microdeletion was employed as a model of the developing prefrontal cortical microcircuitry. This microdeletion E-I co-culture model represents a more general model system for the study of neurodevelopmental disorders as diagnostic specificity is difficult due to the overlapping genetic architecture and comorbidity in patients.

4.6.1 Neurodevelopmental aberrations in NGN2 neurons carrying microdeletions

In a first step, neurite outgrowth and neurite branching of differentiating NGN2-transduced glutamatergic neurons was assessed. In contrast to SCZ post-mortem (226) and SCZ patient-derived iPSC studies (157, 158) that reported reduced neurite arborization and decreased neurite outgrowth capacity, NGN2-transduced glutamatergic neurons with 15q13 and 22q11 microdeletions revealed a strong increase in neurite branching. It is important to mention, that microdeletions in humans account for a range of neurodevelopmental and psychiatric disorders which could explain the divergent results. One study that generated a mouse model with a deletion of chromosome 7qC corresponding to the human 15q13 microdeletion, reported no abnormalities in dendrite branching or arborization in the cortex of 2 months old mice (98). Deviating results were observed in an additional study including heterozygous (*Df(h15q13)*/+) mouse models that reported decreased dendritic arborization in layer II/III PFC neurons at postnatal day P28 (95), which was also observed in adult Del(3.0Mb)/+ mice, representative for the human 22q11 microdeletion, in layer V neurons in the PFC (227). In line with those observations, iPSC-derived NGN2 neurons from patients with a 15q13 and a 22q11 microdeletion syndrome revealed a significant reduction in neurite branching at DIV28 and DIV49 (92, 228). Although the described studies reported opposite results compared to the findings in this study, the fact that neurite alterations were observed during the course of cortical neurodevelopment implies a disturbed development of excitatory glutamatergic

neurons carrying microdeletions that could contribute to impaired formation of cortical networks comparable to SCZ. A possible explanation for the deviating phenotypes could be the developmental state of the NGN2 neurons reported. While neurite branching of NGN2 neurons in this study was measured at DIV5, the described studies reported reduced neurite branching at later time points.

4.6.2 Aberrant synapse formation in E-I co-cultures carrying 15q13 and 22q11 microdeletion syndromes

Heterozygous mouse models (*Df(h15q13)*/+) display phenotypes similar to SCZ, epilepsy and ASD patients (93, 95, 97). One phenotypic discovery in these models are deficiencies in dendritic spine and synapse growth in cortical excitatory neurons (92, 95). In support of this, excitatory presynaptic and synaptic densities were found to be significantly reduced in the E-I co-cultures under study, whereas PSD95-positive cluster densities were unchanged. Interestingly, transcriptome analysis of cortical brain tissue derived from heterozygous mouse models revealed significant enrichment for genes associated with ‘forebrain development’ and identified deficiencies of cortical excitatory neurons in synapse formation (95) suggesting that predominantly cortical glutamatergic development is disrupted. Additionally, they found significantly reduced spine densities in the PFC indicating a loss of excitatory neurons. Several rodent studies identified the gene *OTUD7A*, encoding the deubiquitinating enzyme, as a major driver for the phenotypes observed in the 15q13 microdeletion syndrome sufficient to induce characteristic phenotypes (92, 93, 94, 95). The enzyme was found to be enriched at dendritic spines and membrane compartments of cortical neurons implying a potential role in synaptogenesis (93). In accordance with phenotypes observed in 15q13 microdeletion mice, *Otud7a*-null mice revealed a decreased number of dendritic spines in the frontal cortex that was found to be completely rescued by overexpression of *OTUD7A* (95). Additionally, iPSC-derived NGN2-transduced neurons with a loss-of-function (LoF) mutation in *OTUD7A* exhibited marked reductions of both PSD95 and GluA1 puncta, a subunit of the AMPA glutamate receptor, accumulating in mature glutamatergic synapses (94), which is consistent with findings of *Otud7a*-null mice.

Similar synaptic phenotypes were observed in the E-I co-culture model harbouring a 22q11 microdeletion, which is the most common deletion in humans increasing the predisposition to psychiatric disorders (229). Consistent with those findings, a recent histological analysis of Del(3.0Mb)/+ mice revealed significantly reduced spine density of pyramidal neurons in layer V of the frontal cortex (227). On the contrary, an iPSC study of NGN2-transduced excitatory neurons did not show differences in synapse density between CTR and 22q11 patient lines (230). A further iPSC study performed transcriptome and whole cell proteomics and reported

downregulation of presynaptic proteins in excitatory NGN2 neurons, specifically involved in synaptic vesicle cycle, which was confirmed by immunostaining (231) and was in line with the findings in the E-I co-culture study presented here.

Interestingly, drastic loss of excitatory synapses was observed in both 15q13 and 22q11 E-I co-cultures under study, which was mainly due to a presynaptic (vGLUT1) phenotype. Accordingly, several previous SCZ studies using NGN2-derived neurons reported a reduction of excitatory synapses, mainly driven by a loss of vGLUT1-positive presynaptic terminals (165, 166). *In vivo*, axonal terminals are thought to initiate the assembly of a synapse by targeting the postsynaptic site. This first contact between pre- and postsynaptic sites is mainly mediated by cell adhesion molecules (232). The finding of reduced presynaptic sites explains the drastic loss of excitatory synapses, as less presynaptic sites form less contacts with postsynaptic ones.

Quantification of inhibitory synapses did not reveal changes in inhibitory presynaptic nor in inhibitory synaptic densities, whereas Gephyrin-positive densities showed a slight increase in 15q13 and 22q11 microdeletion E-I co-cultures. Contrary to those observations, one study identified reduced expression levels of the presynaptic marker GAD6, but no change in other interneuron markers in the PFC of (*Df(h15q13)*/+) mice (233), whereas no study reported altered inhibitory synapse formation in neurons with 22q11 microdeletions.

Overall, these reports pinpoint towards deficits in excitatory synaptic signalling, which is consistent with the findings of this study. It is of note, that the observed excitatory synaptic phenotype was due to a drastic reduction of presynaptic sites. Nonetheless, the possible implication of cortical inhibitory synaptic signalling remains largely unstudied in these models.

4.6.3 Altered network connectivity in E-I co-cultures carrying 15q13 and 22q11 microdeletion syndromes

Next, functional characterization was performed by measuring spontaneous calcium activity. In contrast to the previously described ALN-NGN2 co-culture model (as discussed in 4.4), recorded E-I co-cultures exhibited synchronous network activity. *In vivo*, synchronized bursting activity in the cortex is regulated by the precise interplay of excitatory and inhibitory neurons (215). Several studies demonstrated that patients with SCZ have altered cortical gamma oscillations in resting states and in response to stimuli (234), which was also observed in *Df(h15q13)*/+ mice (97). These oscillations are predominantly driven by fast spiking interneurons (126). The *CHRNA7* gene is also affected by the critical 15q13 microdeletion and is mediating inhibitory transmission in the cortex (235). Although *Chrna7*-/- mice have very subtle phenotypes (236), suggesting that *Chrna7* alone is not sufficient to induce characteristic

features observed in *Df(h15q13)*/+ mice, reduced expression may lead to compromised signalling of interneurons. While complex high-frequency oscillations *in vivo* cannot be simply compared to the simplified *in vitro* E-I co-culture model, the observations suggest altered network activity. Concordant to the results observed in the 15q13 microdeletion E-I co-culture model, *Df(h15q13)*/+ mouse cortical neurons *in vitro* demonstrated significantly reduced burst and network burst frequencies (92). Interestingly, the same study also reported elevated burst frequency of cultures comprising NGN2-transduced neurons derived from 15q13 and homozygous *OTUD7A* patients that reversed after eight weeks of cultivation. So far, studies using iPSC-based systems to model 15q13 microdeletions made use of NGN2 neurons. The use of more physiologically relevant culture systems, such as neuronal co-cultures comprising NGN2 and AD2 neurons is largely lacking in this iPSC research field and may contribute to the identification of microdeletion-related phenotypes.

Despite the concordant synaptic phenotypes, functional characterization of 22q11 E-I co-cultures as well revealed similar phenotypes as observed in 15q13 co-cultures. A possible mechanism contributing to altered neuronal activity was observed in a recent study using human 3D cortical spheroids derived from 22q11 patients, in which transcriptional profiling revealed enrichment of genes associated with neuronal excitability and calcium signalling (159). However, in contrast to the E-I co-culture under study, electrophysiological and calcium imaging experiments revealed increased spontaneous peak frequency, which was found to be related to altered membrane potential and deficits in calcium signalling. Additionally, the generation of a heterozygous *DGCR8*+/- isogenic iPSC line was able to recapitulate the functional features of 22q11 neurons and could be rescued by *DGCR8* overexpression (159). Moreover, mitochondrial deficits were identified in NGN2 neurons derived from 22q11 patients contributing to reduced levels of ATP, which primarily resulted from reduced functionality of respiratory complexes I and IV (230). One could speculate that decreased ATP capacity may have an impact on functional properties of neurons and could contribute to reduced peak frequency. Hence, it would be interesting to perform experiments such as Seahorse assays to assess putative mitochondrial dysfunctions in NGN2 and AD2 neurons in the 22q11 E-I co-culture model. The reported loss of excitatory synapses in both 15q13 and 22q11 microdeletion E-I co-culture systems under study, could as well account for the decreased network activity as both excitatory and inhibitory neurons may receive less input resulting in an overall downregulation of neuronal activity. However, this hypothesis needs to be addressed more thoroughly. Taken together, these findings support the hypothesis of aberrant neuronal network activity and suggest pervasive alterations during cortical neurodevelopment

Besides the reduced peak frequency identified in the microdeletion E-I co-cultures, increased synchronicity was observed by the analysis of the GSI. Hypersynchronous neuronal networks

are a characteristic hallmark of epilepsy and are further accompanied by excess excitability (237). In support of this, studies focusing on 15q13 microdeletion mouse models reported epilepsy-related alterations and altered excitability of cortical neurons (97, 238).

In summary, the analysis of synaptic and functional phenotypic features in mutant E-I co-cultures provided a clear indication of a potential E-I imbalance. Aberrations of glutamatergic neurons were already observed during early neurodevelopment and were then reflected in the excitatory synaptic imbalance, which then might result in aberrant neuronal activity.

4.7 Comparison of idiopathic ALN-NGN2 and isogenic E-I co-culture-related phenotypes

In this thesis, morphological and functional phenotypic features in SCZ and related neuropsychiatric disorders were studied using two co-culture models (ALN-NGN2 and E-I) with distinct neuronal compositions. Both co-culture systems were surrogates for distinct neuronal connectivity *in vivo* with NGN2 neurons as the common denominator, thus the aim was to identify common and divergent phenotypes. A comparative overview of observed morphological and functional phenotypes is listed in **Table 27**.

One deviating phenotype in those co-cultures was observed on a functional level. While ALN-NGN2 co-cultures did not show synchronous network activity, E-I co-cultures exhibited synchronous activity with an increased synchronicity in mutant cultures compared to CTR. Similar observations have been made in SCZ patient-derived E-I co-cultures, which demonstrated both synchronous as well as unsynchronous activity, however the synchronicity was decreased in these SCZ co-cultures (164, 239). When focusing on the calcium parameters, opposing effects were identified. While ALN and NGN2 neurons in SCZ co-cultures exhibited increased peak frequency, this parameter was found to be decreased in E-I mutant co-cultures. Divergent observations have been made in the patient-derived E-I co-culture study mentioned above. Both NGN2 and AD2 neurons involved in synchronous network activity exhibited increased peak frequency in SCZ E-I co-cultures (239).

Interestingly, both co-culture systems revealed a shared synaptic phenotype. In SCZ ALN-NGN2 co-cultures, as well as in mutant E-I co-cultures a significant loss of excitatory synapses was observed, which was in both cases due to a decrease in presynaptic sites (vGLUT1).

Overall, shared and divergent phenotypes were observed in both co-cultures system suggesting that regardless of neuronal composition and genetic background, neuronal aberrations occur, which manifest in distinct outcomes. Although, an overarching synaptic phenotype was identified, the functional consequences differed from each other, which could

be due to different neuronal interactions. In addition, these findings suggest different mechanisms are likely at play, that not only depend on the interactions between neurons, but also on the genetic background preserved in these cultures. Moreover, the loss of excitatory synapses in both model systems implies that this phenotype is not SCZ specific but is rather a common phenomenon in neuropsychiatric disorders and manifests in distinct neuronal connectivity. One should also keep in mind that the degree of neuronal maturation can vary between cultures, which might also lead to different results.

However, the comparison of both co-culture systems under study should be regarded with caution, as they differ in their neuronal interactions as well as in their genetic background. The characterization and direct comparison of idiopathic SCZ and isogenic microdeletion models would benefit from the same neuronal co-culture composition. This would on the one hand allow to identify phenotypes shared between SCZ and microdeletion syndromes, and on the other hand help to identify specific SCZ or specific microdeletion-related alterations.

Table 27. Comparison of synaptic and functional phenotypes observed in patient-derived ALN-NGN2 and isogenic 15q13 and 22q11 E-I co-cultures. Shared phenotypes observed in both co-culture model systems are marked with red arrows.

Phenotypes observed	**Idiopathic SCZ ALN-NGN2 co-culture**	**Isogenic 15q13 and 22q11 E-I co-culture**
Excitatory synapses	↓ vGLUT1 on NGN2 ↓ vGLUT1+PSD95 on NGN2 ↓ SYP on ALN and NGN2	↓ vGLUT1 ↓ vGLUT1+PSD95
Inhibitory synapses	-	↑ Gephyrin
Dopaminergic synapses	no differences	-
Calcium imaging	↑ peak frequency no change in AUC ↓ FWHM in ALN no change ΔF/F0	↓ peak frequency ↑ AUC ↑ FWHM ↑ ΔF/F0
Synchronization (GSI)	unsychronous activity	synchronous activity ↑ GSI

4.8 Conclusion and future perspectives

The dopamine hypothesis and cortical E-I imbalances are still leading theories in the pathophysiology of SCZ and related neuropsychiatric disorders. In order to study altered neuron-neuron interactions in SCZ patient-derived neurons, a highly defined iPSC-based co-culture system comprising induced dopaminergic and glutamatergic neurons was established in this thesis. In the second part, isogenic iPSC-based E-I co-culture model systems carrying microdeletions, as genetic risk factors for SCZ, were studied to reveal disease-related neuronal aberrations. For the first time, a dopaminergic-glutamatergic neuronal co-culture model was employed. This newly established co-culture model supports the notion of a hypodopaminergic

phenotype in the PFC, which is suggested to result in cognitive and negative symptoms in SCZ, that so far are hardly addressed by therapeutic strategies. Additionally, the decreased excitatory synaptic connectivity and altered neuronal (network) activity observed in SCZ patient-derived and 15q13/22q11 mutant co-cultures indicate synaptic and functional disbalances as a common feature that occurs during neurodevelopment. Most strikingly, the study presented here demonstrates the importance of employing more complex model systems rather than characterizing one neuronal cell type, as disease-related phenotypes were unique to the co-culture system.

Nevertheless, there are still some limitations and open questions regarding the observed disease-related features underlying the neuron-neuron interactions. For better understanding, single cell RNA sequencing of neuronal co-cultures could help to identify cell type-specific transcriptome profiles and subsequent gene enrichment analysis could provide further information regarding deregulated biological processes and cellular mechanisms. Likewise, detailed electrophysiological characterization of co-cultured neurons could be employed to decipher the neuronal cell type responsible for altered firing patterns, and to reveal alterations in neuronal excitability and neurotransmitter release probability. Despite numerous advantages in modelling neuropsychiatric disorders using 2D iPSC-derived neuronal culture systems, it remains challenging due to improper maturation and the lack of other physiologically relevant cell types such as glial cells and other neuronal cell types. Moreover, the cultivation period of 2D monolayer models is limited making it impossible to examine long-term effects, which would be of great interest since the onset of SCZ is in late adolescence. In order to address these limitations, iPSC-derived 3D brain organoids, which resemble human brains more precisely and have improved maturity, could be used as a further approach. To date, several protocols describe the differentiation of iPSC into brain region-specific organoids allowing to recapitulate developing microcircuits in a more complex macroenvironment (240, 241). For the investigation of neuronal connectivity involving several brain areas such as the mesocortical, midbrain and cortical spheroids could be assembled. Finally, one important aspect to consider when employing 2D and 3D neuronal cultures derived from patients is the high inter-donor variability due to distinct genetic backgrounds. Hence, large sample sizes are required.

5. REFERENCES

1. Howes OD, Murray RM. Schizophrenia: an integrated sociodevelopmental-cognitive model. Lancet. 2014;383(9929):1677-87.
2. McGrath J, Saha S, Welham J, El Saadi O, MacCauley C, Chant D. A systematic review of the incidence of schizophrenia: the distribution of rates and the influence of sex, urbanicity, migrant status and methodology. BMC Med. 2004;2:13.
3. Saha S, Chant D, Welham J, McGrath J. A systematic review of the prevalence of schizophrenia. PLoS Med. 2005;2(5):e141.
4. Picchioni MM, Murray RM. Schizophrenia. BMJ. 2007;335(7610):91-5.
5. Dabiri M, Dehghani Firouzabadi F, Yang K, Barker PB, Lee RR, Yousem DM. Neuroimaging in schizophrenia: A review article. Front Neurosci. 2022;16:1042814.
6. Hardy T, Breier A. Patients on atypical antipsychotic drugs: another high-risk group for type 2 diabetes: response to Lean and Pajonk. Diabetes Care. 2003;26(11):3200-1.
7. De Hert M, McKenzie K, Peuskens J. Risk factors for suicide in young people suffering from schizophrenia: a long-term follow-up study. Schizophr Res. 2001;47(2-3):127-34.
8. Tandon R, Gaebel W, Barch DM, Bustillo J, Gur RE, Heckers S, et al. Definition and description of schizophrenia in the DSM-5. Schizophr Res. 2013;150(1):3-10.
9. Kapur S, Seeman P. Does fast dissociation from the dopamine d(2) receptor explain the action of atypical antipsychotics?: A new hypothesis. Am J Psychiatry. 2001;158(3):360-9.
10. Elsheikh SSM, Muller DJ, Pouget JG. Pharmacogenetics of Antipsychotic Treatment in Schizophrenia. Methods Mol Biol. 2022;2547:389-425.
11. Lally J, MacCabe JH. Antipsychotic medication in schizophrenia: a review. Br Med Bull. 2015;114(1):169-79.
12. Correll CU, Schooler NR. Negative Symptoms in Schizophrenia: A Review and Clinical Guide for Recognition, Assessment, and Treatment. Neuropsychiatr Dis Treat. 2020;16:519-34.
13. Moller HJ, Czobor P. Pharmacological treatment of negative symptoms in schizophrenia. Eur Arch Psychiatry Clin Neurosci. 2015;265(7):567-78.
14. Ackenheil M, Weber K. Differing response to antipsychotic therapy in schizophrenia: pharmacogenomic aspects. Dialogues Clin Neurosci. 2004;6(1):71-7.
15. Gammon D, Cheng C, Volkovinskaia A, Baker GB, Dursun SM. Clozapine: Why Is It So Uniquely Effective in the Treatment of a Range of Neuropsychiatric Disorders? Biomolecules. 2021;11(7).
16. Orsini CA, Moorman DE, Young JW, Setlow B, Floresco SB. Neural mechanisms regulating different forms of risk-related decision-making: Insights from animal models. Neurosci Biobehav Rev. 2015;58:147-67.
17. Coddington LT, Dudman JT. Learning from Action: Reconsidering Movement Signaling in Midbrain Dopamine Neuron Activity. Neuron. 2019;104(1):63-77.
18. Brignani S, Pasterkamp RJ. Neuronal Subset-Specific Migration and Axonal Wiring Mechanisms in the Developing Midbrain Dopamine System. Front Neuroanat. 2017;11:55.
19. Nieuwenhuys R, Geeraedts LM, Veening JG. The medial forebrain bundle of the rat. I. General introduction. J Comp Neurol. 1982;206(1):49-81.
20. Salamone JD, Correa M, Mingote SM, Weber SM. Beyond the reward hypothesis: alternative functions of nucleus accumbens dopamine. Curr Opin Pharmacol. 2005;5(1):34-41.
21. Manitt C, Mimee A, Eng C, Pokinko M, Stroh T, Cooper HM, et al. The netrin receptor DCC is required in the pubertal organization of mesocortical dopamine circuitry. J Neurosci. 2011;31(23):8381-94.
22. Kelley AE, Berridge KC. The neuroscience of natural rewards: relevance to addictive drugs. J Neurosci. 2002;22(9):3306-11.
23. Klein MO, Battagello DS, Cardoso AR, Hauser DN, Bittencourt JC, Correa RG. Dopamine: Functions, Signaling, and Association with Neurological Diseases. Cell Mol Neurobiol. 2019;39(1):31-59.
24. Berridge KC, Robinson TE. What is the role of dopamine in reward: hedonic impact, reward learning, or incentive salience? Brain Res Brain Res Rev. 1998;28(3):309-69.

25. Gerfen CR, Surmeier DJ. Modulation of striatal projection systems by dopamine. Annu Rev Neurosci. 2011;34:441-66.
26. Yager LM, Garcia AF, Wunsch AM, Ferguson SM. The ins and outs of the striatum: role in drug addiction. Neuroscience. 2015;301:529-41.
27. Lambe EK, Krimer LS, Goldman-Rakic PS. Differential postnatal development of catecholamine and serotonin inputs to identified neurons in prefrontal cortex of rhesus monkey. J Neurosci. 2000;20(23):8780-7.
28. Reynolds LM, Flores C. Mesocorticolimbic Dopamine Pathways Across Adolescence: Diversity in Development. Front Neural Circuits. 2021;15:735625.
29. Gurevich EV, Gainetdinov RR, Gurevich VV. G protein-coupled receptor kinases as regulators of dopamine receptor functions. Pharmacol Res. 2016;111:1-16.
30. Toda M, Abi-Dargham A. Dopamine hypothesis of schizophrenia: making sense of it all. Curr Psychiatry Rep. 2007;9(4):329-36.
31. Carlsson A, Roos BE, Walinder J, Skott A. Further studies on the mechanism of antipsychotic action: potentiation by alpha-methyltyrosine of thioridazine effects in chronic schizophrenics. J Neural Transm. 1973;34(2):125-32.
32. Carlsson A, Lindqvist M, Magnusson T. 3,4-Dihydroxyphenylalanine and 5-hydroxytryptophan as reserpine antagonists. Nature. 1957;180(4596):1200.
33. Davis KL, Kahn RS, Ko G, Davidson M. Dopamine in schizophrenia: a review and reconceptualization. Am J Psychiatry. 1991;148(11):1474-86.
34. Howes OD, Kapur S. The dopamine hypothesis of schizophrenia: version III--the final common pathway. Schizophr Bull. 2009;35(3):549-62.
35. Walter H, Kammerer H, Frasch K, Spitzer M, Abler B. Altered reward functions in patients on atypical antipsychotic medication in line with the revised dopamine hypothesis of schizophrenia. Psychopharmacology (Berl). 2009;206(1):121-32.
36. Yui K, Ikemoto S, Ishiguro T, Goto K. Studies of amphetamine or methamphetamine psychosis in Japan: relation of methamphetamine psychosis to schizophrenia. Ann N Y Acad Sci. 2000;914:1-12.
37. Johnstone EC, Owens DG, Bydder GM, Colter N, Crow TJ, Frith CD. The spectrum of structural brain changes in schizophrenia: age of onset as a predictor of cognitive and clinical impairments and their cerebral correlates. Psychol Med. 1989;19(1):91-103.
38. Uno Y, Coyle JT. Glutamate hypothesis in schizophrenia. Psychiatry Clin Neurosci. 2019;73(5):204-15.
39. Mackay AV, Iversen LL, Rossor M, Spokes E, Bird E, Arregui A, et al. Increased brain dopamine and dopamine receptors in schizophrenia. Arch Gen Psychiatry. 1982;39(9):991-7.
40. Howes O, McCutcheon R, Stone J. Glutamate and dopamine in schizophrenia: an update for the 21st century. J Psychopharmacol. 2015;29(2):97-115.
41. Howes OD, Williams M, Ibrahim K, Leung G, Egerton A, McGuire PK, et al. Midbrain dopamine function in schizophrenia and depression: a post-mortem and positron emission tomographic imaging study. Brain. 2013;136(Pt 11):3242-51.
42. Schizophrenia Working Group of the Psychiatric Genomics C. Biological insights from 108 schizophrenia-associated genetic loci. Nature. 2014;511(7510):421-7.
43. Abi-Dargham A, Rodenhiser J, Printz D, Zea-Ponce Y, Gil R, Kegeles LS, et al. Increased baseline occupancy of D2 receptors by dopamine in schizophrenia. Proc Natl Acad Sci U S A. 2000;97(14):8104-9.
44. Goldman-Rakic PS, Castner SA, Svensson TH, Siever LJ, Williams GV. Targeting the dopamine D1 receptor in schizophrenia: insights for cognitive dysfunction. Psychopharmacology (Berl). 2004;174(1):3-16.
45. Silvestri S, Seeman MV, Negrete JC, Houle S, Shammi CM, Remington GJ, et al. Increased dopamine D2 receptor binding after long-term treatment with antipsychotics in humans: a clinical PET study. Psychopharmacology (Berl). 2000;152(2):174-80.
46. Abi-Dargham A, Mawlawi O, Lombardo I, Gil R, Martinez D, Huang Y, et al. Prefrontal dopamine D1 receptors and working memory in schizophrenia. J Neurosci. 2002;22(9):3708-19.
47. Karlsson P, Farde L, Halldin C, Sedvall G. PET study of D(1) dopamine receptor binding in neuroleptic-naive patients with schizophrenia. Am J Psychiatry. 2002;159(5):761-7.

48. Hirvonen J, van Erp TG, Huttunen J, Aalto S, Nagren K, Huttunen M, et al. Brain dopamine d1 receptors in twins discordant for schizophrenia. Am J Psychiatry. 2006;163(10):1747-53.
49. Akil M, Pierri JN, Whitehead RE, Edgar CL, Mohila C, Sampson AR, et al. Lamina-specific alterations in the dopamine innervation of the prefrontal cortex in schizophrenic subjects. Am J Psychiatry. 1999;156(10):1580-9.
50. Halstead JM, Lionnet T, Wilbertz JH, Wippich F, Ephrussi A, Singer RH, et al. Translation. An RNA biosensor for imaging the first round of translation from single cells to living animals. Science. 2015;347(6228):1367-671.
51. Krystal JH, D'Souza DC, Mathalon D, Perry E, Belger A, Hoffman R. NMDA receptor antagonist effects, cortical glutamatergic function, and schizophrenia: toward a paradigm shift in medication development. Psychopharmacology (Berl). 2003;169(3-4):215-33.
52. Egerton A, Grace AA, Stone J, Bossong MG, Sand M, McGuire P. Glutamate in schizophrenia: Neurodevelopmental perspectives and drug development. Schizophr Res. 2020;223:59-70.
53. Javitt DC. Glutamate and schizophrenia: phencyclidine, N-methyl-D-aspartate receptors, and dopamine-glutamate interactions. Int Rev Neurobiol. 2007;78:69-108.
54. Pilowsky LS, Bressan RA, Stone JM, Erlandsson K, Mulligan RS, Krystal JH, et al. First in vivo evidence of an NMDA receptor deficit in medication-free schizophrenic patients. Mol Psychiatry. 2006;11(2):118-9.
55. Catts VS, Lai YL, Weickert CS, Weickert TW, Catts SV. A quantitative review of the postmortem evidence for decreased cortical N-methyl-D-aspartate receptor expression levels in schizophrenia: How can we link molecular abnormalities to mismatch negativity deficits? Biol Psychol. 2016;116:57-67.
56. Basu AC, Tsai GE, Ma CL, Ehmsen JT, Mustafa AK, Han L, et al. Targeted disruption of serine racemase affects glutamatergic neurotransmission and behavior. Mol Psychiatry. 2009;14(7):719-27.
57. Homayoun H, Moghaddam B. NMDA receptor hypofunction produces opposite effects on prefrontal cortex interneurons and pyramidal neurons. J Neurosci. 2007;27(43):11496-500.
58. Robison AJ, Thakkar KN, Diwadkar VA. Cognition and Reward Circuits in Schizophrenia: Synergistic, Not Separate. Biol Psychiatry. 2020;87(3):204-14.
59. Howes OD, Onwordi EC. The synaptic hypothesis of schizophrenia version III: a master mechanism. Mol Psychiatry. 2023;28(5):1843-56.
60. Sullivan PF, Kendler KS, Neale MC. Schizophrenia as a complex trait: evidence from a meta-analysis of twin studies. Arch Gen Psychiatry. 2003;60(12):1187-92.
61. Lichtenstein P, Yip BH, Bjork C, Pawitan Y, Cannon TD, Sullivan PF, et al. Common genetic determinants of schizophrenia and bipolar disorder in Swedish families: a population-based study. Lancet. 2009;373(9659):234-9.
62. Trubetskoy V, Pardinas AF, Qi T, Panagiotaropoulou G, Awasthi S, Bigdeli TB, et al. Mapping genomic loci implicates genes and synaptic biology in schizophrenia. Nature. 2022;604(7906):502-8.
63. Guerrin CGJ, Doorduin J, Sommer IE, de Vries EFJ. The dual hit hypothesis of schizophrenia: Evidence from animal models. Neurosci Biobehav Rev. 2021;131:1150-68.
64. Schmitt A, Malchow B, Hasan A, Falkai P. The impact of environmental factors in severe psychiatric disorders. Front Neurosci. 2014;8:19.
65. Merikangas AK, Shelly M, Knighton A, Kotler N, Tanenbaum N, Almasy L. What genes are differentially expressed in individuals with schizophrenia? A systematic review. Mol Psychiatry. 2022;27(3):1373-83.
66. International Schizophrenia C. Rare chromosomal deletions and duplications increase risk of schizophrenia. Nature. 2008;455(7210):237-41.
67. Dahoun T, Trossbach SV, Brandon NJ, Korth C, Howes OD. The impact of Disrupted-in-Schizophrenia 1 (DISC1) on the dopaminergic system: a systematic review. Transl Psychiatry. 2017;7(1):e1015.
68. Soares DC, Carlyle BC, Bradshaw NJ, Porteous DJ. DISC1: Structure, Function, and Therapeutic Potential for Major Mental Illness. ACS Chem Neurosci. 2011;2(11):609-32.

69. Cannon M, Jones PB, Murray RM. Obstetric complications and schizophrenia: historical and meta-analytic review. Am J Psychiatry. 2002;159(7):1080-92.
70. Varese F, Smeets F, Drukker M, Lieverse R, Lataster T, Viechtbauer W, et al. Childhood adversities increase the risk of psychosis: a meta-analysis of patient-control, prospective- and cross-sectional cohort studies. Schizophr Bull. 2012;38(4):661-71.
71. Cantor-Graae E, Pedersen CB. Full spectrum of psychiatric disorders related to foreign migration: a Danish population-based cohort study. JAMA Psychiatry. 2013;70(4):427-35.
72. Marconi A, Di Forti M, Lewis CM, Murray RM, Vassos E. Meta-analysis of the Association Between the Level of Cannabis Use and Risk of Psychosis. Schizophr Bull. 2016;42(5):1262-9.
73. Weinberger DR. On the plausibility of "the neurodevelopmental hypothesis" of schizophrenia. Neuropsychopharmacology. 1996;14(3 Suppl):1S-11S.
74. Schmitt A, Falkai P, Papiol S. Neurodevelopmental disturbances in schizophrenia: evidence from genetic and environmental factors. J Neural Transm (Vienna). 2023;130(3):195-205.
75. Feigenson KA, Kusnecov AW, Silverstein SM. Inflammation and the two-hit hypothesis of schizophrenia. Neurosci Biobehav Rev. 2014;38:72-93.
76. Davis J, Eyre H, Jacka FN, Dodd S, Dean O, McEwen S, et al. A review of vulnerability and risks for schizophrenia: Beyond the two hit hypothesis. Neurosci Biobehav Rev. 2016;65:185-94.
77. Pos O, Radvanszky J, Buglyo G, Pos Z, Rusnakova D, Nagy B, et al. DNA copy number variation: Main characteristics, evolutionary significance, and pathological aspects. Biomed J. 2021;44(5):548-59.
78. Bray NJ, O'Donovan MC. The genetics of neuropsychiatric disorders. Brain Neurosci Adv. 2019;2.
79. Szecowka K, Misiak B, Laczmanska I, Frydecka D, Moustafa AA. Copy Number Variations and Schizophrenia. Mol Neurobiol. 2023;60(4):1854-64.
80. MacDonald JR, Ziman R, Yuen RK, Feuk L, Scherer SW. The Database of Genomic Variants: a curated collection of structural variation in the human genome. Nucleic Acids Res. 2014;42(Database issue):D986-92.
81. Lupski JR. Genomic disorders: structural features of the genome can lead to DNA rearrangements and human disease traits. Trends Genet. 1998;14(10):417-22.
82. Thapar A, Cooper M. Copy number variation: what is it and what has it told us about child psychiatric disorders? J Am Acad Child Adolesc Psychiatry. 2013;52(8):772-4.
83. Ruderfer DM, Hamamsy T, Lek M, Karczewski KJ, Kavanagh D, Samocha KE, et al. Patterns of genic intolerance of rare copy number variation in 59,898 human exomes. Nat Genet. 2016;48(10):1107-11.
84. Kirov G, Pocklington AJ, Holmans P, Ivanov D, Ikeda M, Ruderfer D, et al. De novo CNV analysis implicates specific abnormalities of postsynaptic signalling complexes in the pathogenesis of schizophrenia. Mol Psychiatry. 2012;17(2):142-53.
85. Cooper GM, Coe BP, Girirajan S, Rosenfeld JA, Vu TH, Baker C, et al. A copy number variation morbidity map of developmental delay. Nat Genet. 2011;43(9):838-46.
86. Marshall CR, Howrigan DP, Merico D, Thiruvahindrapuram B, Wu W, Greer DS, et al. Contribution of copy number variants to schizophrenia from a genome-wide study of 41,321 subjects. Nat Genet. 2017;49(1):27-35.
87. Malhotra D, Sebat J. CNVs: harbingers of a rare variant revolution in psychiatric genetics. Cell. 2012;148(6):1223-41.
88. Bassett AS. Parental origin, DNA structure, and the schizophrenia spectrum. Am J Psychiatry. 2011;168(4):350-3.
89. Ahn Y, Jun Y. Measurement of pain-like response to various NICU stimulants for high-risk infants. Early Hum Dev. 2007;83(4):255-62.
90. Costain G, Lionel AC, Merico D, Forsythe P, Russell K, Lowther C, et al. Pathogenic rare copy number variants in community-based schizophrenia suggest a potential role for clinical microarrays. Hum Mol Genet. 2013;22(22):4485-501.
91. Thelin J, Halje P, Nielsen J, Didriksen M, Petersson P, Bastlund JF. The translationally relevant mouse model of the 15q13.3 microdeletion syndrome reveals deficits in neuronal

spike firing matching clinical neurophysiological biomarkers seen in schizophrenia. Acta Physiol (Oxf). 2017;220(1):124-36.
92. Unda BK, Chalil L, Yoon S, Kilpatrick S, Irwin C, Xing S, et al. Impaired OTUD7A-dependent Ankyrin regulation mediates neuronal dysfunction in mouse and human models of the 15q13.3 microdeletion syndrome. Mol Psychiatry. 2023;28(4):1747-69.
93. Yin J, Chen W, Chao ES, Soriano S, Wang L, Wang W, et al. Otud7a Knockout Mice Recapitulate Many Neurological Features of 15q13.3 Microdeletion Syndrome. Am J Hum Genet. 2018;102(2):296-308.
94. Kozlova A, Zhang S, Kotlar AV, Jamison B, Zhang H, Shi S, et al. Loss of function of OTUD7A in the schizophrenia- associated 15q13.3 deletion impairs synapse development and function in human neurons. Am J Hum Genet. 2022;109(8):1500-19.
95. Uddin M, Unda BK, Kwan V, Holzapfel NT, White SH, Chalil L, et al. OTUD7A Regulates Neurodevelopmental Phenotypes in the 15q13.3 Microdeletion Syndrome. Am J Hum Genet. 2018;102(2):278-95.
96. Yin J, Chen W, Yang H, Xue M, Schaaf CP. Chrna7 deficient mice manifest no consistent neuropsychiatric and behavioral phenotypes. Sci Rep. 2017;7:39941.
97. Fejgin K, Nielsen J, Birknow MR, Bastlund JF, Nielsen V, Lauridsen JB, et al. A mouse model that recapitulates cardinal features of the 15q13.3 microdeletion syndrome including schizophrenia- and epilepsy-related alterations. Biol Psychiatry. 2014;76(2):128-37.
98. Kogan JH, Gross AK, Featherstone RE, Shin R, Chen Q, Heusner CL, et al. Mouse Model of Chromosome 15q13.3 Microdeletion Syndrome Demonstrates Features Related to Autism Spectrum Disorder. J Neurosci. 2015;35(49):16282-94.
99. Crawford K, Bracher-Smith M, Owen D, Kendall KM, Rees E, Pardinas AF, et al. Medical consequences of pathogenic CNVs in adults: analysis of the UK Biobank. J Med Genet. 2019;56(3):131-8.
100. Thomas NS, Durkie M, Potts G, Sandford R, Van Zyl B, Youings S, et al. Parental and chromosomal origins of microdeletion and duplication syndromes involving 7q11.23, 15q11-q13 and 22q11. Eur J Hum Genet. 2006;14(7):831-7.
101. Tripathi A, Spedding M, Schenker E, Didriksen M, Cressant A, Jay TM. Cognition- and circuit-based dysfunction in a mouse model of 22q11.2 microdeletion syndrome: effects of stress. Transl Psychiatry. 2020;10(1):41.
102. Niklasson L, Rasmussen P, Oskarsdottir S, Gillberg C. Autism, ADHD, mental retardation and behavior problems in 100 individuals with 22q11 deletion syndrome. Res Dev Disabil. 2009;30(4):763-73.
103. Fiksinski AM, Hoftman GD, Vorstman JAS, Bearden CE. A genetics-first approach to understanding autism and schizophrenia spectrum disorders: the 22q11.2 deletion syndrome. Mol Psychiatry. 2023;28(1):341-53.
104. Ma J, Zhao M, Zhou W, Li M, Huai C, Shen L, et al. Association Between the COMT Val158Met Polymorphism and Antipsychotic Efficacy in Schizophrenia: An Updated Meta-Analysis. Curr Neuropharmacol. 2021;19(10):1780-90.
105. Fenelon K, Mukai J, Xu B, Hsu PK, Drew LJ, Karayiorgou M, et al. Deficiency of Dgcr8, a gene disrupted by the 22q11.2 microdeletion, results in altered short-term plasticity in the prefrontal cortex. Proc Natl Acad Sci U S A. 2011;108(11):4447-52.
106. Forstner AJ, Degenhardt F, Schratt G, Nothen MM. MicroRNAs as the cause of schizophrenia in 22q11.2 deletion carriers, and possible implications for idiopathic disease: a mini-review. Front Mol Neurosci. 2013;6:47.
107. Frascarelli M, Padovani G, Buzzanca A, Accinni T, Carlone L, Ghezzi F, et al. Social cognition deficit and genetic vulnerability to schizophrenia in 22q11 deletion syndrome. Ann Ist Super Sanita. 2020;56(1):107-13.
108. Liu H, Heath SC, Sobin C, Roos JL, Galke BL, Blundell ML, et al. Genetic variation at the 22q11 PRODH2/DGCR6 locus presents an unusual pattern and increases susceptibility to schizophrenia. Proc Natl Acad Sci U S A. 2002;99(6):3717-22.
109. Ren D, Luo B, Chen P, Yu L, Xiong M, Fu Z, et al. DiGeorge syndrome critical region gene 2 (DGCR2), a schizophrenia risk gene, regulates dendritic spine development through cell adhesion. Cell Biosci. 2023;13(1):134.

110. Biswal SR, Kumar A, Muthuswamy S, Kumar S. Genetic components of microdeletion syndromes and their role in determining schizophrenia traits. Mol Biol Rep. 2024;51(1):804.
111. Ellegood J, Markx S, Lerch JP, Steadman PE, Genc C, Provenzano F, et al. Neuroanatomical phenotypes in a mouse model of the 22q11.2 microdeletion. Mol Psychiatry. 2014;19(1):99-107.
112. Miyashita Y. Operating principles of the cerebral cortex as a six-layered network in primates: beyond the classic canonical circuit model. Proc Jpn Acad Ser B Phys Biol Sci. 2022;98(3):93-111.
113. Espinos A, Fernandez-Ortuno E, Negri E, Borrell V. Evolution of genetic mechanisms regulating cortical neurogenesis. Dev Neurobiol. 2022;82(5):428-53.
114. Islam KUS, Meli N, Blaess S. The Development of the Mesoprefrontal Dopaminergic System in Health and Disease. Front Neural Circuits. 2021;15:746582.
115. Sahara S, Yanagawa Y, O'Leary DD, Stevens CF. The fraction of cortical GABAergic neurons is constant from near the start of cortical neurogenesis to adulthood. J Neurosci. 2012;32(14):4755-61.
116. Rudy B, Fishell G, Lee S, Hjerling-Leffler J. Three groups of interneurons account for nearly 100% of neocortical GABAergic neurons. Dev Neurobiol. 2011;71(1):45-61.
117. Lim L, Mi D, Llorca A, Marin O. Development and Functional Diversification of Cortical Interneurons. Neuron. 2018;100(2):294-313.
118. Sohal VS, Rubenstein JLR. Excitation-inhibition balance as a framework for investigating mechanisms in neuropsychiatric disorders. Mol Psychiatry. 2019;24(9):1248-57.
119. Liu Y, Ouyang P, Zheng Y, Mi L, Zhao J, Ning Y, et al. A Selective Review of the Excitatory-Inhibitory Imbalance in Schizophrenia: Underlying Biology, Genetics, Microcircuits, and Symptoms. Front Cell Dev Biol. 2021;9:664535.
120. Kim JS, Kornhuber HH, Schmid-Burgk W, Holzmuller B. Low cerebrospinal fluid glutamate in schizophrenic patients and a new hypothesis on schizophrenia. Neurosci Lett. 1980;20(3):379-82.
121. Tsai G, Passani LA, Slusher BS, Carter R, Baer L, Kleinman JE, et al. Abnormal excitatory neurotransmitter metabolism in schizophrenic brains. Arch Gen Psychiatry. 1995;52(10):829-36.
122. Song J, Viggiano A, Monda M, De Luca V. Peripheral glutamate levels in schizophrenia: evidence from a meta-analysis. Neuropsychobiology. 2014;70(3):133-41.
123. Osimo EF, Beck K, Reis Marques T, Howes OD. Synaptic loss in schizophrenia: a meta-analysis and systematic review of synaptic protein and mRNA measures. Mol Psychiatry. 2019;24(4):549-61.
124. Berdenis van Berlekom A, Muflihah CH, Snijders G, MacGillavry HD, Middeldorp J, Hol EM, et al. Synapse Pathology in Schizophrenia: A Meta-analysis of Postsynaptic Elements in Postmortem Brain Studies. Schizophr Bull. 2020;46(2):374-86.
125. Fujihara K, Miwa H, Kakizaki T, Kaneko R, Mikuni M, Tanahira C, et al. Glutamate Decarboxylase 67 Deficiency in a Subset of GABAergic Neurons Induces Schizophrenia-Related Phenotypes. Neuropsychopharmacology. 2015;40(10):2475-86.
126. Sohal VS, Zhang F, Yizhar O, Deisseroth K. Parvalbumin neurons and gamma rhythms enhance cortical circuit performance. Nature. 2009;459(7247):698-702.
127. Kwon JS, O'Donnell BF, Wallenstein GV, Greene RW, Hirayasu Y, Nestor PG, et al. Gamma frequency-range abnormalities to auditory stimulation in schizophrenia. Arch Gen Psychiatry. 1999;56(11):1001-5.
128. Uhlhaas PJ, Singer W. Abnormal neural oscillations and synchrony in schizophrenia. Nat Rev Neurosci. 2010;11(2):100-13.
129. Howes OD, Shatalina E. Integrating the Neurodevelopmental and Dopamine Hypotheses of Schizophrenia and the Role of Cortical Excitation-Inhibition Balance. Biol Psychiatry. 2022;92(6):501-13.
130. Michels KB, Binder AM, Dedeurwaerder S, Epstein CB, Greally JM, Gut I, et al. Recommendations for the design and analysis of epigenome-wide association studies. Nat Methods. 2013;10(10):949-55.

131. Banerjee A, Lu Y, Do K, Mize T, Wu X, Chen X, et al. Validation of Induced Microglia-Like Cells (iMG Cells) for Future Studies of Brain Diseases. Front Cell Neurosci. 2021;15:629279.
132. Doss MX, Sachinidis A. Current Challenges of iPSC-Based Disease Modeling and Therapeutic Implications. Cells. 2019;8(5).
133. Zahumenska R, Nosal V, Smolar M, Okajcekova T, Skovierova H, Strnadel J, et al. Induced Pluripotency: A Powerful Tool for In Vitro Modeling. Int J Mol Sci. 2020;21(23).
134. Robinton DA, Daley GQ. The promise of induced pluripotent stem cells in research and therapy. Nature. 2012;481(7381):295-305.
135. Biehl JK, Russell B. Introduction to stem cell therapy. J Cardiovasc Nurs. 2009;24(2):98-103; quiz 4-5.
136. Evans MJ, Kaufman MH. Establishment in culture of pluripotential cells from mouse embryos. Nature. 1981;292(5819):154-6.
137. Lo B, Parham L. Ethical issues in stem cell research. Endocr Rev. 2009;30(3):204-13.
138. Yamanaka S. Strategies and new developments in the generation of patient-specific pluripotent stem cells. Cell Stem Cell. 2007;1(1):39-49.
139. Takahashi K, Yamanaka S. Induction of pluripotent stem cells from mouse embryonic and adult fibroblast cultures by defined factors. Cell. 2006;126(4):663-76.
140. Kamata M, Liu S, Liang M, Nagaoka Y, Chen IS. Generation of human induced pluripotent stem cells bearing an anti-HIV transgene by a lentiviral vector carrying an internal murine leukemia virus promoter. Hum Gene Ther. 2010;21(11):1555-67.
141. Raab S, Klingenstein M, Liebau S, Linta L. A Comparative View on Human Somatic Cell Sources for iPSC Generation. Stem Cells Int. 2014;2014:768391.
142. Al Abbar A, Ngai SC, Nograles N, Alhaji SY, Abdullah S. Induced Pluripotent Stem Cells: Reprogramming Platforms and Applications in Cell Replacement Therapy. Biores Open Access. 2020;9(1):121-36.
143. Brunner JW, Lammertse HCA, van Berkel AA, Koopmans F, Li KW, Smit AB, et al. Power and optimal study design in iPSC-based brain disease modelling. Mol Psychiatry. 2023;28(4):1545-56.
144. Mahajani S, Bahr M, Kugler S. Patterning inconsistencies restrict the true potential of dopaminergic neurons derived from human induced pluripotent stem cells. Neural Regen Res. 2021;16(4):692-3.
145. Telias M. Neural differentiation protocols: how to choose the correct approach. Neural Regen Res. 2023;18(6):1273-4.
146. Ho SM, Hartley BJ, Tcw J, Beaumont M, Stafford K, Slesinger PA, et al. Rapid Ngn2-induction of excitatory neurons from hiPSC-derived neural progenitor cells. Methods. 2016;101:113-24.
147. Barretto N, Zhang H, Powell SK, Fernando MB, Zhang S, Flaherty EK, et al. ASCL1- and DLX2-induced GABAergic neurons from hiPSC-derived NPCs. J Neurosci Methods. 2020;334:108548.
148. Powell SK, O'Shea C, Townsley K, Prytkova I, Dobrindt K, Elahi R, et al. Induction of dopaminergic neurons for neuronal subtype-specific modeling of psychiatric disease risk. Mol Psychiatry. 2023;28(5):1970-82.
149. Das AT, Tenenbaum L, Berkhout B. Tet-On Systems For Doxycycline-inducible Gene Expression. Curr Gene Ther. 2016;16(3):156-67.
150. Shi Y, Kirwan P, Smith J, Robinson HP, Livesey FJ. Human cerebral cortex development from pluripotent stem cells to functional excitatory synapses. Nat Neurosci. 2012;15(3):477-86, S1.
151. Ardhanareeswaran K, Mariani J, Coppola G, Abyzov A, Vaccarino FM. Human induced pluripotent stem cells for modelling neurodevelopmental disorders. Nat Rev Neurol. 2017;13(5):265-78.
152. Noh H, Shao Z, Coyle JT, Chung S. Modeling schizophrenia pathogenesis using patient-derived induced pluripotent stem cells (iPSCs). Biochim Biophys Acta Mol Basis Dis. 2017;1863(9):2382-7.
153. Moslem M, Olive J, Falk A. Stem cell models of schizophrenia, what have we learned and what is the potential? Schizophr Res. 2019;210:3-12.

154. Topol A, Zhu S, Tran N, Simone A, Fang G, Brennand KJ. Altered WNT Signaling in Human Induced Pluripotent Stem Cell Neural Progenitor Cells Derived from Four Schizophrenia Patients. Biol Psychiatry. 2015;78(6):e29-34.
155. Narla ST, Lee YW, Benson CA, Sarder P, Brennand KJ, Stachowiak EK, et al. Common developmental genome deprogramming in schizophrenia - Role of Integrative Nuclear FGFR1 Signaling (INFS). Schizophr Res. 2017;185:17-32.
156. Brennand K, Savas JN, Kim Y, Tran N, Simone A, Hashimoto-Torii K, et al. Phenotypic differences in hiPSC NPCs derived from patients with schizophrenia. Mol Psychiatry. 2015;20(3):361-8.
157. Brennand KJ, Simone A, Jou J, Gelboin-Burkhart C, Tran N, Sangar S, et al. Modelling schizophrenia using human induced pluripotent stem cells. Nature. 2011;473(7346):221-5.
158. Grunwald LM, Stock R, Haag K, Buckenmaier S, Eberle MC, Wildgruber D, et al. Comparative characterization of human induced pluripotent stem cells (hiPSC) derived from patients with schizophrenia and autism. Transl Psychiatry. 2019;9(1):179.
159. Khan TA, Revah O, Gordon A, Yoon SJ, Krawisz AK, Goold C, et al. Neuronal defects in a human cellular model of 22q11.2 deletion syndrome. Nat Med. 2020;26(12):1888-98.
160. Lin M, Pedrosa E, Hrabovsky A, Chen J, Puliafito BR, Gilbert SR, et al. Integrative transcriptome network analysis of iPSC-derived neurons from schizophrenia and schizoaffective disorder patients with 22q11.2 deletion. BMC Syst Biol. 2016;10(1):105.
161. Das D, Sonthalia S, Stein OBG, Wahbeh MH, Feuer K, Goff L, et al. Insights for disease modeling from single-cell transcriptomics of iPSC-derived Ngn2-induced neurons and astrocytes across differentiation time and co-culture. BMC Biol. 2024;22(1):75.
162. Xu J, Hartley BJ, Kurup P, Phillips A, Topol A, Xu M, et al. Inhibition of STEP(61) ameliorates deficits in mouse and hiPSC-based schizophrenia models. Mol Psychiatry. 2018;23(2):271-81.
163. Ma Y, Bendl J, Hartley BJ, Fullard JF, Abdelaal R, Ho SM, et al. Activity-Dependent Transcriptional Program in NGN2+ Neurons Enriched for Genetic Risk for Brain-Related Disorders. Biol Psychiatry. 2024;95(2):187-98.
164. Heider J, Gonzalez EP, Hartmann SM, Kannaiyan N, Vogel S, Wust R, et al. Aberrant neuronal connectivity and network activity of neurons derived from patients with idiopathic schizophrenia. Neurobiol Dis. 2024;201:106678.
165. Heider J, Stahl A, Sperlich D, Hartmann SM, Vogel S, Breitmeyer R, et al. Defined co-cultures of glutamatergic and GABAergic neurons with a mutation in DISC1 reveal aberrant phenotypes in GABAergic neurons. BMC Neurosci. 2024;25(1):12.
166. Breitmeyer R, Vogel S, Heider J, Hartmann SM, Wust R, Keller AL, et al. Regulation of synaptic connectivity in schizophrenia spectrum by mutual neuron-microglia interaction. Commun Biol. 2023;6(1):472.
167. Hartley BJ, Tran N, Ladran I, Reggio K, Brennand KJ. Dopaminergic differentiation of schizophrenia hiPSCs. Mol Psychiatry. 2015;20(5):549-50.
168. Hook V, Brennand KJ, Kim Y, Toneff T, Funkelstein L, Lee KC, et al. Human iPSC neurons display activity-dependent neurotransmitter secretion: aberrant catecholamine levels in schizophrenia neurons. Stem Cell Reports. 2014;3(4):531-8.
169. Robicsek O, Karry R, Petit I, Salman-Kesner N, Muller FJ, Klein E, et al. Abnormal neuronal differentiation and mitochondrial dysfunction in hair follicle-derived induced pluripotent stem cells of schizophrenia patients. Mol Psychiatry. 2013;18(10):1067-76.
170. Stock R, Vogel S, Mau-Holzmann UA, Kriebel M, Wust R, Fallgatter AJ, et al. Generation and characterization of human induced pluripotent stem cells lines from four patients diagnosed with schizophrenia and one healthy control. Stem Cell Res. 2020;48:101961.
171. Burridge PW, Thompson S, Millrod MA, Weinberg S, Yuan X, Peters A, et al. A universal system for highly efficient cardiac differentiation of human induced pluripotent stem cells that eliminates interline variability. PLoS One. 2011;6(4):e18293.
172. Keller AL, Binner A, Breitmeyer R, Vogel S, Anderle N, Rothbauer U, et al. Generation and characterization of the human induced pluripotent stem cell line NMIi010-A from peripheral blood mononuclear cells of a healthy 49-year old male individual. Stem Cell Res. 2021;54:102427.

173. Reinhardt P, Glatza M, Hemmer K, Tsytsyura Y, Thiel CS, Hoing S, et al. Derivation and expansion using only small molecules of human neural progenitors for neurodegenerative disease modeling. PLoS One. 2013;8(3):e59252.
174. Bus C, Zizmare L, Feldkaemper M, Geisler S, Zarani M, Schaedler A, et al. Human Dopaminergic Neurons Lacking PINK1 Exhibit Disrupted Dopamine Metabolism Related to Vitamin B6 Co-Factors. iScience. 2020;23(12):101797.
175. Freel BA, Sheets JN, Francis KR. iPSC modeling of rare pediatric disorders. J Neurosci Methods. 2020;332:108533.
176. Zhang Y, Pak C, Han Y, Ahlenius H, Zhang Z, Chanda S, et al. Rapid single-step induction of functional neurons from human pluripotent stem cells. Neuron. 2013;78(5):785-98.
177. Nehme R, Zuccaro E, Ghosh SD, Li C, Sherwood JL, Pietilainen O, et al. Combining NGN2 Programming with Developmental Patterning Generates Human Excitatory Neurons with NMDAR-Mediated Synaptic Transmission. Cell Rep. 2018;23(8):2509-23.
178. Raabe FJ, Hausruckinger A, Gagliardi M, Ahmad R, Almeida V, Galinski S, et al. Polygenic risk for schizophrenia converges on alternative polyadenylation as molecular mechanism underlying synaptic impairment. bioRxiv. 2024.
179. Schildge S, Bohrer C, Beck K, Schachtrup C. Isolation and culture of mouse cortical astrocytes. J Vis Exp. 2013(71).
180. Li X, Cui D, Jiruska P, Fox JE, Yao X, Jefferys JG. Synchronization measurement of multiple neuronal populations. J Neurophysiol. 2007;98(6):3341-8.
181. Ho SM, Topol A, Brennand KJ. From "directed differentiation" to "neuronal induction": modeling neuropsychiatric disease. Biomark Insights. 2015;10(Suppl 1):31-41.
182. Deas E, Plun-Favreau H, Wood NW. PINK1 function in health and disease. EMBO Mol Med. 2009;1(3):152-65.
183. Vizziello M, Borellini L, Franco G, Ardolino G. Disruption of Mitochondrial Homeostasis: The Role of PINK1 in Parkinson's Disease. Cells. 2021;10(11).
184. Ascherio A, Schwarzschild MA. The epidemiology of Parkinson's disease: risk factors and prevention. Lancet Neurol. 2016;15(12):1257-72.
185. Grace AA. Dysregulation of the dopamine system in the pathophysiology of schizophrenia and depression. Nat Rev Neurosci. 2016;17(8):524-32.
186. Tolleson C, Claassen D. The function of tyrosine hydroxylase in the normal and Parkinsonian brain. CNS Neurol Disord Drug Targets. 2012;11(4):381-6.
187. Domanskyi A, Alter H, Vogt MA, Gass P, Vinnikov IA. Transcription factors Foxa1 and Foxa2 are required for adult dopamine neurons maintenance. Front Cell Neurosci. 2014;8:275.
188. Tian L, Al-Nusaif M, Chen X, Li S, Le W. Roles of Transcription Factors in the Development and Reprogramming of the Dopaminergic Neurons. Int J Mol Sci. 2022;23(2).
189. Li T, Chen CK, Hu X, Ball D, Lin SK, Chen W, et al. Association analysis of the DRD4 and COMT genes in methamphetamine abuse. Am J Med Genet B Neuropsychiatr Genet. 2004;129B(1):120-4.
190. Ford CP. The role of D2-autoreceptors in regulating dopamine neuron activity and transmission. Neuroscience. 2014;282:13-22.
191. Woodworth MB, Greig LC, Liu KX, Ippolito GC, Tucker HO, Macklis JD. Ctip1 Regulates the Balance between Specification of Distinct Projection Neuron Subtypes in Deep Cortical Layers. Cell Rep. 2016;15(5):999-1012.
192. Sugitani Y, Nakai S, Minowa O, Nishi M, Jishage K, Kawano H, et al. Brn-1 and Brn-2 share crucial roles in the production and positioning of mouse neocortical neurons. Genes Dev. 2002;16(14):1760-5.
193. Huang CY, Rasband MN. Axon initial segments: structure, function, and disease. Ann N Y Acad Sci. 2018;1420(1):46-61.
194. Yoon S, Piguel NH, Penzes P. Roles and mechanisms of ankyrin-G in neuropsychiatric disorders. Exp Mol Med. 2022;54(7):867-77.
195. Kathuria A, Lopez-Lengowski K, Watmuff B, Karmacharya R. Comparative Transcriptomic Analysis of Cerebral Organoids and Cortical Neuron Cultures Derived from Human Induced Pluripotent Stem Cells. Stem Cells Dev. 2020;29(21):1370-81.

196. Hoffmann A, Ziller M, Spengler D. Progress in iPSC-Based Modeling of Psychiatric Disorders. Int J Mol Sci. 2019;20(19).
197. Chambers SM, Fasano CA, Papapetrou EP, Tomishima M, Sadelain M, Studer L. Highly efficient neural conversion of human ES and iPS cells by dual inhibition of SMAD signaling. Nat Biotechnol. 2009;27(3):275-80.
198. Kriks S, Shim JW, Piao J, Ganat YM, Wakeman DR, Xie Z, et al. Dopamine neurons derived from human ES cells efficiently engraft in animal models of Parkinson's disease. Nature. 2011;480(7378):547-51.
199. Caiazzo M, Dell'Anno MT, Dvoretskova E, Lazarevic D, Taverna S, Leo D, et al. Direct generation of functional dopaminergic neurons from mouse and human fibroblasts. Nature. 2011;476(7359):224-7.
200. Perlmann T, Wallen-Mackenzie A. Nurr1, an orphan nuclear receptor with essential functions in developing dopamine cells. Cell Tissue Res. 2004;318(1):45-52.
201. Raina A, Mahajani S, Bahr M, Kugler S. Neuronal Trans-differentiation by Transcription Factors Ascl1 and Nurr1: Induction of a Dopaminergic Neurotransmitter Phenotype in Cortical GABAergic Neurons. Mol Neurobiol. 2020;57(1):249-60.
202. Theka I, Caiazzo M, Dvoretskova E, Leo D, Ungaro F, Curreli S, et al. Rapid generation of functional dopaminergic neurons from human induced pluripotent stem cells through a single-step procedure using cell lineage transcription factors. Stem Cells Transl Med. 2013;2(6):473-9.
203. Salesse C, Charest J, Doucet-Beaupre H, Castonguay AM, Labrecque S, De Koninck P, et al. Opposite Control of Excitatory and Inhibitory Synapse Formation by Slitrk2 and Slitrk5 on Dopamine Neurons Modulates Hyperactivity Behavior. Cell Rep. 2020;30(7):2374-86 e5.
204. Jankovic J, Chen S, Le WD. The role of Nurr1 in the development of dopaminergic neurons and Parkinson's disease. Prog Neurobiol. 2005;77(1-2):128-38.
205. Xing G, Zhang L, Russell S, Post R. Reduction of dopamine-related transcription factors Nurr1 and NGFI-B in the prefrontal cortex in schizophrenia and bipolar disorders. Schizophr Res. 2006;84(1):36-56.
206. Lee JY. Normal and Disordered Formation of the Cerebral Cortex : Normal Embryology, Related Molecules, Types of Migration, Migration Disorders. J Korean Neurosurg Soc. 2019;62(3):265-71.
207. Boissart C, Poulet A, Georges P, Darville H, Julita E, Delorme R, et al. Differentiation from human pluripotent stem cells of cortical neurons of the superficial layers amenable to psychiatric disease modeling and high-throughput drug screening. Translational Psychiatry. 2013;3(8):e294-e.
208. Lyon GJ, Abi-Dargham A, Moore H, Lieberman JA, Javitch JA, Sulzer D. Presynaptic regulation of dopamine transmission in schizophrenia. Schizophr Bull. 2011;37(1):108-17.
209. Taylor SF, Koeppe RA, Tandon R, Zubieta JK, Frey KA. In vivo measurement of the vesicular monoamine transporter in schizophrenia. Neuropsychopharmacology. 2000;23(6):667-75.
210. Fusar-Poli P, Meyer-Lindenberg A. Striatal presynaptic dopamine in schizophrenia, Part I: meta-analysis of dopamine active transporter (DAT) density. Schizophr Bull. 2013;39(1):22-32.
211. Sekiguchi H, Pavey G, Dean B. Altered levels of dopamine transporter in the frontal pole and dorsal striatum in schizophrenia. NPJ Schizophr. 2019;5(1):20.
212. Kim SY, Choi KC, Chang MS, Kim MH, Kim SY, Na YS, et al. The dopamine D2 receptor regulates the development of dopaminergic neurons via extracellular signal-regulated kinase and Nurr1 activation. J Neurosci. 2006;26(17):4567-76.
213. Torretta S, Rampino A, Basso M, Pergola G, Di Carlo P, Shin JH, et al. NURR1 and ERR1 Modulate the Expression of Genes of a DRD2 Coexpression Network Enriched for Schizophrenia Risk. J Neurosci. 2020;40(4):932-41.
214. Parnell E, Culotta L, Forrest MP, Jalloul HA, Eckman BL, Loizzo DD, et al. Excitatory Dysfunction Drives Network and Calcium Handling Deficits in 16p11.2 Duplication Schizophrenia Induced Pluripotent Stem Cell-Derived Neurons. Biol Psychiatry. 2023;94(2):153-63.

215. Yao Y, Wu M, Wang L, Lin L, Xu J. Phase Coupled Firing of Prefrontal Parvalbumin Interneuron With High Frequency Oscillations. Front Cell Neurosci. 2020;14:610741.
216. Anzalone A, Lizardi-Ortiz JE, Ramos M, De Mei C, Hopf FW, Iaccarino C, et al. Dual control of dopamine synthesis and release by presynaptic and postsynaptic dopamine D2 receptors. J Neurosci. 2012;32(26):9023-34.
217. Sagar R, Azoidis I, Zivko C, Xydia A, Oh ES, Rosenberg PB, et al. Excitatory Neurons Derived from Human-Induced Pluripotent Stem Cells Show Transcriptomic Differences in Alzheimer's Patients from Controls. Cells. 2023;12(15).
218. Tian R, Gachechiladze MA, Ludwig CH, Laurie MT, Hong JY, Nathaniel D, et al. CRISPR Interference-Based Platform for Multimodal Genetic Screens in Human iPSC-Derived Neurons. Neuron. 2019;104(2):239-55 e12.
219. Flaherty E, Zhu S, Barretto N, Cheng E, Deans PJM, Fernando MB, et al. Neuronal impact of patient-specific aberrant NRXN1alpha splicing. Nat Genet. 2019;51(12):1679-90.
220. Fornito A, Yucel M, Patti J, Wood SJ, Pantelis C. Mapping grey matter reductions in schizophrenia: an anatomical likelihood estimation analysis of voxel-based morphometry studies. Schizophr Res. 2009;108(1-3):104-13.
221. Ducrot C, Bourque MJ, Delmas CVL, Racine AS, Guadarrama Bello D, Delignat-Lavaud B, et al. Dopaminergic neurons establish a distinctive axonal arbor with a majority of non-synaptic terminals. FASEB J. 2021;35(8):e21791.
222. Onwordi EC, Halff EF, Whitehurst T, Mansur A, Cotel MC, Wells L, et al. Synaptic density marker SV2A is reduced in schizophrenia patients and unaffected by antipsychotics in rats. Nat Commun. 2020;11(1):246.
223. Eskenazi D, Malave L, Mingote S, Yetnikoff L, Ztaou S, Velicu V, et al. Dopamine Neurons That Cotransmit Glutamate, From Synapses to Circuits to Behavior. Front Neural Circuits. 2021;15:665386.
224. Obi-Nagata K, Temma Y, Hayashi-Takagi A. Synaptic functions and their disruption in schizophrenia: From clinical evidence to synaptic optogenetics in an animal model. Proc Jpn Acad Ser B Phys Biol Sci. 2019;95(5):179-97.
225. Sudhof TC. The cell biology of synapse formation. J Cell Biol. 2021;220(7).
226. Mizutani R, Saiga R, Takeuchi A, Uesugi K, Terada Y, Suzuki Y, et al. Three-dimensional alteration of neurites in schizophrenia. Transl Psychiatry. 2019;9(1):85.
227. Tabata H, Mori D, Matsuki T, Yoshizaki K, Asai M, Nakayama A, et al. Histological Analysis of a Mouse Model of the 22q11.2 Microdeletion Syndrome. Biomolecules. 2023;13(5).
228. Toyoshima M, Akamatsu W, Okada Y, Ohnishi T, Balan S, Hisano Y, et al. Analysis of induced pluripotent stem cells carrying 22q11.2 deletion. Transl Psychiatry. 2016;6(11):e934.
229. Qin X, Chen J, Zhou T. 22q11.2 deletion syndrome and schizophrenia. Acta Biochim Biophys Sin (Shanghai). 2020;52(11):1181-90.
230. Li J, Ryan SK, Deboer E, Cook K, Fitzgerald S, Lachman HM, et al. Mitochondrial deficits in human iPSC-derived neurons from patients with 22q11.2 deletion syndrome and schizophrenia. Transl Psychiatry. 2019;9(1):302.
231. Nehme R, Pietilainen O, Artomov M, Tegtmeyer M, Valakh V, Lehtonen L, et al. The 22q11.2 region regulates presynaptic gene-products linked to schizophrenia. Nat Commun. 2022;13(1):3690.
232. Favuzzi E, Rico B. Molecular diversity underlying cortical excitatory and inhibitory synapse development. Curr Opin Neurobiol. 2018;53:8-15.
233. Al-Absi AR, Qvist P, Glerup S, Sanchez C, Nyengaard JR. Df(h15q13)/+ Mouse Model Reveals Loss of Astrocytes and Synaptic-Related Changes of the Excitatory and Inhibitory Circuits in the Medial Prefrontal Cortex. Cereb Cortex. 2021;31(3):1609-21.
234. Brenner CA, Krishnan GP, Vohs JL, Ahn WY, Hetrick WP, Morzorati SL, et al. Steady state responses: electrophysiological assessment of sensory function in schizophrenia. Schizophr Bull. 2009;35(6):1065-77.
235. Lin H, Hsu FC, Baumann BH, Coulter DA, Anderson SA, Lynch DR. Cortical parvalbumin GABAergic deficits with alpha7 nicotinic acetylcholine receptor deletion: implications for schizophrenia. Mol Cell Neurosci. 2014;61:163-75.

236. Orr-Urtreger A, Goldner FM, Saeki M, Lorenzo I, Goldberg L, De Biasi M, et al. Mice deficient in the alpha7 neuronal nicotinic acetylcholine receptor lack alpha-bungarotoxin binding sites and hippocampal fast nicotinic currents. J Neurosci. 1997;17(23):9165-71.
237. Toth K, Hofer KT, Kandracs A, Entz L, Bago A, Eross L, et al. Hyperexcitability of the network contributes to synchronization processes in the human epileptic neocortex. J Physiol. 2018;596(2):317-42.
238. Forsingdal A, Fejgin K, Nielsen V, Werge T, Nielsen J. 15q13.3 homozygous knockout mouse model display epilepsy-, autism- and schizophrenia-related phenotypes. Transl Psychiatry. 2016;6(7):e860.
239. Heider J. Neurodevelopmental Alterations in Idiopathic and Isogenic iPSC-derived Psychiatric Disease Models [Doctoral Dissertation]: University of Tübingen; 2024.
240. Monzel AS, Smits LM, Hemmer K, Hachi S, Moreno EL, van Wuellen T, et al. Derivation of Human Midbrain-Specific Organoids from Neuroepithelial Stem Cells. Stem Cell Reports. 2017;8(5):1144-54.
241. Sloan SA, Andersen J, Pasca AM, Birey F, Pasca SP. Generation and assembly of human brain region-specific three-dimensional cultures. Nat Protoc. 2018;13(9):2062-85.
242. Zhang Y, You X, Li S, Long Q, Zhu Y, Teng Z, et al. Peripheral Blood Leukocyte RNA-Seq Identifies a Set of Genes Related to Abnormal Psychomotor Behavior Characteristics in Patients with Schizophrenia. Med Sci Monit. 2020;26:e922426.
243. Richetto J, Meyer U. Epigenetic Modifications in Schizophrenia and Related Disorders: Molecular Scars of Environmental Exposures and Source of Phenotypic Variability. Biol Psychiatry. 2021;89(3):215-26.
244. Markiewicz-Gospodarek A, Markiewicz R, Dobrowolska B, Rahnama M, Loza B. Relationship of Neuropeptide S (NPS) with Neurocognitive, Clinical, and Electrophysiological Parameters of Patients during Structured Rehabilitation Therapy for Schizophrenia. J Clin Med. 2022;11(18).
245. Dennis C. Psychiatric disease: all in the mind of a mouse. Nature. 2005;438(7065):151-2.
246. Zai CC, Tiwari AK, Zai GC, Maes MS, Kennedy JL. New findings in pharmacogenetics of schizophrenia. Curr Opin Psychiatry. 2018;31(3):200-12.
247. Antonacci F, Dennis MY, Huddleston J, Sudmant PH, Steinberg KM, Rosenfeld JA, et al. Palindromic GOLGA8 core duplicons promote chromosome 15q13.3 microdeletion and evolutionary instability. Nat Genet. 2014;46(12):1293-302.
248. Benes FM, Lim B, Matzilevich D, Walsh JP, Subburaju S, Minns M. Regulation of the GABA cell phenotype in hippocampus of schizophrenics and bipolars. Proc Natl Acad Sci U S A. 2007;104(24):10164-9.
249. Charych EI, Liu F, Moss SJ, Brandon NJ. GABA(A) receptors and their associated proteins: implications in the etiology and treatment of schizophrenia and related disorders. Neuropharmacology. 2009;57(5-6):481-95.
250. Marques TR, Ashok AH, Angelescu I, Borgan F, Myers J, Lingford-Hughes A, et al. GABA-A receptor differences in schizophrenia: a positron emission tomography study using [(11)C]Ro154513. Mol Psychiatry. 2021;26(6):2616-25.
251. Brandl EJ, Tiwari AK, Chowdhury NI, Zai CC, Lieberman JA, Meltzer HY, et al. Genetic variation in the GCG and in the GLP1R genes and antipsychotic-induced weight gain. Pharmacogenomics. 2014;15(4):423-31.
252. Monfared RV, Alhassen W, Truong TM, Gonzales MAM, Vachirakorntong V, Chen S, et al. Transcriptome Profiling of Dysregulated GPCRs Reveals Overlapping Patterns across Psychiatric Disorders and Age-Disease Interactions. Cells. 2021;10(11).
253. Sun L, Cheng Z, Zhang F, Xu Y. Gene expression profiling in peripheral blood mononuclear cells of early-onset schizophrenia. Genom Data. 2015;5:169-70.
254. Grunwald LM. iPSC-derived cortical neurons from patients with schizophrenia exhibit changes in early neuronal development [Doctoral Dissertation]: University of Tübingen; 2018.
255. Kim SK, Kang SW, Chung JH, Park HJ, Cho KB, Park MS. Genetic Polymorphisms of Glutathione-Related Enzymes (GSTM1, GSTT1, and GSTP1) and Schizophrenia Risk: A Meta-Analysis. Int J Mol Sci. 2015;16(8):19602-11.

256. Zhang X, Yang J, Liu X, Zhao G, Li X, Xun G. Glutathione S-transferase gene polymorphisms (GSTT1 and GSTM1) and risk of schizophrenia: A case-control study in Chinese Han population. Medicine (Baltimore). 2020;99(36):e21918.
257. Mladinov M, Sedmak G, Fuller HR, Babic Leko M, Mayer D, Kirincich J, et al. Gene expression profiling of the dorsolateral and medial orbitofrontal cortex in schizophrenia. Transl Neurosci. 2016;7(1):139-50.
258. Spalletta G, Piras F, Gravina P, Bello ML, Bernardini S, Caltagirone C. Glutathione S-transferase alpha 1 risk polymorphism and increased bilateral thalamus mean diffusivity in schizophrenia. Psychiatry Res. 2012;203(2-3):180-3.
259. Pak C, Danko T, Mirabella VR, Wang J, Liu Y, Vangipuram M, et al. Cross-platform validation of neurotransmitter release impairments in schizophrenia patient-derived NRXN1-mutant neurons. Proc Natl Acad Sci U S A. 2021;118(22).

6. SUPPLEMENTARY INFORMATION

6.1 Insertion of P2A-Puro sequence into the pLV-TetO-ALN plasmid

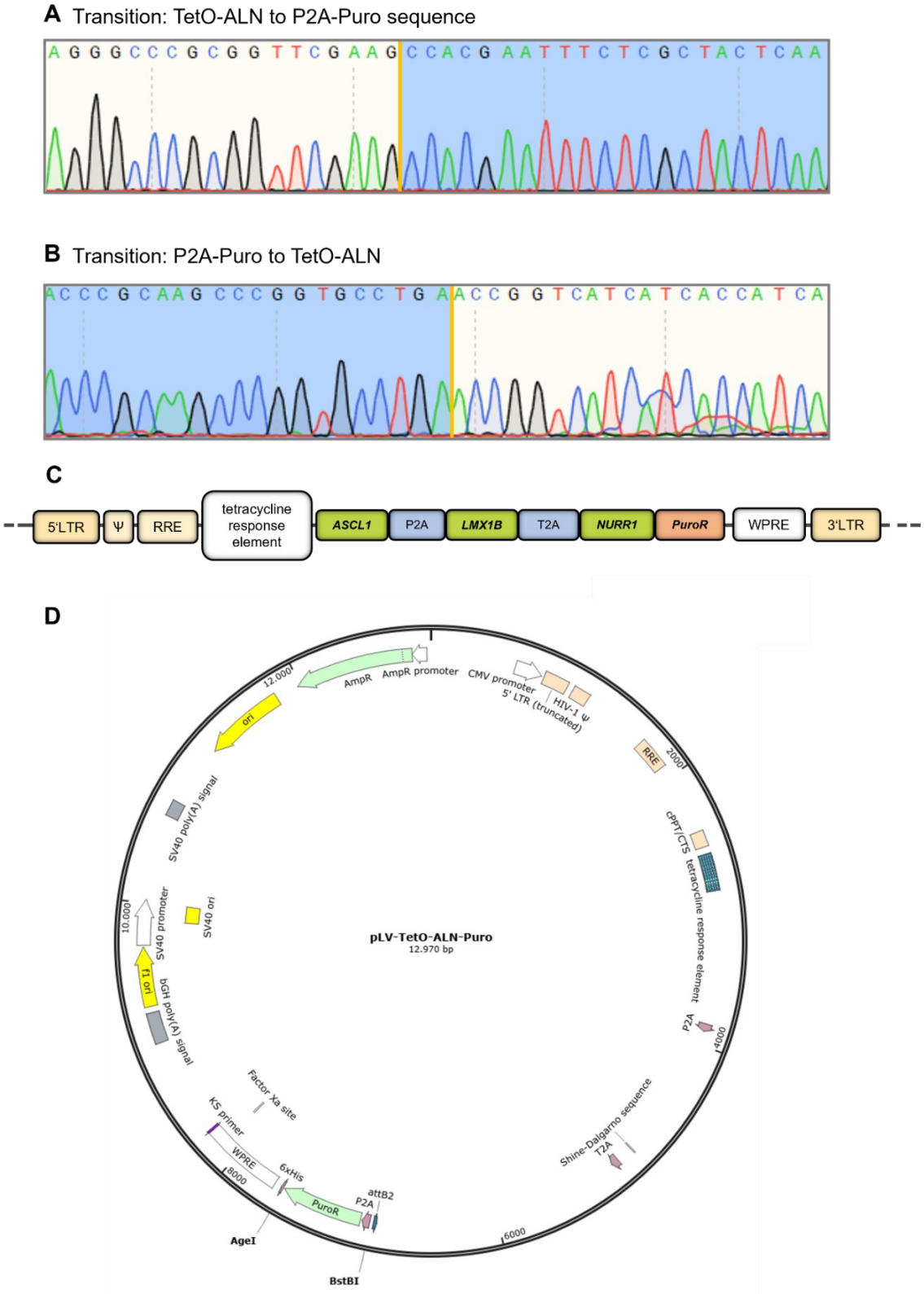

Figure legend on the next page

Supplementary Figure 1: Insertion of a P2A-Puro sequence into the pLV-TetO-ALN plasmid. Puromycin (Puro) resistance gene was inserted at the 3' end of the *ASCL1-LMX1B-NURR1* sequence and separated by a 2A peptide sequence. **(A)** Schematic representation of the transition from TetO-ALN sequence to P2A-Puro sequence (indicated in blue). Confirmation of successful insertion was assessed by Sanger sequencing. **(B)** Schematic representation of the Transition from P2A-Puro sequence (indicated in blue) to TetO-ALN sequence. Confirmation of successful insertion was assessed by Sanger sequencing. **(C)** Schematic representation of the lentiviral vector containing a tetracycline-response element, the ASCL1-LMX1B-NURR1-P2A-Puro sequence and a WPRE fragment. **(D)** Schematic representation of the generated pLV-TetO-ALN-Puro plasmid. The two restriction enzymes AgeI and BstBI indicate the position of the inserted fragment. Created with SnapGene.

6.2 Generation of the lentiviral vector pLV-EF1α-Synaptophysin-mRuby

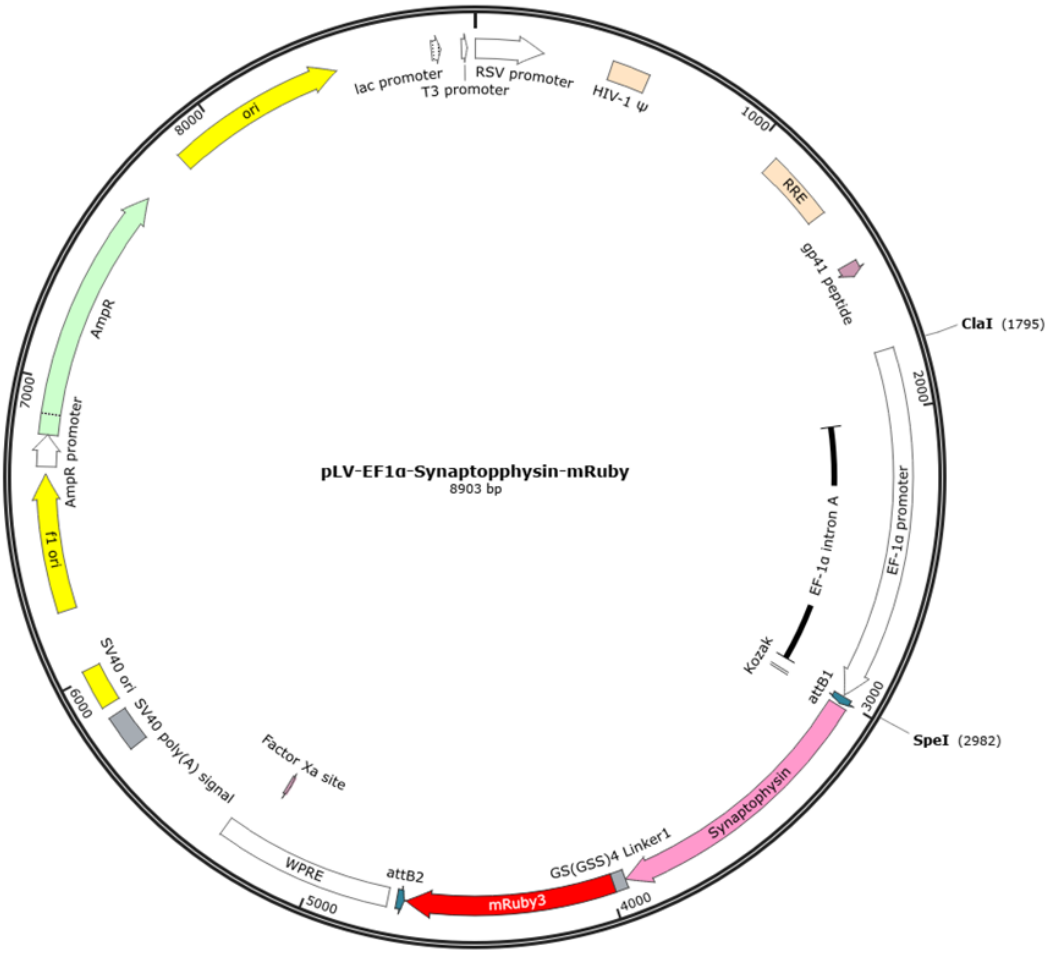

Supplementary Figure 2: Generation of the lentiviral vector pLV-EF1α-Synaptophysin-mRuby. Schematic representation of the generated pLV-EF1α-Synaptophysin-mRuby plasmid. The two restriction enzymes ClaI and SpeI indicate the position of the inserted fragment (EF1α promotor) into the lentiviral backbone. Insertion of the Synaptophysin-mRuby sequence in the plasmid pLV-EF1α/WPRE was done by gateway cloning and resulted in the final plasmid pLV-EF1α-Synaptophysin-mRuby. Created with SnapGene.

6.3 Calcium imaging of ALN and NGN2 monocltures

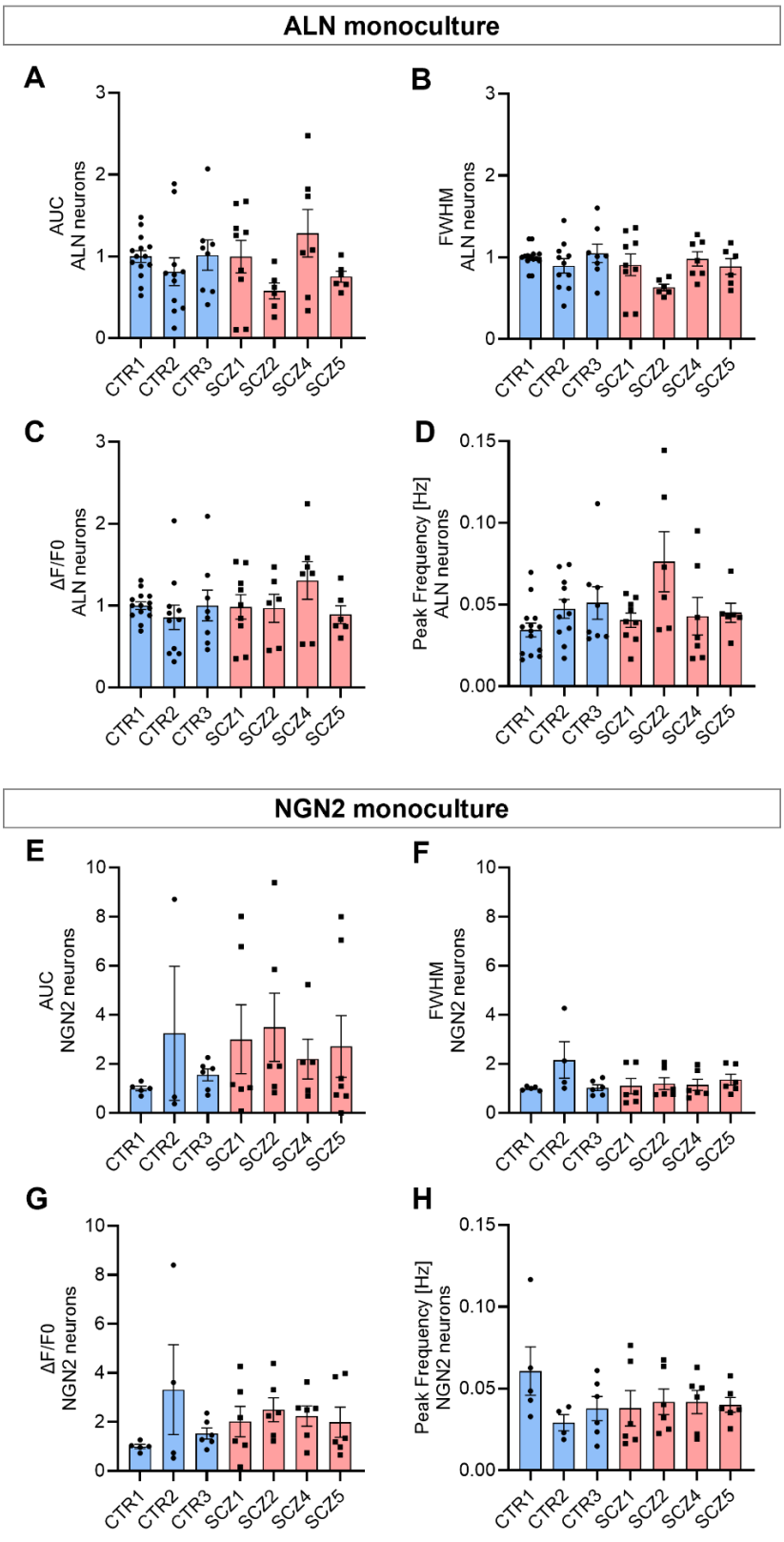

Figure legend on the next page

Supplementary Figure 3. Analysis of spontaneous calcium activity of ALN and NGN2 neurons cultured separately. (A-D) Analysis of spontaneous somatic calcium traces from ALN neurons derived from three CTR and four SCZ lines cultured separately at DIV28. Mean peak parameters are indicated: area under the curve (AUC), full width at half maximum (FWHM), amplitude (ΔF/F0) and peak frequency (Hz) of ALN neurons and NGN2 neurons. **(A)** AUC of ALN neurons, **(B)** FWHM of ALN neurons, **(C)** ΔF/F0 of ALN neurons and **(D)** peak frequency of ALN neurons. CTR1 n=14, CTR2 n1=1, CTR3 n=8, SCZ1 n=9, SCZ2 n=6, SCZ4 n=7, SCZ5 n=6. Data points represent average values from two recordings taken within individual wells ± SEM. Values are normalized to CTR1, while values for peak frequency are represented as absolute values. **(E-H)** Analysis of spontaneous somatic calcium traces from NGN2 neurons derived from three CTR and four SCZ lines cultured separately at DIV21. **(E)** AUC of NGN2 neurons, **(F)** FWHM of NGN2 neurons, **(G)** ΔF/F0 of NGN2 neurons and **(H)** peak frequency of NGN2 neurons. CTR1 n=5, CTR2 n=3, CTR3 n=6, SCZ1 n=6, SCZ2 n=6, SCZ4 n=5, SCZ5 n=7. Data points represent average values from two recordings taken within individual wells ± SEM. Values are normalized to CTR1, while values for peak frequency are represented as absolute values.

6.4 Calcium imaging of ALN and NGN2 co-cultures

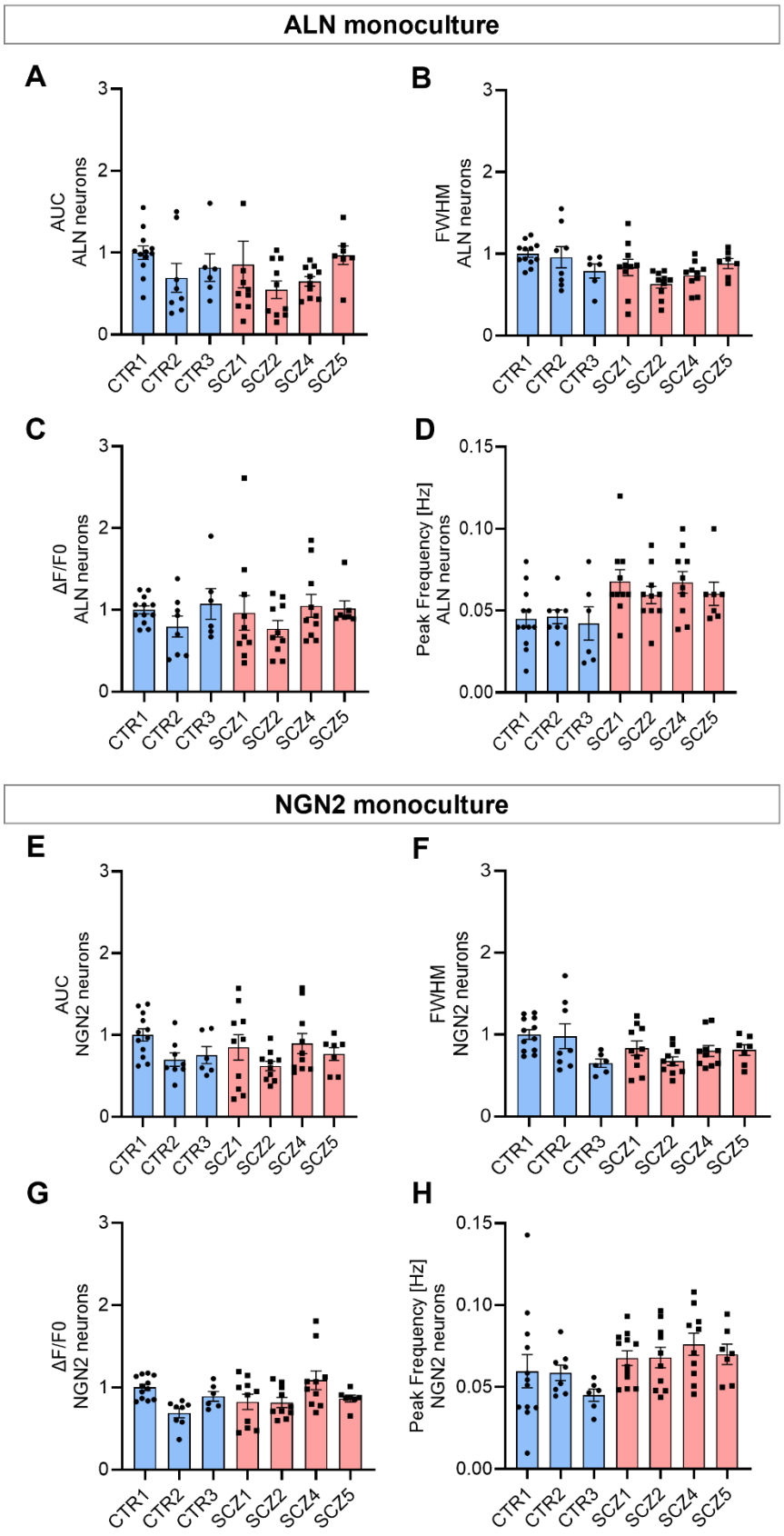

Figure legend on the next page

Supplementary Figure 4. Analysis of spontaneous calcium activity in ALN-NGN2 co-cultures. (A-D) Analysis of spontaneous somatic calcium traces of ALN neurons in ALN-NGN2 co-cultures derived from three CTR and four SCZ lines at DIV28. Mean peak parameters are indicated: area under the curve (AUC), full width at half maximum (FWHM), amplitude (ΔF/F0) and peak frequency (Hz) of ALN neurons and NGN2 neurons. **(A)** AUC of ALN neurons, **(B)** FWHM of ALN neurons, **(C)** ΔF/F0 of ALN neurons and **(D)** peak frequency of ALN neurons. CTR1 n=12, CTR2 n=8, CTR3 n=6, SCZ1 n=10, SCZ2 n=10, SCZ4 n=10, SCZ5 n=7. Data points represent average values from recordings taken within individual wells ± SEM. Values are normalized to CTR1, while values for peak frequency are represented as absolute values. **(E-H)** Analysis of spontaneous somatic calcium traces of NGN2 neurons in ALN-NGN2 co-culture at DIV28. **(E)** AUC of NGN2 neurons, **(F)** FWHM of NGN2 neurons, **(G)** ΔF/F0 of NGN2 neurons and **(H)** peak frequency of NGN2 neurons. CTR1 n=12, CTR2 n=8, CTR3 n=6, SCZ1 n=10, SCZ2 n=10, SCZ4 n=10, SCZ5 n=7. Data points represent average values from recordings taken within individual wells ± SEM. Values are normalized to CTR1, whereas values for peak frequency are represented as absolute values.

6.5 Calcium imaging of ALN and NGN2 co-cultures treated with Pramipexole and Sulpiride

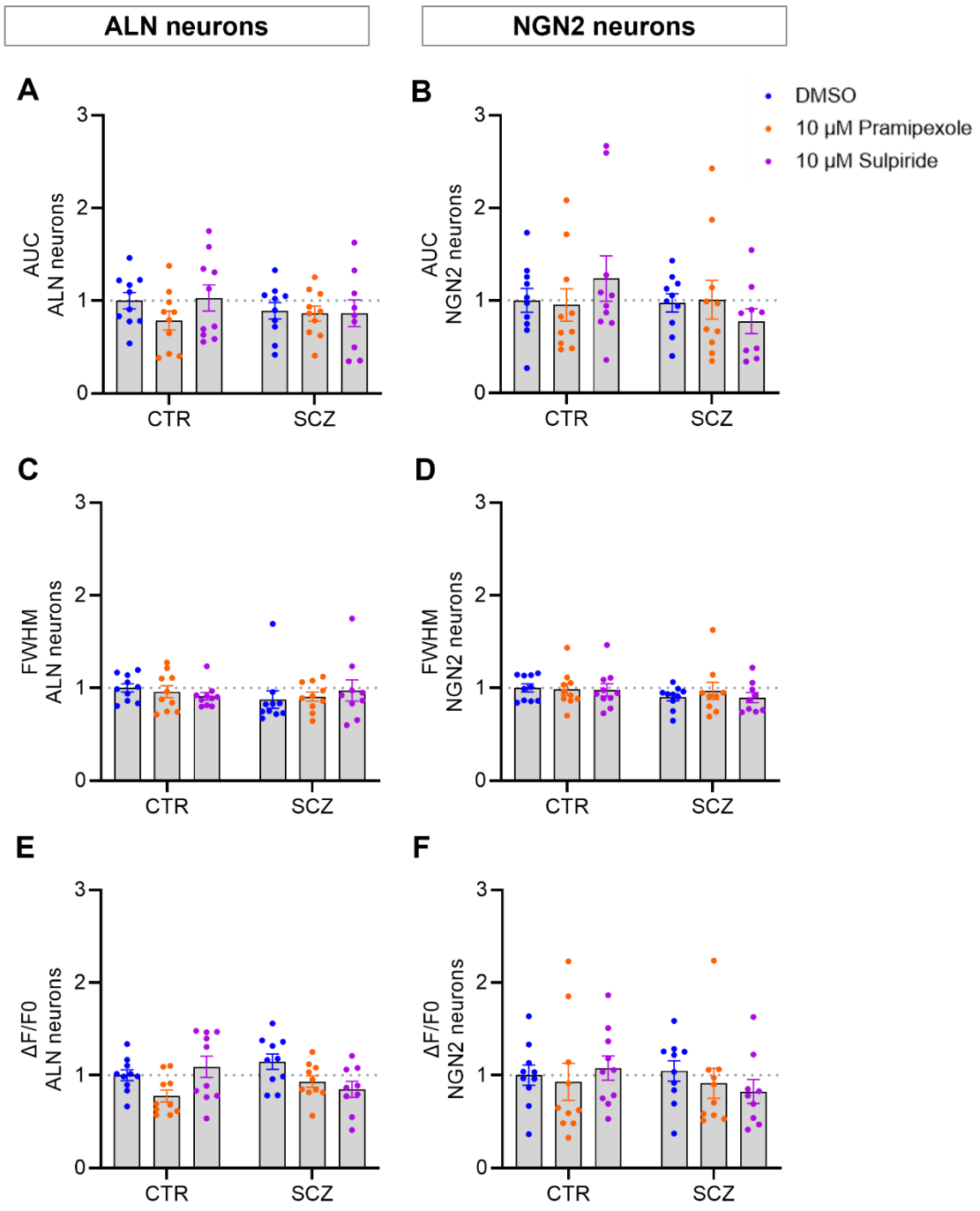

Supplementary Figure 5. Calcium imaging of ALN-NGN2 co-cultures after 24 h treatment with a selective DRD2 agonist/antagonist. (A-F) Analysis of spontaneous somatic calcium activity of ALN and NGN2 neurons in mixed co-culture after 24 h treatment with DMSO, 10 µM Pramipexole (DRD2 agonist) and 10 µM Sulpiride (DRD2 antagonist) at DIV28. Following parameters were analysed: area under the curve (AUC), full width at half maximum (FWHM), amplitude (ΔF/F0) and peak frequency (Hz). **(A)** AUC of ALN neurons, **(B)** AUC of NGN2 neurons, **(C)** FWHM of ALN neurons, **(D)** FWHM of NGN2 neurons, **(E)** ΔF/F0 of ALN neurons and **(F)** ΔF/F0 of NGN2 neurons. CTR DMSO n=10, CTR Pramipexole n=10, CTR Sulpiride n=9, SCZ DMSO n=10, SCZ Pramipexole n=10, SCZ Sulpiride n=9. Data points represent averaged values of recordings taken within individual wells ± SEM. Values are normalized to CTR DMSO.

6.6 Synapse quantification in ALN-NGN2 co-cultures

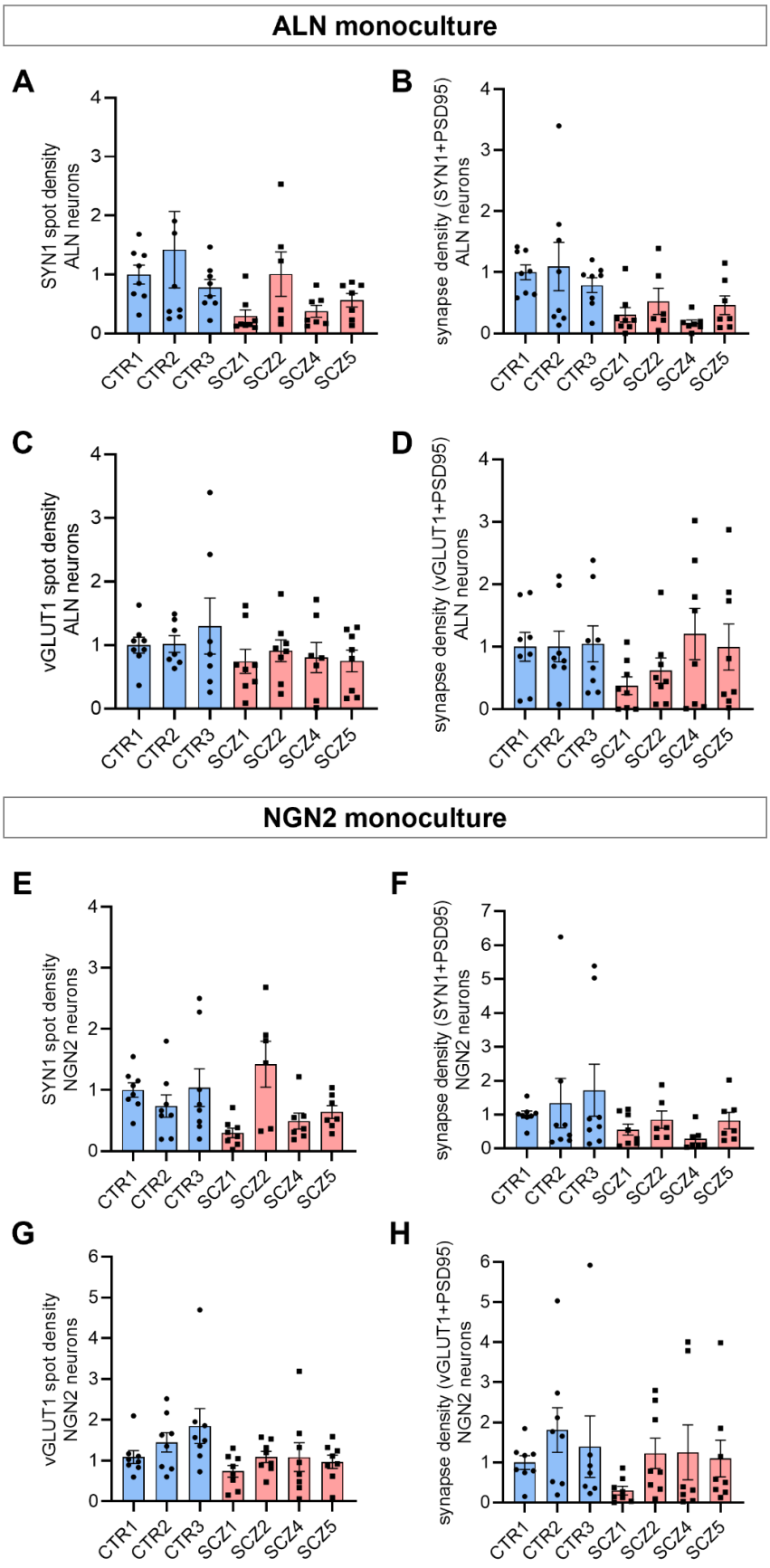

Figure legend on the next page

Supplementary Figure 6. Synapse quantification in ALN-NGN2 co-cultures at DIV28. (A-D) Quantification of synaptic markers on ALN neurons, **(E-H)** and on NGN2 neurons in ALN-NGN2 co-cultures derived from three CTR and four SCZ lines at DIV28. Data points represent average values from individual wells ± SEM. Values are normalized to CTR1. **(A)** Presynaptic density (SYN1) on ALN neurons, CTR1 n=8, CTR2 n=8, CTR3 n=8, SCZ1 n=8, SCZ2 n=6, SCZ3 n=7, SCZ4 n=7. **(B)** Synapse density (SYN1+PSD95) on ALN neurons, CTR1 n=8, CTR2 n=8, CTR3 n=8, SCZ1 n=8, SCZ2 n=6, SCZ3 n=7, SCZ4 n=7. **(C)** Excitatory presynaptic density (vGLUT1) on ALN neurons, CTR1 n=8, CTR2 n=7, CTR3 n=7, SCZ1 n=8, SCZ2 n=8, SCZ3 n=7, SCZ4 n=8. **(D)** Excitatory synapse density (vGLUT1+PSD95) on ALN neurons, CTR1 n=8, CTR2 n=8, CTR3 n=8, SCZ1 n=8, SCZ2 n=8, SCZ3 n=8, SCZ4 n=8. **(E)** Presynaptic density (SYN1) on NGN2 neurons, CTR1 n=8, CTR2 n=8, CTR3 n=8, SCZ1 n=8, SCZ2 n=6, SCZ3 n=7, SCZ4 n=7. **(F)** Synapse density (SYN1+PSD95) on NGN2 neurons, CTR1 n=8, CTR2 n=8, CTR3 n=8, SCZ1 n=8, SCZ2 n=6, SCZ3 n=7, SCZ4 n=7. **(G)** Excitatory presynaptic density (vGLUT1) on NGN2 neurons, CTR1 n=8, CTR2 n=8, CTR3 n=8, SCZ1 n=8, SCZ2 n=8, SCZ3 n=8, SCZ4 n=8. **(H)** Excitatory synapse density (vGLUT1+PSD95) on NGN2 neurons, CTR1 n=8, CTR2 n=8, CTR3 n=7, SCZ1 n=8, SCZ2 n=8, SCZ3 n=7, SCZ4 n=7.

6.7 Synapse quantification in transduced ALN-NGN2 co-cultures

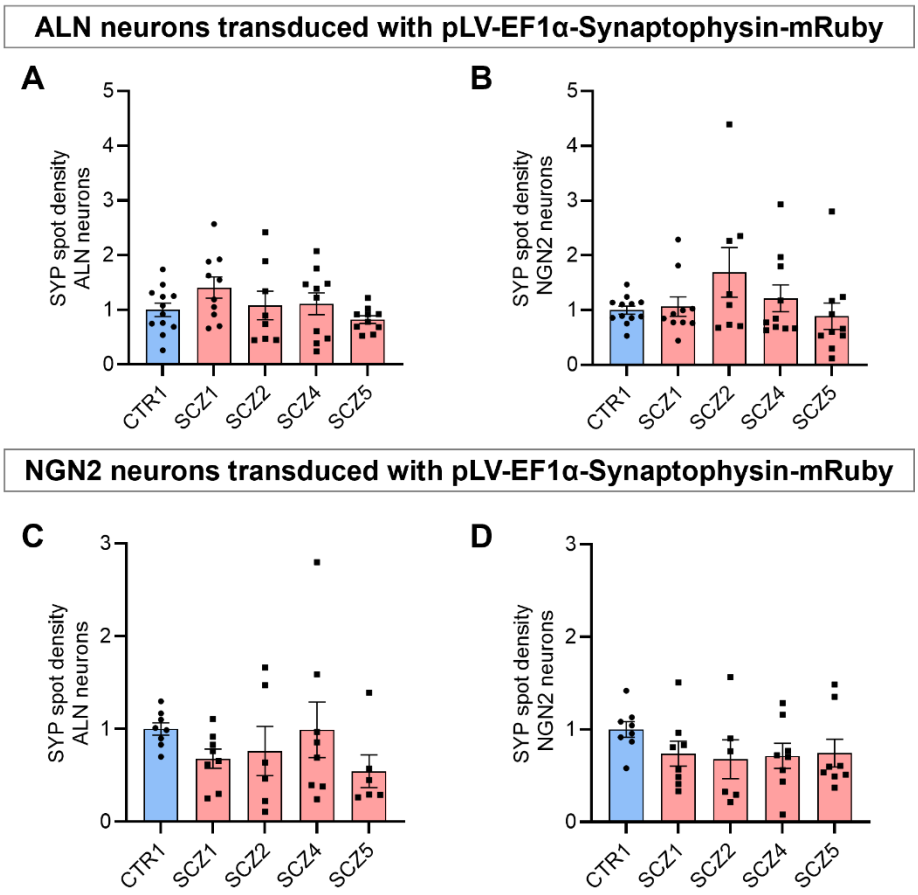

Supplementary Figure 7. Presynaptic SYP-mRuby quantification in ALN-NGN2 co-cultures at DIV28. (A-B) Transduction of ALN neurons and quantification of SYP-mRuby-positive presynaptic boutons on ALN and NGN2 neurons in co-culture. **(C-D)** Transduction of NGN2 neurons and quantification of SYP-mRuby-positive presynaptic boutons on ALN and NGN2 neurons in co-culture derived from one CTR and four SCZ lines at DIV28. Data points represent average values from individual wells ± SEM. Values are normalized to CTR1. **(A)** SYP-mRuby-positive presynaptic densities on ALN neurons, CTR1 n=12, SCZ1 n=10, SCZ2 n=8, SCZ3 n=10, SCZ4 n=10. **(B)** SYP-mRuby-positive presynaptic densities on NGN2 neurons, CTR1 n=12, SCZ1 n=10, SCZ2 n=8, SCZ3 n=10, SCZ4 n=10. **(C)** SYP-mRuby-positive presynaptic densities on ALN neurons, CTR1 n=8, SCZ1 n=8, SCZ2 n=6, SCZ3 n=8, SCZ4 n=8. **(D)** SYP-mRuby-positive presynaptic densities on NGN2 neurons, CTR1 n=8, SCZ1 n=8, SCZ2 n=6, SCZ3 n=8, SCZ4 n=8.

6.8 Top 5 % of DEGs down- and upregulated in SCZ ALN neurons

Supplementary Table 1: Top 5 % of DEGs down- and upregulated in SCZ ALN neurons. Gene ID, gene name, log_2 fold change, as well as the function of the protein encoded by the respective gene, based on the website of the 'Human Protein Atlas' (https://www.proteinatlas.org), are depicted. In addition, research articles, which have also found those genes implicated in SCZ are listed.

Top 5 % of downregulated genes in SCZ				
Gene ID	**Gene**	**Log2FoldChange**	**Function of the protein encoded by the gene**	**Implication in SCZ**
ENSG00000198300	PEG3	-11.83538183	Apoptosis	Not reported
ENSG00000171772	SYCE1	-11.79296336	Cell cycle, Cell division, Meiosis	Not reported
ENSG00000128617	OPN1SW	-10.86263725	G-protein coupled receptor, Photoreceptor protein, Receptor, Retinal protein, Transducer	(242)
ENSG00000182053	TRIM49B	-9.751395702	Protein ubiquitination, Regulation of gene expression	(243)
ENSG00000188886	ASTL	-9.712374284	Hydrolase, Metalloprotease, Protease	Not reported
ENSG00000225581	TRIM53AP	-9.694803279	Pseudogene	Not reported
ENSG00000214285	NPS	-9.486095506	Neuropeptide, involved in positive regulation of GABAergic synaptic transmission	(244)
ENSG00000186223	SSU72P4	-9.466536317	Pseudogene	Not reported
ENSG00000109272	PF4V1	-9.445315243	Cytokine, Heparin-binding, impairs tumor growth and can protect against blood-retinal barrier breakdown	Not reported
ENSG00000116721	PRAMEF1	-9.262235644	May function in reproductive tissues during development	Not reported
ENSG00000120068	HOXB8	-9.257034998	Transcription, Transcription regulation	(245)
ENSG00000215547	DEFB115	-9.104273729	Antibiotic, Antimicrobial, Defensin, a family of antimicrobial and cytotoxic peptides made by neutrophils	(243)
ENSG00000166603	MC4R	-8.938349919	G-protein coupled receptor, Receptor, interacts with adrenocorticotropic and MSH hormones	(246)
ENSG00000162891	IL20	-8.891984713	Cytokine, ansduce its signal through signal transducer and activator of transcription 3 (STAT3) in keratinocytes	Not reported
ENSG00000163534	FCRL1	-8.816530236	Fc receptor-like glycoprotein, may play a	Not reported

			role in the regulation of cancer cell growth	
ENSG00000261739	GOLGA8S	-8.774587315	Predicted to be involved in Golgi organization and Golgi network	(247)
ENSG00000229542	SSU72P7	-8.632514577	Pseudogene	Not reported
ENSG00000202496	RNVU1-20	-8.564446743	Affiliated with the snRNA	Not reported
ENSG00000120952	PRAMEF2	-8.539054346	Predicted to be involved in several processes, including negative regulation of apoptotic process, positive regulation of cell population proliferation	Not reported
ENSG00000230522	MBD3L2	-8.509850393	Related to methyl-CpG-binding proteins	Not reported
ENSG00000138136	LBX1	-8.458821952	Transcription factor required for the development of GABAergic interneurons	(248)
ENSG00000036473	OTC	-8.162639939	Encodes a mitochondrial matrix enzyme	Not reported
ENSG00000145863	GABRA6	-8.048575283	GABA receptor subunit alpha6	(249, 250)
ENSG00000147206	NXF3	-7.527831159	May function as a tissue-specific nuclear mRNA export factor	Not reported
ENSG00000115263	GCG	-7.487182174	Hormone, key role in glucose metabolism and homeostasis	(251)
ENSG00000035720	STAP1	-7.384375757	thought to participate in a positive feedback loop by upregulating the activity of tyrosine-protein kinase Tec	Not reported
ENSG00000142515	KLK3	-7.337514313	Hydrolase, Protease, Serine protease	Not reported
ENSG00000174948	GPR149	-7.219880283	G-protein coupled receptor, Receptor, Orphan receptor	(252)
ENSG00000095627	TDRD1	-7.197414863	Differentiation, Meiosis, RNA-mediated gene silencing, Spermatogenesis	Not reported
ENSG00000251258	RFPL4B	-6.759827035	Predicted to enable metal ion binding activity	(253)
Top 5 % of upregulated genes in SCZ				
Gene ID	**Gene**	**Log2FoldChange**	**Function of the protein encoded by the gene**	**Implication in SCZ**
ENSG00000176728	TTTY14	13.69942899	Long intergenic non-coding RNAs	(254)
ENSG00000206159	GYG2P1	12.88446616	Pseudogene	Not reported
ENSG00000092377	TBL1Y	12.68208204	Involved in the recruitment of the ubiquitin/19S proteasome complex to nuclear	Not reported

			receptor-regulated transcription units	
ENSG00000134184	GSTM1	11.75284824	Involved in the formation of glutathione conjugates, lipid metabolism	(255, 256)
ENSG00000226555	AGKP1	11.17591894	Pseudogene	Not reported
ENSG00000183878	UTY	10.99789332	Chromatin regulator, Dioxygenase, Oxidoreductase	Not reported
ENSG00000136457	CHAD	10.86925779	Cartilage matrix protein thought to mediate adhesion of isolated chondrocyte	Not reported
ENSG00000064218	DMRT3	10.61480144	Differentiation, Sexual differentiation, Transcription, Transcription regulation	Not reported
ENSG00000179097	HTR1F	10.00132364	Enables G protein-coupled serotonin receptor activity and serotonin binding activity. Involved in adenylate cyclase-inhibiting G protein-coupled receptor signaling pathway	Not reported
ENSG00000231007	CDC20P1	9.955421398	Pseudogene	Not reported
ENSG00000067048	DDX3Y	9.812234302	ATP-binding, Nucleotide-binding, involved in ATP binding, hydrolysis, RNA binding	(257)
ENSG00000221710	MIR1298	9.767028859	microRNA	Not reported
ENSG00000162782	TDRD5	9.753216241	Differentiation, Spermatogenesis	Not reported
ENSG00000099725	PRKY	9.593343887	Pseudogene	Not reported
ENSG00000174156	GSTA3	9.270018621	Lipid metabolism, catalyses the double bond isomerization of precursors for progesterone and testosterone	(258)
ENSG00000203489	HMGB1P39	9.230168231	Pseudogene	Not reported
ENSG00000223543	TCEAL4P1	9.21453461	Pseudogene	Not reported
ENSG00000160994	CCDC105	9.148446074	Located in extracellular exosome	Not reported
ENSG00000187513	GJA4	9.138870429	Encoded protein is a component of gap junctions, which are composed of arrays of intercellular channels	Not reported
ENSG00000253649	PRSS51	9.091410257	Predicted to enable serine-type endopeptidase activity. Predicted to be involved in proteolysis	Not reported

ENSG00000251389	YTHDF1P1	9.080192055	Pseudogene	Not reported
ENSG00000130383	FUT5	8.889430701	Lipid metabolism, Predicted to be located in Golgi membrane	(242)
ENSG00000170477	KRT4	8.856444898	Protein encoded by this gene is a member of the keratin gene family	Not reported
ENSG00000236969	GGT8P	8.837332389	Pseudogene	Not reported
ENSG00000170486	KRT72	8.811472082	Encodes a type II keratin that is specifically expressed in the inner root sheath of hair follicles	Not reported
ENSG00000053438	NNAT	7.364011118	Protein encoded by this gene is a proteolipid that may be involved in the regulation of ion channels during brain development	(166, 259)
ENSG00000007350	TKTL1	8.776348656	Calcium, Magnesium, Metal-binding, Thiamine pyrophosphate	Not reported
ENSG00000120949	TNFRSF8	8.745841225	Protein encoded by this gene is a member of the TNF-receptor superfamily	Not reported
ENSG00000227145	IL21-AS1	8.652886434	Antisense RNA	Not reported
ENSG00000239005	ACA64	8.624670058	Small nucleolar RNA	Not reported

6.9 GO enrichment analysis – category ‘cellular component’

Supplementary Table 2: GO enrichment analysis of the category 'cellular components’ (CC, cut-off q-val <0.05) using the online classification system PantherDB (https://www.pantherdb.org/). Complete list with downregulated gene sets, as well as upregulated gene sets is depicted. (FDR=false discovery rate)

Downregulated gene sets			
GO cellular component complete	**raw p-value**	**FDR**	**-log10(pvalue)**
cellular anatomical entity (GO:0110165)	9.73E-11	1.95E-07	10.01188716
synapse (GO:0045202)	4.46E-10	4.45E-07	9.350665141
cellular_component (GO:0005575)	6.66E-10	3.33E-07	9.176525771
neuron projection (GO:0043005)	9.86E-10	3.94E-07	9.006123085
membrane (GO:0016020)	5.12E-09	1.70E-06	8.290730039
extracellular region (GO:0005576)	5.43E-08	1.55E-05	7.26520017
neuronal cell body (GO:0043025)	6.44E-08	1.61E-05	7.191114133
synaptic membrane (GO:0097060)	8.24E-08	1.83E-05	7.084072788
Golgi cis cisterna (GO:0000137)	2.24E-07	4.47E-05	6.649751982

cell body (GO:0044297)	2.58E-07	4.69E-05	6.588380294
axon terminus (GO:0043679)	3.39E-07	5.64E-05	6.469800302
cell periphery (GO:0071944)	4.06E-07	6.24E-05	6.391473966
nuclear protein-containing complex (GO:0140513)	4.56E-07	6.51E-05	6.341035157
organelle membrane (GO:0031090)	5.25E-07	7.00E-05	6.279840697
postsynaptic membrane (GO:0045211)	1.55E-06	1.93E-04	5.809668302
cell junction (GO:0030054)	1.58E-06	1.86E-04	5.801342913
nucleoplasm (GO:0005654)	1.68E-06	1.87E-04	5.774690718
neuron projection terminus (GO:0044306)	2.04E-06	2.15E-04	5.690369833
axon (GO:0030424)	2.15E-06	2.14E-04	5.66756154
nuclear lumen (GO:0031981)	2.16E-06	2.05E-04	5.665546249
extracellular space (GO:0005615)	3.09E-06	2.81E-04	5.510041521
cytoplasm (GO:0005737)	4.18E-06	3.63E-04	5.378823718
terminal bouton (GO:0043195)	8.16E-06	6.79E-04	5.088309841
postsynapse (GO:0098794)	1.16E-05	9.25E-04	4.935542011
somatodendritic compartment (GO:0036477)	2.11E-05	1.62E-03	4.675717545
recycling endosome membrane (GO:0055038)	2.85E-05	2.11E-03	4.54515514
plasma membrane bounded cell projection (GO:0120025)	4.25E-05	3.04E-03	4.37161107
nucleus (GO:0005634)	4.29E-05	2.96E-03	4.367542708
Golgi stack (GO:0005795)	6.06E-05	4.04E-03	4.217527376
plasma membrane (GO:0005886)	6.17E-05	3.98E-03	4.209714836
endomembrane system (GO:0012505)	6.18E-05	3.86E-03	4.209011525
Golgi cisterna (GO:0031985)	6.54E-05	3.96E-03	4.184422252
perikaryon (GO:0043204)	7.04E-05	4.14E-03	4.152427341
MHC class I protein complex (GO:0042612)	9.28E-05	5.30E-03	4.032452024
cell projection (GO:0042995)	1.07E-04	5.93E-03	3.970616222
acetylcholine-gated channel complex (GO:0005892)	1.14E-04	6.18E-03	3.943095149
endoplasmic reticulum (GO:0005783)	1.37E-04	7.22E-03	3.863279433
transport vesicle membrane (GO:0030658)	1.54E-04	7.89E-03	3.812479279
presynapse (GO:0098793)	1.60E-04	8.01E-03	3.795880017
endoplasmic reticulum membrane (GO:0005789)	1.68E-04	8.18E-03	3.774690718

endoplasmic reticulum subcompartment (GO:0098827)	1.74E-04	8.28E-03	3.759450752
nuclear outer membrane-endoplasmic reticulum membrane network (GO:0042175)	2.71E-04	1.26E-02	3.567030709
distal axon (GO:0150034)	3.04E-04	1.38E-02	3.517126416
organelle subcompartment (GO:0031984)	3.33E-04	1.48E-02	3.477555766
GABA receptor complex (GO:1902710)	3.40E-04	1.48E-02	3.468521083
transmembrane transporter complex (GO:1902495)	3.53E-04	1.50E-02	3.452225295
early endosome membrane (GO:0031901)	3.62E-04	1.51E-02	3.441291429
Golgi apparatus (GO:0005794)	5.06E-04	2.06E-02	3.295849483
membrane protein complex (GO:0098796)	5.33E-04	2.13E-02	3.273272791
transport vesicle (GO:0030133)	5.63E-04	2.21E-02	3.249491605
plasma membrane region (GO:0098590)	7.30E-04	2.81E-02	3.13667714
chromosomal region (GO:0098687)	8.78E-04	3.31E-02	3.056505484
receptor complex (GO:0043235)	8.96E-04	3.32E-02	3.04769199
transporter complex (GO:1990351)	9.02E-04	3.28E-02	3.044793462
excitatory synapse (GO:0060076)	9.13E-04	3.26E-02	3.039529222
collagen type I trimer (GO:0005584)	9.15E-04	3.21E-02	3.038578906
extrinsic component of endosome membrane (GO:0031313)	9.15E-04	3.15E-02	3.038578906
neuronal dense core vesicle (GO:0098992)	9.71E-04	3.29E-02	3.01278077
vesicle (GO:0031982)	9.97E-04	3.32E-02	3.001304842
dense core granule (GO:0031045)	1.05E-03	3.43E-02	2.978810701
respirasome (GO:0070469)	1.05E-03	3.39E-02	2.978810701
ribonucleoprotein complex (GO:1990904)	1.12E-03	3.56E-02	2.950781977
monoatomic ion channel complex (GO:0034702)	1.18E-03	3.64E-02	2.928117993
mitochondrial membrane (GO:0031966)	1.18E-03	3.68E-02	2.928117993
Golgi membrane (GO:0000139)	1.23E-03	3.73E-02	2.910094889
intracellular non-membrane-bounded organelle (GO:0043232)	1.33E-03	3.92E-02	2.876148359
non-membrane-bounded organelle (GO:0043228)	1.33E-03	3.97E-02	2.876148359
organelle lumen (GO:0043233)	1.39E-03	4.04E-02	2.8569852
intracellular organelle lumen (GO:0070013)	1.39E-03	3.98E-02	2.8569852
membrane-enclosed lumen (GO:0031974)	1.39E-03	3.92E-02	2.8569852

extracellular exosome (GO:0070062)	1.56E-03	4.34E-02	2.806875402
extracellular vesicle (GO:1903561)	1.62E-03	4.44E-02	2.790484985
extracellular organelle (GO:0043230)	1.63E-03	4.39E-02	2.787812396
extracellular membrane-bounded organelle (GO:0065010)	1.63E-03	4.33E-02	2.787812396
mitochondrial envelope (GO:0005740)	1.70E-03	4.46E-02	2.769551079
Upregulated gene sets			
GO cellular component complete	**raw p-value**	**FDR**	**-log10(pvalue)**
plasma membrane bounded cell projection (GO:0120025)	8.97E-06	1.79E-02	5.047207557
apical part of cell (GO:0045177)	1.17E-05	1.17E-02	4.931814138
cilium (GO:0005929)	1.18E-05	7.89E-03	4.928117993
cell periphery (GO:0071944)	2.81E-05	1.40E-02	4.55129368
cell projection (GO:0042995)	3.61E-05	1.44E-02	4.442492798
cell surface (GO:0009986)	9.07E-05	3.02E-02	4.042392713
axoneme (GO:0005930)	1.01E-04	2.90E-02	3.995678626
ciliary plasm (GO:0097014)	1.08E-04	2.69E-02	3.966576245
extracellular matrix (GO:0031012)	1.18E-04	2.62E-02	3.928117993
external encapsulating structure (GO:0030312)	1.21E-04	2.42E-02	3.91721463
cell junction (GO:0030054)	1.80E-04	3.27E-02	3.744727495
FACIT collagen trimer (GO:0005593)	2.62E-04	4.37E-02	3.581698709

7. STATEMENT OF CONTRIBUTIONS

Following iPSC lines were a kind gift from other groups and used in this study:

1) **Names and shares of colleagues:** one isogenic CTR and two *PINK1* K.O. (*PINK1* Δ8.9 and *PINK1* Δ40.7) iPSC lines were a kind gift from Dr. Julia Fitzgerald (Hertie Institute for Clinical Brain Research, Tübingen).
2) **Names and shares of colleagues:** one isogenic CTR and three deletion iPSC lines (one iPSC clone with a deletion in chromosome 15q13 and two iPSC clones with a deletion in chromosome 22q11) were a kind gift from Prof. Dr. Moritz Rossner (Department of Psychiatry and Psychotherapy, Munich).
3) **Names and shares of colleagues:** one CTR iPSC line (CTR3) was a kind gift from the Tumorbiology group (NMI, Reutlingen).

Colleagues who contributed to the following experiments in this study:

4) **Framework of the experiment:** Transcriptome analysis of iPSC-derived dopaminergic neurons and subsequent GO enrichment analysis, as well as hierarchical cluster analysis were performed. This experiment is described in **chapter 3.2.2** 'RNA expression profiling reveals thousands of differentially expressed genes in SCZ ALN neurons'.

   Names and shares of colleagues: Aaron Stahl (Assay Development, NMI, Reutlingen) performed the hierarchical cluster analysis in the MeV software (see Figure 8B).

   My own contribution: I differentiated the respective iPSC lines into dopaminergic neurons until DIV21 and prepared cell pellets for following RNA sequencing. Data processing necessary for hierarchical cluster analysis was performed by me.

5) **Framework of the experiment:** Calcium imaging of mixed iPSC-derived dopaminergic and glutamatergic co-cultures to identify a neuronal cell type responsible for elevated neuronal activity. This experiment is described in **chapter 3.5.3** 'SCZ ALN neurons as possible driver for elevated neuronal activity in co-cultures'.

   Names and shares of colleagues: Patricia Pizarro Garcia (Master student, Molecular Neurobiology, NMI, Reutlingen) differentiated the neurons, seeded the cells into mixed co-cultures and performed calcium imaging. Three biological replicates were analysed by her.

   My own contribution: I supervised Patricia Pizarro Garcia in seeding the cells, performing calcium imaging of the mixed co-cultures and analysing the data. I transduced the starting

cell types with the lentiviral vectors. Two additional biological replicates were analysed by me.

6) **Framework of the experiment:** iPSC-derived dopaminergic and glutamatergic neurons were transduced with the lentiviral vector pEF1α-Synaptophysin-mRuby to label presynaptic boutons, respectively. This experiment is described in **chapter 3.7.3** 'Development of a lentiviral vector for cell type-specific presynaptic-bouton labelling'.

   Names and shares of colleagues: Cloning of EF1α-Synaptophysin-mRuby into the lentiviral backbone pLV-04CAMKII-s/WPRE and generation of the pLV-EF1α-Synaptophysin-mRuby lentivirus were performed by Lisa-Sophie Wüstner (Molecular Neurobiology, NMI, Reutlingen).

   My own contribution: Transduction of respective cell types with this lentiviral vector, differentiation into dopaminergic and glutamatergic neurons, immunocytochemistry and synapse quantification were carried out by me.

7) **Framework of the experiment:** Neurite outgrowth and neurite branching assays with differentiating NGN2 neurons carrying microdeletions were performed to identify early neurodevelopmental aberrations. This experiment is described in **chapter 3.8.1** 'Aberrant neurite branching in NGN2 neurons carrying microdeletions'.

   Names and shares of colleagues: Sabrina Vogel (Molecular Neurobiology, NMI, Reutlingen) seeded the cells and analysed two of the four biological replicates.

   My own contribution: I seeded the cells and analysed two of the four biological replicates. I developed the analysis procedure.

8) **Framework of the experiment:** The GSI as a measure for the level of synchronization within the E-I co-cultures was analysed. This experiment is described in **chapter 3.8.4** 'Increased synchronization in E-I co-cultures carrying microdeletions'.

   Names and shares of colleagues: Emilio Pardo Gonzalez (Electrophysiology group, NMI, Reutlingen) wrote a Python code that allowed to analyse the GSI based on the calcium imaging raw data.

   My own contribution: I differentiated the neurons, seeded the co-culture, performed calcium imaging and processed the data. I applied the Python code to the raw data to obtain the GSI for each recording.

8. STATEMENT OF PUBLICATIONS

Parts of this thesis are included in the following submitted article:

Hartmann SM, Pizarro Garcia P, Heider J, et al. A co-culture model of dopaminergic and glutamatergic neurons derived from patients with idiopathic schizophrenia reveals a hypodopaminergic phenotype.

The transcriptome data discussed in this thesis have been deposited in NCBI's Gene Expression Omnibus (GEO) and are part of the submitted article. The data are accessible through GEO Series accession number GSE275064 (https://www.ncbi.nlm.nih.gov/geo/query/acc.cgi?acc=GSE275064).

Following data, that are part of this thesis, can be found in the above-mentioned submitted article:

Characterization of ALN-induced dopaminergic neurons	Described in section 3.1.2	Figure 4B
Differentiation efficiency of ALN-induced dopaminergic neurons	Described in section 3.1.3	Figure 5C
Transcriptome analysis of ALN-induced dopaminergic neurons	Described in section 3.2 (3.2.2; 3.2.3; 3.2.4; 3.2.5)	Figure 8; Figure 9; Figure 10; Figure 11
Functional characterization of ALN and NGN2 neurons	Described in section 3.5 (3.5.1; 3.5.2; 3.5.3; 3.5.4)	Figure 15; Figure 16; Figure 17; Figure 18; Figure 19
Morphological characterization of ALN and NGN2 neurons	Described in section 3.7 (3.7.1; 3.7.2; 3.7.4)	Figure 22; Figure 23; Figure 24; Figure 26; Figure 27

9. DANKSAGUNG

An dieser Stelle möchte ich mich herzlich bei den zahlreichen Personen bedanken, die mich während des Schreibens dieser Arbeit unterstützt haben. Ich bin euch sehr dankbar und weiß das sehr zu schätzen.

Zunächst gilt mein größter Dank Prof. Dr. Hansjürgen Volkmer, der mir das Anfertigen dieser Doktorarbeit in seiner Arbeitsgruppe ermöglicht hat. Danke für deine stetige Unterstützung, dein großes Vertrauen, sowie die zahleichen und wertvollen wissenschaftlichen Diskussionen. Ich danke dir für die stets vielen Möglichkeiten und Freiheiten, die du mir gegeben hast, auf internationale Konferenzen zu gehen, um dort meine Arbeit zu präsentieren und mich fachlich weiterzubilden.

Ich bedanke mich ebenfalls bei Dr. Julia Fitzgerald und Prof. Dr. Jan Benda, die Teil meines Advisory Boards waren und zahlreiche Ideen, sowie konstruktive Anmerkungen im Rahmen unseres jährlichen AB-Meetings hatten.

Danken möchte ich ebenfalls Prof. Dr. Stefan Liebau, der kurzerhand als Zweitgutachter eingesprungen ist und damit einverstanden war, meine Arbeit zu begutachten.

Ganz besonders möchte ich mich bei Johanna Heider, Lisa-Sophie Wüstner, Verena Singer und Sabrina Vogel bedanken. Ich danke euch für die fabelhafte Zusammenarbeit und die großartige Unterstützung während dieser Zeit. Danke, für die vielen tollen Stunden, die wir gemeinsam verbracht haben, sei es in der Zellkultur, im Großraumbüro oder beim Basteln der vielen Geschenke. Danke für eure aufmunternden Worte, wenn mal nicht alles glatt lief. Zudem bin ich unendlich dankbar für die Freundschaften, die daraus entstanden sind.

Des Weiteren gilt ein großer Dank allen Kolleginnen und Kollegen des 3. Stocks. Unsere gemeinsamen Mittags- und Kaffeepausen, sowie die zahlreichen lustigen Ausflüge innerhalb und außerhalb des NMIs bleiben unvergesslich und werde ich in sehr guter Erinnerung behalten.

Von Herzen möchte ich meiner Familie und Freunden danken, die mir in jeder Situation zur Seite standen und eine sehr große Stütze in dieser Zeit waren.

Zuletzt noch ein ganz besonderer Dank an meinen Freund Moritz Rothweiler. Ich danke dir für die große Unterstützung und dein unglaubliches Verständnis, vor allem während dem Schreiben dieser Arbeit. Du hast mich immer wieder motiviert und ermutigt nach vorne zu blicken.